

# Advanced Center for Research in High Energy Meterials ACRHEM

# EXCITED STATE DYNAMICS AND FEMTOSECOND NONLINEAR OPTICAL STUDIES OF NOVEL PORPHYRINS, PHTHALOCYANINES USING TRANSIENT ABSORPTION SPECTROSCOPY AND Z SCAN TECHNIQUES

Thesis submitted by
Somdatta Bhattacharya
15ACPA02
Under supervision of
Prof. Soma Venugopal Rao



November 2020



# Excited State Dynamics and Femtosecond Nonlinear Optical Studies of Novel Porphyrins, Phthalocyanines using Transient Absorption Spectroscopy and Z-scan Techniques

A Thesis Submitted to the **University of Hyderabad**for the award of the degree in **Doctor of Philosophy in Physics** 

by Ms. Somdatta Bhattacharya (15ACPA02)
under the guidance of
Prof. Soma Venugopal Rao



#### November 2020

Advanced Centre of Research in High Energy Materials (ACRHEM),
School of Physics, University of Hyderabad,
Hyderabad 500046, Telangana, India

#### **DECLARATION**

I, Somdatta Bhattacharya, hereby declare that this thesis entitled "Excited State Dynamics and Femtosecond Nonlinear Optical Studies of Novel Porphyrins, Phthalocyanines using Transient Absorption Spectroscopy and Z-scan Techniques" submitted by me under the guidance of Dr. S. Venugopal Rao, Professor, ACRHEM, School of Physics, University of Hyderabad, is a bonafide research work which is also plagiarism free. I also declare that it has not been submitted previously in part or in full to this University or any other University or Institution for the award of any degree or diploma. I hereby agree that my thesis can be deposited in Shodhganga/INFLIBNET.

A report on plagiarism statistics from the University Librarian is enclosed.

Date: 04-11-2020

Somdatta Bhattacharya.

Somulatia Bhattachai ya

Reg. No: 15ACPA02

# University of Hyderabad, Central University (P.O.), Gachibowli, Hyderabad-500 046, India

#### CERTIFICATE

This is to certify that the thesis entitled "Excited State Dynamics and Femtosecond Nonlinear Optical Studies of Novel Porphyrins, Phthalocyanines using Transient Absorption Spectroscopy and Z-scan Techniques" being submitted to the University of Hyderabad by Somdatta Bhattacharya (Reg. No: 15ACPA02), for the award of the degree of Doctor of Philosophy in Physics, is a bonafide work carried out by her under my supervision and guidance which is a plagiarism-free thesis. The thesis has not been submitted previously in part or in full to this or any other University or Institution for the award of any degree or diploma.

Henrapai las

Prof. S. Venugopal Rao

Thesis Supervisor

ACRHEM, University of Hyderabad.

Dr. S. VENUGOPAL RAO Professor Advance Centre of Research in High Energy Materials (ACRHEM) UNIVERSITY OF HYDERABAD Hyderabad-500 046. T.S. INDIA.

Head of the Department

Dr. V. KAMESWARA RAO

Advanced Centre of Research in High Energy Materials

UNIVERSITY OF HYDERABAD
P.O. Central University, Prof. C.R. Rao Road,
HYDERABAD-500 046. TELANGANA, INDIA.

**ACRHEM** 

School of Physics, University of Hyderabad DEAN

School of Physics University of Hyderabad

Hyderabad-500 046, INDIA



#### CERTIFICATE

This is to certify that the thesis entitled "Excited State Dynamics and Femtosecond Nonlinear Optical Studies of Novel Porphyrins, Phthalocyanines using Transient Absorption Spectroscopy and Z-scan Techniques" submitted by Somdatta Bhattacharya bearing registration number 15ACPA02 in partial fulfillment of the requirements for award of Doctor of Philosophy in physics at ACRHEM, School of physics, University of **Hyderabad** is a bonafide work carried out by him under my supervision and guidance. This thesis is free from plagiarism and has not been submitted previously in part or in full to this or any other University or Institution for award of any degree or diploma. Further, the student has the following publications before submission of the thesis for adjudication.

- 1. S. Bhattacharya, G.Reddy, S.Paul, Sk S. Hossain, S.S.K.Raavi, L.Giribabu, A.Samanta and S. Venugopal Rao, "Comparative Photophysical and Femtosecond Nonlinear Optical Properties of Novel Imidazole Substituted Metal Phthalocyanines", Dyes and Pigments 2021, 184, 108791.
- 2. S. Bhattacharya, C. Biswas, S. S. K. Raavi, J. V. S. Krishna, D. Koteshwar, L. Giribabu and S. Venugopal Rao, "Optoelectronic, Nonlinear Optical Properties and Excited State Dynamics of a Triphenyl Imidazole Induced Phthalocyanine Derivative", RSc Advances 2019, 9, 36726-36741.
- 3. S. Bhattacharya; C. Biswas; S. S. K. Raavi; J. V. S. Krishna; N. V. Krishna; L. Giribabu; S. Venugopal Rao, "Synthesis, optical, electrochemical, DFT studies, NLO properties and ultrafast excited state dynamics of carbazole induced phthalocyanine derivatives", The Journal of Physical Chemistry C 2019, 123, 11118-11133.
- 4. M.S.S. Bharati, S. Bhattacharya, J.V. Suman Krishna, L. Giribabu, S. Venugopal Rao, "Femtosecond, broadband nonlinear optical studies of a porphyrin and phthalocyanine", Optics and Laser Technology 2018, 108, 418-425.

The following courses have taken as the part of the course work:

Course No.	Department	Title of the course	Credits	Pass/Fail
1	SEST	Characterization of Material Microscopy	4	Pass
2	SEST	Material Processing and Characterization	4	Pass
3	SoP	Advanced Experimental techniques	4	Pass
4	ACRHEM	Research methodology	4	Pass
5	5 ACRHEM High Energy Materials		4	Pass

04/11/2020

Henrippal (las

Prof. Soma Venugopal Rao

ACRHEM,

University of Hyderabad, India

Director

ACRHEM,

University of Hyderabad,

India

Dean

School of Physics, University of

Hyderabad, India

DEAN

School of Physics University of Hyderabad Hyderabad-500 046, INDIA.

Dr. S. VENUGOPAL RAO

Professor Advance Centre of Research in High Energy Materials (ACRHEM) UNIVERSITY OF HYDERABAD Hyderabad-500 046. T.S. INDIA.

Dr. V. KAMESWARA RAO

DI. V. NAMES VARA RAO
Director
Advanced Centre of Research in High Energy Materials
(ACRHEM)
UNIVERSITY OF HYDERABAD
P.O. Central University, Prof. C.R. Rao Road,
HYDERABAD-500 046, TELANGANA, INDIA.

4 | Page

#### **ACKNOWLEDGEMENTS**

Undertaking this PhD has been a truly life-changing experience for me and it would not have been possible to do without the support and guidance that I received from many people. I would like to first say a very big thank you to my supervisor Prof. Soma Venugopal Rao for all the support and encouragement he gave me throughout the entire journey. Without his guidance and constant feedback this PhD would not have been achievable. Many thanks also to Dr Sai Santosh Kumar Raavi who mentored me on femtosecond transient absorption spectroscopy – a major work part of my doctoral degree work which would have been quite challenging otherwise due to lack of immediate seniors to rely on for the knowledge. I gratefully acknowledge the funding received towards my PhD from the Defense Research and Development Organization DRDO fellowship. Thanks to Prof. A.K. Chaudhary and Prof. Sunil Singh for their encouragement and valuable input as members of the Doctoral Committee. I am also grateful to the former and current director(s) of ACRHEM for granting various research opportunities along with auxiliary funding opportunities. I greatly appreciate the support received through the collaborative work undertaken with the IICT Hyderabad under the guidance of Prof. L. Giribabu and his group – for excellent support in the chemistry and synthesis of the novel optoelectronic molecules that were studied in this thesis. My thanks also go out to the Chinmoy Biswas, PhD IITH, for fruitful collaboration and valuable group work as a teammate to contribute to my thesis work. I am also very grateful to Prof. Anuj Vargeese and Prof. P.K. Panda from ACRHEM who have provided me with essential chemicals whenever deemed necessary. Special thanks to Prof. A. Samanta and his group for allowing me to use their laboratory instruments for various photophysical studies through valuable collaboration and feedback. On that note, the Center for Nanotechnology and Center for Instruments Laboratory, UoH, also deserves many thanks on my behalf, for absorption studies and liquid O<sub>2</sub> supply required for essential studies. This PhD study would not have been possible without the corporation and support extended by the ACRHEM offices by taking care of various administrative documentations and scholarship formalities. I find myself lucky to be bestowed with great friends/colleagues who have been constant pillars of support for me in the span of the entire 5 years and without whom I couldn't have steadied myself after several difficult moments experienced in-between. I would especially thank Ms Archana Kumari, PhD ACRHEM, who has been and will always be my unwavering

support system in life and without whom the PhD would be more challenging to achieve. Last but not the least, I am incredibly thankful to my friends – Shazia, Ritu, Navya and others from hostel, for all the amazing cheering up sessions and self-invited parties they threw to keep me cheerful and motivated.

Finally, a thousand thanks to my Parents – Narendu Bhattacharya (father) and Dr. Anindita Sharma (mother) for the unconditional love and support. The doctoral degree earned, equally belongs to them. And to The Almighty – Thank you God for keeping the faith and perseverance alive in me and to give me the strength to stand tall at the end of the road.

Somdatta Bhattacharya 15ACPA02

Cont	tents:	Page No:	
1. Intro	duction and Motivation	10 – 33	
1.1. Org	ganic dyes as sensors in explosive detection.	15	
1.2. Org	ganic dyes as Dye Sensitized Solar Cells.	16	
1.3. Org	ganic dyes as Photosensitizers.	17	
1.4. Org	ganic dyes as Optical Limiters.	18	
1.5. Re	Gerences.	25	
2. Theo	ry and Experimental Techniques	34 – 83	
2.1. The	eory		
2.1.	1. Nonlinear Optics.	34	
2.1.	2. Ultrafast Lasers and their characterization.	37	
2.1.	3. Transient Absorption Spectroscopy.	42	
2.1.	4. Z-scan technique.	47	
2.1.	5. Porphyrins and Phthalocyanines.	54	
2.2. Ins	trumentation and characterization		
2.2.	1. Z-scan setup.	56	
2.2.	2. fs-TAS setup.	58	
2.3. Op	tical Instruments.		
2.3.	1. LIBRA laser.	59	
2.3.	2. TOPAS C.	63	
2.3.	3. HELIOS.	65	
2.4. Da	ta Analysis Z-scan technique.	66	
2.5. TA	S data analysis.		
2.5.	Data Analysis using Surface Xplorer.	69	
2.5.	2. Data Analysis using Glotaran 1.5.1.	71	
2.6. Sai	nple Experiment.		
2.6.	1. The Z-scan Experiment.	74	
2.6.	2. Conclusions.	81	
2.6.	3. Sources of Error.	81	
2.7. Re	Gerences.	82	

3.	<b>Excited State Dynamics and NLO Properties of Carbazole</b>						
	<b>Substituted Zinc Phthalocyanines</b>	<b>84 – 107</b> 85 86 91					
	3.1. Introduction.						
	3.2. Experimental Details and Results.						
	3.2.1. Z-scan with MHz pulses.						
	3.2.2. Z-scan with kHz pulses.	92					
	3.2.3. fs-TAS with kHz pulses.	96					
	3.3. Conclusions.	99					
	3.4. References.	101					
4.	<b>Excited State Dynamics and Nonlinear Option</b>	cal Studi	es of a				
	Triphenylamine Imidazole Substituted	Novel	Zinc				
	Phthalocyanine	106 – 129					
	4.1. Introduction.	107 108					
	4.2. Experimental Details and Results.						
	4.2.1. Z-scan with MHz pulses.	110					
	4.2.2. Z-scan with kHz pulses.	111					
	4.2.3. fs-TAS with kHz pulses.	117					
	4.3. Conclusions.	123					
	4.4. References.	124					
5.	Femtosecond to Microsecond Photophysical S	tudies an	d NLO				
	Properties of Novel Imidazole Subs	tituted	Metal				
	Phthalocyanines	130	<b>- 152</b>				
	5.1. Introduction.	131					
	5.2. Experimental Details and Results.	133					
	5.2.1. Absorption and Emission studies.	133					
	5.2.2. Theoretical Studies.	138					
	5.2.3. Z-scan studies with kHz pulses.	139					
	5.2.4. fs-TAS studies.	141					
	5.2.5. ns-TAS Analysis.	145					
	5.3. Conclusions.	147					

5.4. References. 149

6.	Excited	State	<b>Dynamics</b>	of	Octa-alkox	y Substituted
	Porphyrins in the Presence of Nitroaromatic and Nitramine					
	Energe	153 – 175				
	6.1. Introd	154				
	<ul><li>6.2. Experimental Details and Results.</li><li>6.2.1. Absorption and Emission studies.</li></ul>					155
						156
	<ul><li>6.2.2. fs-TAS studies.</li><li>6.2.3. Porphyrins with Nitroaromatics.</li></ul>				157	
					164	
	<ul><li>6.2.4. Porphyrins with Nitro-amines.</li><li>6.3. Conclusions.</li><li>6.4. References.</li></ul>					166
						170
						171
<b>7.</b>	<b>Conclusion and Future Scope</b>					176 – 189
	<ul><li>7.1. Conclusions.</li><li>7.2. Future Scope in the experiments.</li></ul>			177		
				180		
	7.2.1.	fs-TAS UV	-mid IR wavelen	gth ran	ge.	180
	7.2.2.	Hyperspect	ral fs-TAS study.			182
	7.3. Future Scope with Phthalocyanines.		182			
	7.3.1.	Phthalocyar	nines as Supramo	lecular	complexes.	182
	7.3.2.	Phthalocyar	nines in Organic	LEDs (	OLEDs).	183
	7.3.3. Phthalocyanines in triplet-triplet annihilated up-con			nihilated up-conv	ersion. 184	
	7.4. References.				186	

# **Chapter 1**

## **Introduction and Motivation**

Organic molecules such as porphyrins (P), phthalocyanines (Pc) and their derivatives are synthetic dyes with unique molecular structure possessing huge potential in the world of photonics and photomedicine [1, 2, 3, 4, 5]. Porphyrin molecules contain four pyrrole rings linked by the methane carbon bridges. On the other hand, Pc molecules are composed of four indole units which are pyrrole rings linked by nitrogen atoms conjugated with benzene rings [6]. These molecules have conjugated aromatic structure with 18  $\pi$ delocalized electrons [7]. These electrons give rise to interesting optical and photophysical properties like very high absorption in visible to IR wavelength and long-lived excited state components which is ideal for photovoltaics [5] and biological applications [8]. For appropriate light intensity, the free electron cloud of a porphyrin or phthalocyanine can give rise to polarizability in electric field giving rise to nonlinear optical (NLO) effect [9]. These NLO properties find potential application in optical devices such as saturable absorbers, optical data storage, optical limiters, multiphoton filament formation, frequency mixing, and up-conversion, etc. [10, 11, 12, 13]. Porphyrins and phthalocyanines can exist as free bases or as metallo-complexes usually achieved by incorporating a metal at the center of their core structure in which case the central metal can accept or donate electron to the P or Pc moiety [14]. In photovoltaic cells, the dye molecules absorb solar light energy which in turn generates electronically excited states. The excited state can migrate to an interface where an electron transfer takes place, enabling the oxidized and reduced species (holes and electrons) to be able to migrate to the opposite sides of the cell, collected as electrical energy [5]. The first reported case of using organic dyes such as porphyrins and phthalocyanines for photovoltaics was in 1986 by C.W. Tang [15], who constructed an organic solar cell constituting a heterojunction bilayer. The bilayer was composed of Cuphthalocyanine along with a perylene derivative. They later came to be termed as DSSC or dye sensitized solar cells. Compared to commercial silicon based solar cells, DSSCs have low cost, are low in toxicity and easy to produce [16]. However, DSSC comes with some major challenges which makes it difficult to be manufactured commercially like – low solar cell efficiency and no long-term stability. These challenges can be dealt with a detailed

understanding of the carrier transfer and energy transfer mechanisms of the excited dynamics of the system. Recently hybrid perovskites have been able to show high performance in terms of efficiency ~23% (reported by the agency U.S. National Renewable Energy Laboratory (NREL) [15]. The porphyrin and phthalocyanine metallo-complexes can promote efficient singlet state to triplet state transitions with long lived triplet lifetimes making them good photosensitizers for medicinal purposes [17].

Metalloporphyrins and metallophthalocyanines are organic dyes that are naturally suitable for different types of medical imaging, therapy. As photosensitizers, numerous porphyrin-based photosensitizers have obtained clinical approval as well as entered clinical trials [18, 19, 20]. Many studies have reviewed these investigations extensively in the literature, the first one being Photofrin (1993) for treatment of bladder cancer [21]. The phthalocyanines are chemically more stable structures than the porphyrins and displays superior optical nonlinearity, structural stability along with longer reaction lifetimes upon excitation [22]. Phthalocyanines also favors the functionalization of various substituent moieties at their peripheral positions which helps to increase their solubility (especially in common organic solvents) over and above the minimization of aggregation making them more desirable for photomedicine as well as optoelectronic applications [23]. Novel phthalocyanines that have been developed in the recent past that various microbial pathogens with very low dark toxicity have shown good inactivation of [24]. The central atom linked to phthalocyanine enhances antimicrobial property by increasing the quantum yield and the triplet lifetime which helps in singlet oxygen generation that helps in destruction of pathogenic microbe [25, 26]. Studies have shown that conjugation of metal nanoparticle to a porphyrin or phthalocyanine moiety improves permeability and retention effect which also reduces the aggregation in biological tissues and aqueous media [27, 28]. The crucial properties that make porphyrins and phthalocyanines excellent photosensitizers for photodynamic therapy (PDT) are: (a) absorption peak in the 600-800 nm range, which is within the biological window that helps in forming significant yield of the reactive oxygen species when irradiated with light, (b) efficient and long lived triplet state and (c) high singlet oxygen quantum yield ( $\Phi_{\Delta} > 0.4$ ) [29]. To improve the performance of these molecules as photosensitizers, a detailed study of their excited state dynamics is essential. Combining PDT with multiphoton processes have been found to enhance the effective treatment by a significant scale [30]. The NLO process is intrinsic to the photosensitizer used and both porphyrins and phthalocyanines show excellent NLO properties making them ideal for multiphoton PDT applications [31, 32]. Thus, the ever-increasing scope and challenges with these molecules make them an interesting field of research in optics. However, processes like energy transfer, charge transfer or multiphoton absorption can be only observed in the realm of ultrafast optics.

The processes within the timescale window of 10<sup>-9</sup>s (ns) to 10<sup>-18</sup>s (as) are known as ultrafast processes. All chemical reaction dynamics occur within this timescale and are studied using time-resolved ultrafast spectroscopic methods. Since the understanding of the ultrafast regime in nature is imperative to mankind, to do so scientists came up with the idea of pulsed lasers around the year 1962 [33]. Pulsed lasers produce short outbursts of laser pulses within the time duration of ns – as which can be used to capture all phenomena occurring within that timescale window. These ultrafast phenomena are studied using femtochemistry – a technique introduced by Dr. Ahmed Zewail (Nobel laureate 1999) [34] which later came to be known more popularly as the pump-probe spectroscopy. Transient absorption spectroscopy (TAS) or pump-probe spectroscopy is a time-resolved spectroscopic technique under femtochemistry domain, where the molecule under study is excited by an ultrashort pump pulse and the excited state dynamics is monitored over time by another ultrashort probe pulse. It is a nonlinear light-matter interaction between the excited molecule and the probe pulse. By monitoring finite number of probe measurements at varied delay time, the time dependence of the excited molecular processes can be mapped [35]. The scope of time resolved spectroscopy is immense which encompasses the world of physical chemistry and biology [36]. It can be studied for solids, fluids (dense and liquids), gas phase, clusters, thin films or surfaces [37]. TAS is used to study the various types of photoinduced inter/intramolecular transitions such as energy transfer, charge transfer, formation of intermediate charge complexes, isomerization, bong breakage, etc. [5] In DSSCs (solar cells), long term stability is still a challenge which is caused by ion migration within the defect states of the semiconductor material [17]. TAS measurements play an important role in the investigation of ion migration and charge transfer mechanism of DSSCs to improve the solar cell performance. In photodynamic therapy PDT, TAS is primarily used to study the singlet to triplet intersystem crossing efficiency of a molecule and their triplet state lifetimes. Since, oxygen in its ground state stays in triplet state as <sup>3</sup>O<sub>2</sub>, the longer the photosensitizer's triplet lifetime, the greater number of singlet oxygen and free radicals are created [38]. These cytotoxic species (singlet oxygen and free radicals) in turn undergo reaction (Type I/II) with the target cells and destroy them [39]. Apart from

that transient absorption spectroscopy can be used to study other biological processes like photosynthetic processes, protein dynamics, charge transfer in DNA and antimicrobial therapy [40, 41, 42].

Since ultrafast pulses are capable of producing high-power light output compared to conventional CW (continuous wave) laser, the light-matter interaction goes from linear to non-linear regime where all material characteristics (like absorption, refraction, etc.) become intensity dependent [43]. This opens up a new field of study known as non-linear optics (NLO). There are several techniques to measure the NLO properties of a material viz. degenerate four wave mixing (DWFM), optical Kerr effect, two beam coupling and others [44]. One of the simplest among them is the Z-scan technique (proposed by M. Sheikh Bahae et al. in the year 1990) that allows simultaneous calculation of the nonlinear absorption (related to the imaginary part of third-order NLO susceptibility) and nonlinear refractive index (related to the real part of third-order NLO susceptibility) of the samples under investigation [45]. Through NLO studies one can witness multiphoton absorption processes which finds a number of applications in the area of photonics. Among porphyrins and phthalocyanines, two photon absorption process, being the most widely used NLO process, finds its application in two photon fluorescence spectroscopy and imaging, microscopy, three-dimensional optical data storage, optical limiting and many more [46, 47, 48]. Replacing two photon absorption process with higher-order nonlinear absorption processes (e.g. three-, four- or five-photon absorption) has been demonstrated to further improve spatial resolution and light penetration for applications in optical power limiting [49], fluorescence imaging [50, 51, 52], and fluorescence up-conversion applications [53]. Porphyrins and phthalocyanines are most widely known as potential nonlinear optical limiters [54]. Nonlinear optical limiters provide a wavelength-agile means of protection against pulsed lasers by limiting the transmitted output to safe levels. For efficient optical limiting, the molecule should have large nonlinearity, broadband spectral response, intrinsically fast response time, and ease of processing. Porphyrins and phthalocyanines are particularly attractive candidates for nonlinear optical limiting for all the above reasons in addition to their ability of changing NLO properties via suitable structural modifications [54].

Another very important application of porphyrins and phthalocyanines are as sensors. Porphyrins and phthalocyanines are conjugated fluorescent organic dyes that have been

reported to show significant fluorescent quenching in the presence of nitrated explosives (RDX, HMX, TNT, etc.) [55, 56, 57]. In fluorescence quenching, the fluorescence of a molecule (called fluorophore) is decreased (or quenched) in the presence of an explosive [58]. Fluorescence quenching can be qualitatively observed via fluorescence spectroscopy while quantitatively one can measure the quench through TCSPC (time-correlated single photon counting). Transient absorption spectroscopy (TAS) can also be used to study and detect high energy materials, HEMs or explosives which are categorized according to their molecular structure. For instance, RDX and HMX are nitroamines, TNT and NB are nitroaromatics, PETN and NG are nitroesters and so on. The performance of a HEM is hence hugely dependent on the molecular structure and its material characteristics – most importantly detonation sensitivity [59]. Transient absorption spectroscopic studies have shown that molecular excited states play a crucial role in studying the detonation sensitivity of energetic molecules upon shock application (in the form of heat, light or pressure) [60, 61]. In recent years, inordinate efforts have been dedicated to develop novel fluorescent materials like polymer sensors [62], optical chemosensors [63], conjugated polymers [64, 65], luminescent metal-organic frameworks [66], and nanomaterials [67] for explosive detection so as to achieve high selectivity, fast response time, as well as super-sensitivity. Fluorophore sensors like porphyrins and phthalocyanines prefer collisional or dynamic quenching that results from collision between the quencher and the fluorophore. There are multiple mechanisms that results in fluorescence quenching such as (i) resonance energy transfer (RET), (ii) photo-induced electron transfer (PET), (iii) intermolecular charge transfer, (iv) electron exchange, etc. [68]. These phenomena can be studied primarily using transient absorption spectroscopy with the help of other spectroscopic techniques like UV-vis absorption, fluorescence spectroscopy, electrochemical studies, DFT studies and others.

Keeping in mind the potential of organic compounds: Porphyrins and Phthalocyanines in the world of optoelectronics, explosive detection and sensing as well as photomedicines, this thesis focuses on the study of the NLO properties and excited state dynamics of various types of novel Phthalocyanine and Porphyrin derivatives for application in optoelectronics (solar cells and optical limiters), photodynamic therapy (PDT) and detection of high energy materials (nitro-explosives based on fluorescence quenching phenomenon). Here, we will have brief discussion on each of the aforementioned applications to understand the prospects of our study.

#### 1.1 Organic dyes as sensors in explosive detection:

Explosives detection plays a crucial role for humanitarian agencies and security providers along with law enforcement and armed forces operations. The target compounds used for explosives detection are varied, including

- nitroaromatics [e.g. trinitrotoluene (TNT), picric acid],
- nitramines (e.g. RDX),
- nitrate esters (e.g. PETN),
- nitroaliphatics (e.g., DMNB, nitromethane),
- organic peroxides (e.g., TATP and HMTD) and
- nitrate salts (e.g., ammonium nitrate).

Improvised explosive devices (IEDs) in current/previous warzones employ/employed traditional nitro-containing materials outstanding from previous conflicts and, therefore, the detection/demolition of such compounds is an important target for new detection systems being developed. Various detection techniques/methodologies have been developed over the last few year and deployed to varying extent such as (a) ion mobility spectrometers [69] (b) mm wave and X-ray backscatter imaging scanners [70, 71] (c) calorimetric kits [72] (d) Raman-based spectroscopies [73] and (e) fluorescence based detectors [74, 75]. Fluorescence-based detectors are mainly promising since they possess the potential to combine trace-level detection (via vapour-based sampling) in a compact, robust device form that is easy to use for non-technical persons. Changes in the luminescence (emission) of the sensing material is the basic principle behind fluorescencebased finding of nitro-containing explosive molecule vapours. The process includes favourable energetics for the transfer of an electron via photo-induced transfer from the sensing material to the analyte, the analyte vapour pressure (or concentration present in the ambient atmosphere) of the analyte and the binding strength amongst the sensing material. Porphyrins and Phthalocyanines are among the popular fluorophores that can be and have been used for selective sensing applications [76, 77]. Their emission can be quenched in presence of nitro-contained explosives via photoinduced charge transfer or resonance energy transfer process. Mostly, porphyrin-based sensors show high sensitivity and selectivity accompanied by good reproducibility. Whereas, porphyrins are also prone to slow reaction rates when a species is incorporated into the porphyrin ring with poor aqueous solubility are involved. For example, the porphyrin ring metal ion incorporation is around 109 times slower in comparison to the metal ion complex formation with noncyclic ligands. In order to overcome the shortcomings, several metal as well as non-metal porphyrin derivatives have been developed and reviewed over the years [78]. Phthalocyanines are an improved replacement to the porphyrins in terms of structural flexibility, chemical stability and improved selectivity [79]. In this thesis, we will discuss the potential sensor capabilities of metalloporphyrin derivatives for commonly used explosives.

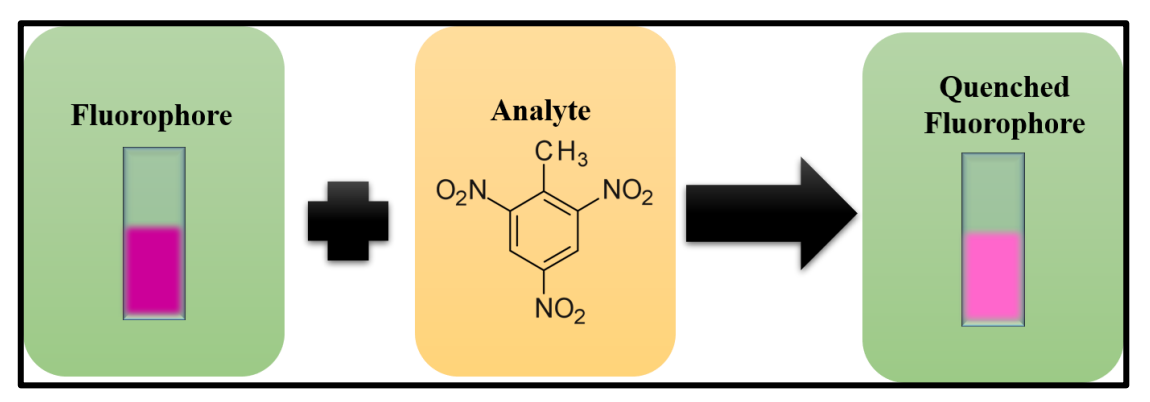


**Figure 1.1** Fluorescence quenching occurs in an organic fluorophore (e.g. Porphyrin) in presence of an analyte (e.g. explosives) which can be used in sensing devices for trace detection.

#### 1.2 Organic dyes as Dye Sensitized Solar Cells:

A technical-cum-economical credible alternative to the p-n junction photovoltaic devices are dye-sensitized solar cells (DSSCs). DSSCs are thin-film solar cells under extensive more than two decades of due to their simple preparation methodology, low cost, ease of production and low toxicity. DSSC consists of a working electrode that is soaked with a dye or sensitizer followed by sealing around the thin electrolyte layer of counter electrode (with the help of a hot melt tape for preventing electrolyte leakage). The extreme absorption of input incident light is achieved with the dye component of DSSC. For any material to qualify as a dye component suited for DSSC, must have the following photophysical, electrochemical properties:

- The absorption spectra should range from UV-NIR which makes up the biological window for living tissues.
- ii. The dye's periphery is preferred to be hydrophobic (this is to enhance the long-term stability of these cells).
- iii. The highest occupied molecular orbital (HOMO) should be situated away surface of the TiO<sub>2</sub> conduction band while and the lowest unoccupied molecular orbital (LUMO) should be positioned close to the TiO<sub>2</sub> surface.
- iv. HOMO level should lie below the level belonging to that of redox electrolytes.

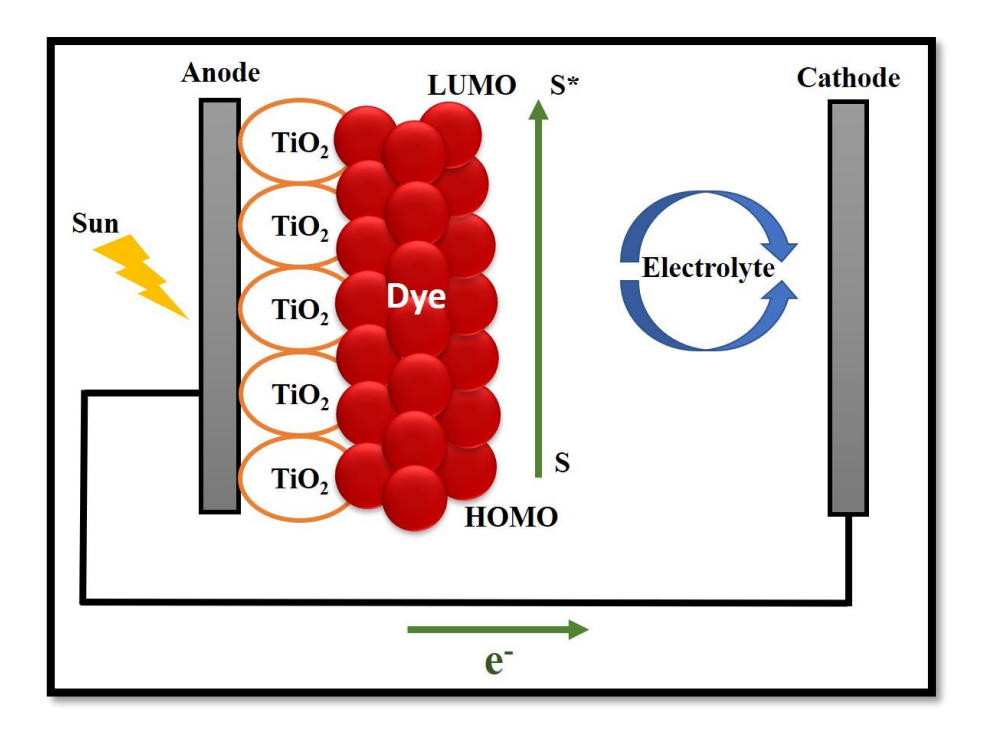


Figure 1.2 Working schematic of a dye sensitized solar cell (DSSC).

Porphyrins, phthalocyanines and their derivatives are organic dyes that have been long exploited for DSSC applications as they meet all the aforementioned criteria. Also, these molecules can accommodate more than 70 non-metallic and metallic ions in the cavity at their center and ligands at the periphery, giving the ability to tailor make the molecules suiting a particular application [80]. Recently Milan et al. [81] recently reported SnO<sub>2</sub> NPs being used as electron transport material in DSSCs, containing two peripherally substituted push-pull zinc phthalocyanines. Those phthalocyanines had (i) electron-donating diphenylamine substituents and (ii) carboxylic acid anchoring groups acting as light harvesters. While it was expected to enhance the DSSC performance, experimentally, the device efficiency was found <1%. They speculated that this might be due to (a) poor charge injection from the excited Zinc phthalocyanine to the conduction band of SnO<sub>2</sub> along with the low capability of Zinc phthalocyanine in contributing to stop the recombination at the FTO & electrolyte interface. The results indicate that several parameters to act in the solar energy converting devices' working mechanism and unexpected parameters may prove to be more serious than expected. In this chapter, we tried to investigate these crucial properties in Phthalocyanines and their derivates for optimal solar cell efficiency and compare with the most recent developments in the contemporary field.

#### 1.3 Organic dyes as Photosensitizers:

Cancer has affected the society in every corner of the world can be described as the uncontrolled cell division that can spread from cells to other parts of body leading to metastatic cancer. According to Indian Council of Medical Research (ICMR) 2020, India's cancer cases are likely to increase by 12% over the coming five years, with an estimate of 1.5 million people to get affected from the non-communicable disease (by 2025) [82]. Currently, few of the effective treatments against the dreadful disease are - surgery, chemotherapy, radiotherapy, immunotherapy, hormone therapy and others. The most practised method to treat localized tumours (that has not spread to other body parts yet) is surgery. However, since it is invasive, there is possibility of normal cells being affected in order to avoid recurrence. Another common technique is Chemotherapy where is treatment with drugs to destroy cancer cells. This could be used before surgery to shrink tumour or after surgery to remove the remaining tumour cells and to kill the metastatic tumour cells in other parts of the body [83]. This treatment is not only very costly, but also may lead to severe side effects if the normal healthy tissues are exposed to radiation [84]. Thus, the need of non-invasive that is affordable and accessible cancer treatment modalities started to be most sought of which the Photodynamic therapy or PDT gained importance. PDT involves the use of a light, photosensitizer (PS), and endogenous molecular oxygen to destroy microbes or cancer cells [85]. When irradiated with light, a PS undergoes a number of photochemical reactions leading to formation of singlet oxygen species that are highly reactive and responsible for cytotoxicity leading to cell death via apoptosis.

Porphyrins are the 1<sup>st</sup> generation PSs with the very first clinically approved PS being Photophrin [86]. Photofrin® (Porfimer sodium from Axcan Pharma, Inc.) was the first permitted PDT agent for the treatment of obstructive esophageal cancer in the year 1995 [87]. Later it has been used to treat bladder cancer, cervical cancer, lung cancer, etc [88, 89]. However, some of the major limitations of the molecule are

- lack of penetration depth (i.e. excitation wavelength ~630 nm),
- high dark toxicity,
- lack of solubility (in most common solvents) along their tendency to aggregate.

This made the PDT community to move on to 2<sup>nd</sup> generation PS. They include Chlorfins, Phthalocyanines, etc. that had a larger range of penetration depth i.e. from visible to IR

with minimal aggregation and low dark toxicity [90]. Some of the applications of PDT using 2<sup>nd</sup> gen PS are head and neck cancer [91], prostate cancer [92], breast cancer [93] to name a few. Currently, 3<sup>rd</sup> generation PS have been making quite a stir which include conjugated organic molecules, upconversion nanoparticles, QDs, etc. In this chapter we deal with optimizing the basic monomeric phthalocyanine derivative for PDT or multiphoton PDT applications.

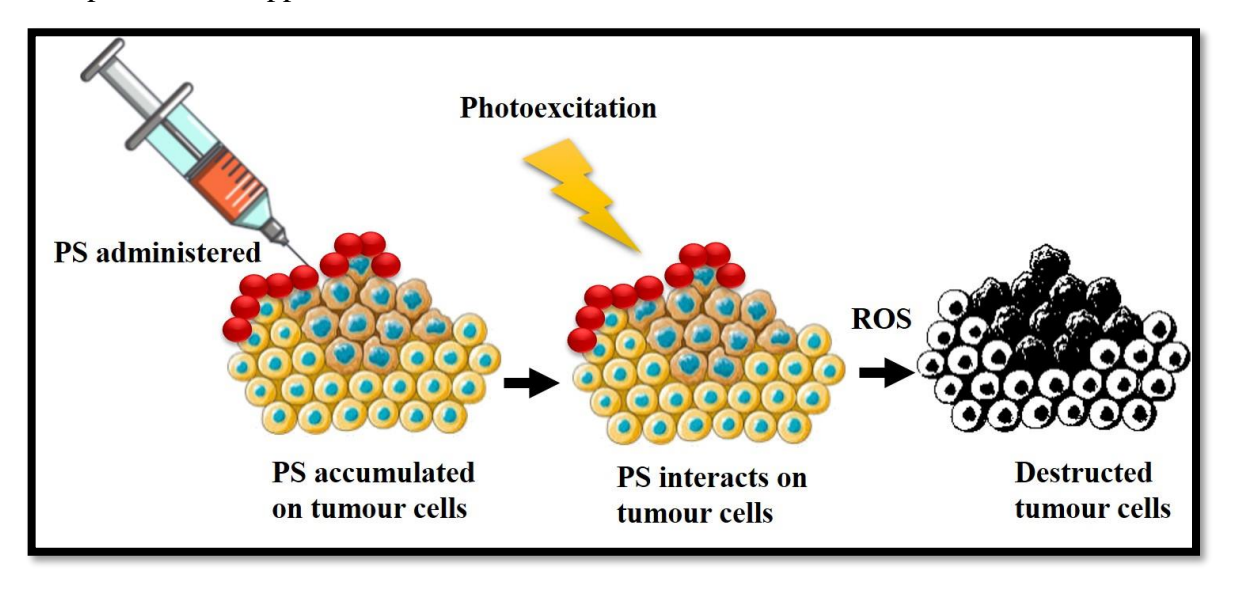


Figure 1.3 Schematic showing the mechanism of photodynamic therapy on targeted tumour cells.

## 1.4 Organic dyes as Optical Limiters:

High-power laser has been growing popularity in the current times due to the number of possible applications including the search for new nonlinear optical materials for optical limiters (passive) which are used in solid-state optical sensors to protect us from intense laser beams as well as to protect human eyes. An optical limiter can be defined as a material that exhibits linear transmittance at low powers, whereas become slightly opaque at higher intensities. Thus, its true purpose is to keep the irradiance, power, fluence or energy transmitted by an optical system to be below a specified upper limit, irrespective of the input magnitude. Other applications of an optical limiter besides defense of sensitive optical sensors (including human eye) and optical components from laser induced damage, can include (a) stabilization/restoration of signal levels in optical data transmission, logic systems and (b) laser power regulation. Optical limiting is a consequence of various intensity-dependent NLO processes such as (i) nonlinear refraction (NLR) (ii) nonlinear absorption (NLA) (iii) photo-refraction (PR) (iv) nonlinear scattering (NLS) and (v)

optically induced phase transitions. The least criteria acknowledged for any NLO material to be considered as an effective optical limiter are:

- (i) The presence of a high linear transmittance
- (ii) A low limiting threshold (the input corresponding to the breakpoint in the curve)
- (iii) A fast response time (faster than a few nanoseconds/picoseconds)
- (iv) A broad band nonlinear response (e.g., the entire visible and/or near-IR spectrum)
- (v) Low optical scattering [94].

Thus far, a wide variety of organic/inorganic NLO materials have been investigated to achieve this efficient optical limiting [95, 96]. Organic materials such as porphyrins and phthalocyanines have many advantages—over inorganic counterparts. From the aspect of technological applications of these organic materials, the current research focused is in five technical areas:

- Structural, multi-functional materials
- Energy & power materials
- Photonic & electronic materials
- Functional organic, hybrid materials
- Bio-derived/bio-inspired materials [97, 98].

A few advantages of organic nonlinear materials over non-inorganic are listed below [99]:

- Easy Process Engineering- these materials do not require electric poling or the large single crystal preparation methods, which makes their process engineering easier for development of inorganic optical materials.
- 2. **Cost minimalization** Ease of processing definitely leads to a lower fabrication cost.
- 3. **Superior Second and Third Order NLO Susceptibility** The organic materials exhibit excellent performance in frequency conversion (doubling and tripling of light frequency) passing through it making them comparable to inorganic counterparts.
- 4. **Low Dielectric Constant -** This technology does not require a poling voltage while maintaining its refractive index.
- 5. **High Electro-Optic Coefficient** making them apposite for electro-optic modulation (application for high speed devices).
- 6. **Transparency** The capacity of the frequency doubling material prevents the absorption of visible light, allowing a huge spectrum of input light frequencies to be doubled.

- **7. Tailorability** It is easy to engineer these materials by simply replacing the central metal ions and/or through easy peripheral substitution.
- 8. **Resistant to Laser Damage** The frequency doubling and tripling materials can sustain intense laser pulses (nanosecond pulses at few Hz repetition rate) without damage making them ideal for usage in various photonic applications.

Savelyev et al. [100] recently studied the threshold effect in optical limiters using J-type phthalocyanine dimers (Zn or Mg) with single-walled carbon nanotubes in water. Created conjugates showed application in not only protecting eyes and light-sensitivity elements, but for forming three-dimensional tissue-engineered structures too. In our studies, we focus on porphyrin and phthalocyanine derivatives to engineer and characterize them for application as optical limiters. Figure 1.4 shows a typical response of an optical limiter. They have applications in protection of expensive and complex sensors (human eyes being one of them).

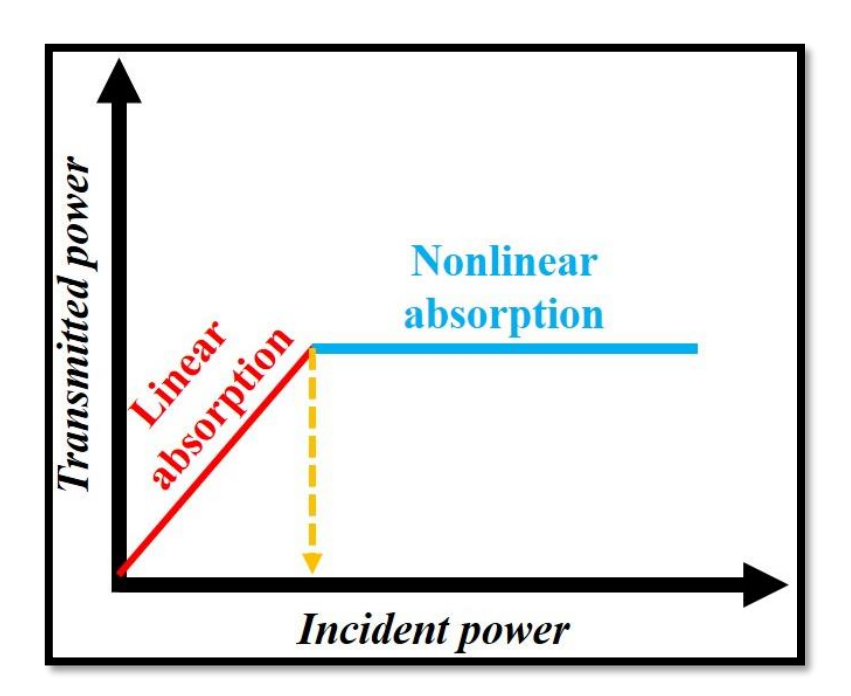


Figure 1.4: Typical Optical response of an optical limiter to incident power.

The thesis is organized further as follows:

**Chapter 2**: This chapter includes all the necessary instrumental setup details starting with (a) Instrumentation and characterization, followed by various tools and techniques involved (b) data analysis. The experimental results from the broadband NLO studies of a porphyrin and a phthalocyanine molecule using the Z-scan technique with femtosecond, MHz repetition rate pulsed laser (in the wavelength range of 700–950 nm) are presented. The

detailed comparative study reveals that the phthalocyanine molecule TPA-ZnPc shows superior NLO properties over the porphyrin ZnTPP. The study focuses on application of the above molecules as optical limiters.

**Chapter 3**: This chapter is dedicated to the excited state studies and NLO properties of two carbazole substituted zinc phthalocyanines namely CBZPC1 and CBZPC2. It is subdivided as: [3.1] Introduction [3.2] Experimental details [3.3] Data analysis [3.4] Results and discussion. Both molecules were studied in the solution form where CBZPC1 was dissolved in THF (tetrahydrofuran) and CBZPC2 in DCM (dichloromethane). The carbazole group results in broadened absorption (in the Soret band). The NLO studies were done using the Z-scan technique with fs pulses – 50 fs, 1 kHz repetition rate and 150 fs, 80 MHz repetition rate in the 600–900 nm wavelength. The molecules exhibited large two-photon absorption cross-sections ranging from 3.1 to 275 GM for kHz pulses and (8.1-48.9)×10<sup>4</sup> GM for MHz pulses. For excited state dynamics studies, transient absorption spectroscopic (TAS) studies were performed using 50 fs, 1 kHz pulses at Q-band excitations – 650 nm for CBZPC1 and 690 nm for CBZPC2. Excited state dynamics in the case of both the phthalocyanines demonstrated a likelihood of long-lived triplet states along with the singlet states due to intersystem crossing (CBZPC1 - >1.0 ns, CBZPC2 ~100-800 ps). A complete analysis showed the potential of both the molecules in optical limiting and photovoltaic or solar cell applications.

**Chapter 4**: This chapter focuses on the excited state dynamics and NLO properties of a triphenylamine imidazole substituted phthalocyanine, PBIPC in solution form. It is subdivided as: **[4.1]** Introduction **[4.2]** Experimental details **[4.3]** Data analysis **[4.4]** Results and discussion. The NLO studies were performed with 50 fs, 1 kHz pulses in the visible to near-IR (NIR) wavelength range. The obtained data was later compared with 150 fs, 80 MHz pulses in the visible range. PBIPC showed efficient multi-photon absorption with positive nonlinearity ranging from (0.4–54.0)×10<sup>-13</sup> esu. The two photon (2P) phenomena dominated visible wavelengths 600–800 nm, three-photon (3P) was predominant in the 1.0–1.2 μm spectral region while four-photon (4P) absorption dominated 1.3–1.5 μm wavelength regime. The NLO cross-sections obtained were large with 1570 – 7080 GM for 2PA, (2.5–3.0)×10<sup>-78</sup> cm<sup>6</sup>s<sup>2</sup> for 3PA and (3–62)×10<sup>-108</sup> cm<sup>8</sup>s<sup>3</sup> for 4PA processes. These studies can find applications in optical limiting, multi-photon spectroscopy and imaging as well as optical storage. The photophysical properties obtained

from femtosecond transient absorption (TAS) data along with global fitting revealed efficient intersystem crossing ( $\tau_{ISC}$  =5.9 ns) from excited singlet to triplet state due to presence of the imidazole group. Additionally, the high triplet quantum yield ( $\phi_T$ ) of 0.62, makes PBIPC desirable for application in photomedicines.

Chapter 5: This chapter is a comparative study of photophysical and femtosecond NLO properties of two novel imidazole substituted metal phthalocyanines – ImCuPc and ImZnPc. It is subdivided as: [5.1] Introduction [5.2] Experimental details [5.3] Data analysis [5.4] Results and discussion. These molecules are excited around Soret (B) band to perform TAS studies in femtosecond regime with 50 fs, 1 kHz laser and nanosecond regime with 8 ns, 20 Hz laser. Femtosecond TAS studies revealed efficient intersystem crossing from singlet to triplet state in both the molecules [ImCuPc = 8.5 ns and ImZnPc = 10.1 ns]. The nanosecond TAS studies showed long lived triplet states in them [ImCuPc = 1.4  $\mu$ s and ImZnPc = 1.2  $\mu$ s]. These properties prove ImCuPc and ImZnPc as potential photosensitizers for use in photodynamic therapy (PDT) with ImCuPc having higher quantum yield ( $\phi$ T ~0.51) than ImZnPc ( $\phi$ T ~0.27). The NLO studies, carried out at 800 nm with 50 fs, 1 kHz pulses, demonstrated large nonlinear absorption cross-sections – 381 GM (ImCuPc) and 994 GM (ImZnPc). This is useful for performing multi-photon PDT with higher selectivity and longer tissue penetration depth.

Chapter 6: In this chapter, three beta octa alkoxy porphyrins – H<sub>2</sub>EP (βoctaethylporphyrin), H<sub>2</sub>OMP  $(\beta$ -octamethoxyporphyrin) and H<sub>2</sub>OBuP  $(\beta$ octabutoxyporphyrin), labelled as samples 9, 10 and 11 respectively, were studied for explosive (HEM) sensing for (a) TNT (trinitrotoluene) (b) RDX (Research Department Explosive) and (c) HMX (High Melting Explosive). It is subdivided as: [6.1] Introduction [6.2] Experimental details [6.3] Data analysis [6.4] Results and discussion. Being excellent fluorophores, these porphyrins have been reported (by A. Rana et al. [55]) to show dynamic fluorescence quenching in the presence of nitroaromatic HEMs like TNT using fluorescence spectroscopy and thus can be used as an explosive detection tool [69]. Fluorescence quenching is a radiative process and hence the ease of sensing using fluorescence spectroscopy. In this paper, however, we do not limit ourselves to the measurement of radiative lifetimes and utilize the fs-TAS technique to understand even the non-radiative energy transfer processes that accompanies the quenching process. It was identified that TNT is more electron deficient than RDX and HMX. As a result, TNT with the electron-rich porphyrin samples 9–11 demonstrated quenching in fluorescence possibly via photoinduced electron transfer (PET). For HMX and RDX, energy transfer was dominant with no significant quenching of fluorescence in the porphyrins. However, due to energy transfer between porphyrin donor molecules and the explosive acceptor molecules, a significant quenching in decay rates was evident. This data can explain the reasons behind selective detection of porphyrins towards nitroaromatics like TNT and not nitramines such as RDX, HMX.

**Chapter 7**: This chapter summarizes all of the above work done in this thesis emphasizing on the end results and potential applications accompanying these studies on the novel molecules. There is a brief section explaining the current trends of ultrafast spectroscopic studies on newly developed organic molecules. Finally, the chapter ends with discussion on the future scope in the world of ultrafast spectroscopy and plausible ways to achieve it. The future of porphyrins and phthalocyanines are also discussed in this chapter.

#### 1.5 References:

- [1] M. Maaza, N. Mongwaketsi, M. Genene, G. Hailu, G. Garab, B. Sahraoui and D. Hamidi, "Nonlinear photonics properties of porphyrins nanocomposites and self-assembled porphyrins," *J. Porphy. Phth.*, vol. 16, p. 985–995, 2012.
- [2] Y. Zhang and J. Lovell, "Recent applications of phthalocyanines and naphthalocyanines for imaging and therapy," *Wiley Interdiscip. Rev. Nanomed. Nanobiotechnol.*, vol. 9(1), p. 1–24., 2017.
- [3] H. Huang, W. Song, J. Rieffel and J. Lovell, "Emerging applications of porphyrins in photomedicine," *Front. Phys.*, vol. 3 (23), p. 1–15, 2015.
- [4] P. Gregory, "Industrial applications of phthalocyanines," *J. Porphy. Phth.*, vol. 4, p. 432–437, 2000.
- [5] M. Waltera, A. Rudineb and C. C. Wamser, "Porphyrins and phthalocyanines in solar photovoltaic cells," *J. Porphy. Phth.*, vol. 14, p. 759–792., 2010.
- [6] C. Leznof and A. Lever, Phthalocyanines, Properties and Applications, New York: VCH Publishers, 1989...

- [7] G. d. l. Torre, G. Bottari, M. Sekita, A. Hausmann, D. Guldi and T. Torres, "A voyage into the synthesis and photophysics of homo- and heterobinuclear ensembles of phthalocyanines and porphyrins," *Chem. Soc. Rev.*, vol. 42, p. 8049–8105., 2013.
- [8] X.-F. Zhang, Y. Lin, W. Guo and J. Zhu, "Spectroscopic insights on imidazole substituted phthalocyanine photosensitizers: Fluorescence properties, triplet state and singlet oxygen generation," *Spectrochim. Acta A*, vol. 133, p. 752–758., 2014.
- [9] M. D. Garcia, "Nonlinear optical properties of phthalocyanines and related compounds," *J. Porphy. Phth.*, vol. 13, p. 652–667, 2010.
- [10] M. Calvete, G. Yang and M. Hanack, "Porphyrins and phthalocyanines as materials for optical limiting," *Synth. Met.*, vol. 141, p. 231–243., 2004.
- [11] T. Yamada, H. Hoshi, T. Manaka, K. Ishikawa, H. Takezoe and A. Fukuda, "Resonant enhancement of second-harmonic generation of electric quadrupole origin in phthalocyanine films," *Phys. Rev. B*, vol. 53, p. 13314–13317., 1996.
- [12] M. Hercher, W. Chu and D. Stocmian, "An experimental study of saturable absorbers for ruby lasers," *IEEE J. Quantum Electron.*, vol. 4, no. 11, p. 954–968., 1968.
- [13] S. Taniguchi, N. Suzuki, M. Masuda, S. Hisanaga, T. Iwatsubo, M. Goedert and M. Hasegawa, "Inhibition of heparin-induced tau filament formation by phenothiazines, polyphenols, and porphyrins," *J. Biol. Chem.*, vol. 280, no. 9, p. 7614–7623, 2005.
- [14] C. Fierro, A. Anderson and D. A. Scherson, "Electron donor-acceptor Properties of porphyrins, phthalocyanines, and related ring chelates: A molecular orbital approach," *J. Phys. Chem.*, vol. 92, p. 6902–6907., 1988.
- [15] C.W. Tang, "Two-layer organic photovoltaic cell," *Appl. Phys. Lett.*, vol. 48, p. 183–185., 1986.
- [16] K. Sharma, V. Sharma and S. S. Sharma, "Dye-sensitized solar cells: Fundamentals and current status," *Nanoscale Res. Lett.*, vol. 13, p. 381–427., 2018.
- [17] A. Jena, A. Kulkarni and T. Miyasaka, "Halide perovskite photovoltaics: background, status, and future prospects," *Chem. Rev.*, vol. 119, p. 3036–3103., 2019.
- [18] D. Dolmans, D. Fukumura and R. Jain, "Photodynamic therapy for cancer," *Nat. Rev. Cancer.*, vol. 3, no. 5, p. 380–387., 2003.

- [19] N. Brussel, "Photodynamic therapy of subfoveal choroidal neovascularization in age-related macular degeneration with verteporfin: two-year results of 2 randomized clinical trials-tap report 2," *Arch. Ophthalmol.*, vol. 119, no. 2, p. 198–207, 2001.
- [20] M. Ochsner., "Photophysical and photobiological processes in the photodynamic therapy of tumours," *J. Photochem. Photobiol. B.*, vol. 39, p. 1–18, 1997.
- [21] T. Dougherty, C. Gomer, B. Henderson, G. Jori, D. Kessel, M. Korbelik, J. Moan and Q. Peng, "Photodynamic therapy," *Natl. Cancer Inst.*, vol. 90, p. 889–905, 1998.
- [22] R.-M. Ion, "Phthalocyanines and some current applications," in *Intech Open*, (DOI:10.5772/intechopen.68654), 2017.
- [23] S. Bhattacharya, C. Biswas, S. Raavi, J. Krishna, D. Koteshwar, L. Giribabu and S. V. Rao, "Optoelectronic, femtosecond nonlinear optical properties and excited state dynamics of a triphenyl imidazole induced phthalocyanine derivative," *RSc Adv.*, vol. 9, p. 36726–36741, 2019.
- [24] N. Rapulenyane, "Photophysicochemical and photodynamic antimicrobial chemotherapeutic studies of novel phthalocyanines conjugated to silver nanoparticles," *M.S. thesis*, pp. 1-134, Rhodes University, 2013.
- [25] C. Fabris, M. Soncin and E. M. e. al., "A novel tetracationic phthalocyanine as a potential skin phototherapeutic agent," *Experimental Dermatology*, vol. 14, p. 675–683, 2005.
- [26] R. Ruiz-González, M. Agut, E. Reddi and S. Nonell, "A comparative study on two cationic porphycenes: Photophysical and antimicrobial photoinactivation evaluation," *Int. J. Mol.*, vol. 16, p. 27072–27086, 2015.
- [27] N. Tam, P. McVeigh, T. MacDonald, A. Farhadi, B. Wilson and G. Zheng, "Porphyrin–lipid stabilized gold nanoparticles for surface enhanced Raman scattering based imaging," *Bioconjug. Chem.*, vol. 23, p. 1726–1730., 2012.
- [28] I. Zafar, M. Arfan, R. Nasir and A. Sheikh., "Aluminum phthalocyanine derivatives: Potential in antimicrobial PDT and photodiagnosis," *Austin Biomolecules: Open Access*, vol. 1(2), pp. 1-7, 2016.
- [29] S. Nyamu, L. Ombaka, E. Masika and M. Nganga, "Antimicrobial Photodynamic Activity of Phthalocyanine Derivatives," *Adv. Chem.*, vol. 2018, ID 2598062, 2018. https://doi.org/10.1155/2018/2598062

- [30] K. Ogawa and Y. Kobuke, "Recent Advances in Two-Photon Photodynamic Therapy," *Anti-Cancer Agents in Medicinal Chemistry*, vol. 8, no. 3, p. 269–279., 2008.
- [31] F. Bolze, S. Jenni, A. Sour and V. Heitz, "Molecular photosensitisers for two-photon photodynamic therapy," *Chem Commun.*, vol. 53, p. 12857–12877, 2017.
- [32] C.M.-Jimenez, M. Henry, D. Aggad, L. Raehm, X. Cattoën, M. Man, C. Charnay, S. Alpugan and V. A. e. al., "Porphyrin- or phthalocyanine-bridged silsesquioxane nanoparticles for two-photon photodynamic therapy or photoacoustic imaging," *Nanoscale*, vol. 9, pp. 16622-16626, 2017.
- [33] Photonics Media (www.photonics.com).
- [34] A. Zewail, "Femtochemistry," J. Phys. Chem., vol. 97, no. 48, pp. 12427-12446, 1993.
- [35] J. C. Gonzalez, G. Gracini and G. Lanzani, "Pump-probe spectroscopy in organic semiconductors: Monitoring fundamental processes of relevance in optoelectronics," *Adv. Mat.*, vol. 23, p. 5468–5485, 2011.
- [36] "Introduction to time-resolved spectroscopy." (http://web.vu.lt/ff/m.vengris/images/TR\_spectroscopy02.pdf).
- [37] A. Zewail., "Femtochemistry: Recent progress in studies of dynamics and control of reactions and their transition states," *J. Phys. Chem.*, vol. 100, p. 12701–12724 1996.
- [38] M. Jarvi, M. Patterson and B. Wilson, "Insights into photodynamic therapy dosimetry: Simultaneous singlet oxygen luminescence and photosensitizer photobleaching measurements," *Biophys. J.*, vol. 102, p. 661–671, 2012.
- [39] L. Benov, "Photodynamic therapy: current status and future directions," *Med. Princ. Pract.*, vol. 24, p. 14–28, 2015.
- [40] J. Kennis, D. Larsen, K. Ohta, M. Facciotti, R. Glaeser and G. Fleming, "Ultrafast protein dynamics of bacteriorhodopsin probed by photon echo and transient absorption spectroscopy," *J. Phys. Chem. B*, vol. 106, no. 23, p. 6067–6080, 2002.
- [41] M. Fujitsuka and T. Majima, "Charge transfer dynamics in DNA revealed by time-resolved spectroscopy," *Chem. Sci.*, vol. 8, pp. 1752-1762, 2017.
- [42] U. Chilakamarthi and L. Giribabu, "Photodynamic therapy: past, present and future," *The Chem. Rec.*, vol. 17, no. 8, pp. 775-802, 2017.

- [43] R. Boyd, "Nonlinear optics, 3<sup>rd</sup> Ed.," in *Ch. 1*, Academic Press, 2008.
- [44] S. Pramodini, "Third order optical nonlinearity and optical power limiting of organic materials under CW laser illumination," *Doctoral Thesis*, Submitted to Manipal University, India, 2015.
- [45] M. Sheik-Bahae, A. Said, T.-H. Wei, D. J. Hagan and E. W. V. Stryland., "Sensitive measurement of optical nonlinearities using a single beam," *IEEE J. Quant. Electron.*, vol. 26, pp. 760-769, 1990.
- [46] F. Helmchen, *In Vivo Optical Imaging of Brain Function*, 2<sup>nd</sup> E., CRC Press/Taylor & Francis, 2009.
- [47] Q. Li, C. Liu, Z. Liu and Q. Gong, "Broadband optical limiting and two-photon absorption properties of colloidal GaAs nanocrystals," *Opt. Express*, vol. 13, no. 6, pp. 1833-1838, 2005.
- [48] S. Huang, A. Heika and W. Webb, "Two-photon fluorescence spectroscopy and microscopy of NAD(P)H and flavoprotein," *Biophys. J.*, vol. 82(5), pp. 2811-25, 2002.
- [49] G. S. He, J. D. Bhawalkar, P. N. Prasad and B. A. Reinhardt, "Three-photon-absorption-induced fluorescence and optical limiting effects in an organic compound," *Opt. Lett.*, vol. 20, p. 1524–1526, 1995.
- [50] M. Gu, "Resolution in three-photon fluorescence scanning microscopy," *Opt. Lett.*, vol. 21, p. 988–990, 1996.
- [51] I. Gryczynski, H. Malak and J. Lakowicz, "Three-photon excitation of p-quaterphenyl with a mode-locked femtosecond Ti:sapphire laser," *J. Fluoresc.*, vol. 6, pp. 139-145, 1996.
- [52] F. Hernández, K. Belfield, I. Cohanoschi, M. Balu and K. Schafer, "Three- and four-photon absorption of a multiphoton absorbing fluorescent probe," *Appl. Opt.*, vol. 43, pp. 5394-5398, 2004.
- [53] D. Correa, L. D. Boni, D. Balogh and C. Mendonca, "Perylene derivatives with large two-photon-absorption cross-sections for application in optical limiting and upconversion lasing," *Adv. Mater.*, vol. 17, no. 15, p. 1890–1893, 2005.
- [54] M. Calvete, G. Y. Yang and M. Hanack, "Porphyrins and phthalocyanines as materials for optical limiting," *Synth. Met.*, vol. 141, p. 231–243, 2004.

- [55] A. Rana, S. Sahoo and P. Panda, "β-Octaalkoxyporphyrins: Versatile fluorometric sensors towards nitrated explosives," *J. Porphy. Phth.*, vol. 23, p. 1–9, 2019.
- [56] A. Gupta, M. Kim and J. Park, "Efficient fluorescence quenching of tert-butyl substituted phthalocyanines with picric acid," *J. Korean Soc. Dye. and Finish.*, vol. 26, p. 277–282, 2014.
- [57] S. Kasthuri, P. Gawas, S. Maji, N. Veeraiah and N. Venkatramaiah, "Selective detection of trinitrophenol by amphiphilic dimethylaminopyridine-appended Zn(II)phthalocyanines at the near-Infrared region," *ACS Omega*, vol. 4, p. 6218–6228, 2019.
- [58] S. J. Toal and W. C. Trogler, "Polymer sensors for nitroaromatic explosives detection," *J. Mater. Chem.*, vol. 16, pp. 2871-2883, 2006.
- [59] W. Zhang, Y. Tang, A. Shi, L. Bao, Y. Shen, R. Shen and Y. Ye, "Recent developments in spectroscopic techniques for the detection of explosives," *Materials*, vol. 11, p. 1364 1388, 2018.
- [60] C. Rajchenbach, G. Jonusauskas and C. Rulliere, "Sub-picosecond time resolved spectroscopy of energetic materials: The nitromethane and nitro-stilbenes," *J. de Phys. IV*, vol. 5, p. 365–378, 1995.
- [61] S. D. McGrane, N. C. Dang, V. H. Whitley, C. A. Bolme and D. S. Moore, "Transient absorption spectroscopy of laser shocked explosives," *International Detonation Symposium 2010*, Idaho USA, 2010.
- [62] I. A. Buryakov, T. I. Buryakov and V. T. Matsaev, "Optical chemical sensors for the detection of explosives and associated substances," *J. Anal. Chem.*, vol. 69, p. 616—631, 2014.
- [63] S. W. Thomas, G. D. Joly and T. M. Swager, "Chemical Sensors Based on Amplifying Fluorescent Conjugated Polymers," *Chem. Rev.*, vol. 107, p. 1339 -1386, 2007.
- [64] A. Alvarez, J. Costa-Fernández, R. Pereiro, A. Sanz-Medel and A. Salinas-Castillo, "Fluorescent conjugated polymers for chemical and biochemical sensing," *Trends Anal. Chem.*, vol. 30, p. 1513 - 1525, 2011.
- [65] L. Martelo, T. d. Neves, L. M. J. Figueiredo, A. Fedorov, A. Charas, M.N.B-Santos and H. Burrows, "Towards the development of a low-cost device for the detection

- of explosives vapors by fluorescence quenching of conjugated polymers in solid matrices," *Sensors*, vol. 17, p. 2532–2545, 2017.
- [66] Z. Hu, B. J. Deibert and J. Li, "Luminescent metal-organic frameworks for chemical sensing and explosive detection," *Chem. Soc. Rev.*, vol. 43, p. 5815-5840, 2014.
- [67] Y. Ma, S. Wang and L. Wang, "Nanomaterials for luminescence detection of nitroaromatic explosives," *Trends Anal. Chem.*, vol. 65, p. 13-21, 2015.
- [68] J. Lakowicz, "Principles of Fluorescence Spectroscopy," 3rd ed., in Ch 8, Boston, MA, Springer 2008, p. 277–330.
- [69] R. Ewing, D. Atkinson, G. Eiceman and G. Ewing, "A critical review of ion mobility spectrometry for the detection of explosives and explosive related compounds," *Talanta*, vol. 54, p. 515–529, 2001.
- [70] D. M. Sheen, D. L. McMakin and T. E. Hall, "Three-dimensional millimeter-wave imaging for concealed weapon detection," *IEEE Trans. Microwave Theory Tech.*, vol. 49, p. 1581–1592, 2001.
- [71] G. Harding, "X-ray scatter tomography for explosives detection," *Rad. Phys. Chem.*, vol. 71, p. 869–881, 2004.
- [72] M. E. Germain and M. J. Knapp, "Optical explosives detection: from color changes to fluorescence turn-on," *Chem. Soc. Rev.*, vol. 38, pp. 2543-55, 2009.
- [73] D. S. Moore and R. J. Scharff, "Portable Raman explosives detection," *Anal. Bioanal. Chem.*, vol. 393, p. 1571–1578, 2008.
- [74] M. Fisher, M. I. Grone and J. Sikes, "Implementation of serial amplifying fluorescent polymer arrays for enhanced chemical vapor sensing of landmines," in *Detection and Remediation Technologies for Mines and Minelike Targets VIII* (*Proc. SPIE*), 2003, vol. 5089, pp. 991–1000.
- [75] T. Caron, M. Guillemot, P. Montmeat, F. Veignal, F. Perraut, P. Prene and F. Serein-Spirau, "Ultra trace detection of explosives in air: Development of a portable fluorescent detector," *Talanta*, vol. 81, p. 543–548, 2010.
- [76] P. E. Shaw and P. L. Burn, "Real-time fluorescence quenching-based detection of nitro-containing explosive vapours: what are the key processes?," *Phys. Chem. Chem. Phys.*, vol. 19, p. 29714, 2017.

- [77] X. Sun, Y. Wang and Y. Lei, "Fluorescence based explosive detection: from mechanisms to sensory materials," *Chem. Soc. Rev.*, vol. 44, p. 8019, 2015.
- [78] L. Wang, H. Li, J. Deng and D. Cao, "Recent Advances in Porphyrin-Derived Sensors," *Current Organic Chemistry*, vol. 17, pp. 3078-3091, 2013.
- [79] S. Rao, A. Thilakan, A. Thomas and R. Philip, "Nonlinear Absorption and Excited State Dynamics of Porphyrin and Phthalocyanine in the Presence of Explosive Molecules," *Chem. Phys. Lett.*, vol. 641, 2015.
- [80] S. Bhattacharya, C. Biswas, S. Raavi, J. Krishna, N. Krishna, L. Giribabu and S. V. Rao, "Synthesis, optical, electrochemical, DFT studies, NLO properties, and ultrafast excited state dynamics of carbazole-Induced phthalocyanine derivatives," *J. Phys. Chem. C.*, vol. 123, pp. 1118-33, 2019.
- [81] R. Milan, G. Selopal, M. Cavazzini, S. Orlandi, R. Boaretto, S. Caramori, I. Concina and G. Pozzi, "Zinc phthalocyanines as light harvesters for SnO2-based solar cells: a case study," *Scientific Reports*, vol. 10, p. 1176, 2020.
- [82] "12% rise in India's cancer burden predicted," *The Pharma Letter*, pp. https://www.thepharmaletter.com/article/12-rise-in-india-s-cancer-burden-predicted, 24 August 2020.
- [83] P. King and M. Perry, "Hepatotoxicity of chemotherapy," *The Oncologist*, vol. 6, p. 162–176., 2001.
- [84] T. Lawrence, R. Haken and A. Giaccia, Principles of Radiation Oncology, In: DeVita VT Cancer: Principles and Practice of Oncology, 8<sup>th</sup> ed., Philadelphia: Lippincott Williams and Wilkins, 2008.
- [85] M. Olivo, R. Bhuvaneswari, S. Lucky, N. Dendukuri and P. Thon, *Pharmaceuticals*, vol. 3, pp. 1507-1529, 2010.
- [86] C. G. T.J. Dougherty, B. Henderson, D. K. G. Jori, M. Korbelik, J. Moan and Q. Peng, "Photodynamic Therapy," J. Natl. Cancer Inst., vol. 90, no. 12, pp. 889-905, 1998.
- [87] T. Reynolds, "Photodynamic therapy expands its horizons.," *J. Natl Cancer Inst.*, vol. 89, p. 112–4., 1997.
- [88] R. Allison and C. Sibata, "Oncologic photodynamic therapy photosensitizers: a clinical review," *Photodiag. Photodyn. Ther.*, vol. 7, p. 61–75, 2010.

- [89] J. Breskey, S. Lacey, B. Vesper, W. Paradise, J. Radosevich and M. Colvard, "Photodynamic therapy: occupational hazards and preventative recommendations for clinical administration by healthcare providers.," *Photomed. Laser Surg.*, vol. 31, p. 398–407, 2013.
- [90] R. Baskaran, J. Lee and S.-G. Yang, "Clinical development of photodynamic agents and therapeutic applications," *Biomater. Res.*, vol. 22, p. 25, 2018.
- [91] P. Lou, H. Jager, L. Jones, T. Theodossy, S. Bown and C. Hopper, "Interstitial photodynamic therapy as salvage treatment for recurrent head and neck cancer," *Br. J Cancer.*, vol. 91, p. 441–446, 2004.
- [92] A. Azzouzi, S. Lebdai, F. Benzaghou and C. Stief, "Vascular-targeted photodynamic therapy with TOOKAD(R) soluble in localized prostate cancer: standardization of the procedure.," *World J. Urol.*, vol. 33, p. 937–944, 2015.
- [93] S. Bown, A. Rogowska, D. Whitelaw, W. Lees, L. Lovat, P. Ripley and e. al, "Photodynamic therapy for cancer of the pancreas.," *Gut.*, vol. 50, p. 549–557, 2002.
- [94] D. Oluwole, A. Yagodin, J. Britton, A. Martynov, Y. Gorbunova, A. Tsivadze and T. Nyokong, "Optical limiters with improved performance based on nanoconjugates of thiol substituted phthalocyanine with CdSe quantum dots and Ag nanoparticle," *Dalton Trans.*, vol. 46, pp. 16190-16198, 2017.
- [95] J. WAng and W. J. Blau, "Inorganic and hybrid nanostructures for optical limiting," J. Opt. A Pure and Applied Optics, vol. 11, no. 2, 2009.
- [96] Y.-P. Sun and J. Riggs, "Organic and inorganic optical limiting materials. From fullerenes to nanoparticles," *Int. Rev. Phys. Chem.*, vol. 18, no. 1, pp. 43-90, 2010.
- [97] A. Mahmood, J.-Y. Hu, B. Xiao, A. Tang, X. Wang and E. Zhou, "Recent progress in porphyrin-based materials for organic solar cells.," *J. Mater. Chem. A*, vol. 6, pp. 16769-16797, 2018.
- [98] D. Dini, M. Barthel and M. Hanack, "Phthalocyanines as Active Materials for Optical Limiting," *Eur. J. Org. Chem.*, vol. 20, pp. 3759-3769, 2001.
- [99] S. Aithal, P. S. Aithal and G. K. Bhat, "Characteristics of ideal optical limiter and realization scenarios using nonlinear organic materials," *International Journal of Advanced Trends in Engineering and Technology*, vol. 1, no. 1, pp. 73-84, 2017.

[100] M. Savelyev, A. Gerasimenko, A. Kuksin, V. Podgaetsky, A. Tolbin, P. Vasilevsky and S. Tereschenko, "Threshold effect in optical limiters based on conjugates J-type phthalocyanine dimers Zn and Mg with single-walled carbon nanotubes," in *Proc. SPIE 10684, Nonlinear Optics and its Applications*, 2018.

# **Chapter 2**

# **Theory and Experimental Techniques**

The chapter discusses the details of experimental setups of femtosecond (fs) transient absorption spectroscopy (TAS) setup as well as the Z-scan technique. The chapter also includes the theoretical and experimental details of photophysical and nonlinear optical properties accompanying the organic chromophores – Porphyrins, Phthalocyanines and their derivatives that are key to the experiments conducted in following chapters. Starting with the Ti:sapphire fs lasers, the parametric amplifier (TOPAS C) and femtosecond TAS (HELIOS) setups are described in detail. This chapter also provides a detailed discussion on all the relevant optical instruments used in the TAS and Z-scan experiments.

#### 2.1 Theory:

#### 2.1.1 Nonlinear Optics:

Nonlinear optics (NLO) encompasses the phenomena that occur in a material system in which the applied optical field depends on the optical field strength in a nonlinear manner. Typically, only laser light is sufficiently intense to modify the optical properties of a material system. Basically, the two stages of a typical NLO process involve – nonlinear response of the medium induced by a coherent intense beam of light followed by the influence of the medium to affect the optical radiation in a nonlinear way [1]. An induced polarization, P, as a result of the interaction with electric field E, can be written as:

$$P = \varepsilon_0 \chi E + \varepsilon_0 \chi^{(2)} E.E + \varepsilon_0 \chi^{(3)} E.E.E + \dots$$
 (2.1)

Here,  $\chi^n$  is the  $n^{th}$  order susceptibility of the NLO material. It is to be noted that, to estimate orders of magnitude of the nonlinear susceptibilities, we consider nonlinearity of electronic origin. The NLO effect gives rise to a lot of phenomena like Kerr effect, frequency mixing, multiphoton absorption, etc. Let us discuss few of the relevant phenomena below:

#### 2.1.1.a. Optical Kerr Effect:

The optical Kerr effect is also known as the AC Kerr effect where the light itself induces the electric field, resulting in a variation in refractive index which is proportional to the local light irradiance as given below mathematically:

$$\Delta \phi = \frac{2\pi}{\lambda} \Delta n \ [2]$$

This variation in the refractive index is the basis for Kerr-lens mode locking and can also lead to phenomena like **self-focusing**, **self-phase modulation** (**SPM**) and **modulational instability**. This effect can be significantly observed for very intense beams (e.g. from lasers).

- i. **Self-focusing/de-focusing:** A gaussian beam profile with a positive  $\chi^{(3)}$  shows an effectively increased RI (refractive index) on the inner area due to the higher optical intensities along the beam axis when compared to the spatial intensity distribution in the winds (see figure 2.1). This makes the modified RI distribution to behave like a focusing lens which is termed as self-focusing or thermal lensing [3, 4]. In case of a ve  $\chi^{(3)}$  nonlinearity, an opposite behavior is observed that is called self-defocusing, and the Kerr lens has a reduced RI along the beam axis.
- ii. **Self-phase modulation:** A nonlinear phase delay is induced from intense light passing through a medium which has the same temporal shape as the optical intensity (see figure 2.1). Here, the Kerr effect results in a time-dependent phase shift from the time-dependent input pulse intensity that can induce chirp in an initially unchirped optical pulse (a temporally varying instantaneous frequency) [5]. Mathematically, it is represented as

$$\Delta n = n_2 I$$

iii. **Cross-phase modulation:** Similar to self-phase modulation, here the change in the optical phase is a result of the interaction between two different beams in a nonlinear medium. Mathematically it is represented as,

$$\Delta n^{(2)} = 2n_2 I^{(1)}$$

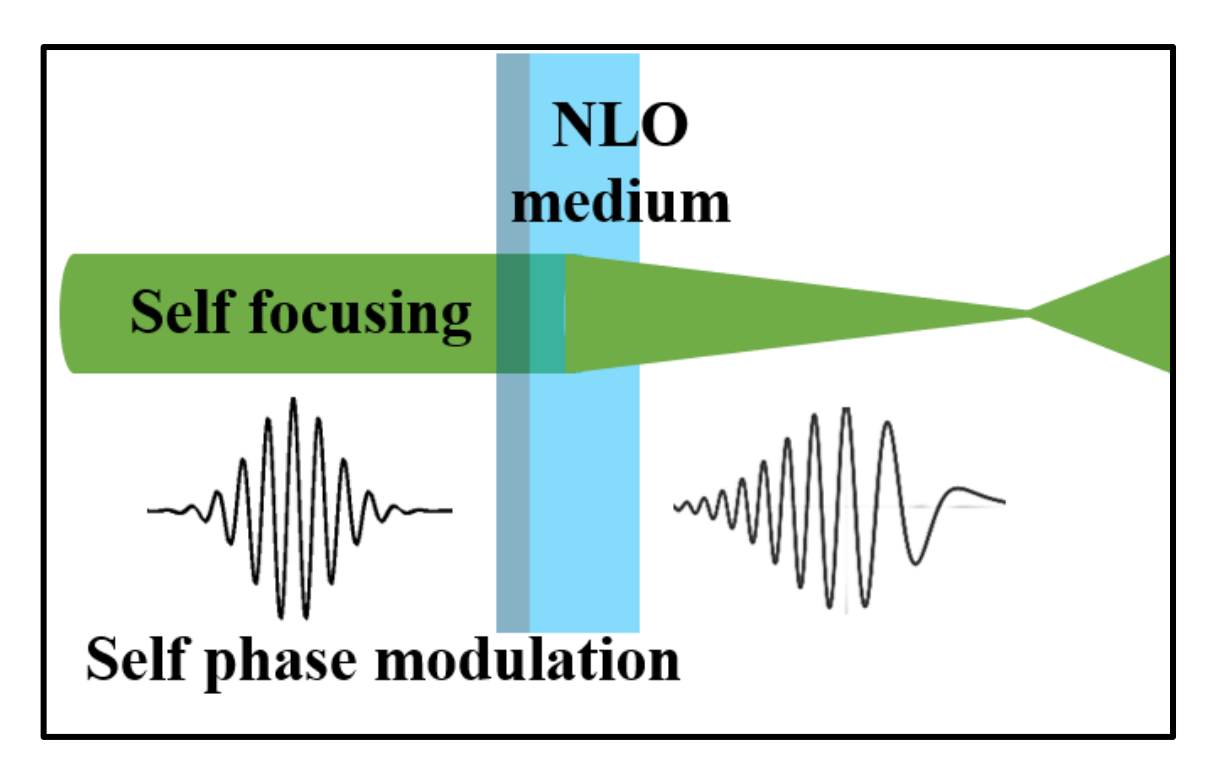


Fig 2.1 Nonlinear Optical Kerr Effect denoting self-focusing and self-phase modulation (SPM) phenomena.

#### 2.1.1.b. Frequency Mixing [6]:

For a nonlinear medium, we can write the wave equation as:

$$\nabla^2 \mathbf{E} - \frac{1}{C^2} \frac{\partial^2 \mathbf{E}}{\partial t^2} = \mu_0 \frac{\partial^2 \mathbf{P}_{NL}}{\partial t^2}$$
(2.2)

In general, an *n*-th order nonlinearity will lead to (n + 1)-wave mixing. In this thesis, we are focused on second and third order nonlinearity (i.e.  $\chi^{(2)}$  and  $\chi^{(3)}$ ). For  $2^{nd}$  order phenomena or three wave mixing, the polarization  $P_{NL}$  takes the form:  $P_{NL} = \epsilon_0 \chi^{(2)} \mathbf{E}^2(t)$ .

For, 
$$E(t) = \frac{1}{2}E_1e^{-i\omega lt} + \frac{1}{2}E_2e^{-i\omega 2t} + c.c.$$
 (2.3)

Thus,

$$\mathrm{P_{NL}} = \frac{\varepsilon_0}{4} x^{(2)} \left[ E_1^2 e^{-i^2 \omega_1 t} + E_2^2 e^{-i^2 \omega_2 t} + 2 E_1 E_2 e^{-i(\omega_1 + \omega_2) t} + 2 E_1 E_2 i^{i(\omega_1 - \omega_2) t} + 1 + c. \, c \right]$$

Here, the frequency components obtained are  $2\omega_1$ ,  $2\omega_2$ ,  $\omega_1 + \omega_2$ ,  $\omega_1 - \omega_2$ , and 0 which are known as: second-harmonic generation (SHG), sum-frequency generation (SFG), difference-frequency generation (DFG) and optical rectification (OR), respectively as depicted in figure 2.2(a).

All these processes, in which the quantum state of the NLO material remains unchanged after optical field interactions, can be categorized as parametric processes and are instantaneous in nature. Phase matching is a critical condition in parametric process given by the relation:  $\mathbf{k}_3 = \mathbf{k}_2 + \mathbf{k}_1$  where  $\mathbf{k}_i$  is the wave vector for respective field components [7]. A direct application of the optical parametric process is the optical parametric oscillator OPO [8], that converts an input laser wave (called as "pump") with frequency  $\omega_p$  into two output waves at a lower frequency [termed as signal ( $\omega_s$ ) and idler ( $\omega_i$ )] by means of second-order NLO interaction:  $\omega_p = \omega_s + \omega_i$  [see figure 2.2 (b)]. An OPO, placed inside a cavity, is known as an Optical Parametric Amplifier (OPA).

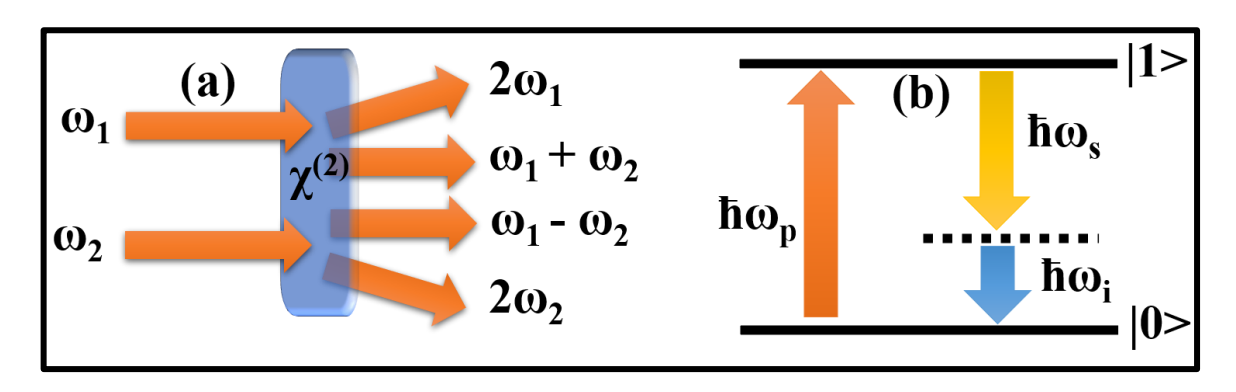


Fig 2.2 (a) Frequency mixing second order NLO parametric process (b) Optical parametric oscillation energy diagram.

### 2.1.2. Ultrafast Lasers and their characterization:

A LASER (Light Amplification by Stimulated Emission of Radiation) where a gain medium or active medium is activated inside an optical cavity to excite atoms in such a manner that they produce photons of same energy and coherence. The optical cavity has an optical feedback mechanism which allows the light to get amplified before exiting from an output coupler resulting in an intense collimated monochromatic spatially coherent light. The light from a laser can lase in a continuous manner, called a CW (Continuous Wave) laser or in the form of short bursts of light, called Pulsed laser. Pulsed lasers have very high peak intensities as each pulse contains similar energy of CW power that is concentrated for short time, typically of the order of  $10^{-9}$  s (ns). Further shorter pulse durations ranging from  $\sim 10^{-12}$  s (ps) to sub-fs ( $\sim 10^{-15}$  and lower) fall under Ultrafast pulses. Due to their high intensity and ultrashort time window ( $10^{-9} - 10^{-18}$  s), pulsed lasers and ultrafast pulses are primarily used for time-resolved spectroscopic studies [9]. Based on their working principle and material used, their laser characteristics – pulse duration, repetition rate, wavelength and average power/ peak power, vary. In this chapter we will be discussing about the

working principles of Q-switched and mode-locked lasers which lase in the time window of  $10^{-9} - 10^{-15}$  s as is relevant to our experiments.

### 2.1.2.a. Q-switched lasers:

Q-switched lasers produce intense laser pulses with pulse duration of few nanoseconds. Here, variable losses are introduced in the cavity to change the quality or Q-factor and hence the name [10, 11]. In a Q-switched laser, the active medium amplifies the input light entering the cavity which acts as a positive feedback (see figure 2.3 (left)). Initially, the cavity losses are made high resulting in no lasing and promoting very strong population inversion in the active medium. After all the atoms of active medium has reached their metastable excited states, the losses are switched off resulting in the sudden rise of the Q-factor and the laser starts lasing. Here, the laser radiation grows extremely fast and disappears equally fast producing short bursts of high intensity radiation. The lasing in a Q-switched laser produces a train of repetitive pulses of nanosecond duration. The variable attenuator in Q-switching can be: a saturable absorber (passive), electro-optic modulator (active) or an acousto-optic modulator (active).

Active Q-switching increases the Q-factor in the laser medium by using an externally controlled variable attenuator like an electrical signal. Active Q-switching can be used to externally control the pulse repetition rate. The active control material can be spinning mirror/prism placed inside the cavity (commonly a mechanical device, for example, a shutter, chopper wheel) or it may be some form of modulator such as a magneto-optic effect device, an acousto-optic device, or an electro-optic device - a Pockels cell/Kerr cell. For example, an electro-optic Pockels cell is a crystal where high voltage (~kV) induces birefringence making it a half waveplate. Along with a crystal, a polarizer is also inserted into the cavity. For high voltages, the polarized light is blocked inside the cavity resulting in no lasing. Accumulation of sufficient amount of gain in the laser medium can lead to population inversion via half-lambda voltage. This rotates the polarization of the beam which can pass through the polarizer without any losses. This results in a giant pulse of ~ns pulse duration and several Hz – MHz repetition rate.

In **passive Q-switching**, no external control for Q-factor gain is required, rather the losses are self-modulated with a saturable absorber. Here, the initial losses in the medium is high making the medium opaque to light exiting the active medium until most of the absorbed atoms are excited to higher level creating population inversion. In this stage, the

medium becomes transparent, thus decreasing the cavity losses. The most common Q-switch laser used has active medium as Nd:YAG with pulse duration ~10 ns and pulse energy in ~J. They produce light in wavelengths 1064 nm and 532 nm with repetition rate of 10–20 Hz.

### **2.1.2.b. Mode-locked lasers** [10, 11]:

Mode-locking laser is used to produce picosecond (ps) to femtosecond (fs) pulses. Here, the laser resonator consists of a mode locking device that can either be an active element (e.g., optical modulator) or a passive element (e.g., a saturable absorber) leading to formation of ultrashort pulses circulating within the cavity. A pulse is emitted each time a pulse hits the output coupler mirror, leaving a train of pulses with pulse duration within few ps to fs. Now, the feedback pulses inside the laser cavity of length 'L' can survive in the cavity if they interfere constructively for which the condition is:

$$L = n\frac{\lambda}{2}$$
 ;  $[n = 1, 2, 3, .....]$ 

In order for the longitudinal modes to be mode-locked, the identical phases are added whose intensity (square of sum of phase) is an equidistant train of pulses with each adjacent pulse being at a distance of double the length of the cavity [see figure 2.3 (right)]. Once modelocking is achieved, the resultant beam exits from the output coupler mirror. Adding number of modes in the cavity can shorten the duration of the resultant, because the extent of space (time) wherever all the modes are at their maxima will be briefer. In this thesis we use mode-locked femtosecond lasers of kHz and MHz repetition rate. Like Q-switching, mode-locking can be active (like an acousto-optic or an electro-optic modulator), passive (like a saturable absorber) or both. Saturable absorbers are already driven by shorter pulses in comparison to an electronic modulator and hence can generate much shorter (femtosecond) pulses. The most common example is the solid state dye lasers – titaniumdoped sapphire (Ti:sapphire, Ti:Al<sub>2</sub>O<sub>3</sub>) lasers permitting the generation of light in the 690-1050 nm spectral range with a maximum gain near 800 nm. It works on Kerr lens mode locking where the medium obtains refractive index that is intensity dependent as:  $n = n_0 + n_0$  $n_2I$  [ $n_0$  is linear refractive index valid for low intensities]. Here, the gaussian beam starts to self-focus as it experiences higher index of refraction along the gaussian beam center as compared to the edges and keeps contracting in size until it reached the diffraction limit.

Using this, the Ti:sapphire laser generates a train of pulses with duration of few tens of femtoseconds, repetition frequency usually around 80 MHz and energy within the range of 1-6 nJ.

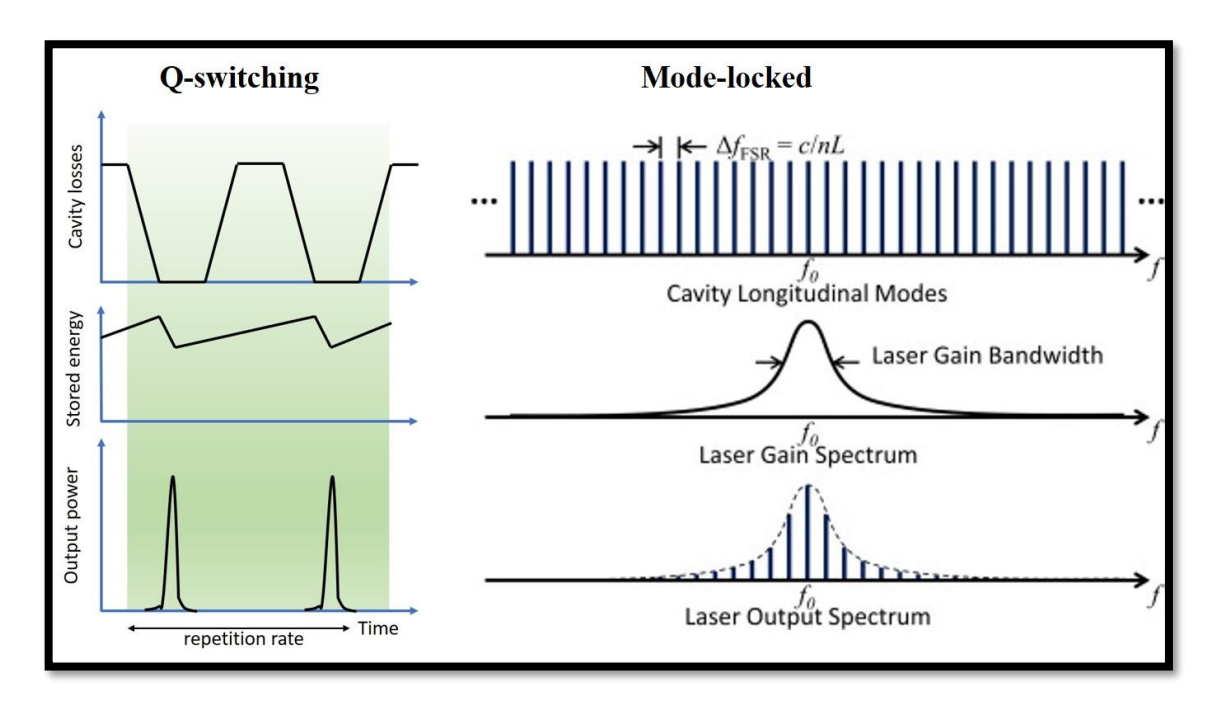


**Figure 2.3** (**left**) Generation of laser pulse (~ns) by Q-switching and (**right**) mode-locking mechanism of generating laser pulse (~fs).

#### 2.1.2.c. Laser pulse characterization:

Laser pulse characterization can be achieved by measuring the following parameters using respective techniques [10]:

- **i. Pulse repetition rate:** A pulse repetition rate is the number of pulses emitted per second by the pulsed laser (e.g. Q-switched or mode-locked). The measurement technique requires a fast photodiode along with an electronic spectrum analyzer.
- ii. Pulse duration: Pulse duration,  $\tau$ , in a laser is typically the time measured across a single pulse, often defined by its full width at half maxima (FWHM) as shown in figure 2.4 (a). Common techniques to measure the pulse duration are autocorrelators, a streak camera, or optical sampling.
- **iii. Pulse energy:** The pulse energy, E<sub>p</sub> is the total optical energy in a light pulse, calculated from the repetition rate and average power.
- **iv. Optical center frequency** and **spectral shape** can be obtained with an optical spectrum analyzer. Frequency-resolved optical gating (FROG) technique can be used to measure the chirp of the ultrashort pulse.

Assuming the pulse envelope to be a standard Gaussian, where,  $\omega_0$  is the central (carrier) frequency of the pulse while  $\tau$  is the input pulse duration. Since the frequency domain of the gaussian pulse is the Fourier transform of its temporal domain and is also a gaussian as:

$$E(t) = E_0 e^{\frac{-t^2}{2\zeta^2}} e^{-i\omega_0 t}$$

$$E(\omega) = E_0 \zeta e^{\frac{-(\omega - \omega_0)^2}{2\sigma^2}}$$
 where,  $\sigma$  is the spectral width.

Thus,
$$\sigma^2 = \frac{1}{\zeta^2} \equiv \sigma \zeta = 1$$
 (2.4)

The constant on the right-hand side of eqn. (2.1), which is equal to one, is called **time-bandwidth product**, **TBP**. A pulse can be defined as a transform-limited pulse when its bandwidth in dictated by Fourier Transform with a minimum value of 1, indicating a proper symmetric Gaussian electromagnetic pulse.

v. Autocorrelation: The basic principle of operation of an autocorrelator is to check the correlation of the temporal pulse trace with itself. This is achieved by superimposition of two pulses (separated by a beam splitter) overlapping temporarily in a nonlinear medium, where they non-linearly interact based on the type of interaction in the medium. Some of the autocorrelators are: intensity, interferometric and two-photon autocorrelators. The most commonly used intensity autocorrelator uses two pulses: the input pulse is split in two, and one of the pulses is delayed by time 'τ'. The two pulses are focused into a nonlinear optical crystal in a non-collinear fashion leading to second order nonlinearity when phase matching is achieved. The dependence of the autocorrelation signal on the temporal delay is given by:

$$I_{AC}(\zeta) = \int_{-\infty}^{\infty} P(t)P(t-\zeta) dt \propto \int_{-\infty}^{\infty} I(t)I(t-\zeta) dt$$
 (2.5)

Where, 'P(t)' is the nonlinear polarizability which is proportional to the intensity 'I(t)' convolution of the pulses with a finite delay ' $\tau$ '. The typical schematic of an intensity autocorrelator is shown in Figure 2.4(b) below.

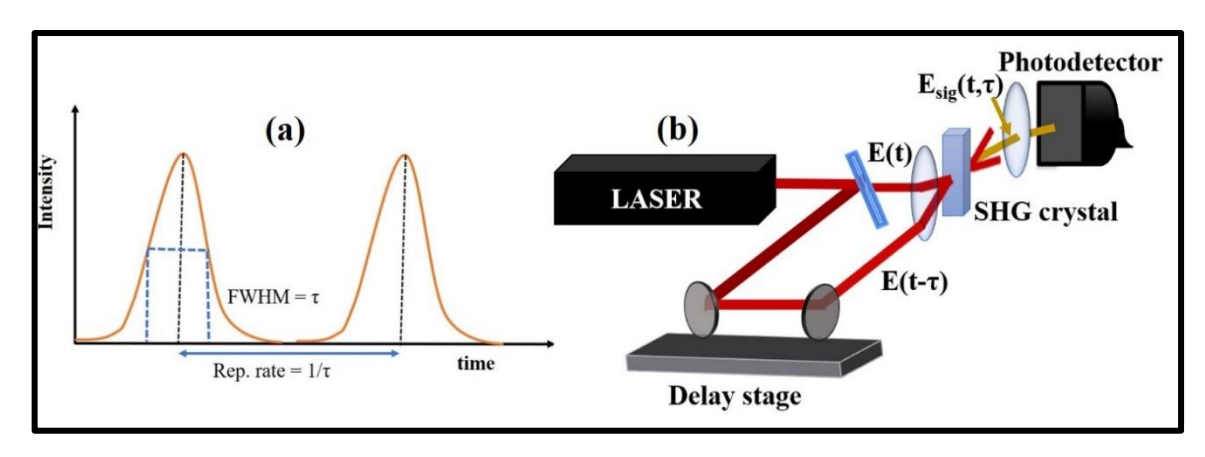


**Figure 2.4 (a)** Laser pulse characterization parameters **(b)** Schematic showing Intensity Autocorrelator setup.

vi. FROG (frequency resolved optical grating): works in a similar way to the intensity autocorrelator, with a spectrograph being placed in the place of a photodetector. giving a complete pulse characterization which not only includes pulse duration but also pulse energy, phase and chirp information. The FROG signal is generally a convolution of the unknown electric field [E(t)] with the gating field [g(t)]. The gating is a nonlinear sampling with  $\chi^{(2)}$  or  $\chi^{(3)}$  medium. Thus, the spectrally frequency-resolved intensity,  $S_F(\tau,\omega)$  is given by,

$$S_F(\zeta,\omega) \propto \left| \int_{-\infty}^{\infty} E(t) \cdot g(t-\zeta) e^{-i\omega t} dt \right|^2$$
 (2.6)

To reconstruct the pulse shape from FROG trace Spectrogram includes a computer program of complex iterative phase retrieval algorithm.

# 2.1.3. Transient Absorption Spectroscopy:

Transient Absorption Spectroscopy (TAS) is a time-resolved spectroscopic technique which is also referred to as pump-probe technique. TAS is used to understand the electronic/structural properties of transitory excited states of different photochemically and/or photophysically relevant molecules. In pump-probe the sample is excited using a short pulse which alters the photophysical state of the molecule. The excited state can be captured by another shorter weak pulse that arrives after a certain delay. By varying the arrival time of the 2<sup>nd</sup> laser pulse with respect to the 1<sup>st</sup> laser pulse, one can measure the complete time-dependence of the change in absorption [9]. The delay is induced with a retroreflector while alternating pump pulses are caused by an optical chopper. On excitation by pump pulse, some of the molecules transition from ground state to the excited state via

linear absorption which further interacts with a delayed probe pulse kicking the excited species to further higher excited states through nonlinear interactions. As a result, some of the species can gain enough energy to transition to higher excited levels which is a nonlinear interaction. The signal obtained by the Photodetector contains both spectral and kinetic information of the probe pulse taken over specific delay time. The signal appears as the difference absorption of the probe pulse with and without the pump pulse, i.e.  $\Delta A$  (absorbance) =  $A_{pump\ on} - A_{pump\ off} = log(I_{pump\ off}/I_{pump\ on})$  with respect to wavelength ( $\lambda$ ) or delay time (t) for spectral and kinetic picture respectively. A typical TAS spectrum is depicted in figure 2.5 (right) below.

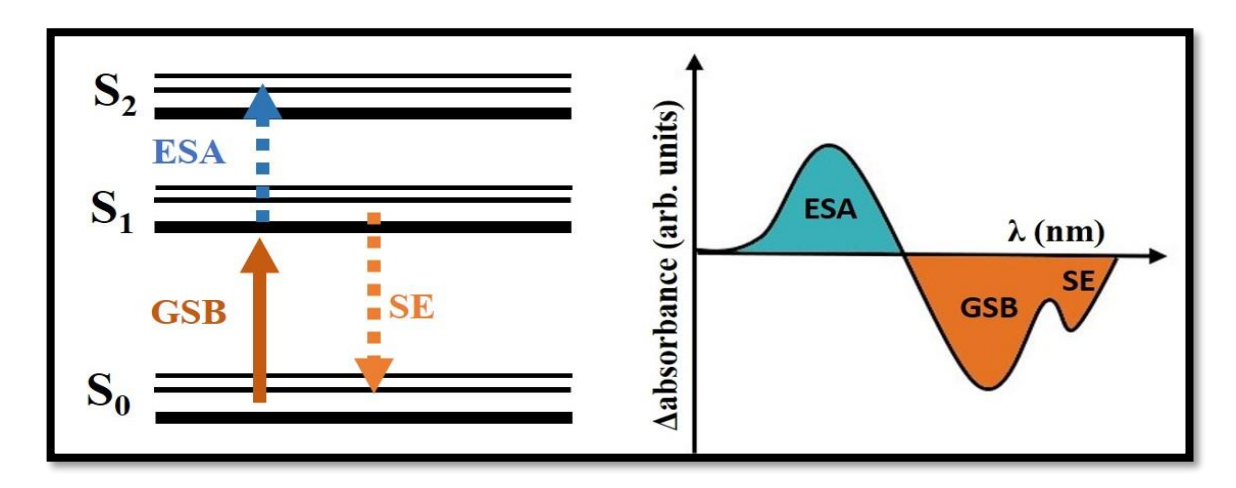


**Figure 2.5 (left)** Jablonski energy diagram showing excited species transitions corresponding to **(right)** TAS spectrum obtained in pump-probe spectroscopy.

Let us discuss the spectral bands obtained in a TAS spectrum in details:

- i. Ground state bleach (GSB): When a part of the molecular population is excited to the higher energy state through pump pulse irradiation, the ground state molecular population is decreased. Hence, the ground-state absorption is reduced in the excited sample compared to its non-excited state. This is reflected as a negative signal in the ΔA spectrum with respect to wavelength region as shown in figure 2.5 by the orange region in the TA spectrum (right) and orange arrow in the Jablonski diagram (left).
- ii. Excited state absorption (ESA): Also known as photoinduced absorption (PIA) and is a nonlinear optical phenomenon. Upon pump beam excitation, excited species can further populate in optically allowed transitions that may exist in certain wavelength regions, and absorption of the probe pulse at these wavelengths will occur. This is seen as a positive signal in the  $\Delta A$  spectrum as depicted as blue region in figure 2.5 (right).

It is to be noted that the due to weak intensity of the probe pulse, excited-state population is not significantly affected by the excited-state absorption process.

iii. Stimulated emission (SE): As the probe pulse passes through the excited population, stimulated emission takes place. It takes place for specific optically allowed transitions only which matches the spectral profile of the fluorescence spectrum of the excited species, while Stokes shifted with respect to the ground state. Here, one photon from the probe pulse interacts with the excited molecule to emit another photon while returning to its ground state which when detected, results in an increase of light intensity on the detector, corresponding to a negative ΔA signal as shown in Fig. 2.5 (orange region) and dotted arrow.

Now, apart from the general distribution of excited molecules of the transient spectra, each excited species is capable of showing variable dynamics in their kinetic domain. To understand the TAS kinetic picture, a brief theoretical discussion is necessary [12].

We know, the absorbance  $A(\lambda)$  of each probe pulse is defined by the intensity of the incident and transmitted light,  $I_0(\lambda)$  and  $I(\lambda)$ , in the Beer–Lambert law:  $A(\lambda) \propto \frac{I_0(\lambda)}{I(\lambda)}$ 

Experimentally, we tend to examine the change in absorbance  $\Delta A(\tau,\lambda)$  induced by the pump pulse which is defined as the difference between the pump absorbance,  $A_p(\tau,\lambda)$  and the unpumped sample,  $A_u(\lambda)$ , i.e.

$$\Delta A(\lambda, \tau) = A_p(\lambda, \tau) - A_u(\lambda) \propto \frac{I_u(\lambda)}{I_p(\lambda, \tau)}$$
(2.7)

On excitation, let the change in level population of  $i^{th} \rightarrow j^{th}$  level be  $N \rightarrow N + \Delta N$ , then, from Beer-Lambert's law, absorption coefficient,  $\alpha(v) = \sigma_{ij}(v) (N_i - N_j) l$  (2.8) where  $\sigma_{ij}$  is the absorption cross-section and l is the sample length with  $N_i = N$  and  $N_j = N + \Delta N$ . Using equation (2.8), we get,

$$\frac{\Delta A}{A} = -\Sigma \alpha(\nu) = -\sum_{ij} \sigma_{ij}(\nu) \Delta N_j(t) l$$
 (2.9)

Now, at a particular delay 't', the level population,  $\Delta N_i$  can be written as

$$\Delta N_j(t) \propto N_j(0) e^{\left(\frac{-t}{\tau}\right)}$$
 (2.10)

This gives us, 
$$\frac{\Delta A}{A} = -\sum_{i} A_{i} e^{\frac{-t}{\tau}}$$
 (2.11)

where,  $A_i$  is the constant (proportionality) given as the amplitude to the exponential equation.

Equation (2.11) indicates that the excited state decay follows an exponential path in the TAS spectra as shown in figure 2.6(a) below.

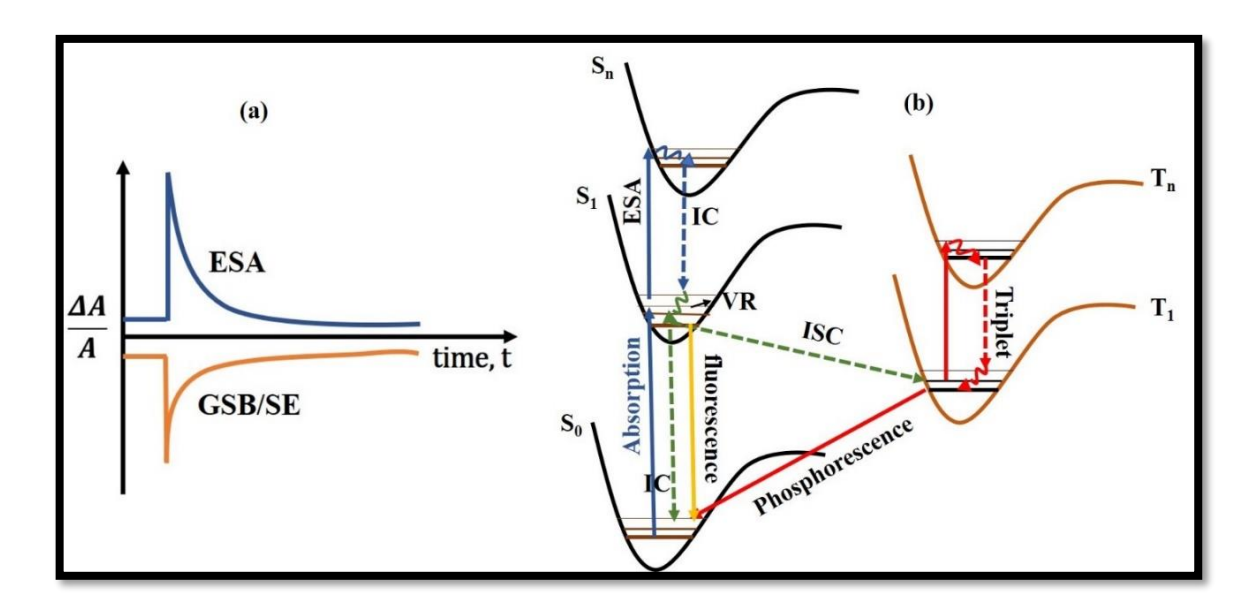


**Figure 2.6 (a)** TAS kinetic spectrum showing excited species evolution trend with time for ESA, GSB and SE **(b)** Jablonski diagram showing various phenomena accompanying the kinetic evolution of the excited molecule. The notations stand for: IC=Internal Conversion; VR= Vibrational Relaxation; ISC= Intersystem Crossing.

The kinetics provide information about a number of processes that undergoes with the excited species like: vibrational relaxation, internal conversion, intersystem crossing, phosphorescence and others. An energy diagram that best describes the processes consists of energy on a vertical axis known as the Jablonski diagram. Each column in the diagram usually represents a specific spin multiplicity for a particular species where the horizontal lines indicate eigenstates for that particular molecule where the bold lines depicted electronic levels and the multiple thin lines above it showing vibrational levels as shown in figure 2.6(b). Each of the processes [9] are described briefly below:

i. Vibrational Relaxation (VR): An excited species (e.g. an electron) can dissipate its energy in a multiple way – first one is through vibrational relaxation (non-radiative)

where the deposited photon energy into the electron is transferred to other vibrational modes in the form of kinetic energy [illustrated as curvy lines in figure 2.6 (b)]. The energy may be transferred to surrounding molecules or may stay within the molecule or within approx.  $10^{-14} - 10^{-11}$  s.

- ii. Internal Conversion (IC): Sometimes, the excited electron can transition within the vibrational levels of two electronic states e.g. S<sub>2</sub> and S<sub>1</sub>. This happens if there is a strong overlap in the vibrational energy levels with electronic energy levels. This process is termed as internal conversion (non-radiative) and is shown as dashed arrows in the figure 2.6(b). Thus, greater the overlap between the vibrational and electronic level between two states, higher the chances of internal conversion, i.e. for energy levels higher to first excited state (like S<sub>2</sub> and higher).
- **Fluorescence:** This process also involves emission of a photon as a relaxation pathway to deal with energy received from higher level photons of same spin multiplicity and is termed as fluorescence (radiative). It is depicted as yellow solid arrow in figure 2.6 (b). This slow process can occur in the order of 10<sup>-9</sup> to 10<sup>-7</sup> seconds in which case, it is highly unlikely for an electron to dissipate energy at electronic energy states higher than the first excited state.
- iv. Intersystem Crossing (ISC): Sometimes, an electron changes spin multiplicity from an excited singlet to triplet state [non-radiative transition from one column to another of the Jablonski diagram as shown in figure 2.6 (b) as green dashed arrow]. This is a slower process of several orders of magnitude slower than typical fluorescence since it is a forbidden transition based on electronic selection rules but becomes weakly allowed when coupled to vibrational factors.
- **v. Phosphorescence:** This is also a radiative transition that takes place from an excited triplet to a singlet ground state as shown as a red solid arrow from  $T_1$  to  $S_0$  in figure 2.6(b).

Other than the above-mentioned processes, a molecule can also undergo energy transfer via delayed fluorescence, Forster's resonance energy transfer (FRET), Dexter energy transfer, molecular collisions and others. This will be discussed briefly within concerned chapters where we witness these processes.

# 2.1.4. Z-scan technique:

When a high intensity laser light (pulsed or continuous) is incident on a sample (preferably a nonlinear material), the characteristic properties of the material (like absorption, refractive index, susceptibility etc.) becomes intensity dependent in a non-linear like  $n = n_0 + n_2 I$  where  $n_0$  is the linear refractive index while  $n_2$  is the nonrelation linear contribution. In a linear medium, the relation between the induced electric polarization and the electric field is linear as:  $\mathbf{P} = \varepsilon_0 \chi \mathbf{E}$  where  $\varepsilon_0$  is the permittivity of vacuum and  $\chi$  is the dielectric susceptibility of the medium. For a non-linear medium, the polarization in the dielectric medium follows the relation:  $P(E) = \varepsilon_0(\chi^{(1)}E + \chi^{(2)}E.E +$  $\chi^{(3)}$ **E.E.**E +....). Centrosymmetric materials possess inversion symmetry for which the second order susceptibility  $\chi^{(2)} = 0$  along with other even terms. In our upcoming chapters, we deal with centrosymmetric media. Considering higher harmonic contributions  $\chi^{(5)}$ ,  $\chi^{(7)}$ ,... negligible, we focus our attention to third order nonlinearity  $\chi^{(3)}$  itself. Now the  $\chi^{(3)}$ contains its real and imaginary parts which correspond to the nonlinear refraction and nonlinear absorption respectively. One of the simplest experiments to determine simultaneously the nonlinear absorption coefficient  $\alpha_2$  and refractive index  $n_2$  is the Z-scan technique proposed by Sheikh Bahae et al in the year 1990 [13]. Z-scan technique is a simple, single beam technique where the sample under investigation (either solution, bulk solid, or thin film) is moved along (translated linearly along the Z-axis) a tightly focused Gaussian laser beam [see figure 2.7(a) for a schematic]. Different intensities are experienced by the sample along the sample position that is relative to the focus (Z=0) which results in various nonlinear effects such as multi-photon absorption, self-focusing or defocusing effects which will be discussed below. These NLO properties have potential applications in areas such as photonics (as optical limiters, saturable absorbers, etc.).

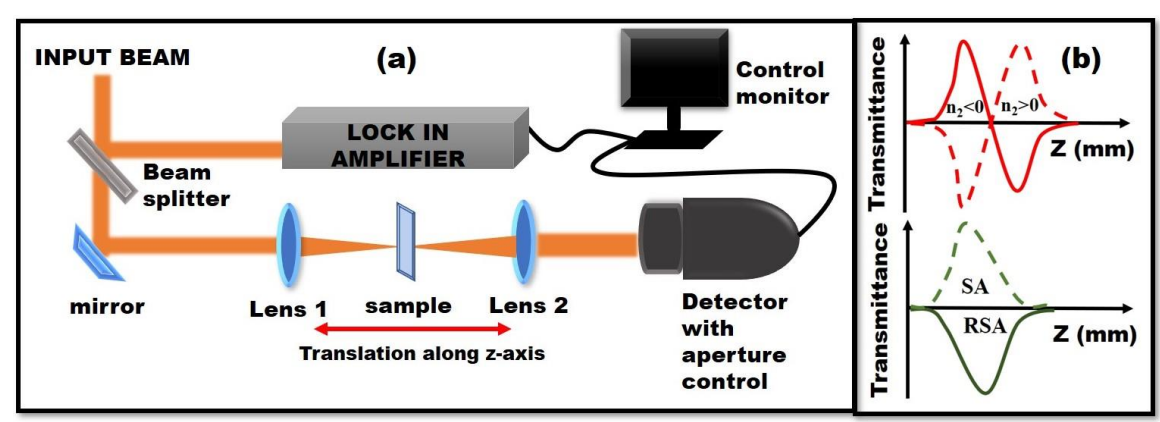


Figure 2.7 (a) Z-scan schematic (b) closed (top) and open (bottom) aperture Z-scan signals.

In the Z-scan, the beam aperture through which the transmitted light enters the detector is crucial to measurement of the NLO coefficients – (nonlinear refractive index)  $n_2$  or (nonlinear absorption coefficient)  $\alpha_2$ .

In **open aperture Z-scan** [14], the control aperture is fully open allowing the entire transmitted light to enter the detector. This method is used to measure  $\alpha_2$ . Expected open aperture Z-scan trace must be symmetric with respect to the focus (Z=0) where the transmittance is at minimum as shown in bottom of figure 2.7(b). At the far field, the intensity is low and hence linear absorption occurs. As the sample approaches focus, a decrease or increase in the detector transmittance is observed. At the focus, the resultant signal can form a valley or peak which can indicate to a saturable or reverse saturable absorption respectively [see figure 2.7(b) bottom]. Open aperture Z-scan signal gives us the value nonlinear absorption coefficient, which is related to the imaginary part of  $\chi^{(3)}$ .

In **closed aperture Z-scan** [14], the nonlinear index of refraction n<sub>2</sub> of the NLO medium varies with higher intensity or fluence. Here, the control aperture is half-closed, allowing only a fraction of the transmitted light to the detector. A NLO material medium can act like an intensity dependent lens (called Kerr lens) when a Gaussian laser beam is made to pass through the material medium. Based on the sample location along the z-axis, the transmitted amount of energy through the aperture varies (see figure 2.7 (b) top). For example, let us consider a material with negative nonlinear refractive index (n<sub>2</sub><0) which have defocusing behavior. When the sample is far away from the focus (far-field case), the intensity of the input Gaussian beam is not strong enough to invoke any nonlinearity within the sample and the measured transmitted power on the detector remains more or less constant. As the sample translates towards focus, the nonlinear absorption and refraction are enhanced and, therefore, the sample acts like a (variable) lens. The diverged beam passes through the small aperture resulting in increase in measured transmittance [see figure 2.7(b) top]. As the sample moves away from the focus, the refraction strength decreases due to lower peak intensity resulting in a decreased transmittance. Finally, when the sample reaches far field, the peak intensity again is weak to induce nonlinearity. Hence, the measured output power on the detector remains constant as shown in see figure 2.7(b) top. The signal reverses for positive nonlinearity  $(n_2>0)$  as they promote self-focusing behavior. The experimentally obtained data from open and closed aperture data is further fitted using standard formulae to calculate all the NLO coefficients specific to the sample under study which was used by Sheikh-Bahae et al. in 1990 [13]. The theory behind is explained below.

#### **2.1.4.a.** Theory of **Z**-scan [14]:

Considering a gaussian beam, 
$$E(r,t,z) = E_0(t) \frac{\omega_0}{\omega(z)} \cdot \exp\left(-\frac{r^2}{\omega^2(z)} - \frac{ikr^2}{2R(z)}\right) e^{-i\varphi(z,t)}$$
 (2.12)

Where,  $E_0(t)$  is the radial electric field of pulse envelope at the waist with  $e^{-i\phi(z,t)}$  being temporal phase evolution which is independent of radial 'r' contribution.

Beam radius is given by,  $\omega(z)=\omega_0\left(1+\frac{z^2}{z_0^2}\right)^{1/2}$  and R(z) is the radius of curvature of wave front given by,  $R(z)=z\left(1+\frac{z_0^2}{z^2}\right)$ 

Since, dielectric constant of a medium is  $\epsilon_1 = \chi^{(1)} + 1$  and the relation with linear refractive index is  $n_0 = (\epsilon)^{1/2}$ . Therefore, refractive index in a medium is  $n^2 = 1 + \chi(|\mathbf{E}|^2)$ .

i.e.

$$n_0 + \frac{\chi^{[3]}|E|^2}{2n_0^2} \equiv n_0 + \frac{n_2}{2}I \tag{2.13}$$

Equation **2.13** gives us total nonlinear refractive index with  $n_2$  being the nonlinear refractive coefficient. The Z-scan technique follows slowly varying envelope approximation (SVEA) which assumes a slowly varying forward travelling wave in time and space as compared to its wavelength or period. Thus, here we consider only the radial phase of the beam,  $\phi(r)$ . For thin samples where the sample length,  $L << z_0/\Delta \phi_0$  [ $z_0$ : Rayleigh range and  $\Delta \phi_0$ : radial phase shift at z=0], we can write,

$$\frac{\mathrm{d}\Delta\varphi(r,t,z,L)}{\mathrm{d}\mathbb{Z}} = \Delta n(I)k$$

Which gives us,

$$\Delta\phi(r,z,t,L) = \Delta\phi_0(z,t,L) \exp\left(\frac{-2r^2}{\omega^2(z)}\right)$$
Where 
$$\Delta\varphi_0(z,t) = \frac{\Delta\varphi_0(t)}{1 + \left(\frac{z}{z_0}\right)^2} \quad \text{and,} \quad \Delta\varphi_0(t) = k\Delta n_0(t) L_{\text{eff}}.$$
(2.14)

With Leff being the effective sample length through which the nonlinearity is affected,

$$Leff = 1 - \frac{e^{-(n-1)\alpha_0 L}}{(n-1)\alpha_0}; \quad [n=1, 2, ...., n]$$
 (2.15)

Thus, electric field exiting the sample is given by,  $E_{ex}(r, z, t) = E(z, r, t)e^{-\alpha L/2} e^{i\Delta\phi(z,r,t)}$ 

According to Gaussian decomposition method [15], we carry out a Taylor expansion of the nonlinear part to the above equation as,

$$e^{i\Delta\varphi(z,r,t)} = \sum_{m=0}^{\infty} \frac{[i\Delta\varphi_0(z,t)]^m}{m!} e^{\frac{-2mr^2}{\omega^2(z)}}$$
(2.16)

Now, the nonlinear absorption in a material is intensity, I dependent and can be written as,

$$\frac{\partial I}{\partial z} = -\alpha(\omega)I - \beta(\omega)I^2 - \gamma(\omega)I^3 - H \cdot 0 \cdot T$$
(2.17)

Where  $\alpha$ ,  $\beta$ ,  $\gamma$  and so on... are 1-photon, 2-photon, 3-photon absorption coefficients respectively. Here, we will consider only contributions from 2-photon absorption (2PA) giving us,  $I(z)=I_0/(1+\beta I_0 z)$ . Here H.O.T. refers to higher order terms.

If the electric field at the aperture is 'E<sub>a</sub>', then transmittance power obtained at the detector can be written as:  $P_T(\Delta \varphi_0(t)) = c\varepsilon_0 n_0 \pi \int_0^{r_a} |E_a(r,t)|^2 r \, dr$ . (2.18)

The instantaneous input power is given by  $P_i(t) = \frac{\pi \omega_0^2 I_0(t)}{2}$ . Therefore, output transmittance measured,  $T(z) = \frac{\int_{-\infty}^{\infty} P_T(\Delta \varphi_0(t)) dt}{S \int_{-\infty}^{\infty} P_i(t) dt}$  where S=1-exp(-2r<sub>a</sub><sup>2</sup>/ $\omega_a$ <sup>2</sup>) is the linear aperture transmittance with  $\omega_a$  being the beam radius.

Let, 
$$q(z,r,t) = \beta I(z,r,t) L_{eff}$$
, then,  $I_e(z,r,t) = \frac{I(z,r,t)e^{-\alpha L}}{1+q(z,r,t)}$  [from eqn. 2.16 and 2.18]

And 
$$\Delta \varphi(z,r,t) = \frac{k\gamma}{\beta} ln[1 + q(z,r,t)]$$
 (2.19)

Then, electric field at aperture can be written as:

$$E_a = E(z, r = 0, t)e^{-\alpha L/2} \sum_{m=0}^{\infty} \frac{[i\Delta\varphi_0(z, t)]^m}{m!} \frac{\omega_{m_0}}{\omega_m} exp\left(-\frac{r^2}{\omega_m^2} - \frac{ikr^2}{2R_m} + i\theta_m\right) \text{ and eqn. 2.10}$$

can be written as, 
$$E = E(z, r, t)e^{-\alpha L/2} \sum_{m=0}^{\infty} \frac{q(z, r, t)^m}{m!} \left[ \prod_{n=0} \left( \frac{ik\gamma}{\beta} - \frac{1}{2} - n + 1 \right) \right]$$
 (2.20)

From eqn. 2.19, we can write transmitted power as,

$$P(z,t) = P_i(t)e^{-\alpha L} \frac{\ln[1+q_0(z,t)]}{q_0(z,t)} \text{ where } q_0(z,t) = \beta I_0(t) L_{\text{eff}} / (1+\frac{z^2}{z_0^2})$$
 (2.21)

In case of the temporal profile of a Gaussian pulse, equation 2.14 can be integrated with time to give the normalized energy transmittance

$$T(z, S = 1) = \frac{1}{\sqrt{\pi}q_0(z, 0)} \int ln[1 + q(z, 0)e^{-\tau^2}] d\tau$$
 (2.22)

For open aperture measurements, S=1. Assuming  $|q_0|<1$ , eqn. 2.18 can be expanded and simplified as

$$T(z,S=1) = \sum_{m=0}^{\infty} \frac{[-q_0(z,0)]^m}{(m+1)^{3/2}}$$
 (2.23)

Thus, the nonlinear absorption coefficient  $\beta$  can be determined from the open aperture (S = 1) Z-scan experimental data. But for closed aperture conditions, S is affected by  $|\phi_0|$ . For small  $|\Delta\phi_0|$ , the peak and valley occur at the same distance with respect to focus while for large  $|\Delta\phi_0|$ , symmetry no longer holds [see eqns. 2.22 and 2.23] and the peak and valley move along the z-axis for the corresponding sign of nonlinearity ( $\pm\Delta\phi_0$ ). On normalization, the peak (p) to valley (v) transmittance variation  $\Delta T_{p-v}$  was numerically fit and a linear relation between  $\Delta T_{p-v}$  and  $|\Delta\phi_0|$  was established as:  $\Delta T_{p-v} \approx 0.406(1-S)^{0.25}|\Delta\phi_0|$  for  $|\Delta\phi_0| \leq \pi$  and  $\Delta T_{p-v} \approx 0.21(1-S)^{0.25}|\Delta\phi_0|$  for larger values of  $|\Delta\phi_0|$ .

Plotting **eqn. 2.23** we obtain open aperture Z-scan signal as shown in figure 2.8(a) and 2.8(b) which gives us the nonlinear absorption ' $\beta$ ' coefficient. On the other hand, **eqn. 2.24** shows the closed aperture Z-scan result [see figure 2.8 (c)] which can give us the value of nonlinear refractive index n<sub>2</sub>.

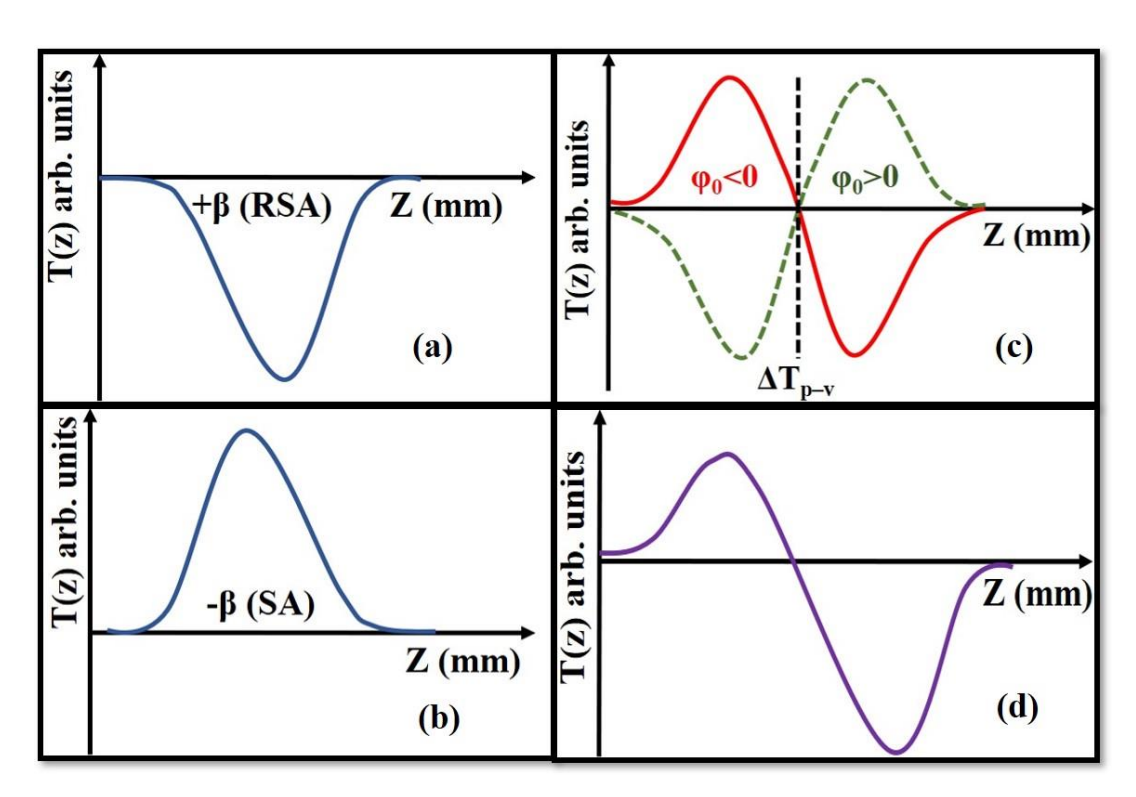


**Figure 2.8** (a) open aperture Z-scan signal showing reverse saturable absorption (RSA,  $\beta$  +ve) (b) open aperture Z-scan showing saturable absorption (SA,  $\beta$  -ve) (c) closed aperture Z-scan showing peak-valley transmittance variation  $\Delta T_{p-v}$  w.r.t Z-axis. For  $\phi_0$ <0, negative nonlinearity is observed while for  $\phi_0$ >0, positive nonlinearity is observed following eqn. 2.8. (d) Z-scan signal containing contributions from both nonlinear absorption and refraction coefficients.

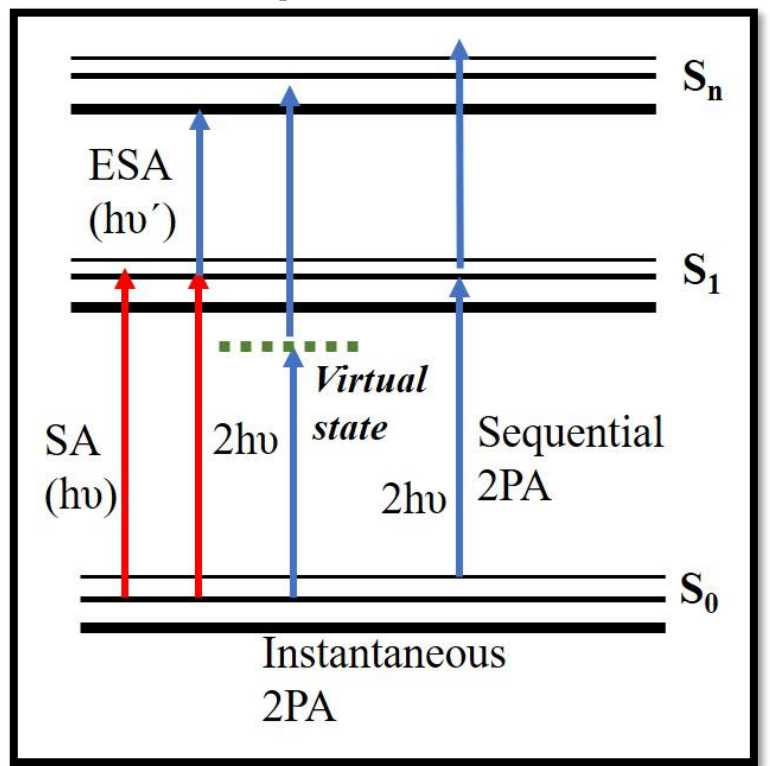


**Figure 2.9** Energy diagram showing various absorption processes. For multiphoton absorption processes, the instantaneous and sequential processes are demonstrated with the help of two-photon absorption phenomenon.

Mostly, closed aperture Z-scan measurements contain both nonlinear absorption (NLA) and nonlinear refraction (NLR) contribution resulting in a signal as shown in Figure 2.8 (d). Hence, it is necessary to divide the open aperture signal from the obtained combined signal to reveal the accurate closed aperture data as shown in figure 2.8 (c). The third order nonlinear susceptibility,  $\chi^{(3)}$  is a complex quantity given by:  $\chi^{(3)} = \chi_R^{(3)} + i\chi_I^{(3)}$  where, imaginary part is associated with two-photon nonlinear absorption as:  $\chi_I^{(3)} = \frac{n_0^2 \varepsilon_0 c^2}{\omega} \beta$  and real part is associated with nonlinear refraction coefficient  $n_2$  as:  $\chi_R^{(3)} = 2n_0^2 \varepsilon_0 cn_2$ 

When a material undergoes the nonlinear absorption process, there are possibilities of either of the following phenomena to take place:

- i. Saturable absorption (SA): Here the material tends to become more and more transparent or its absorption decreases with increase in intensity, i.e.  $\frac{dI}{dz} = -\frac{\alpha I}{1+\frac{I}{I_0}}$  with ' $\alpha$ ' being the linear absorption coefficient and ' $I_0$ ' being the saturation intensity. In this case the ground state atoms of the excited material, get excited to the upper level at a rate such that the excited atoms don't get sufficient time to relax back resulting the upper level to saturate. This property finds its application in passive Q-switching and mode-locking in pulsed lasers, semiconductor lasers, etc.
- ii. Reverse saturable absorption (RSA): In contrast to SA, when the absorption of the material increases as the input laser intensity is increased, it is termed as reverse saturable absorption (RSA). RSA generally arises in a molecular system as a result of the excited state absorption (ESA) cross being larger than the ground state cross section [16]. RSA can occur due to simple ESA or multiphoton absorption (nPA) such as 2PA, 3PA, 4PA and so on depending on the incident laser pulse properties (e.g. wavelength, input intensity and pulse duration) as well as sample properties like excited state lifetimes of singlet/triplet states [17]. Multiphoton absorption like 2PA can either occur instantaneously (S<sub>0</sub>→S<sub>n</sub>) via a virtual state or it can occur via S₁ which is a real state and is known as a sequential or resonant process (see figure 2.9). RSA finds a wide range of application as optical limiters, fiber communications, multi-photon imaging, etc.

Often a nonlinear optical material is capable of switching its behavior from SA to RSA or from RSA to SA by changing few experimental parameters [18, 19, 20]. This property is extensively used in optical switches which are used in photonics and optoelectronics.

Furthermore, certain materials under specific experimental focusing conditions also show exotic nonlinear absorption behavior such as RSA to SA to RSA or SA to RSA to SA. Such a behavior is rare to observe but has been reported.

### 2.1.5. Porphyrins and Phthalocyanines:

Porphyrins (P) and Phthalocyanines (Pc) are an important class of synthetic organic dyes which show a huge scope of application in the world of photonics. These molecules show strong nonlinear optical properties and other photophysical properties. They can serve as photosensitizers in photovoltaics and as catalysts and photocatalysts in different reactions, photodynamic therapy of cancer, and also as sensors for material detection via fluorescence quenching [21, 22, 23].

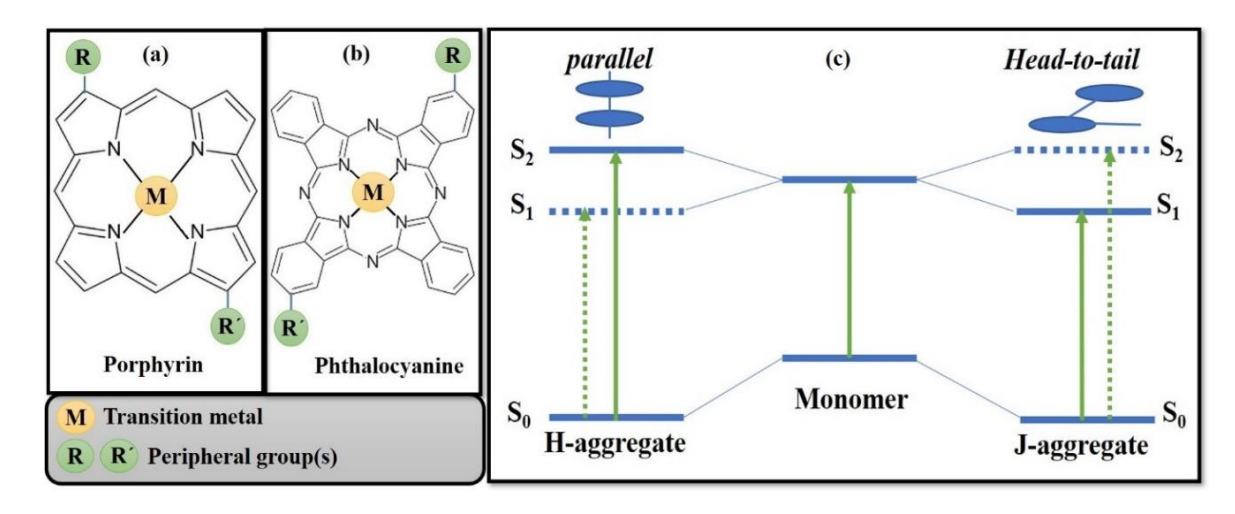


**Figure 2.10** Typical molecular structure of: (a) a porphyrin P. (b) a phthalocyanine Pc. (c) Schematic showing shift in energy level of a Pc monomer for (left) H-aggregate showing blue shift and (right) J-aggregate showing red shift.

Porphyrins are a class of the molecules with tetrapyrrolic rings which are linked by methane carbon bridges as shown in figure 2.10(a). They can exist as metallo complexes when incorporated with a central metal ion in the pyrrole ring center as free bases. Also, other peripheral groups can be attached to the outer rings of the methane bridges or isoindole units to form different Por and Pc structures respectively [24]. Similar to porphyrins, phthalocyanine molecules (Pc) contain four indole units—pyrrole rings linked by nitrogen atoms conjugated with benzene rings and capable of holding metals at their center along with different range of various peripheral groups [see figure 2.10(b)]. The typical absorption band(s) of P and Pc ligand are around 600 – 800 nm which is most ideal wavelength window for biomedical applications [24]. This band arises due to characteristic

ligand based  $\pi$  -  $\pi$ \* transitions referred to as the Q band. The 18 $\pi$  delocalized conjugated electrons present in their molecular structure gives these organic compounds particular stability and other interesting photochemical and photophysical properties. A conjugated system has an overlapping p orbitals region (or d-orbitals for transition metals) that allow a  $\pi$  electrons delocalization across all the adjacent aligned p orbitals giving the molecule (P or Pc) a stable lower energy structure. They are also capable of accepting or donating electrons easily due to the presence of transition metal ion [25]. The P or Pc moiety can easily changes its oxidation state by electron exchange with the complexed transition metal ion that. For both P and Pcs containing diamagnetic metals show higher triplet lifetimes are (e.g. Mg, Cd, Zn) compared to the ones with paramagnetic metals (Cu, Ni) [26, 27]. These organic molecules can organize themselves in the form of monomers, polymers  $(\alpha, \beta, \eta, \gamma)$ and x), stacks, dyads, supramolecules and many more, broadening their scope of applications [28, 29, 30]. When compared to porphyrins (P), phthalocyanines (Pc) are more stable and their lifetimes during different reactions are longer. However, Pcs tend to undergo self-aggregation in polar environments [31] which reduces their solubility in common solvents and in turn significantly affect their photophysical and photochemical properties in those media. The two most common form of aggregates formed are head-totail form called J-aggregates and face-to-face form called H-aggregates (see figure 2.10 (c)). The aggregation can be observed in the absorption spectra as a red shift for J while a blue shift for H-aggregates. This can be hugely reduced by incorporating proper peripheral substituents to the Pc-moiety [32, 33]. The excited state dynamics of porphyrins and phthalocyanines are extremely useful for application in photovoltaics (solar cells), photosensitizer for photodynamic therapy (PDT) in cancer treatment as well as detection of molecules (like high energy materials, HEMs) via quenching mechanism. Each application has certain criteria to be fulfilled and hence a complete picture of the excited state dynamics of the P or Pc molecule is imminent. Among these some of the process like charge transfer, electron transfer, intersystem crossing etc. are ultrafast events [34]. Besides, these compounds make distinguished NLO materials with variable figures of merit thus affecting the nonlinear absorption by the aforementioned processes. In this thesis, we explore the photophysical and NLO properties of various P and Pc derivatives and identify the potential applications possible.

### 2.2 Instrumentation and characterization

As mentioned above, to perform the transient absorption spectroscopy (TAS) studies as well as nonlinear optical (NLO) studies with Z-scan technique a number of optical instruments were used to build the necessary experimental setups. In this section, a detailed description of the Z-scan and TAS setup is given. In addition to that, the working principle of all optical instruments (laser, OPA, etc.) involved in those setups are also described here.

### **2.2.1 Z-scan setup:**

In this thesis, we use two setups for Z-scan measurements – MHz repetition rate and kHz repetition rate with femtosecond pulses.

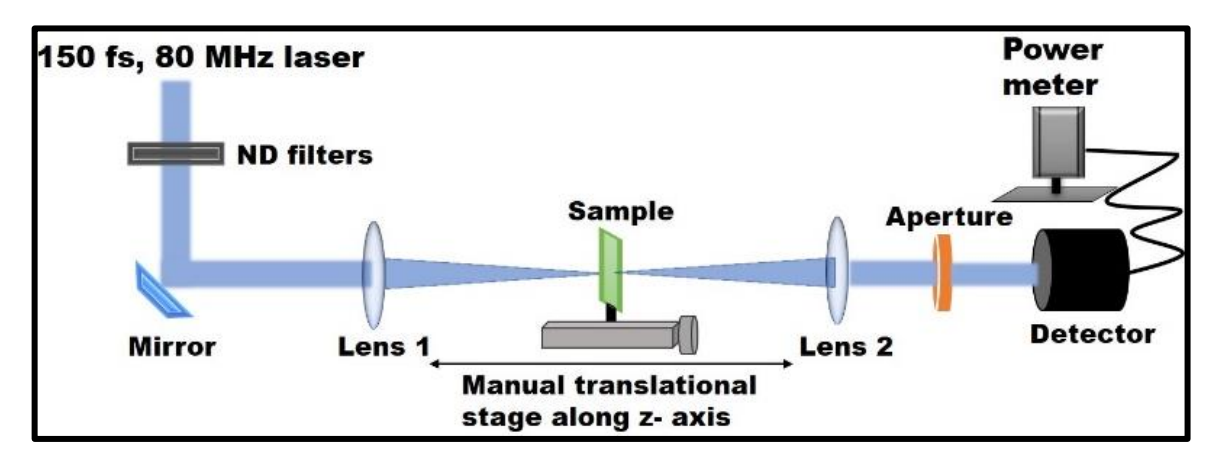


**Fig 2.11** Schematic layout of the Z-scan setup in the MHz regime with a tunable laser (Chameleon from M/s Coherent Inc., USA).

i. **150 fs, 1 MHz repetition rate Chameleon laser** is used for Z-scan measurements in the MHz regime. It is a tunable Ti:sapphire laser with a wavelength range of 680 nm–1080 nm. The setup is shown in figure 2.11 below.

Here, the input wavelength of the tunable laser is set through computer control. The input light intensity is adjusted using neutral density (ND) filters. This light is then passed through focusing lens 1 of focal length 100 mm which is collected by lens 2 after passing through the sample. The sample is mounted on a 15 cm translational stage which can be manually translated along the z-axis. The transmitted light is collected at the detector. An aperture placed between lens 2 (focal length of 75 mm) and the detector controls the amount of transmitted light reaching the detector which allows to take open and closed aperture Z-scan data. The NLO signal can be recorded by measuring the transmitted power displayed

on the power meter w.r.t the distance traversed by the Z-axis which is later plotted on Origin 8.5 software. Data fitting is done using standard set of formulae as mentioned in chapter 2.2.

ii. 50 fs, 1 kHz repetition rate Libra HE laser is used for Z-scan measurements in the kHz regime. The laser operates at a central wavelength of 800 nm. Hence, to tune it to other wavelengths, an optical parametric amplifier TOPAS C is used which can ideally have the wavelength range of 260 nm–2.6 μm. The Z-scan setup (kHz regime) is shown in figure 2.12

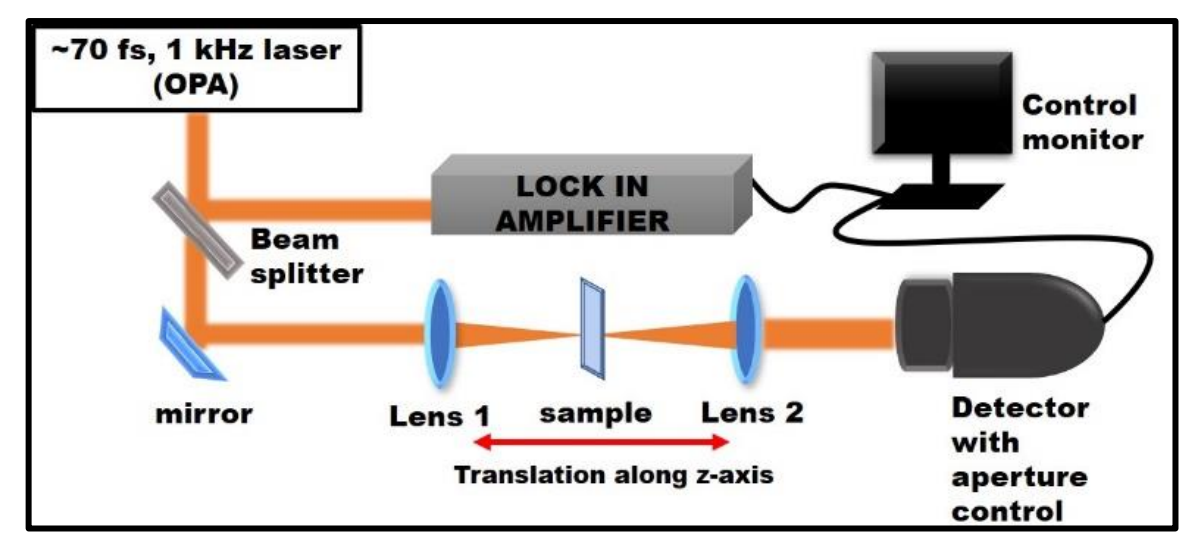


**Fig 2.12** Schematic layout of the Z-scan setup in kHz regime with Libra Ti:Sapphire mode-locked laser. The incident pulse is obtained from TOPAS C as ~70 fs, 1 kHz repetition rate pulses.

In this experimental setup, the 50 fs, 800 nm laser pulse enters TOPAS C where it undergoes frequency mixing via NLO phenomena (such as SHG, SFG, etc.). In this process, the output beam pulse broadens to ~70 fs duration at a desired wavelength. The output beam is then directed to two paths — one part of the beam travels to a lock-in amplifier which is connected to the computer system, the other beam travels through a focusing lens 1 (focal length 150 mm), to the sample whose transmitted light is recollected by lens 2 (focal length 75 mm). The detector has an aperture control to measure open and closed aperture z scan data. The transmitted beam collected at the detector is corrected with the reference beam from lock-in amplifier and recorded real-time on a computer system using LABVIEW software. The translational stage is also controlled by the LABVIEW software. To adjust the input beam intensity, ND filters are used in front of lens 1. Collected data is later fitted in Origin 8.5 using standard set of formulae as mentioned in section 2.4.

### **2.2.2 fs-TAS setup**:

The femtosecond transient absorption spectroscopy setup is shown in figure 2.13.

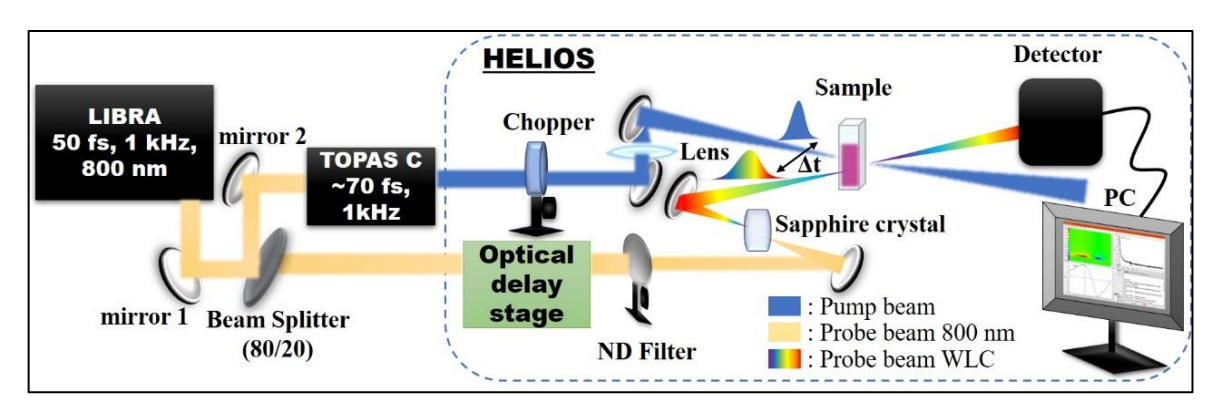


**Fig 2.13** Schematic layout of the fs-TAS setup which comprises of Libra mode-locked laser, OPA TOPAS C and HELIOS TAS setup.

In fs-TAS measurements, the excitation source is a Ti:Sapphire laser of 50 fs pulse duration, 1 kHz repetition rate, operating at 800 nm central wavelength. The output beam passes through a beam splitter (80-20), splitting the beam in the pathways – 80% to the optical parametric amplifier (TOPAS C) to produce pump excitation at a particular wavelength while 20% is directed towards white light generated probe beam. The 800 nm beam on entering the TAS setup HELIOS by Ultrafast Systems interacts with a Sapphire crystal to convert 800 nm beam to a white light continuum (WLC). The optical delay line installed inside HELIOS provided a delay range up to ~5 ns and can be controlled by a LabVIEW based system software. An optical chopper halves the pump frequency from 1 kHz to 500 Hz. The pump and probe beams are focused at the sample at a so-called magic angle (~54.7°). The transient signal is then collected by fiber-coupled multichannel detectors with kHz scan rates and the data is plotted with the help of the inbuilt Surface Xplorer software. The obtained TAS data can be globally fitted using a specialized program called Glotaran which is explained in details in section 2.5.2.

# 2.3. Optical Instruments:

Now that we have a detailed description of each of the optical setups involved in all the experiments discussed in this thesis, let us discuss about each significant optical instrument involved in the various experimental setups used in the present thesis.

# 2.3.1 LIBRA laser [35].

LIBRA is an ultrafast laser amplifier system manufactured by Coherent Inc. It is classified as a Class IV laser (under EN60825-1, clause 9) which produces ~50 fs, 1 kHz repetition rate output pulses at a central wavelength of 800 nm [35]. The Libra is an all-inone regenerative amplifier and ultrafast oscillator laser system. The six primary components are – Libra optical bench assembly, synchronization and delay generator (SDG), Vitesse (seed laser) power supply, Evolution (pump amplifier) power supply, closed loop water chiller and computer system with control software. The closed loop water chiller dissipates heat generated by the system and stabilizes the Vitesse, Evolution and amplifier cavity to typically ~21°C. The computer contains Windows-based control software for the Vitesse, Evolution and the SDG which can be remotely controlled with multiple serial-to-USB adaptors from the components' real panel to the computer. A brief description of Vitesse, Evolution and SDG which comprises the optical bench assembly is given below,

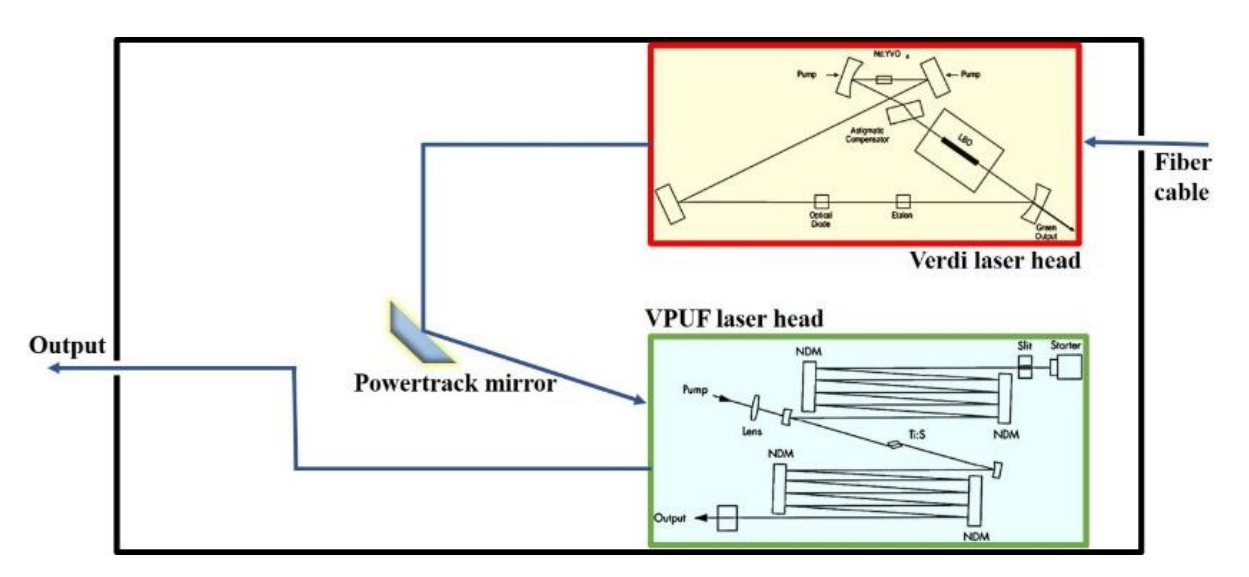


Fig 2.14 Schematic layout of Vitesse (seed) laser head of LIBRA. (consulted from Operator's manual).

i. VITESSE [36]: Vitesse is a compact Verdi pumped ultrafast laser that produces mode-locked, sub-100 fs pulses at 80 MHz repetition rate with an output power >200 mW (average power) at 800 nm (see figure 2.14). The laser head of Vitesse seed laser consists of 532 nm Verdi laser head as the pump laser, a power track mirror and the Verdi Pumped Ultrafast (VPUF) laser head.

The **Verdi pump laser** contains a single frequency ring cavity with cavity mirrors mounted on a kinematically mounted Invar plate. The Invar provides both mechanical strength and

low coefficient of expansion. The cavity is sealed hermetically to reduce environmental impact on laser head components. Astigmatism introduced by off-axis spherical mirrors is compensated by a tipped plate in the focused beam. The Verdi pumped gain medium is Nd:YVO4 (Neodymium: Yttrium Orthovanadate) which has high absorption coefficient in 808 nm, large stimulated emission cross-section around 1064 nm and a strong line of emission around 1064 nm. This makes Nd:YVO<sub>4</sub> an ideal choice for pump laser. Being anisotropic in nature, Nd:YVO4 shows two different focal lengths for light polarized perpendicular to the optic axis and two different focal lengths for light polarized parallel to the optic axis. This leads to astigmatism which can be minimized by regulating the material's temperature. An LBO crystal is used for second harmonic generation. It is because, LBO has low absorption in visible to IR (infrared) range, high damage threshold and is non-hygroscopic. It is a Type I, non-critical phase matching medium where the fundamental wavelength, 1064 nm, is phase-matched with second harmonic, 532 nm, at a crystal temperature of ~148°C. While the optical diode in the Verdi pump forces unidirectional operation, the etalon placed in the cavity insures single-frequency operation by suppressing unwanted longitudinal modes from lasing. The etalon used in the pump laser is temperature-controlled. Thus, adjustment of etalon temperature (operating range: 10-70°C) can shift the etalon loss curve to be tuned to a desired mode. A **power track mirror** actively maintains optimum pump beam alignment into the VPUF cavity serving to minimize the fluctuations in the ultrafast output power. The **VPUF** is an ultrafast cavity that uses Ti:sapphire as the gain medium. Multiple reflections from the NDMs (Negative Dispersion Medium) provide total negative dispersion required to produce sub-100 fs pulses. VPUF is built on an Invar plate that uses Kerr-lens mode-locking (KLM) to produce desired pulses. In Vitesse, initially the laser operates in CW mode, then a proper cavity length is introduced which induces very high-power fluctuations. Once an instantaneous power becomes sufficiently high, a Kerr lens is formed narrowing the beam enough to pass unattenuated through the slit. The pulse is then amplified and become the dominant pulse that form the mode-locked output. An ultrashort laser pulse is intense and consists of a distribution of wavelengths accompanied by NLO effects. This can lead to various undesired optical phenomena that affects the laser output. Hence, it is essential to compensate these phenomena as listed below:

*Group Velocity Dispersion, GVD:* causes temporal re-shaping (broadening or narrowing) of wave-packets from their initial conditions. This is known as chirp. A positive chirp is

when the blue spectral components are retarded with respect to the red spectral components while the opposite is true for a negatively chirped pulse.

Self-phase Modulation, SPM: here an intense pulse propagating through a dense medium create a local index of refraction that is dependent on the light field intensity. This is also known as the Kerr effect which can essentially lead to certain parts of the wave moving faster than the rest, thus, altering the pulse shape. To compensate for GVD and SPM, NDM filters are used which use the technique of Gires-Tournois Interferometer [37] with the help of dielectric mirrors (reflectance >99.95%) to provide negative group velocity dispersion over the expanded femtosecond bandwidth.

**ii. SDG** [38]: The Synchronization and Delay Generator, SDG Elite, provides digital control of the timing signals and high voltages required to operate a regenerative amplifier laser system. The front panel (see figure 2.15(a)) indicates to various control buttons while the rear panel (see figure 2.5(b)) indicates the different connections with the regenerative amplifier system.



**Fig 2.15** (a) Front panel of SDG Elite showing all necessary controls of regenerative amplifier. (b): Rear panel showing all possible connection ports of device to SDG. (taken from SDG Operator's manual).

Here the regenerative amplification is dependent on the precise coordination of the mode-locked seed source, amplifier pump source and amplifier Pockels cells which control pulse injection and ejection. The SDG Elite accepts input from the seed laser (Vitesse) and pump laser (Evolution), then outputs a trigger signal for each Pockels cell at an adjustable delay. Additional delays are provided for synchronization which can operate at the pump laser frequency or a divisor thereof.

iii. Evolution [39]: The Evolution-HE is a diode-pumped, intra-cavity doubled, Q-switched Nd:YLF laser capable of producing 45W of average power and >45mJ of 527nm pulse energy at 1 kHz. It is most suitable for pumping high-power Ti:sapphire amplifiers and for materials processing. The Evolution-HE laser system mainly comprises of an optical laser bench assembly, power supply assembly and a control computer. The Evolution-HE optical laser bench contains a diode-pumped, water-cooled, Nd:YLF laser head (pump chamber), an optical resonator, an acousto-optical Q-switch, a LBO frequency-doubling crystal in a temperature controlled oven and safety shutter. The power supply assembly includes a master control board and all the electronics to drive the laser diodes, stabilize the temperature of the LBO crystal, Q-switch the laser, and monitor interlocks. The Evolution-HE comes with a commercial laptop computer and software to control and monitor the functions of the laser via a RS-232 interface

#### **Pulse duration of LIBRA HE:**

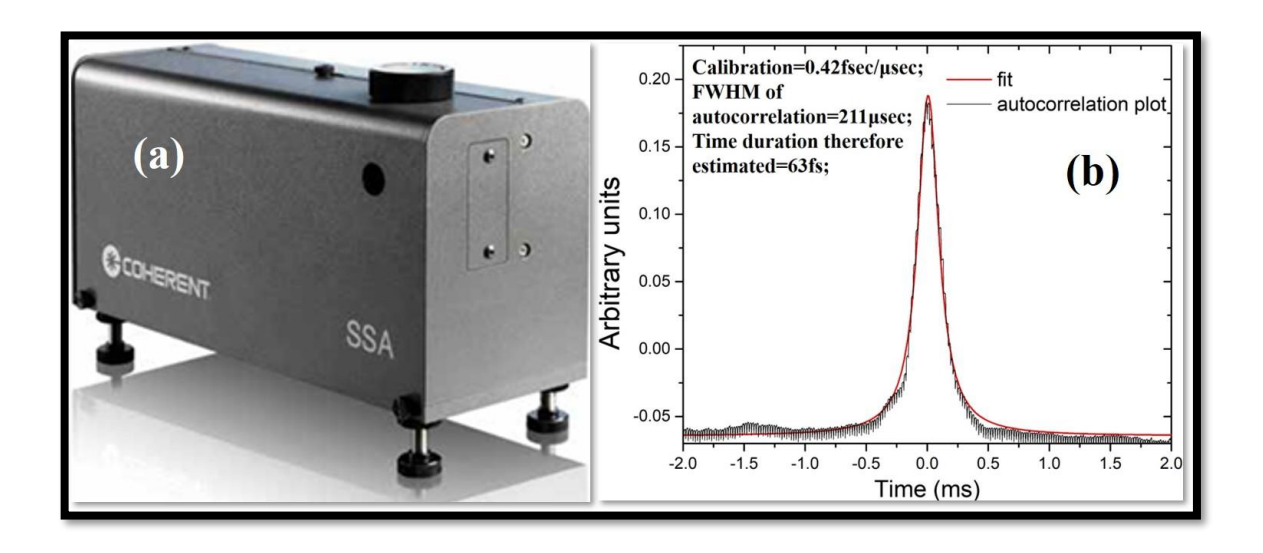


Fig 2.16 (a): SSA by Coherent. Inc. (b): LIBRA HE pulse characterization using the SSA.

The LIBRA HE is manufactured to ideally produce ~50 fs, 1 kHz pulses at 800 nm central wavelength. However, various optical and environmental conditions can broaden the pulses which can slightly deviate from the ideal pulse duration value. This is important for experimental precision in our measurements and calculated using a Single Shot Autocorrelator (SSA) by M/s Coherent Inc. [figure 2.16(a)]. The obtained data is fitted using Gaussian fit showing obtained pulse duration to be ~63 fs [figure 2.16(b)].

# 2.3.2. TOPAS C [40]:

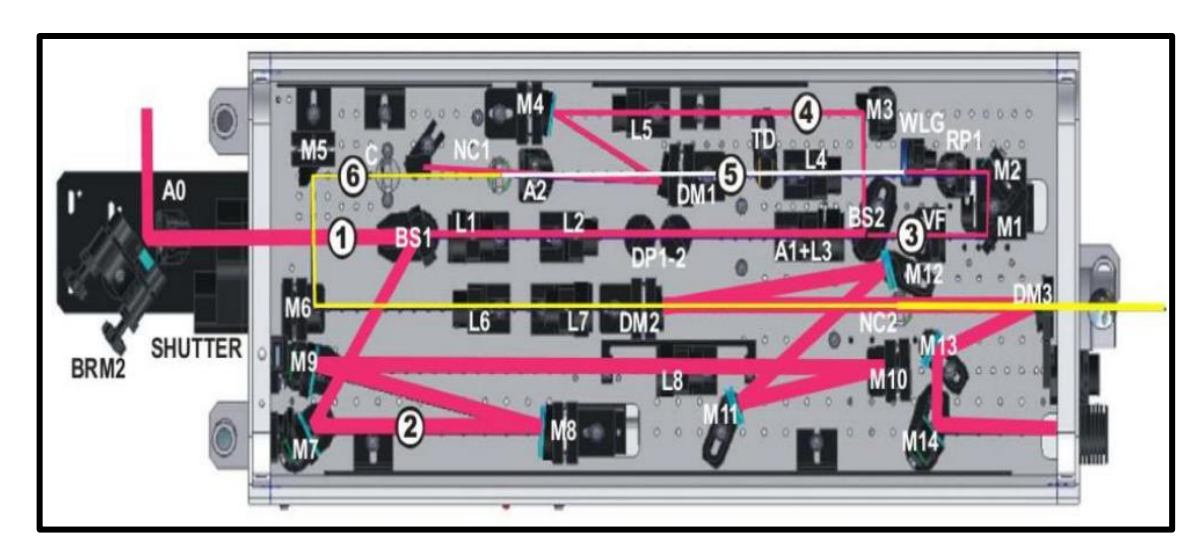
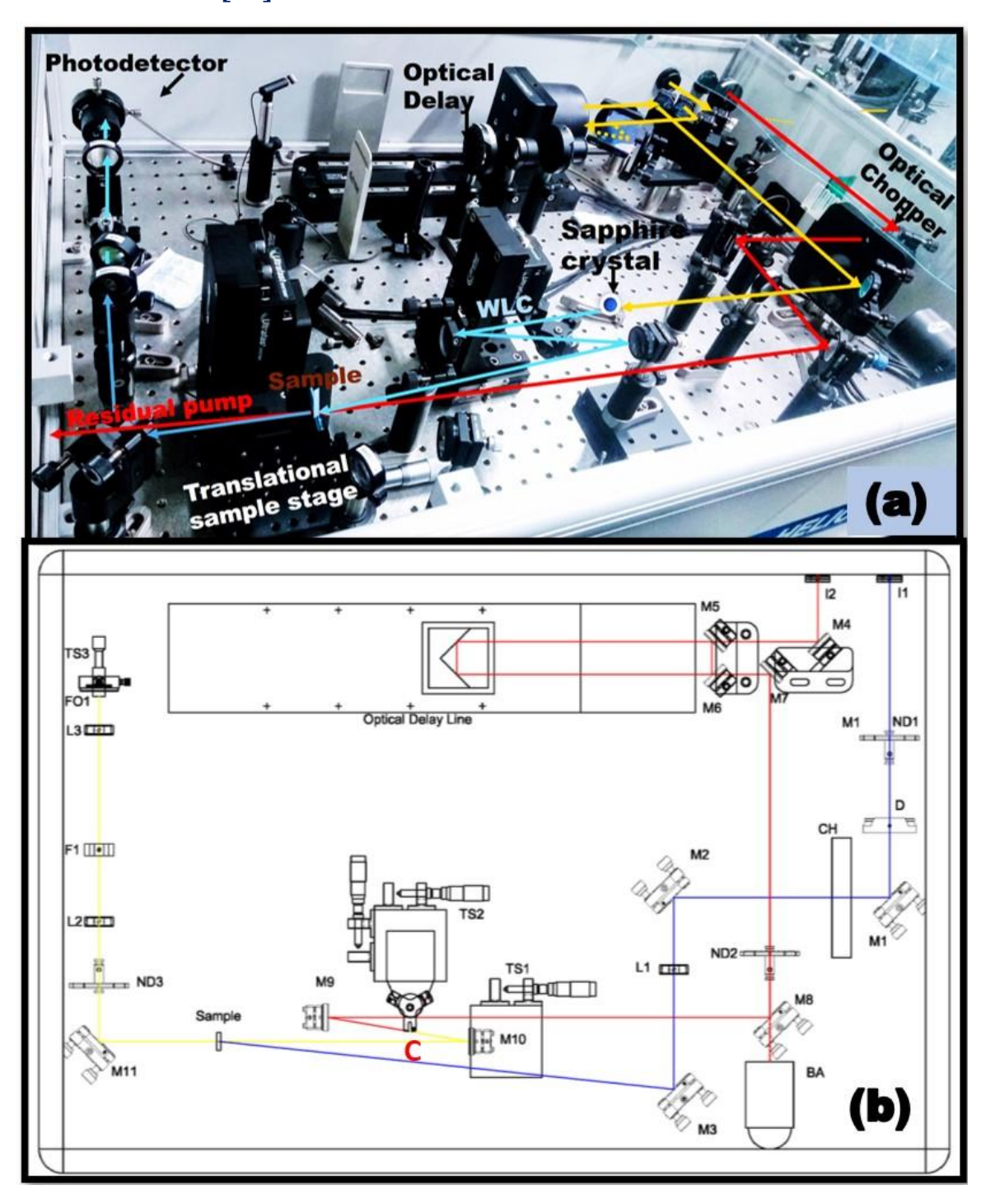


Fig 2.17 Optical layout of TOPAS-C (taken from TOPAS C Operator's manual).

The Travelling wave Optical Parametric Amplifier-C (TOPAS-C) comprises of a two-stage amplifier with the most important components being – pre-amplification stage PA1, WLC and second amplification stage PA2. From the schematic in figure 2.17, the OPA receives 80% of the 800 nm beam from Libra, which is again split for WLC generation (~μJ) and the PA1. For WLC, a sapphire crystal is used which is focused on a BBO crystal (NC1) non-collinearly with the remaining part of the 800 nm beam. Here parametric amplification takes place and then the amplified beam is further expanded and collimated to PA2. In PA1, wavelength tuning can be done by adjusting the WLC delay of the pulse with respect to the NC1 crystal phase matching angle and the pump pulse. In PA2, the power amplifier is pumped by another bulk of the 800 nm pump beam followed by the pump and signal beam to overlap in the second BBO crystal NC2 where a well collimated signal and idler beam is created. Here, the tuning is done by optimizing the NC2 angle and the signal delay w.r.t the second pump beam. It is to be noted that the 800 nm pump beam quality is equally crucial for an optimized stable OPA output and hence, a good beam profile with proper mode-locking is important.

# 2.3.3. HELIOS [41]:



**Fig 2.18** (a) Inside layout of HELIOS TAS setup showing beam propagation of pump (red arrow) and probe (yellow and blue arrows) pulses along with labelled major optical components involved (b): Schematic layout of HELIOS TAS setup for visible wavelength range. (*taken from HELIOS 6.9.1 Operator's manual*).

Helios is a pump-probe transient absorption spectrometer (broadband) which is intended to work with an femtosecond Ti:sapphire amplifier to produce the spectral and kinetic data needed for investigations of photoexcitation events on the fs and/or longer timescales. The

actual setup used in lab has been shown in figure 2.18(a) while the schematic layout is given in figure 2.18(b). The HELIOS has been configured for the spectral window in the visible range of 450–800 nm with a spectral resolution of 1.5 nm. The temporal resolution is around 7 fs with a time window of 3.3 ns. The instrument response function (irf) is roughly 1.4×(FWHM of pump pulse). The optical chopper is depicted as 'Ch' in figure 2.18(b). The layout shows that pump beam enters through iris 1 (I1) while the probe beam enters though iris 2 (I2). The delay line configuration consists of a series of reflecting mirrors to maximize the probe delay in a confined area. To align the probe beam with optical delay line, a BA tool is provided in the software which is connected to a CCD placed along the beam line as shown in the figure.

Neutral density filters ND1 and ND2 are used to adjust pump and probe beam intensities respectively, prior to sample interaction. The WLC is generated at 'C' in figure 2.18(b) where a Sapphire crystal is mounted on a moveable stage to adjust the WLC profile. Mirrors M3 and M10 are used to make the pump and probe beams interact with the sample at the magic angle. The transmitted probe pulse is then detected at FO1–a fibre optics coupled multichannel spectrometer with CMOS sensor with maximum spectral acquisition rate of 9500 spectra/s. The data acquisition along with data collection parameters and translational stages inside the setup are computer-controlled via the in-built software HELIOS<sup>TM</sup>. HELIOS produces a 3-D wavelength-time-absorbance data matrix in a form of an ASCII (CSV) file, which can be easily processed with Surface Xplorer or any third-party/home-made software.

# 2.4. Data Analysis Z-scan technique:

The analysis of Z-scan data is mostly theoretical using a set of formulae provided in the literature by Sheikh Bahae et al. 1999 [13]. To compare the quality of the fit with experimental results, Microsoft Origin 8.5 was used. In Origin, the raw data is plotted for the Transmittance versus Z axis in mm as shown in figures 2.19(a) and 2.19(b). Both the X and Y-axes are normalized before fitting as shown in figures 2.19(c) and 2.19(d).

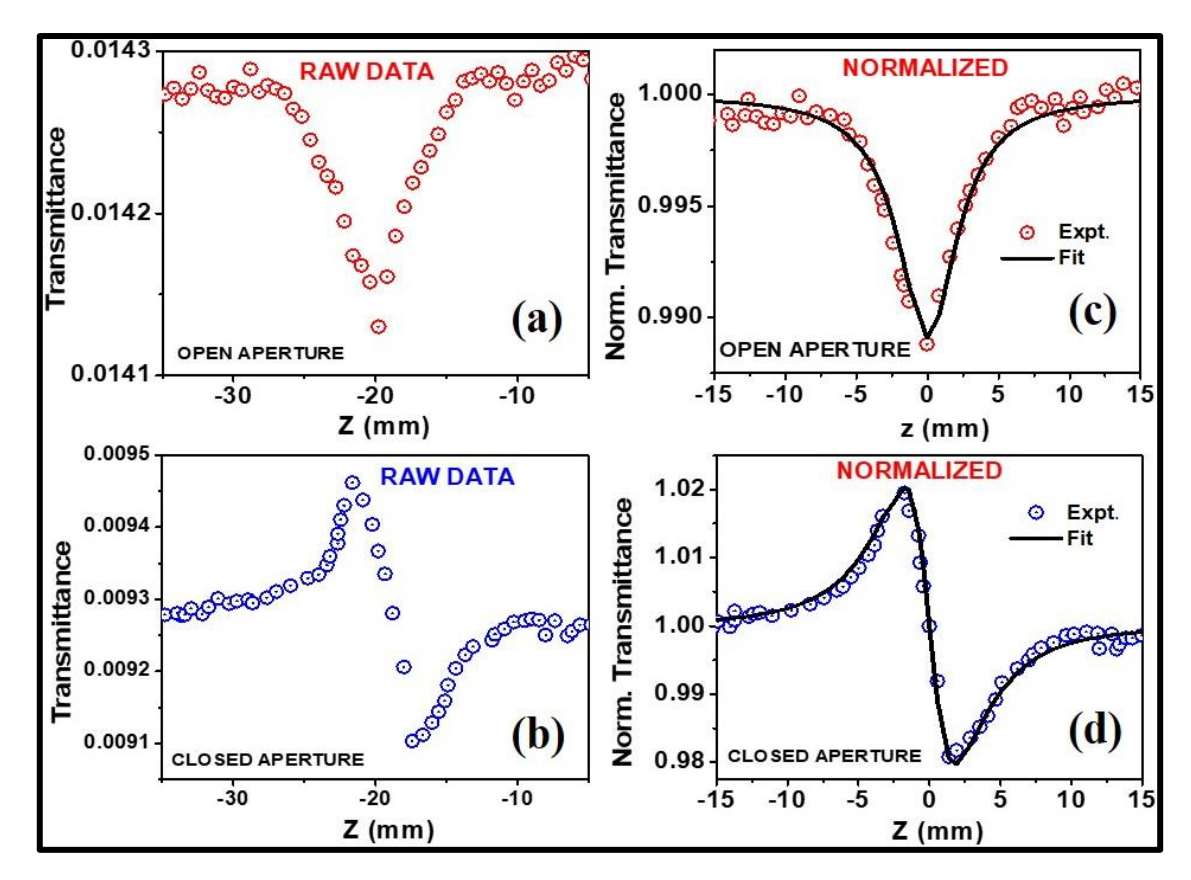


**Fig 2.19:** Raw data obtained from Z-scan experiment taken for dichloromethane (DCM) solvent at 800 nm shown as **(a):** red circles for open aperture data and **(b):** blue circles for closed aperture data. **(c):** Normalized raw data (red circles) for open aperture, best fitted as black solid line. **(d):** Normalized raw data (blue circles) for closed aperture, best fitted as black solid line.

In order to fit the graph, we need to ascertain few parameters obtained from the experimental conditions – input intensity (I<sub>0</sub>), linear transmittance (L<sub>T</sub>), Rayleigh range (Z<sub>0</sub>) and beam waist ( $\omega_0$ ). As the cuvette length used is 1 mm (mentioned in previous section), the effective length can be calculated as:  $L_{eff} = 1 - \frac{e^{-(n-1)\alpha_0 L}}{(n-1)\alpha_0}$  where  $\alpha_0$  is linear transmittance that can be obtained from L<sub>T</sub> while 'n' determines the type of nonlinear interaction which can be 2 for two-photon absorption, 3 for three photon absorption and so on. Using the above values, we can fit the experimental result for open aperture data as follows:

$$T_{nOA} = \frac{1}{\left[1 + (n-1)\alpha_n L_{eff} \left[\frac{I_0}{1 + \left(\frac{Z}{Z_0}\right)^2}\right]^{(n-1)}\right]^{\frac{1}{(n-1)}}}$$
(2.25)

Here, ' $\alpha_n$ ' is the fitting parameter which is also the nonlinear absorption co-efficient. Similarly, the closed aperture studies were fitted using the following expression:

$$T_{CA} = 1 \pm \frac{4\Delta\varphi(\frac{z}{z_0})}{\left[\left(\frac{z}{z_0}\right)^2 + 9\right]\left[\left(\frac{z}{z_0}\right)^2 + 1\right]}$$
(2.26)

where the radial phase ' $\Delta \varphi$ ' is the fitting parameter which is used to obtain the nonlinear refractive index  $n_2$  as:  $n_2 = \frac{\Delta \varphi \lambda}{2\pi I_0 L_{eff}}$  (2.27)

The solid lines in figures 2.19(c) and 2.19(d) depict the best fitted Z-scan data in Origin for open and closed apertures respectively. From the fitted data, we obtain the value of nonlinear absorption  $\alpha_n$  and nonlinear refractive index  $n_2$  (using eqns. 2.25 and 2.27). Using the values of  $\alpha_n$  and  $n_2$ , the third order nonlinear susceptibility  $\chi^{(3)}$  was calculated using the expression,

$$\chi^{(3)} = [(\chi_{R}^{(3)})^{2} + (\chi_{I}^{(3)})^{2}]^{1/2}$$
(2.28)

where 
$$\chi_R^{(3)} = 2cn_0^2 \varepsilon_0 n_2$$
 and  $\chi_I^{(3)} = \frac{c^2 \varepsilon_0 n_0^2 \alpha_n}{\omega}$  (2.29)

with  $n_0$  =linear refractive index (e.g. ~1.5 for glass),  $\varepsilon_0$  = absolute permittivity,  $\omega$  = laser frequency.

The nonlinear absorption cross-section can be calculated as:

$$\sigma_n = \frac{(\hbar\omega)^{n-1}}{N} \alpha_n. \tag{2.30}$$

Here,  $\hbar$  is the reduced Planck's constant while 'N' is the number of solute molecules in the given solution given by:  $N = N_A \times$  (sample molar concentration);  $N_A$  is Avogadro's number.

Molecules possessing good optical nonlinearity often find their application as optical limiters (as discussed in Chapter 1), the quality of which can be determined using fluence measurements.

From Z-scan technique, one can measure the sample fluence

Fluence = 
$$\frac{4\sqrt{\ln 2}E_{in}}{\pi^{3/2}\omega^2(z)}$$
 (2.31)

where  $E_{in}$  is the input laser pulse energy and  $\omega(z)$  is the beam radius at a z-position. To understand the NLO characterization using Z-scan technique, we demonstrate a study as a sample experiment below.

# 2.5 TAS data analysis:

# 2.5.1. Data Analysis using Surface Xplorer [42]:

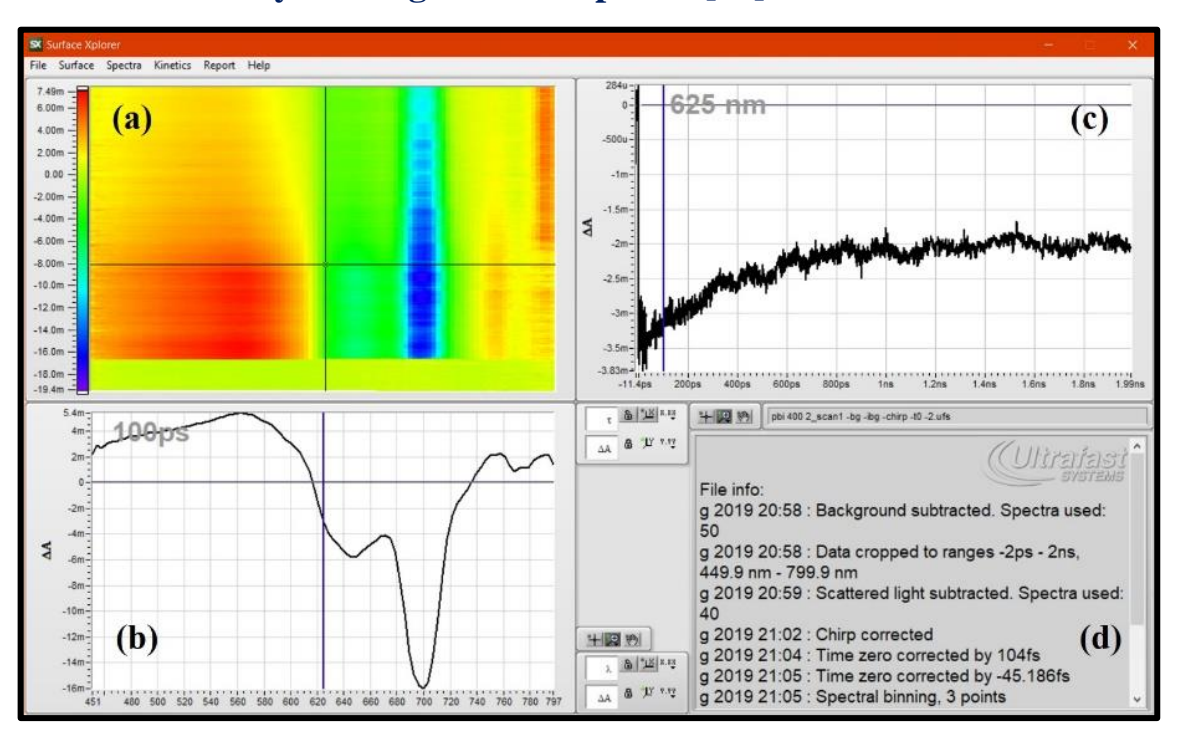


**Figure 2.20** (a) 3D surface plot of TAS data with X-axis as wavelength (nm), Y-axis as time delay (ps) and Z-axis is difference absorption  $\Delta A$  which is depicted in terms of a colour scale showing minimum to maximum transition from blue to red (b): Spectral evolution at a particular time (e.g. 100 ps). (c): Kinetic evolution at a particular wavelength (e.g. 625 nm) (d): Data pre-processing (e.g. background, chirp correction, time zero, etc.)

Surface Xplorer is an in-built software that comes with the HELIOS, Ultrafast Systems. All recorded data from Helios can be directly opened in Surface Xplorer as a '.ufs' file as shown in figure 2.20 below. The data window is divided into four quarters – (a), (b), (c) and (d). While quadrant (a) shows the entire data acquired at various delays (as Y-axis) over the entire visible spectrum (as X-axis) with corresponding change in the difference absorption (as Z-axis), quadrant (b) shows the spectral evolution only and quadrant (c) shows only the kinetic information. The obtained data can be further cleaned and preprocessed using the 'Surface' option on the top left menu of the Surface Xplorer window as shown in the figure 2.20. Here, the data can be cropped, corrected for background noise followed by chirp correction. The scatter and spikes can also be corrected before you obtain a clean processed data that is ready for analysis. All these modifications are accordingly

reflected on quadrant (d). The spectral data can be plotted for various delays to observe how the particular transient spectra evolves, the positive signal (i.e.  $\Delta A > 0$ ) denotes contribution from excited state absorption or ESA while the negative signal (i.e.  $\Delta A < 0$ ) can indicate contribution from ground state bleaching (GSB) and/or stimulated emission (SE). The kinetic data evolves along with the spectra and fitting the kinetic curve can give us the decay lifetime of the particular excited state component denoted by ' $\tau$ '. In order to fit a particular kinetic data, we can go choose the 'Fit kinetic' option from 'Kinetic' tab on the menu bar in the Surface Xplorer window (see Figure 2.20 top left side). A data fitting window appears as shown in figure 2.21 below. Based on a multiexponential decay model:

$$y(t) = t_0 + \sum_{i=0}^{n-1} irf \otimes A_i e^{\frac{-t}{\tau_i}}$$
 where  $t_0$  is defined as time zero or zero delay from which

the transient signal rises, ' $\tau_i$ ' is the corresponding lifetime component with amplitude ' $A_i$ ' and  $\otimes$  denotes the convolution of decay signal with instrumental response function or *irf*, the data is fitted and best fit parameters are shown as (a) in figure 2.21. These parameters can be played with for a best fitted curve that is shown as red solid line in (b) with blue circles showing the experimental data. Accuracy of the fit can be determined from the standard deviation shown in the bottom left corner of the window (in figure. 2.21).

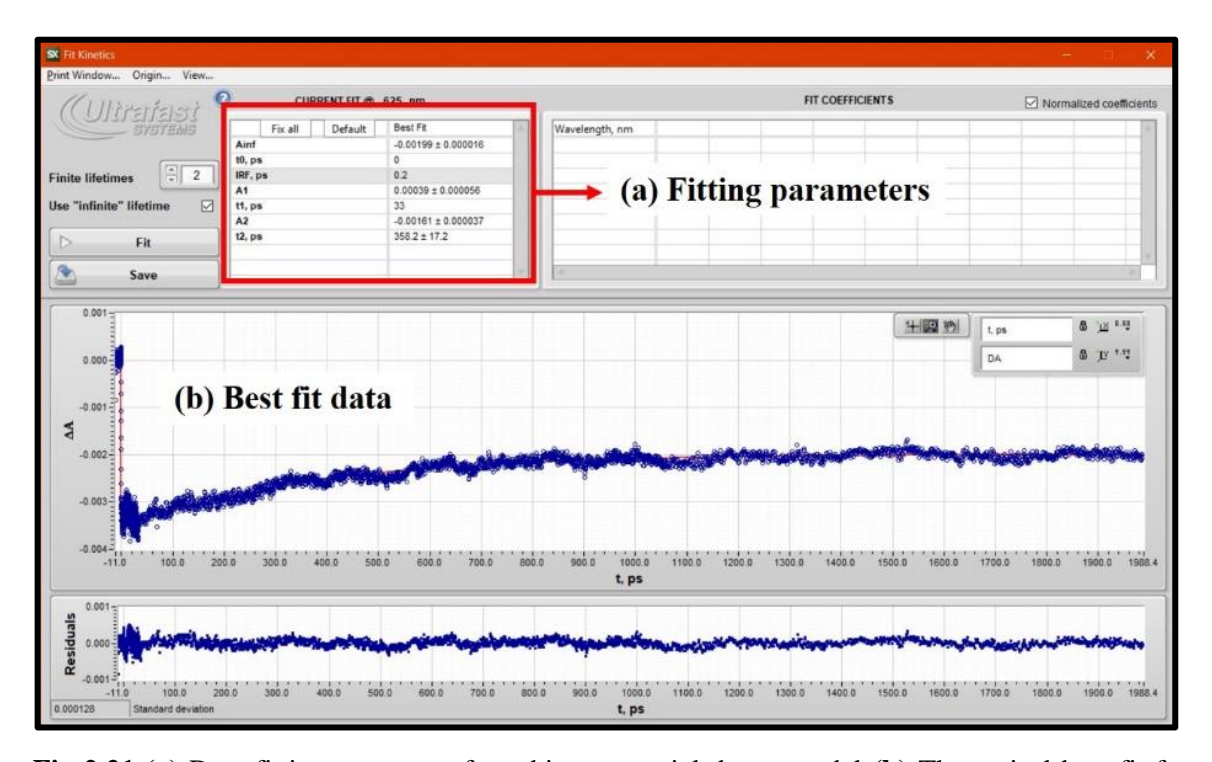
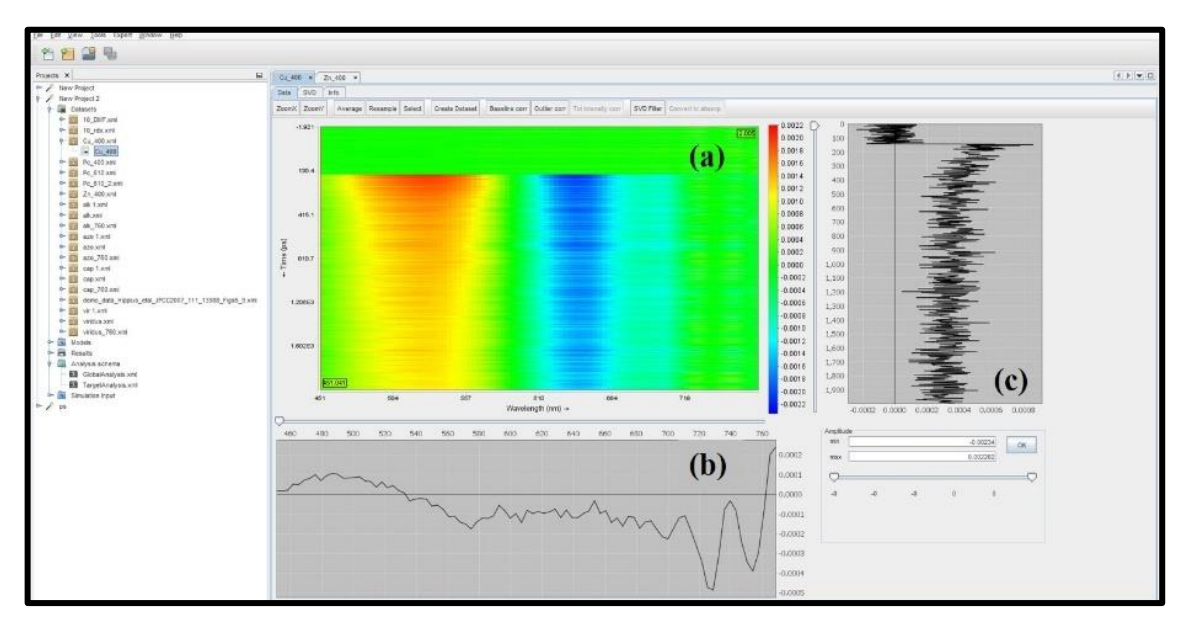


Fig 2.21 (a) Data fitting parameter for a bi-exponential decay model (b) Theoretical best fit for given parameters shown as red solid line over experimental data shown by blue circles.

Usually, in a TAS data, the kinetics at each band maxima are analyzed for decay lifetime components in order to understand the relaxation dynamics of the particular sample. The single wavelength technique is however, often insufficient or inconclusive to determine the exact lifetime components of the particular excited sample. This is due to the fact that, in most cases multiple processes occur within the same time scale. To solve this, advanced spectro-temporal parameterization like global analysis technique is implemented.

### 2.5.2. Data Analysis using Glotaran 1.5.1:

Introduced in 2008 by Snellenburg, Van Stokkum, and Mullen [43], Glotaran is an R-based GUI which stands for **Glo**bal and **tar**get **an**alysis. It is an easy-to-use modelling and data analysis tool that find its application in large and complex time-resolved spectroscopy and microscopy datasets. A time-resolved spectroscopic data for a variable wavelength range can be written as a data matrix with 'n' number of superimposed components:  $\Psi(\lambda,t) = \sum_{i=1}^{n} c_i(t)\varepsilon_i(\lambda)$  where,  $c_i$  and  $\varepsilon_i$  are the unknown concentration profile and spectrum of component 'i' respectively. The dataset can be imported to Glotaran in the form of '.ascii' or '.csv' file.



**Fig 2.22 (a)** Sample dataset showing a 3D profile with **(b)** horizontal axis showing spectral profile and **(c)** vertical axis showing the corresponding temporal profile.

For global analysis, the steps involved are:

i. **Data pre-processing:** Once the dataset is loaded on Glotaran, the dataset window appears as shown in figure 2.21. The vertical axis indicates the time profile [figure 2.22 (b)] while the horizontal axis indicates the spectral profile [figure 2.22 (c)]. The menu

bar on the top of the dataset (a) contains options to process the raw data for averaging, baseline correction, outlier correction, etc. The processed data can then be saved using "Create dataset" option.

**ii. Singular Value Decomposition (SVD):** The SVD factorizes the obtained data matrix into a number of spectrally and temporally independent components that indicates to the number of independent components in the data. Mathematically,

$$\psi(\lambda, t) = \sum_{n=1}^{n_{max}} u_n(t) \omega_n(\lambda) S V_n$$
 (2.32)

where,  $n_{max}$  is the minimum number of independent components in the dataset. Ideally, the singular values  $SV_n$  satisfy the condition:  $SV_1 \ge SV_2 \ge ..... \ge SV_{n_{comp}} > SV_{n_{comp}+1} = 0$ ;  $n_{comp}$  being total number of independent components. Figure 2.23 shows the SVD window in Glotaran where (a) shows the singular values on a logarithmic scale in decreasing order followed by the corresponding (b) left and (c) right singular vectors denoted as ' $u_n(t)$ ' and ' $\omega_n(\lambda)$ ' in eqn. 2.32, respectively.

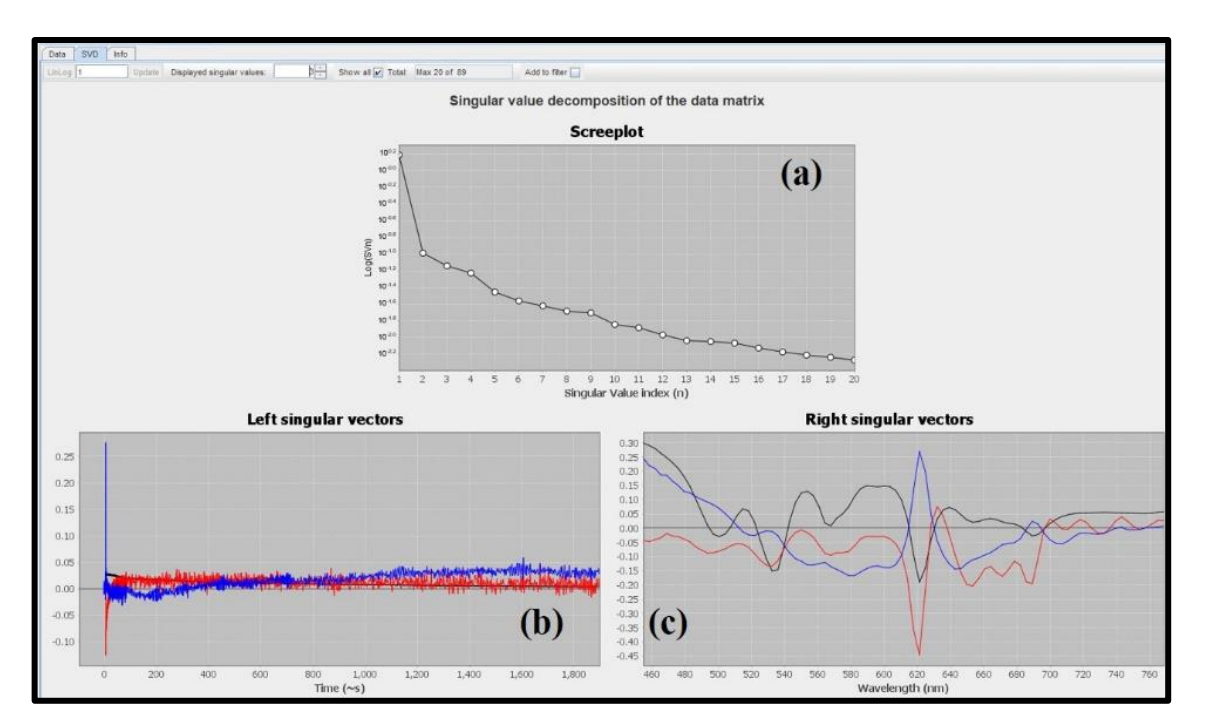


**Figure 2.23:** Singular value decomposition of the data-matrix of a sample dataset where (a) is the screen plot, (b) left singular vectors (temporal profile) and (c) right singular vectors (spectral profile) obtained from the dataset depicted as black, red and blue lines.

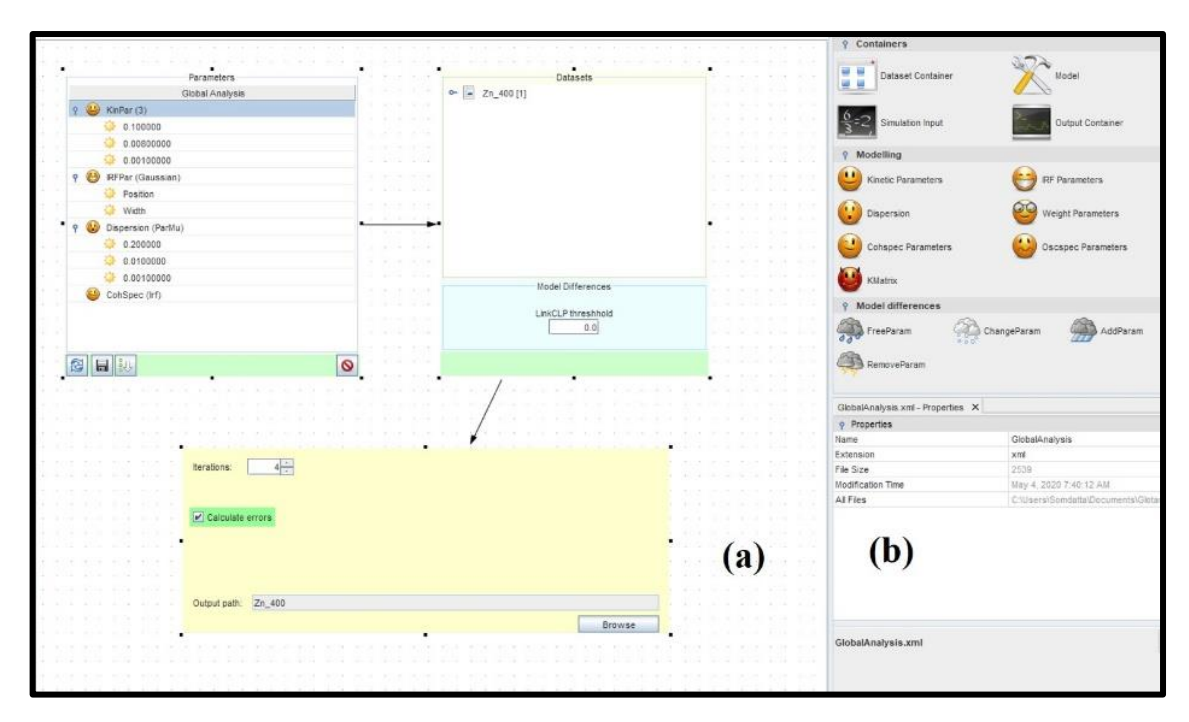


**Figure 2.24** Analysis scheme window where (a) is the visual modelling window which consists of input window to load data (right), parameter window to initial parameters to the model (left) and output window (bottom middle) and (b) various modelling parameters to be introduced to the kinetic model.

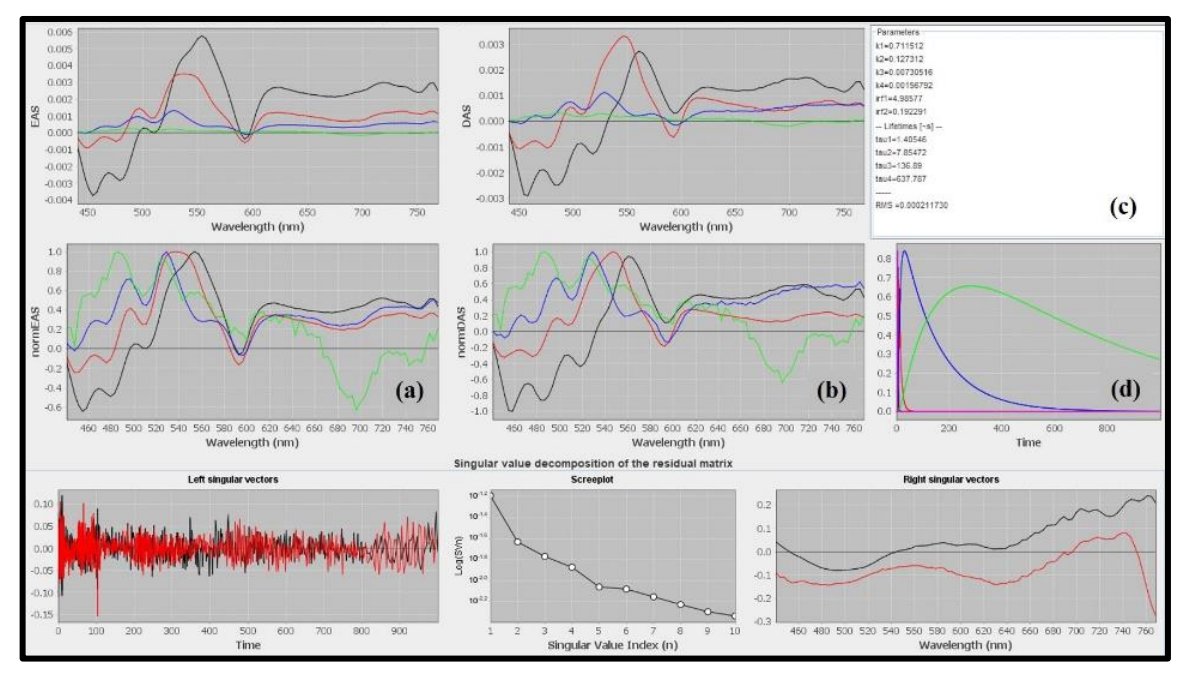


**Figure 2.25** Analysis scheme window where (a) is the visual modelling window which consists of input window to load data (right), parameter window to initial parameters to the model (left) and output window (bottom middle) and (b) various modelling parameters to be introduced to the kinetic model.

**iii. Visual modeling:** In this section, we open an analysis scheme window where a kinetic model can be specified for the current data and initial parameters defined (see figure 2.24). It uses a global analysis scheme (pre-loaded in the software) where one can load

the dataset in a window and link it to a parameter window as shown in figure 2.24(a). In the parameter window, we can assign few initial values estimating from the dataset and run iterations in the output window placed at the bottom middle in figure 2.24 (a). The modelling parameters can be called in from a list of various parameters as shown in figure 2.24(b).

**iv. Result analysis:** On running the kinetic model for a decent number of iterations, the resultant output window is shown in figure 2.25. In the visual modelling section, the global analysis kinetic model can be a parallel rate model resulting in corresponding to decay associated spectra or DAS as:

$$\Psi(\lambda, t) = \sum_{i=1}^{n_{comp}} c_i^{DAS}(t, \theta) DAS_i(\lambda)$$
 (2.33)

where  $c_i^{DAS}(t,\theta)$  is exponentially decaying concentration of 'i' component convoluted with *irf*. The DAS spectra is shown in figure 2.25 (b). In a sequential or unbranched unidirectional kinetic model, the associated spectra are called evolution associated spectra (EAS) with successive lifetimes and can be written as:

$$\Psi(\lambda, t) = \sum_{i=1}^{n_{comp}} c_i^{EAS}(t, \theta) EAS_i(\lambda)$$
 (2.34)

The EAS spectra is shown in figure 2.25 (a) with the obtained rate constants and lifetimes in figure 2.25 (c). Figure 2.25 (d) shows how the excited species population evolves over the delay range corresponding to each spectrum. The accuracy of the kinetic model can be determined by the rms or root mean squared values of the obtained lifetime components along with the SVD residual matrix tab where black line is the experimental fit while red line is the data fit.

### 2.6. Sample Experiment

## 2.6.1. The Z-scan Experiment

A novel phthalocyanine molecule TPA-ZnPc (Triphenylamine Zinc Phthalocyanine,  $C_{104}H_{68}N_{12}Zn$ ) and a novel porphyrin ZnTPP (Zinc Tetraphenylporphyrin,  $C_{44}H_{28}N_4Zn$ ) were studied for NLO properties using the Z-scan technique. Their respective molecular structures and absorption spectra can be seen in figure 2.26 below. This work has been published in JOLT 2018 [44].

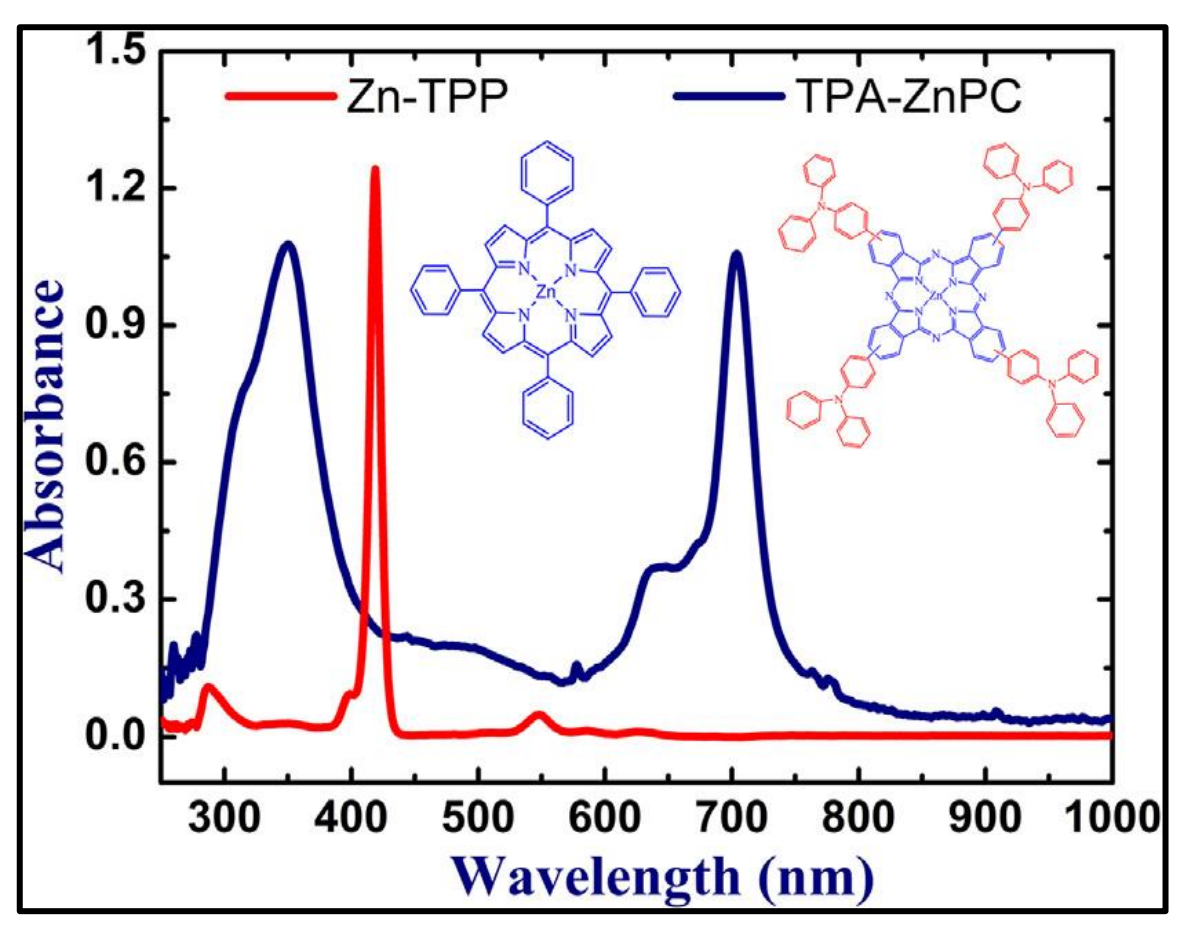


**Fig 2.26** UV-vis absorption spectra of TPA-ZnPc (blue solid line) and ZnTPP (red solid line) with their molecular structures as insets – ZnTPP on left and TPA-ZnPc on right.

The samples were investigated in the 700–950 nm range of wavelengths using a Ti:Sapphire femtosecond tunable laser. The Chameleon is a 150 fs, 80 MHz rep. rate laser with a tunable range of 680–1080 nm. Both TPA-ZnPc and ZnTPP were studied in 1–10  $\mu$ M solution in dichloromethane or DCM. In the experimental setup as shown in Figure 2.11, lens 1 has a focal beam (f) of 100 mm which focusses the ~2mm (d) input beam onto the sample. The Rayleigh range for the aforementioned wavelength ( $\lambda$ ) range was calculated to be 2.2–3 mm from the expression:  $z_0 = \frac{\pi \omega_0^2}{\lambda}$  where  $\omega_0$  is the beam waist calculated as:  $\omega_0 = \frac{2 \times f \times \lambda}{\pi \times D}$ . The input light intensity,  $I_0$  was kept within the range 2.6–47 MW/cm². In this incident intensity range, both the molecules show strong RSA of which TPA-ZnPc show two-photon absorption or 2PA within 700–850 nm excitation as shown in figures 2.27(a)–(d). In figures 2.27(e) and 2.27(f), three-photon absorption or 3PA was dominant for 900 nm and 950 nm wavelengths. The closed aperture studies as shown in

figures 2.27(g)–(l) show a clear peak followed by a valley. This is indicative of negative n<sub>2</sub> or self-defocusing behavior of the molecule.

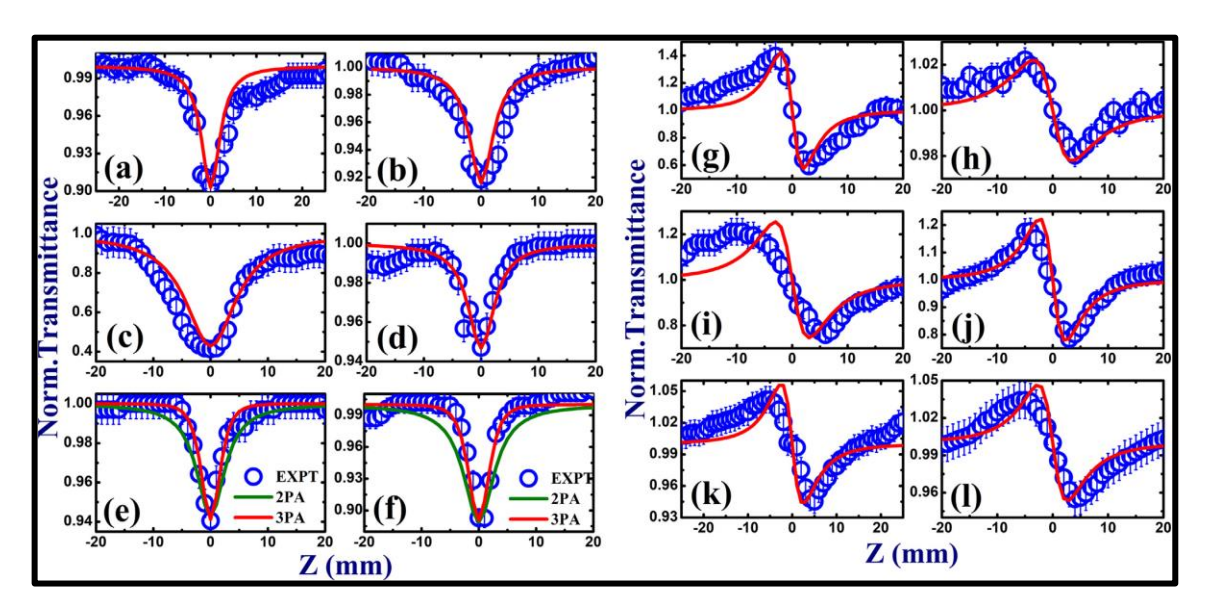


**Figure 2.27:** Open aperture Z-scan data of TPA-ZnPc at (a) 700 nm, (b) 750 nm, (c) 800 nm, (d) 850 nm, (e) 900 nm and (f) 950 nm. Closed aperture Z-scan studies of TPA-ZnPc at (g) 700 nm, (h) 750 nm, (i) 800 nm, (j) 850 nm, (k) 900 nm and (l) 950 nm. Blue circles denote to experimental points while the solid lines denote fitted data.

Similar results were obtained for the porphyrin ZnTPP except ZnTPP showed three-photon absorption at 950 nm only [see figures 2.28(a)–(f)]. The closed aperture studies showed a self-defocusing behavior similar to TPA-ZnPc [see figures 2.28(g)–(l)]. The obtained data for both the molecules were fitted using equations mentioned in section 2.4. where the fitted data is depicted as the solid red line in figures 2.27 and 2.28 (a)–(l). The green solid lines in figures 2.27(e), 2.27(f) and 2.28(f) illustrate that the 2PA does not fit the given data best but 3PA (shown as red solid line) does. From the fitted data, NLO coefficients obtained has been summarized in Table 2.1 below. In order to determine and compare the optical limiting response of TPA-ZnPc and ZnTPP, fluence measurements were performed using equation 2.31. The fluence was further plotted against transmittance and the obtained curve was extrapolated (figure 2.29) to obtain fluence thresholds given in table 2.1.

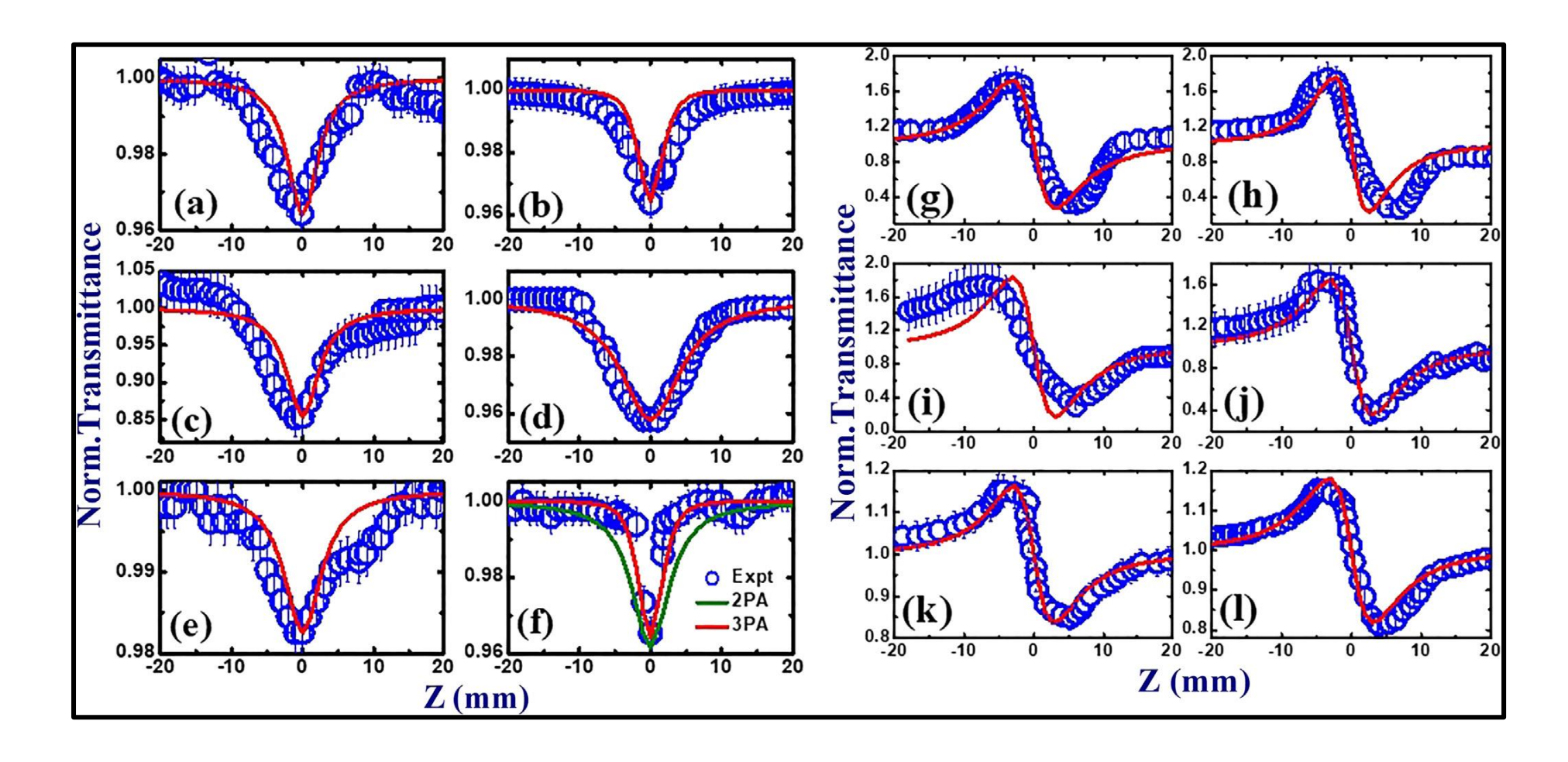


Figure 2.28 Open aperture Z-scan data of ZnTPP at (a) 700 nm, (b) 750 nm, (c) 800 nm, (d) 850 nm, (e) 900 nm and (f) 950 nm. Closed aperture Z-scan studies of ZnTPP at (g) 700 nm, (h) 750 nm, (i) 800 nm, (j) 850 nm, (k) 900 nm and (l) 950 nm. Blue circles denote to experimental points while the solid lines denote fitted data.

Table 2.1 Summary of the NLO coefficients of TPA-ZnPc, ZnTPP obtained from the present study.

	TPA-ZnPc									
λ (nm)	n <sub>2</sub> ×10 <sup>-15</sup> (m <sup>2</sup> /W)	n <sup>2</sup> ×10 <sup>-7</sup> (e.s.u.)	$ \chi_R^{(3)}  \times 10^{-17}$ $(m^2/V^2)$	α <sub>2</sub> ×10 <sup>-7</sup> (cm/W)	σ <sub>2</sub> ×10 <sup>7</sup> (GM)	α <sub>3</sub> ×10 <sup>-14</sup> (cm <sup>3</sup> /W <sup>2</sup> )	σ3×10 <sup>-70</sup> (cm <sup>6</sup> s <sup>2</sup> /photon <sup>2</sup> )	$ \chi_1^{(3)}  \times 10^{-18}$ $(m^2/V^2)$	χ <sup>(3)</sup>  ×10 <sup>-</sup> 9 (e.s.u)	Limiting threshold (山/cm²)
700	-9.0	3.2	11	3.6	17	-	-	2.4	7.7	7.2
750	-0.6	0.2	0.8	0.2	0.8	-	-	1.5	0.5	86.3
800	-3.0	1.1	3.5	9.5	39	-	-	7.2	2.6	3.6
850	-2.0	0.7	2.4	0.2	0.7	-	-	0.1	1.8	101
900	-0.7	0.2	0.8	-	-	0.5	41	-	-	19.4
950	-4.4	1.5	5.0	-	-	1.2	87	-	-	10.1
	ZnTPP									
700	-2.3	0.8	2.7	4.0	1.8	-	-	27	0.2	289
750	-2.4	0.8	2.8	9.0	3.9	-	-	64	0.2	117
800	-16	5.7	17	5.0	2.0	-	-	38	1.3	37
850	-0.5	0.2	0.6	9.0	3.5	-	-	73	0.06	22
900	-0.7	0.2	0.8	7.0	2.5	-	-	60	0.07	179
950	-0.9	3.1	11	-	-	0.1	7.2	-	-	5.4

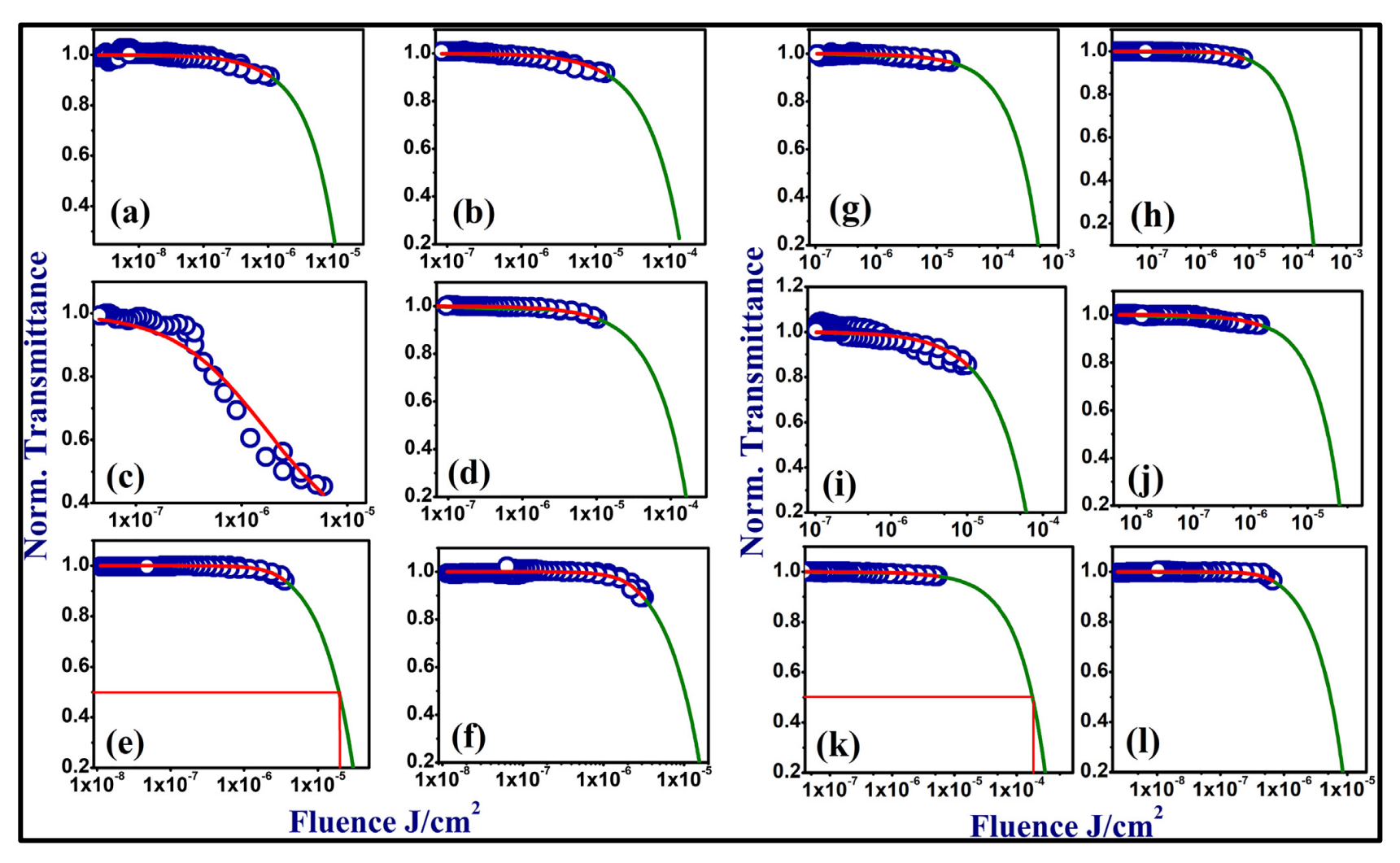


Figure 2.29 Optical limiting response of TPA-ZnPc (left) and ZnTPP (right) at (a) 700 nm (b) 750 nm (c) 800 nm (d) 850 nm (e) 900 nm (f) 950 nm, Symbols (blue) represents experimental OA Z-scan data, solid, red lines represent the theoretical fits and solid, green lines represent the extrapolated fit.

#### 2.6.2. Conclusions:

- Here we demonstrated the study of NLO behavior in two organic molecules TPA-ZnPc and ZnTPP using the Z-scan technique. From the above studies, it can be concluded that both phthalocyanine TPA-ZnPc and porphyrin ZnTPP exhibit strong NLO properties with TPA-ZnPc showing larger NLO coefficients than ZnTPP which can be associated with the larger number of delocalized electrons in a Pc molecule over Por.
- TPA-ZnPc was found to have higher damage threshold compared to ZnTPP. For the wavelength range of 700 850 nm, both molecules show two-photon absorption while beyond that, multi-photon processes dominate due to reduction in photon energy with increase in wavelength. The NLO absorption processes can be assumed to be instantaneous as the laser pulse duration is ~150 fs.
- Thus, NLO studies show Pc and Por molecules exhibiting similar NLO properties with TPA-ZnPc being superior NLO material over the Por - ZnTPP for optical limiting applications.

#### 2.6.3. Sources of Error:

- i. The experimental errors that are random includes concentration measurements, estimation of spot size at the focus, data fitting, input power measurements and others that approximately makes up to  $\pm 10\%$ .
- ii. Accumulated thermal nonlinearities accompanying the electronic contributions may be present in the measured NLO coefficients and cross-sections due to high rep. rate of the laser pulses i.e.~80MHz.

#### 2.7. References:

- [1] Y. Shen, The Principles of Nonlinear Optics, Hoboken, New Jersey, USA: Wiley; ISBN: 0-471-43080-3, 2003. 563 p..
- [2] M. R. R. Vaziri, "Comment on "Nonlinear refraction measurements of materials using the moiré deflectometry," *Opt. Commun.*, vol. 357, p. 200–201, 2015.
- [3] R. Y. Chiao, E. Garmire and C. H. Townes, "Self-trapping of optical beams," *Phys. Rev. Lett.*, vol. 13, no. 15, p. 479, 1964.
- [4] P. W. e. al., "Self-focusing collapse distance in ultrashort pulses and measurement of nonlinear index," *Opt. Lett.*, vol. 36, no. 13, p. 2542, 2011.
- [5] R. Paschotta, "Effect of self-phase modulation on the pulse bandwidth," *RP Photonics*.
- [6] R. Boyd, "Nonlinear optics, 3rd Ed.," in *Ch 1*, Academic Press, 2008.
- [7] M. V. Hobden, "Phase-matched second harmonic generation in biaxial crystals," *J. Appl. Phys.*, vol. 38, no. 11, p. 4365, 1967.
- [8] J. A. Giordmaine and R. C. Miller, "Tunable coherent parametric oscillation in LiNbO3 at optical frequencies," *Phys. Rev. Lett.*, vol. 14, no. 24, p. 973, 1965.
- [9] "Introduction to time-resolved spectroscopy." (http://web.vu.lt/ff/m.vengris/images/TR\_spectroscopy02.pdf).
- [10] "Pulse characterization by RP Photonics," https://www.rp-photonics.com/pulse\_characterization.html.
- [11] "Ultrafast Optics lecture notes, chapter 10, 'pulse characterisation'," (https://ocw.mit.edu/courses/electrical-engineering-and-computer-science/6-977-ultrafast-optics-spring-2005/lecture-notes/chapter10.pdf).
- [12] R. Berera, R. v. Grondelle and J. T. M. Kennis, "Ultrafast transient absorption spectroscopy: principles and application to photosynthetic systems," *Photosynth. Res.*, vol. 101, p. 105–118, 2009.
- [13] M. Sheik-Bahae, A. Said, T. -H. Wei, D. J. Hagan and E. W. V. Stryland., "Sensitive measurement of optical nonlinearities using a single beam," *IEEE J. Quant. Electron.*, vol. 26, pp. 760-769, 1990.

- [14] S. Pramodini, "Third order optical nonlinearity and optical power limiting of organic materials under CW laser illumination," in *Thesis*, Submitted to Manipal University, India, 2015.
- [15] D. Weaire, B. S. Wherrett, D. A. B. Miller and S. D. Smith, "Effect of low-power nonlinear refraction on laser-beam propagation in InSb," *Opt. Lett.*, vol. 4, no. 10, pp. 331-3, 1979.
- [16] D. Swain, "Ultrafast Excited State Dynamics and Dispersion Studies of Optical Nonlinearities in Porphycenes, Naphthobipyrroles, Phthalocyanines, and Porphyrins," Ph.D. Thesis, University of Hyderabad, India, 2013.
- [17] P. Anusha, "Studies of Ultrafast Excited State Dynamics in Corroles, Naphthosapphyrins, Phthalocyanines and Porphyrins," Ph. D. thesis, ACRHEM, University of Hyderabad, Hyderabad, India, 2015.
- [18] P. B. Anand and S. Jayalekshmi, "Observation of switching between SA and RSA in silver/goldpolyaniline nanocomposite films," in *Proc. SPIE* 8809 (2B), (https://doi.org/10.1117/12.2027206), 2013.
- [19] C. Liu, Y. Yuan, L. Cheng, J. Su, X. Zhang, X. Li, H. Zhang, X. Zhang and J. Li, "Tunable nonlinear optical absorption in amorphous and crystalline Sb<sub>2</sub>Se<sub>3</sub> thin films.," *J. Alloys Compd.*, vol. 791, p. 753–760, 2019.
- [20] V. Sreeramulu, K. Haldar, A. Patra and D. N. Rao, "Nonlinear optical switching and enhanced nonlinear optical response of Au-CdSe heteronanostructures," *J. Phys. Chem. C*, vol. 118, pp. 30333-30341, 2014.
- [21] X.-F. Zhang, Y. Lin, W. Guo and J. Zhu, "Spectroscopic insights on imidazole substituted phthalocyanine photosensitizers: Fluorescence properties, triplet state and singlet oxygen generation," *Spectrochim. Acta A*, vol. 133, p. 752–758., 2014.
- [22] N. Krishna, J. Krishna, S. Singh, L. Giribabu, A. Islam and I. Bedja, "Bulky nature phenanthroimidazole-based porphyrin sensitizers for dye-sensitized solar cell applications," *J. Phys. Chem. C*, vol. 121, pp. 25691-25704, 2017.
- [23] A. Rana and P. K. Panda, "Fluorescent turn-off based sensing of nitrated explosives using porphyrins and their Zn(II)-derivatives," *RSC Adv.*, vol. 2, p. 12164–12168, 2012.
- [24] R.-M. Ion, "Phthalocyanines and some current applications," in *Intech Open*, (DOI:10.5772/intechopen.68654)., 2017.

- [25] C. Fierro, A. Anderson and D. A. Scherson, "Electron donor-acceptor Properties of porphyrins, phthalocyanines, and related ring chelates: A molecular orbital approach," *J. Phys. Chem.*, vol. 92, p. 6902–6907., 1988.
- [26] D. Wrobel and R. Ion, "Photovoltaic and spectral properties of tetraphenyloporphyrin and metallotetraphenyloporphyrin dyes," J. Goc, J. Mol. Struct., vol. 450, p. 239–246, 1998.
- [27] D. Frackowiak, A. Planner, A. Waszkowiak, A. Boguta, H. Manikowski, R. Ion and K. Wiktorowicz, "Yield of intersystem (singlet-triplet) crossing in phthalocyanines evaluated on the basis of a time in resolved photothermal method," *J. Photochem. Photobiol*, vol. 141, pp. 101-108, 2001.
- [28] İ. Özceşmeci, A. Geli and A. Gül, "Synthesis and photophysical properties phthalocyanine–pyrene dyads," *Dyes Pigm.*, vol. 92, p. 954–960, 2012.
- [29] M. Brasch, A. d. l. Escosura, Y. Ma, C. Uetrecht, A. Heck, T.Torres and J. Cornelissen, "Encapsulation of Phthalocyanine Supramolecular Stacks into Virus-like Particles," *J. Am. Chem. Soc.*, vol. 133, no. 18, pp. 6878-6881, 2011.
- [30] M. Liao and K. Kuo, "Phthalocyanine polymers. I. Synthesis and characterization of fused copper phthalocyanine polymers," *J. Polym. Sci. Part A*, vol. 28, no. 9, p. 2349–57, 1990.
- [31] N. Mckeown, 23. N.B. Mckeown, The porphyrin handbook: Phthalocyanines: Synthesis of symmetrical phthalocyanines; K. Kadish, R. Cuilard, K. Smith Eds, MA, USA: Academic Press: Burlington, 2003, 15, 61–124...
- [32] B. Sesalan, A. Koca and A. Gul, "Water soluble novel phthalocyanines containing dodeca-amino groups," *Dyes Pigm.*, vol. 79, p. 259–264, 2008.
- [33] K. D. Oliveira, F. d. Assis, A. Ribeiro, C. Neri, A. Fernandes, M. Baptista, N. Lopes, O. Serra and Y. Iamamoto, "Synthesis of phthalocyanines—ALA conjugates: Water-soluble compounds with low aggregation," *J. Org. Chem.*, vol. 74, p. 7962–65, 2009.
- [34] B. Valeur, *Molecular Fluorescence: Principles and Applications* (2nd edition), Germany: Wiley: Weinheim, 2002.
- [35] Manual, Libra Ultrafast Amplifier Laser System by Coherent., http://smos.sogang.ac.kr/wiki/images/b/b7/Libra\_HE\_RevAC\_Operator%27s\_Manual.pdf.

- [36] Manual, Vitesse Diode Pumped Laser User Manual, https://docplayer.net/30024882-Vitesse-laser-operator-s-manual.html.
- [37] "Gires-Tournois Interferometers, RP Photonics Encyclopedia.," in (https://www.rp-photonics.com/gires\_tournois\_interferometers.html)..
- [38] Manual, SDG Elite, https://www.manualslib.com/manual/1517725/Coherent-Sdg-Elite.html.
- [39] Manual, Operator's Manual Evolution-HE High-Power Q-Switched Laser System, https://www.coherent.com/assets/pdf/1299437AA\_Revolution\_preinstall.pdf.
- [40] Manual, User's Manual of TOPAS-C https://sphotonics.ru/company/partnery/%D0%A1%D0%B5%D1%80%D0%B8% D1%8F%20Topas-C.pdf.
- [41] Manual, HELIOS User Manual, Version 6.9.1 https://www.helios.de/support/manuals/wsUB64-e/.
- [42] Manual, Surface Xplorer manual, HELIOS<sup>TM</sup> http://ultrafastsystems.com/download/surface-xplorer/SurfaceXplorerManual.pdf.
- [43] J. Snellenburg, I. V. Stokkum and K. Mullen, "TIMPGUI: A Graphical User Interface for the Package TIMP," in *The R User Conference 2008*, (http://www.statistik.uni-dortmund.de/useR)., 2008.
- [44] M. Bharati, S. Bhattacharya, J. S. Krishna, L. Giribabu and S. V. Rao, "Femtosecond, broadband nonlinear optical studies of a zinc porphyrin and zinc phthalocyanine," *Opt. and Laser Tech.*, vol. 108, p. 418–425, 2018.

# **Chapter 3**

# Excited State Dynamics and NLO Properties of Carbazole Substituted Zinc Phthalocyanines.

The chapter encompasses the detailed theoretical, optical and photophysical studies of two carbazole substituted ZnPc named as CBZPC1 [Zinc(II) 2,10,16,24-tetrakis(9-phenyl-9Hcarbazol-2-yl)-phthalocyanine] and CBZPC2 [Zinc(II) 2,10,16,24-tetrakis(4-(9Hcarbazol-9-yl)phenyl)phthalocyaninel. Both the molecules were studied in solution phase with CBZPC1 in THF and CBZPC2 in DCM solvent. The molecules exhibited a broad Soret (B) absorption bands with emission around 700 nm. The emission spectrum was significantly Stokes shifted in CBZPC1 compared to CBZPC2. The radiative lifetime components obtained from time-resolved fluorescence data were estimated to be ~7.5 ns and ~130 ps with quantum yields of 0.18 and 0.22, respectively. The theoretical optimized energy level molecular structures of CBZPC1 and CBZPC2 was carried out using B3LYP hybrid functional theory and 6-31G(d,p) basis set in the Gaussian 09 package. The non-radiative lifetimes were measured using fs-TAS technique and global fit analysis. The results revealed that the excited molecules underwent ISC with a decay rate with a lifetime component of >1 ns for CBZPC1 and ~0.7 ns for CBZPC2. This data illustrates that both these molecules can be used as a potential photosensitizer in dye-sensitized solar cells (DSSCs) and Organic LEDs. The Pc molecule was also studied for its NLO behavior for the wavelength range: 600–900 nm using the standard Z-scan technique with both MHz and kHz repetition femtosecond pulses. Two-photon absorption (2PA) was observed in the visible range of 600–900 nm for both the cases. CBZPC1 exhibited self-focusing behaviour for all the wavelengths while self-defocusing was prevalent in CBZPC2.

#### Part of the presented work in this chapter has been published as:

S. Bhattacharya; C. Biswas; S. S. K. Raavi; J. V. S. Krishna; N. V. Krishna; L. Giribabu; S. Venugopal Rao, "Synthesis, optical, electrochemical, DFT studies, NLO properties and ultrafast excited state dynamics of carbazole induced phthalocyanine derivatives", *The Journal of Physical Chemistry C* 2019, 123, 11118–11133.

#### 3.1 Introduction

Nonlinear optics (NLO) is one of the few revolutionary technologies that have opened several possibilities in the technological world of photonics, optoelectronics, and biomedicine [1, 2, 3, 4, 5]. Optical signal processing and telecommunications have been extensively developed and studied using various NLO moieties [6, 7]. In this regard, one of the most common good NLO materials are dyes [8, 9, 10]. The origin of strong NLO properties in these types of organic compounds are the network of  $\pi$ -delocalized electrons, which can lead to an enhancement in the triplet excited state lifetimes. This carved the purpose of the development of novel  $\pi$ -conjugated materials [11]. Phthalocyanines (or Pc) and its metallic derivatives are the tetrapyrrolic pigments with incredible thermal, chemical, and optical stability that possess superior NLO properties and can be structurally modified due to their ability of holding more than 70 (70) non-metallic and metallic ions in the cavity. There are several synthetic procedures to develop phthalocyanines with desired ultrafast and large third-order nonlinearity [12, 13, 14, 15]. In case of metallic phthalocyanines or MPc, interesting chemical and optical properties can be studied, for example, MPc thin films give information about the material's microscopic characteristics – their third order electronic susceptibility  $[\chi^{(3)}]$  being dependent on factors such as the temperature of the annealing process, filled "d" valence orbitals and the type of central metal ion the planarity of the molecule [16, 17]. Further enhancement in the NLO properties of MPc thin films were made by nanocrystals (NCs) and nanoparticles deposition [18]. As per discussions in the previous chapters, optical limiting is one of the major applications of NLO materials like phthalocyanines [19] and is typically influenced by phenomena like reverse saturable absorption (RSA), two-photon absorption and/or nonlinear reflection and refraction [20, 21]. Due to the macrocyclic nature a phthalocyanine, it can favourably functionalize various peripheral/non-peripheral substituents within its structure to enhance the solubility.

In general, phthalocyanines have an intense absorption band in the 600–700 nm (Q-band) spectral range with a less intense absorption band in the 300–400 nm region (Soret band) as a result of  $\pi$ – $\pi$ \* transitions. Q-band molar extinction coefficients are very high with typical values of  $10^5$  M<sup>-1</sup>cm<sup>-1</sup>making them excellent candidates for optoelectronic applications [22, 23]. Solubility and aggregation can influence the optical properties of phthalocyanines. The planar nature of phthalocyanine macrocycles may lead to aggregation, which in turn hinders several device applications. Therefore, the development

of highly soluble and aggregation-minimized phthalocyanines have been explored and developed over the decades [24, 25, 26, 27]. For the past few years, our research team has developed quite a few novel phthalocyanines along with their metallic derivatives by introducing substituents either at peripheral/non-peripheral positions, followed by the investigation of their excited state dynamics and third-order NLO properties [28, 29, 30].

In this chapter, we present results from the design, synthesis, and investigations of two carbazole-substituted phthalocyanines. In these molecules the carbazole moiety is tethered to the phthalocyanine using two different positions of the carbazole to achieve the strong NLO coefficients. The carbazole ring substituted (9-phenyl-9H-carbazol-2-yl) molecule is named as CBZPC1 and N phenyl substituted (4-(9H-carbazol-9-yl)phenyl) phthalocyanine as CBZPC2. According to recent literature reports, the carbazoles make excellent candidates for optoelectronic applications due to their rich photochemistry [31]. Additionally, the incorporation of these carbazole moieties at the MPc periphery is likely to influence the electronic and sterical characteristics of the macromolecule, solubility in polar aprotic solvents and shifting of the redox potential towards the positive. Thus, herein we provide a detailed view of the structural, electrochemical, optical (linear and nonlinear) and photophysical studies (excited state dynamics) of CBZPC1 and CBZPC2. The electrochemical and optical (steady state and time resolved) properties were studied and compared in different solvents at varying concentrations to realise their structure—property relationship.

# 3.2 Experimental Details and Results:

CBZPC1 [Zinc(II) 2,10,16,24-tetrakis(9-phenyl-9H-carbazol-2-yl)- phthalocyanine] and CBZPC2 [Zinc(II) 2,10,16,24-tetrakis(4-(9Hcarbazol-9-yl)phenyl)phthalocyanine] are the concerned molecules with structures as shown in figures 3.1(a) and 3.1(b), were studied for NLO and photophysical properties. Shimadzu UV-3600, UV-visible-NIR spectrophotometer recorded the steady state absorption spectra of the given molecules. Fluorolog-3 spectrofluorometer (Spex model, JobinYvon) recorded the steady-state fluorescence spectra at 0.06 optical density. For fluorescence qantum yield calculations, zinc tertbutyl phthalocyanine (=0.37 in benzene) was used as the reference. [32]. A picosecond emitting diode laser (NanoLED, λex= 670 nm) by IBH Horiba Jobin Yvon - FluoroLog3- Triple Illuminator was used to record the corresponding fluorescence

lifetimes of the molecules. The decay curves were recorded at  $\lambda_{em} = 700$  nm which is the phthalocyanine macrocycle fluorescence emission maxima. Detector used was the Photomultiplier tube (R928P, M/s Hamamatsu). A dilute solution of Ludox in water acted as a scatterer to record the lamp profile. The instrument response function was calculated by the excitation source (~635 ps at 670 nm) full width half maximum (FWHM). Data fitting the decay curves were performed using nonlinear least-squares iteration process with the help of IBH DAS6 (version 2.3) decay analysis software. The quality of the fits was adjudicated by the  $\chi^2$  values along with distribution of the residuals. The absorption of the CBZPC1 solution and CBZPC2 in different solutions were found to have a broadened Soret band with peak around 350 nm and an intense B-band at 690 nm which is typical to the Pc moiety as shown in figures 3.2(a) and 3.2(b). Emission studies (using  $\lambda_{exc.} \sim 670$  nm, ps pulses), showed Stokes's shifted peak for CBZPC1 at ~708 nm following the rule of mirror symmetry as indicated in figure 3.2(c) while CBZPC2 emission was not significantly Stokes shifted [figure 3.2 (d)] for the respective common organic solvents. The fluorescence lifetime, measured using TCSPC, were measured with the relative quantum yields. The lifetimes obtained for the carbazole substituted Pcs in polar solvents such as DCM, DMF and DMSO results from two competing excited molecular species formed when in the excited state that have respective fluorescence state lifetimes  $\tau_f$ :  $\tau_{f1}$  and  $\tau_{f2}$  as shown in table 3.1.

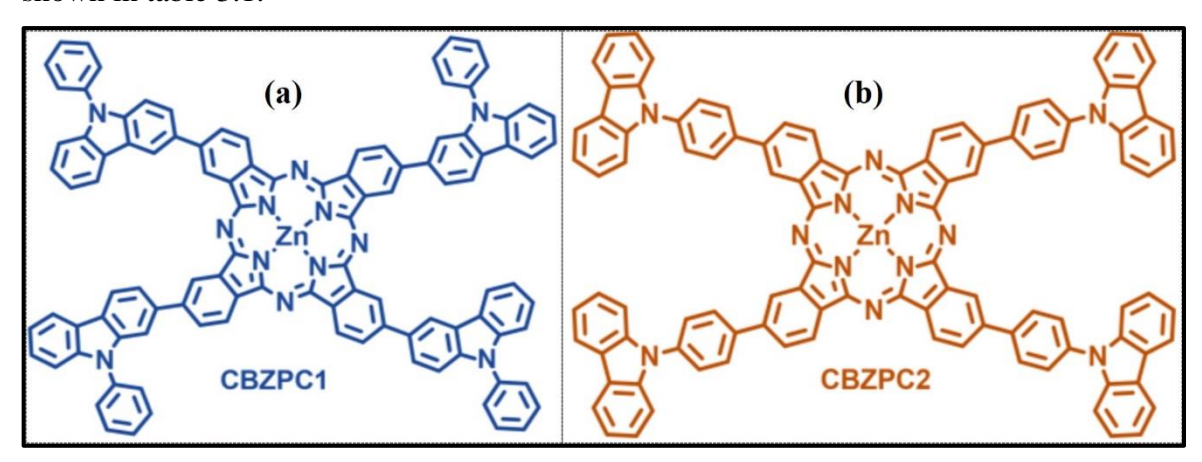
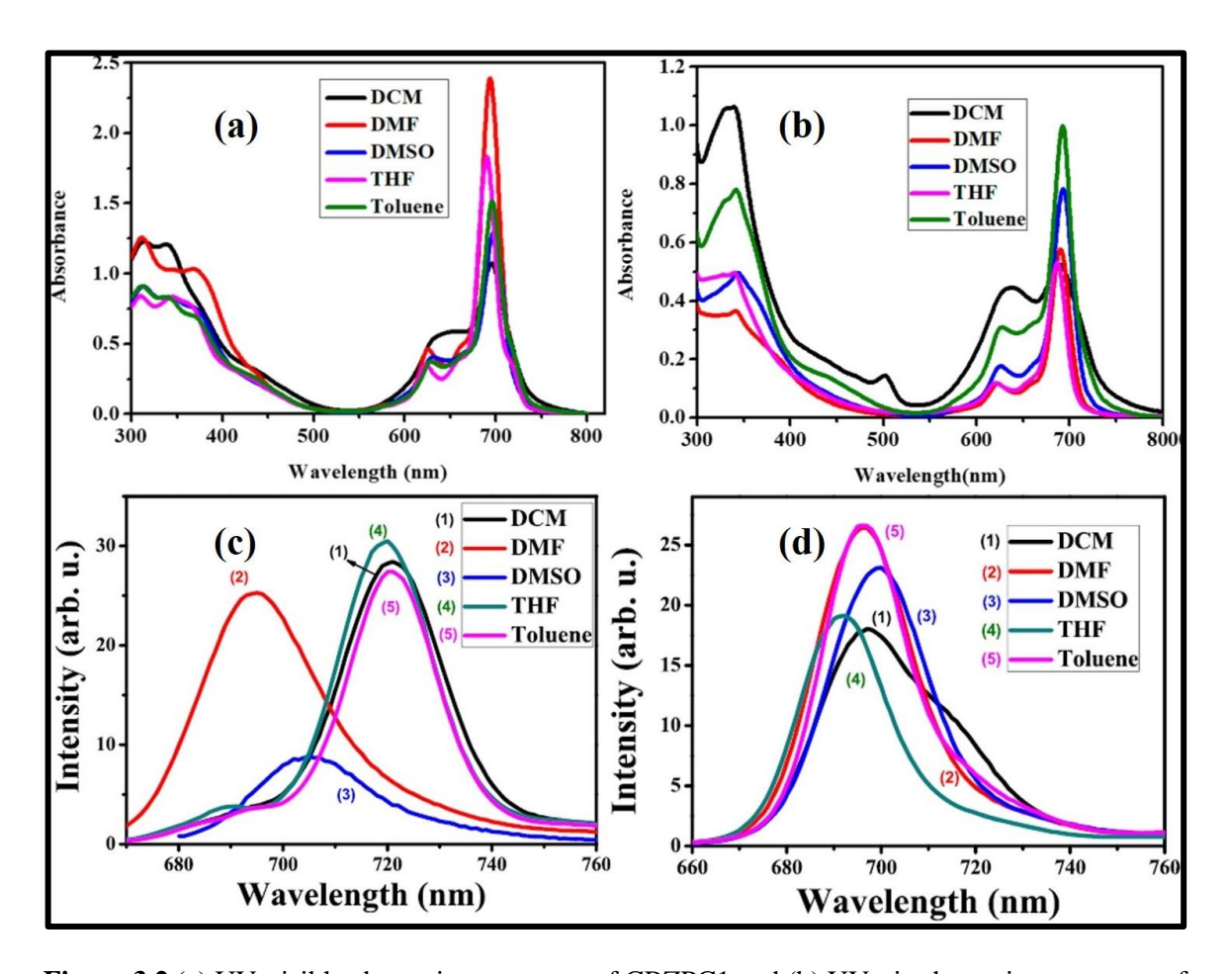


Figure 3.1 (a) Molecular structure of CBZPC1. (b) Molecular structure of CBZPC2

The density functional theory (DFT) and time-dependent DFT studies are run in a functional basis set of the B3LYP/6-31G (d,p) level [Gaussian 09 package] to determine the theoretical information about structural, optical, and redox properties of CBZPC1 and CBZPC2. The phthalocyanine derivatives with two different positions of the carbazole units in phthalocyanine of CBZPC1 and CBZPC2 constitutes the optimized energy

structures as shown in Figures 3.3(a) and 3.3(b). Here, the HOMO, LUMO, and HOMO–LUMO gap energies with ground state dipole moment are given in Debye units. For CBZPC1 electron distribution, the optimized structure consists of HOMO and LUMO predominantly on the phthalocyanine ring at -2.675 and -4.764 levels respectively while the HOMO–1 was on phthalocyanine ring and at -5.41 and LUMO+1 at -2.64 on carbazole moiety. Similarly, HOMO–2 electron cloud resided on phthalocyanine moiety (-5.41) and LUMO+2 on carbazole moiety at (-1.29).



**Figure 3.2** (a) UV-visible absorption spectrum of CBZPC1 and (b) UV-vis absorption spectrum of CBZPC1 in solvents – DCM (black), DMF (red), DMSO (blue), THF (purple) and toluene (green). (c) Emission spectrum of CBZPC1 and (b) Emission spectrum of CBZPC2 in solvents depicted as (1) DCM (2) DMF (3) DMSO (4) THF and (5) Toluene.

For CBZPC2, phthalocyanine ring occupied the HOMO (-5.08) and LUMO (-2.99) levels while HOMO-1 (-5.40), HOMO-2 (-5.40) and LUMO+1(-2.96), LUMO+2 (1.56) pairs were occupied by both phthalocyanine and carbazole moieties. Thus, no distinct donor-acceptor characteristics were predominant in both the molecules. (All these measurements were carried out at IICT, Hyderabad [33]).

**Table 3.1** Absorption and emission data of the molecules CBZPC1 and CBZPC2 in different solvents.

Sample	Solvent	λ <sub>max</sub> (nm):	λ <sub>max</sub> (nm):	φ <sub>f</sub> (yield)	τ <sub>f</sub> (ns)
		Absorption	Emission		$[\tau_{f1}(A_1), \tau_{f2}(A_2)]$
CBZPC1	DCM	694	720	0.24	0.04 (38.8), 3.44 (61.1)
	DMF	693	695	0.11	0.25 (40.3), 4.54 (59.7)
	DMSO	697	705	0.13	8.30 (100)
	THF	690	718	0.18	7.46 (100)
	Toluene	695	720	0.26	7.85 (100)
CBZPC2	DCM	690	698	0.22	0.13 (100)
	DMF	689	691	0.12	0.07 (20.2), 2.63 (79.8)
	DMSO	692	697	0.10	1.27 (18.3), 3.32 (81.7)
	THF	686	696	0.20	7.46 (100)
	Toluene	692	701	0.27	7.85 (100)

 $<sup>\</sup>tau_{f1}$ ,  $\tau_{f2}$  are lifetime components of fluorescence lifetime,  $\tau_f$  with  $A_1$ % and  $A_2$ % species contribution, respectively.

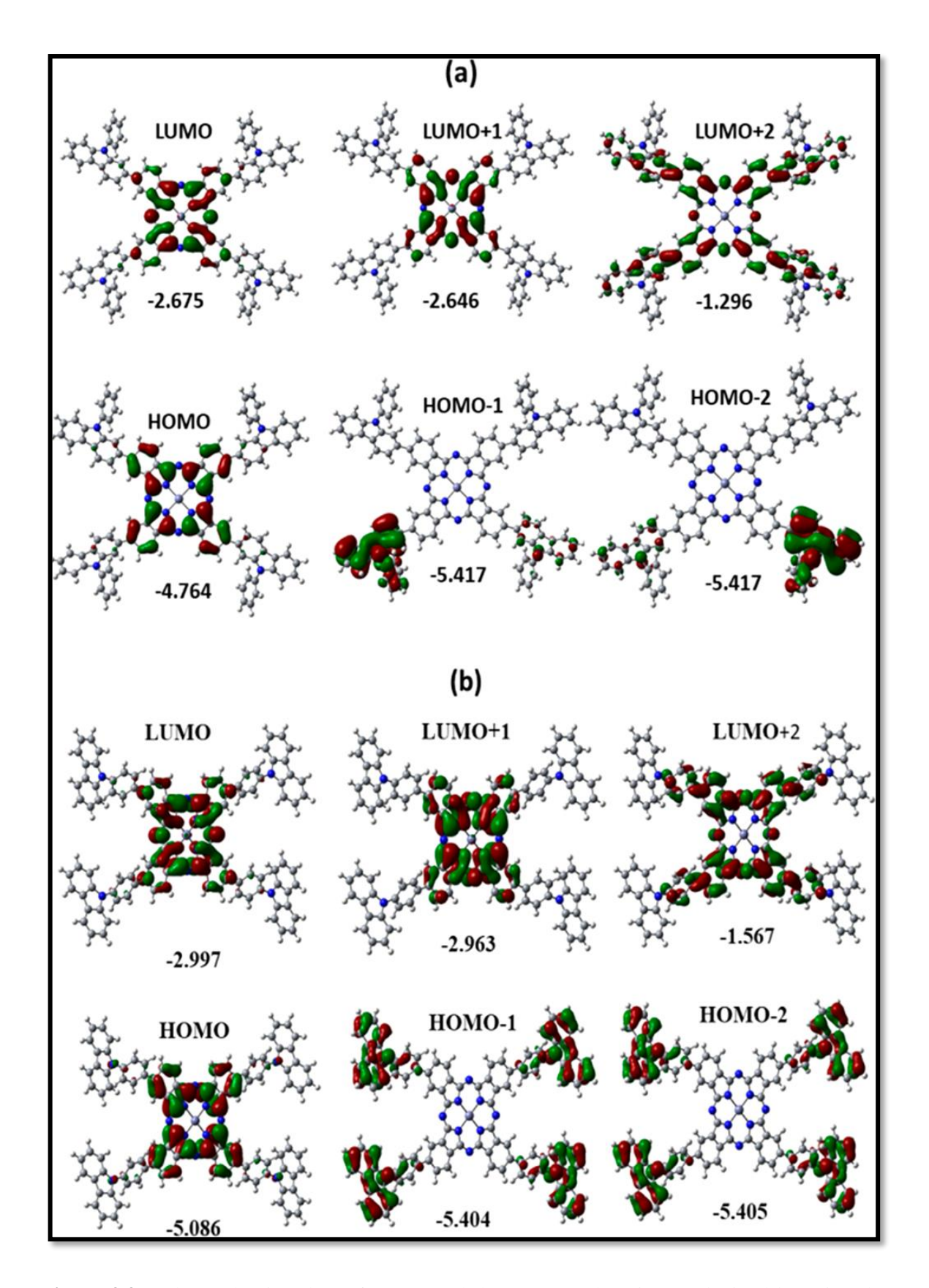


**Figure 3.3** (a, b) Isodensity plots of FMOs and the energy values in eV obtained by using the B3LYP method 6-31G (d,p) for CBZPC1 and CBZPC2, respectively.

#### 3.2.1. Z-scan with MHz pulses:

CBZPC1 and CBZPC2 were studied in the 700–900 nm excitation range using ~150 fs, 80 MHz pulses using the setup as shown in figure 2 described in the Chapter 2. Due to high molar extinction coefficients of both the carbazole substituted phthalocyanines, typically 50–70  $\mu$ M concentrations (of the solution) were used for the present study. Also, low concentration ensured the absence of any aggregation within the solution. The input intensity was kept  $1.3-6.2 \times 10^{11}$  W/cm² and the Rayleigh range were in the 2.2–3.6 mm range for given wavelength window. 1 mm glass cuvette was used for the study. Calculations and data fitting were carried out using the formulae mentioned in Chapter 2.

For CBZPC1, the open aperture Z-scan data depicted RSA behaviour for the aforementioned input intensities with 2PA being the dominant phenomenon [see data in figures 3.4(a)–(c)]. The obtained 2PA coefficient was  $\sim (1.9-2.8)\times 10^{-8}$  cm/W with an absorption cross-section,  $\sigma_2 \sim (8.1-14.7)\times 10^4$  GM. The closed aperture studies [see data presented in figures 3.4(d)-3.4(f)] demonstrated a positive nonlinearity with the coefficient,  $n_2 \sim (1.7-$ 2.3)×10<sup>-12</sup> cm<sup>2</sup>/W indicating a self-focusing behaviour. For CBZPC2, the open aperture studies showed RSA for the afore-mentioned input intensities with 2PA being the dominant phenomenon [see figures 3.5(a)-3.5(c) data]. The obtained 2PA coefficient was  $\sim (1.9 - 1.0)$  $8.0\times10^{-8}$  cm/W with the corresponding absorption cross-sections,  $\sigma_2 \sim (13.1-48.9)\times10^4$ GM. The closed aperture data presented in figures 3.5(d)-3.5(f) depicted a negative nonlinearity with the coefficient,  $n_2 \sim (0.3 - 3.7) \times 10^{-11}$  cm<sup>2</sup>/W, indicating a self-defocusing behaviour. In the MHz regime, no solvent contribution was detected and, hence, we can relate the obtained data to NLO behaviour of purely Pc molecules. Although, MHz pulses include contributions from both electronic and thermal phenomena, from earlier studies on similar molecules demonstrated that the major contribution to the nonlinear absorption when excited with nJ, MHz, 800 nm pulses (from fs oscillator) was predominantly from the instantaneous TPA. However, due to the high repetition rate of the input pulses there is a possibility of thermal contribution to the observed nonlinearities. Therefore, Z-scan measurements with kHz pulses were essential.

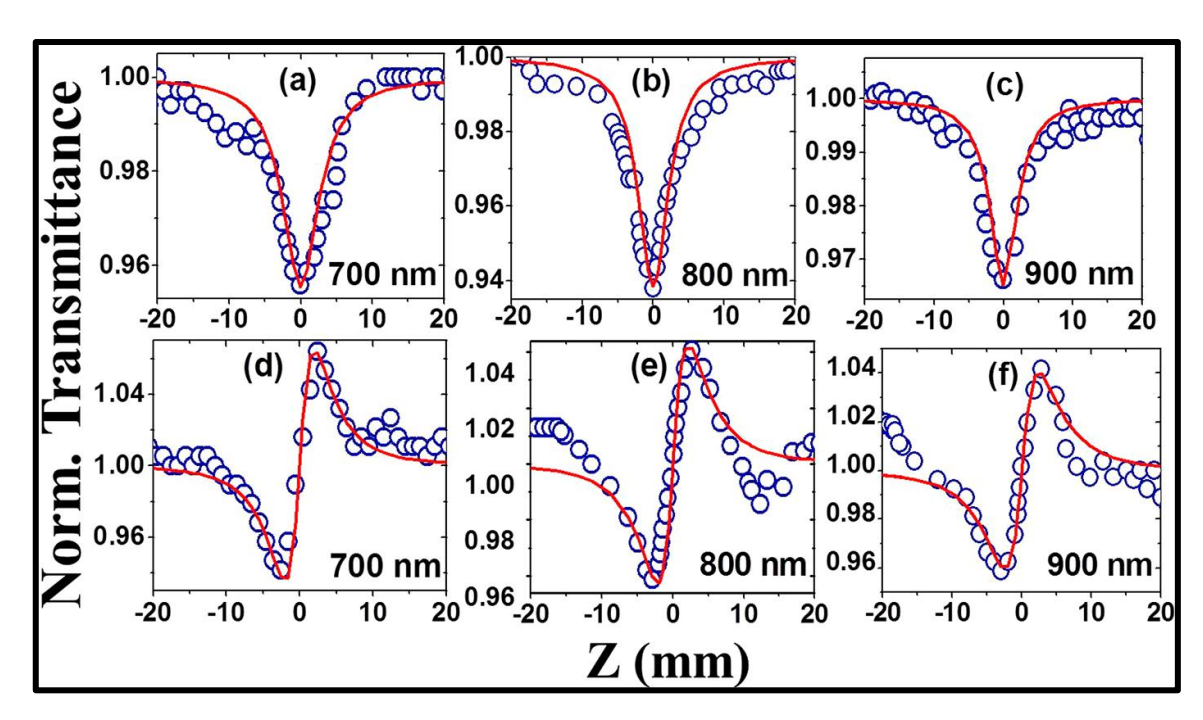


**Figure 3.4** (a), (b) and (c) Open aperture Z-scan data and (d), (e) and (f) closed aperture Z-scan data of CBZPC1 recorded at wavelengths of 700 nm, 800 nm and 900 nm, respectively, with 150 fs, 80 MHz pulses. The experimental data (blue, open circles) are best fitted (red, solid lines) for 2PA and positive nonlinear refraction.

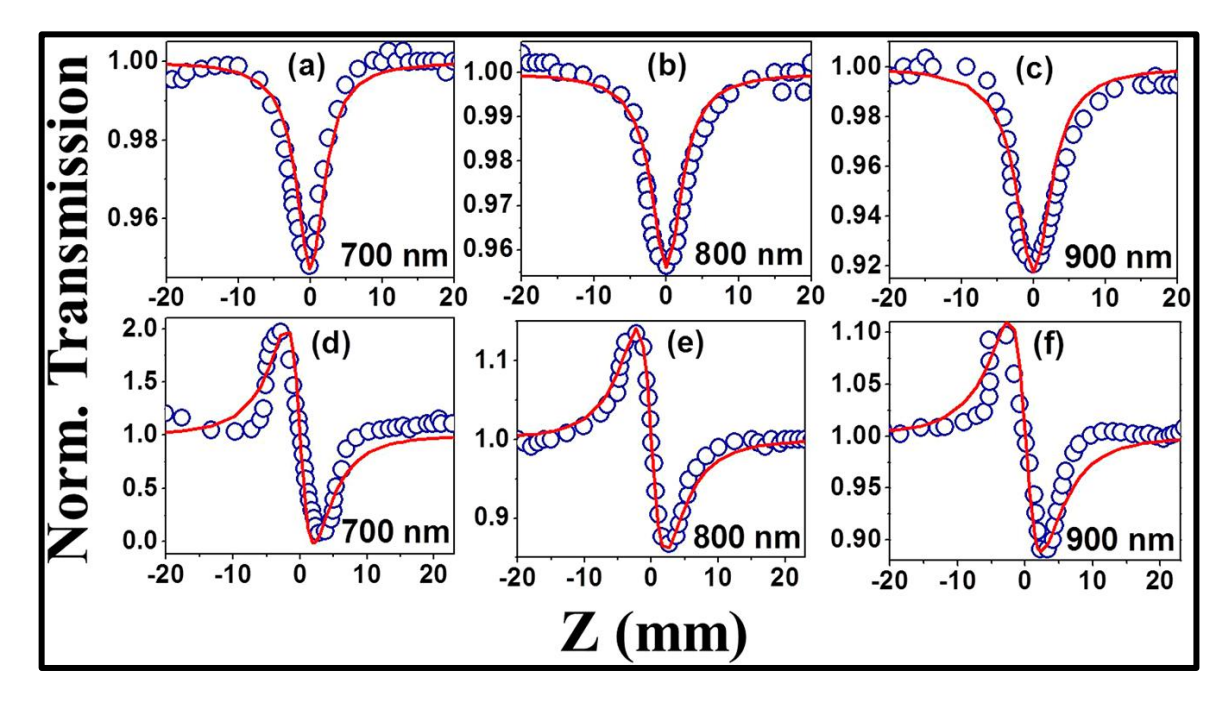


**Figure 3.5** (a), (b) and (c) Open aperture Z-scan data and (d), (e) and (f) closed aperture Z-scan data of CBZPC1 recorded at wavelengths of 700 nm, 800 nm and 900 nm, respectively, with 150 fs, 80 MHz pulses. The experimental data (blue, open circles) are best fitted (red, solid lines) for 2PA and positive nonlinear refraction.

#### 3.2.2. Z-scan with kHz pulses:

The NLO results from MHz pulse regime might contain additional thermal contribution due to higher repetition rate with larger pulse width. Thus, in order to look at

purely electronic contributions, CBZPC1 and CBZPC2 were studied for 600 nm - 800 nm excitation range using 70 fs, 1 kHz pulses using the setup as shown in figure 3 in Chapter 2. Typically, solutions with  $50\text{-}70 \mu\text{M}$  concentration were used and the Rayleigh lengths were in the 1.9-4.7 mm range for given wavelength window. A 1-mm glass cuvette was used for all the studies.

For the visible range of 600 nm - 800 nm wavelength range, CBZPC1 showed RSA phenomena with predominantly 2PA [see figures 3.6(a)–3.6(c)] with absorption coefficient of  $\alpha_2 \sim (0.5-1.2)\times 10^{-12}$  cm/W and absorption cross-section in the range of 0.5-5.5 GM (see table 3.2). In the 2PA regime, CBZPC1 depicted positive nonlinearity with  $n_2 \sim (0.18-0.46)\times 10^{-16}$  cm<sup>2</sup>/W as shown in figures 3.6(d)–3.6(f). CBZPC2 showed similar 2PA behaviour with  $\alpha_2 \sim (0.5-7.0)\times 10^{-11}$  cm/W [data is presented in figures 3.7(a)–3.7(c)] and absorption cross-sections were estimated to be in the range of 42–550 GM. In the 2PA regime, CBZPC1 depicted negative nonlinearity with  $n_2 \sim (6.2-9.2)\times 10^{-16}$  cm<sup>2</sup>/W as shown in figures 3.7(d)–3.7(f). Under current experimental conditions ( $\sim 70$  fs, 1 kHz pulse), we can assume that the multiphoton absorption processes aren't instantaneous like MHz regime but sequential. The detailed summary of all the NLO coefficients obtained from z-scan study in MHz as well kHz pulse regime has been shown in Table 3.2 below.

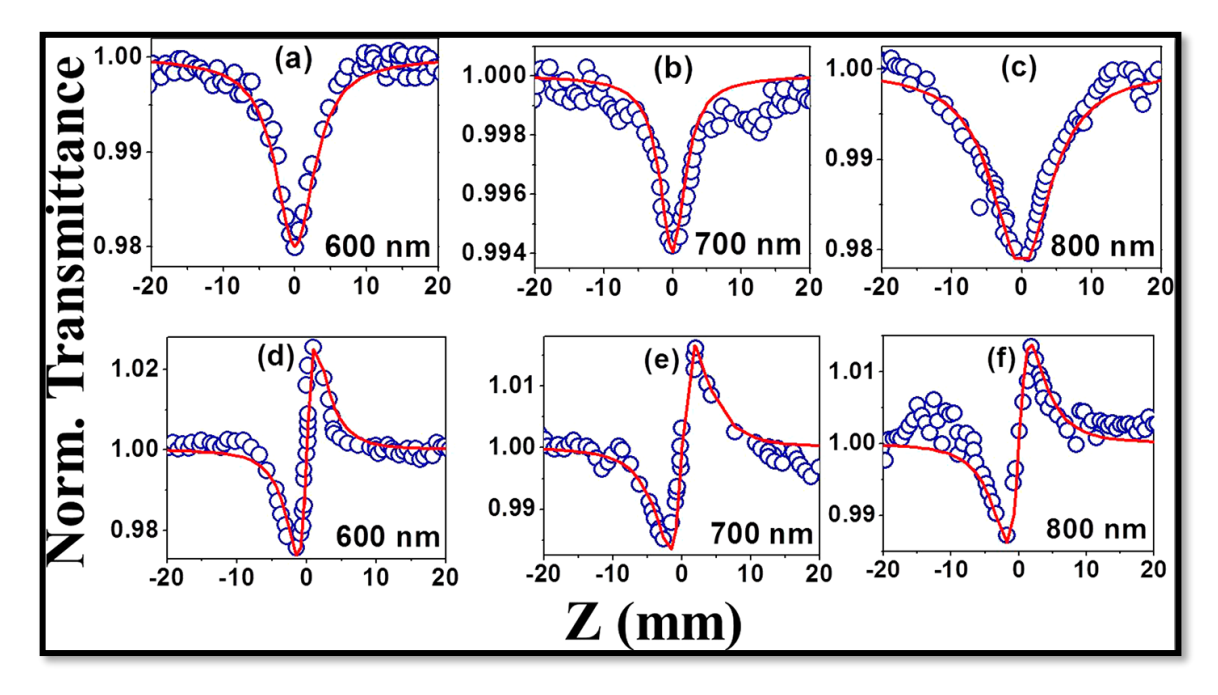


**Fig. 3.6** (a), (b) and (c) Open aperture Z-scan data (d), (e) and (f) closed aperture Z-scan data of CBZPC1 recorded at wavelengths of 600 nm, 700 nm and 800 nm, respectively, with 70 fs, 1 kHz pulses. The experimental data (in blue, open circles) are best fitted (red, solid lines) for 2PA and positive nonlinear refraction.

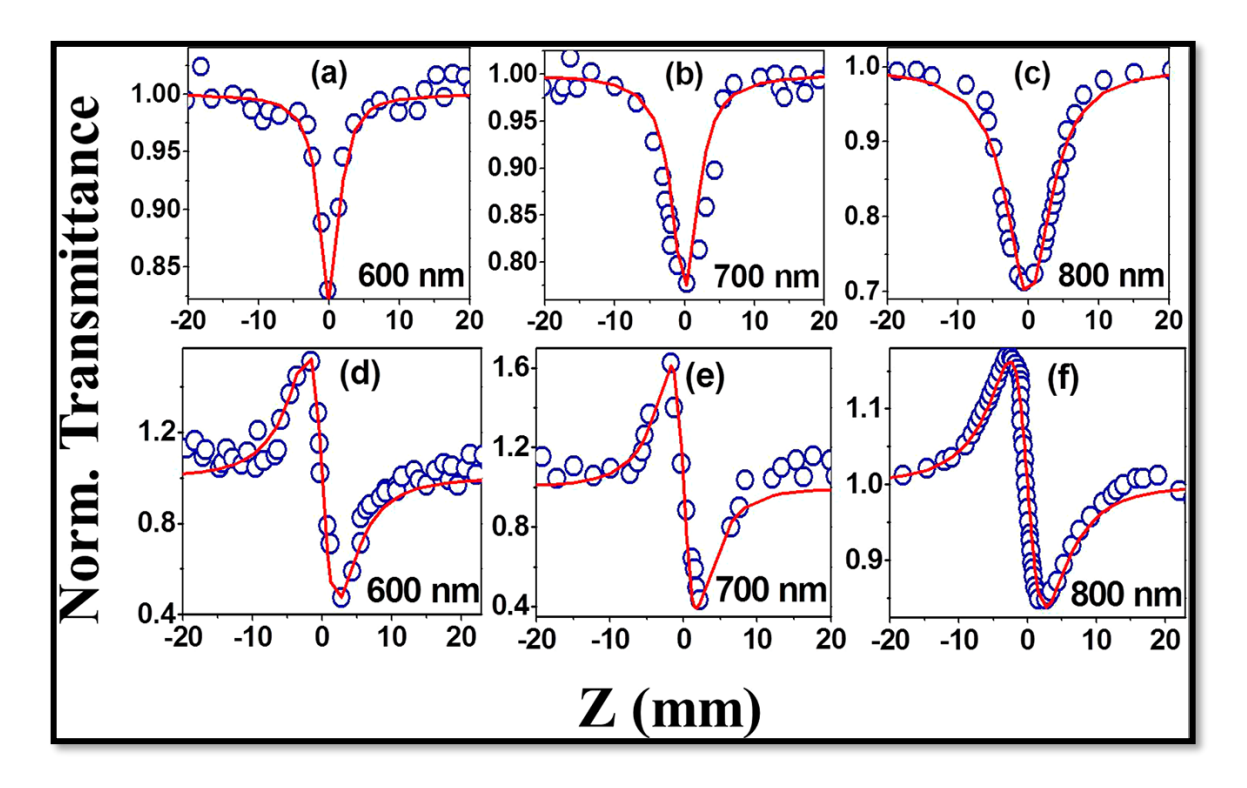


**Fig. 3.7** (a), (b) and (c) Open aperture Z-scan data (d), (e) and (f) closed aperture Z-scan data of CBZPC2 recorded at wavelengths of 600 nm, 700 nm and 800 nm, respectively, with 70 fs, 1 kHz pulses. The experimental data (in blue, open circles) are best fitted (red, solid lines) for 2PA and positive nonlinear refraction.

From the above studies and the data obtained, it is evident that CBZPC1 and CBZPC2 possesses superior NLO properties with large 2PA cross-sections in both regimes (kHz and MHz), which are on par with a few of the recently reported phthalocyanines used for Optical limiting applications [34, 35, 36]. Recent studies on different carbazoles have shown promising NLO properties. Balakrishna et al. [37] synthesized carbazole based NLO polymer, whose 2PA coefficient (β) was found to be 5.1×10<sup>-12</sup> m/W in the femtosecond domain. The charge distribution study done at computational level indicated that HOMO concentrated the total charge at the center of the molecule while LUMO consisted of the charge being spread out from the molecular center. On the other hand, Majeed et al. [38] investgiated the carbazole-substituted phthalocyanines conjugated to graphene quantum dots which showed significant photophysical properties enhancements in the complexes when conjugated with the nanomaterial. The results discussed above only confirms the excellent NLO characteristics carbazole based molecules hold and our molecules show equally excellent results when compared to the recent results discussed above.

**Table 3.2** Summary of NLO coefficients of PBIPC for different wavelengths at both kHz and MHz pulse regime.

λ (nm)	n <sub>2</sub> (cm <sup>2</sup> /W) ×10 <sup>-16</sup>	n <sub>2</sub> (e.s.u.) ×10 <sup>-13</sup>	$\chi_{R(^{3)}}$ $m^2/V^2$ $\times 10^{-23}$	α <sub>2</sub> (cm/W) ×10 <sup>-11</sup>	σ <sub>2P</sub> (GM)	$\chi_{\rm I}^{(3)}$ $m^2/V^2$ $\times 10^{-23}$	χ <sup>(3)</sup> e.s.u. ×10 <sup>-15</sup>	
	CBZPC1 (kHz repetition rate pulses)							
600	0.12	0.43	0.14	2.0	1570	1.14	1.31	
700	0.81	2.90	0.97	3.0	2019	1.99	7.08	
800	0.92	0.57	0.19	12.0	7080	9.13	6.68	
	CBZPC2 (kHz repetition rate pulses)							
600	15.2	54.0	18.4	-	-	-	-	
700	38.6	13.8	4.60	-	-	-	-	
800	31.9	11.4	3.81	-	-	-	-	
λ	n <sub>2</sub>	n <sub>2</sub>	χR( <sup>3)</sup>	α2	$\sigma^2 \times 10^4$	χι <sup>(3)</sup>	χ <sup>(3)</sup>	
(nm)	(cm <sup>2</sup> /W) ×10 <sup>-12</sup>	(e.s.u.) ×10 <sup>-8</sup>	$m^2/V^2 \times 10^{-18}$	(cm/W) ×10 <sup>-8</sup>	(GM)	m <sup>2</sup> /V <sup>2</sup> ×10 <sup>-20</sup>	e.s.u. ×10 <sup>-10</sup>	
(nm)		×10-8		×10 <sup>-8</sup>	, ,			
700		×10-8	×10 <sup>-18</sup>	×10 <sup>-8</sup>	, ,			
	×10 <sup>-12</sup>	×10 <sup>-8</sup>	×10 <sup>-18</sup> ZPC1 (MHz r	×10 <sup>-8</sup> epetition ra	te pulses)	×10 <sup>-20</sup>	×10 <sup>-10</sup>	
700	×10 <sup>-12</sup>	<b>CB</b>	×10 <sup>-18</sup> ZPC1 (MHz r  2.55	×10 <sup>-8</sup> epetition ra  2.48	te pulses)	×10 <sup>-20</sup>	×10 <sup>-10</sup>	
700	2.14 2.14	CB 0.76 0.76 1.75	×10 <sup>-18</sup> ZPC1 (MHz r  2.55  2.55	2.48 5.00 3.20	1.67 2.94 1.67	16 38 27	1.83 1.85	
700	2.14 2.14	CB 0.76 0.76 1.75	×10 <sup>-18</sup> ZPC1 (MHz r  2.55  2.55  5.84	2.48 5.00 3.20	1.67 2.94 1.67	16 38 27	1.83 1.85	
700 800 900	2.14 2.14 4.89	CB 0.76 0.76 1.75 CB	×10 <sup>-18</sup> ZPC1 (MHz r  2.55  2.55  5.84  ZPC2 (MHz r	2.48 5.00 3.20 epetition ra	te pulses)  1.67  2.94  1.67  te pulses)	×10 <sup>-20</sup> 16  38  27	1.83 1.85 4.19	

#### 3.2.3. fs-TAS with kHz pulses:

The molecules [CBZPC1 in THF and CBZPC2 in DCM] were excited at shoulder end of B-band at 650 nm for CBZPC1 and 690 nm for CBZPC2. They were probed in the visible spectral range of 440-800 nm and up to a delay of 2 ns. The obtained data is shown in figures 3.8(a)-3.8(d) indicating band maxima and minima. The data presented here had been corrected for the possible artifacts accompanying the transient absorption measurements (coherent artifact, chirp correction, background correction, etc.).

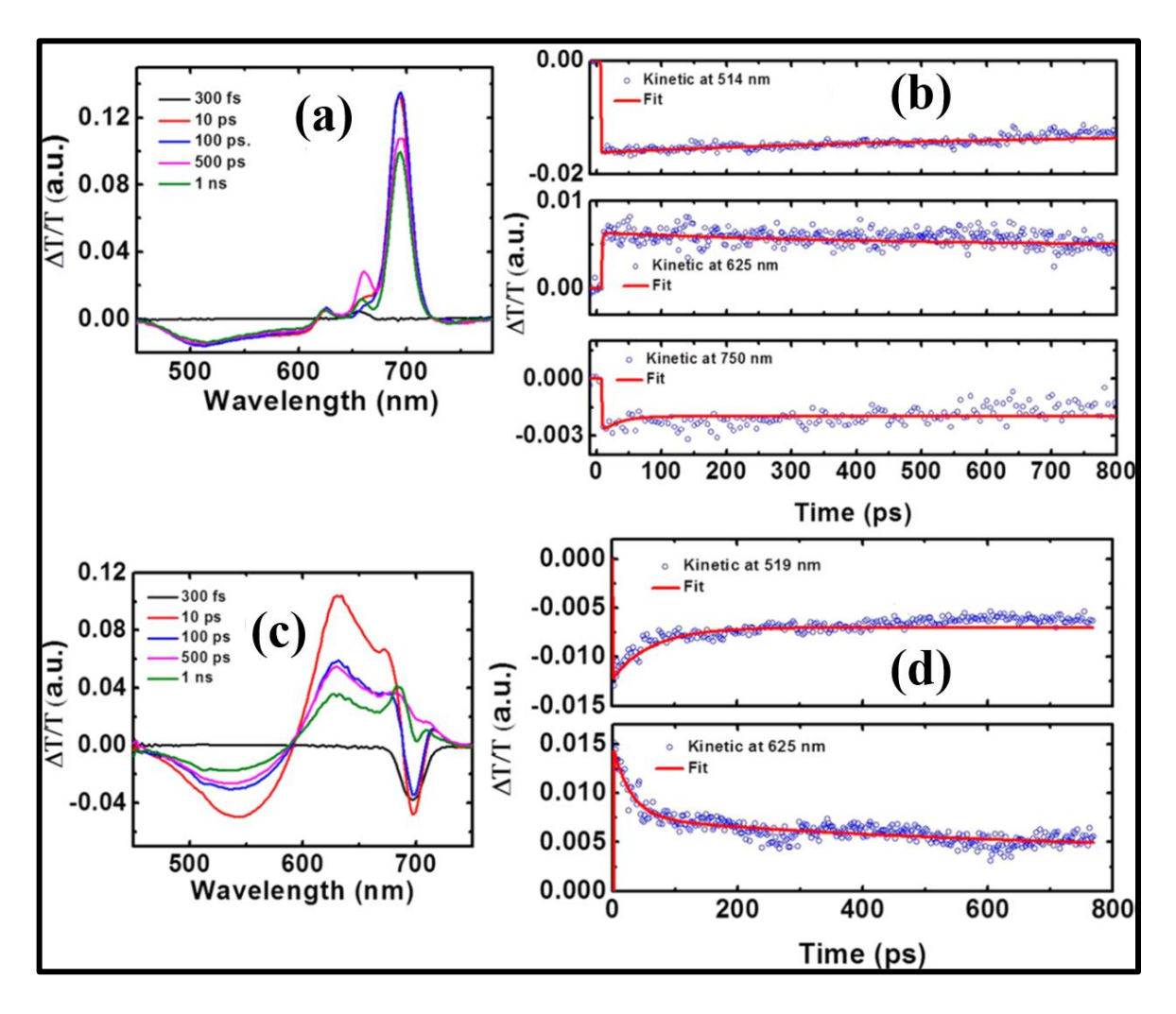


**Fig. 3.8** (a) Femtosecond transient absorption data for CBZ-Pc1 recorded for the time scales ranging from 300 fs to 1 ns. (b) Kinetics at probe wavelengths of 514, 625, and 750 nm. Open circles represent the experimental data while the solid lines are the theoretical fits. (c) Femtosecond transient absorption data for CBZ-Pc1 recorded for the time scales ranging from 300 fs to 1 ns. (d) Kinetics at probe wavelengths of 514 and 625 nm. Open circles represent the experimental data while the solid lines are the theoretical fits.

From figures 3.8(a)–3.8(d) data, it is evident that the excited state of CBZPC1 is longer lived than CBZPC2. There is a presence of pump residue around 690 nm [figure 3.8] (c)] which is taken care of for later measurements. The molecules showed a broad ESA with peak at ~514 nm while the GSB minima seen at ~625 nm and 750 nm. From emission studies [figures 3.2(c) and 3.2(d)] we can assume additional SE contribution around 750 nm. The absorption spectra of CBZPC1 (in THF solvent) and CBZPC2 (in DCM solvent) dyes illustrated two regions – in the visible to NIR we observe an intense band denoting  $S_0$  $\rightarrow$  S<sub>1</sub> transition and in the near-UV region, a S<sub>0</sub>  $\rightarrow$  S<sub>n</sub> (n  $\geq$  2) transition band of comparatively lower intensity. It has been reported that the larger size of a typical cyanine, structural inertia in them may lead to slow structural relaxation, which results in a slow internal conversion  $S_2 \rightarrow S_1$  [39, 40]. And this phenomenon is distinguishably visible in our excited state dynamics studies of the phthalocyanine molecules CBZPC1 and CBZPC2. For Q-band excitation at 650 and 690 nm for CBZPC1 and CBZPC2, respectively, 1 ns delay data were collected up and plotted as  $\Delta T/T$  versus wavelength ( $\lambda$  in nm). A negative band which was blue shifted to the absorption band ( $S_0 \rightarrow S_1$ : 570 to 750 nm) in the region of 450 to 615 nm region, denotes the ESA mediated reverse saturable absorption (RSA), correlated to higher state transitions  $S_1 \rightarrow S_n$ . On the other hand, the regions 615 to 644 nm for CBZPC1 and 590 to 698 nm for CBZPC2, showed a positive band in the  $\Delta T/T$  versus wavelength (λ in nm) graph indicating the ground state bleach (GSB) with stimulated emission (SE) processes. Corresponding to each band maxima, the kinetics (lifetime components) at those wavelengths were evaluated with the help of a sum of multiexponential functions [see figures 3.8(b) and 3.8(d)] with the corresponding lifetimes summarized in Table 3.3. The fitted kinetics for CBZPC1 (in THF) showed a biexponential decay fit revealing two distinct lifetime components at 515 nm (ESA maximum) - 473 ps  $(\tau_1)$  and 1.025 ns  $(\tau_2)$ , whereas, CBZPC2 (in DCM), showed its decay lifetime at 519 nm (ESA maximum) - 25.46 ps ( $\tau_1$ ) and 185.2 ps ( $\tau_2$ ). The fitted kinetics around 625 nm which corresponds to the SE+GSB band, also showed two lifetimes -725.3 ps ( $\tau_1$ ) and 1.59 ns  $(\tau_2)$  for CBZPC1 (THF) and 25.46 ps  $(\tau_1)$  and 780 ps  $(\tau_2)$  for CBZPC2 (DCM). This region indicates the population relaxation pathways of the molecules with  $\tau_1$  showing intersystem crossing (ISC) to the triplet state (T<sub>1</sub>) for CBZPC1 while internal conversion from higher singlet excited state  $(S_n)$  to first excited state for CBZPC2  $(S_1)$ . The slightly polar nature of THF and DCM solvents may make them prone to inducing aggregation within the molecular solution but the presence of carbazole groups at the periphery of the moieties prevented the molecule to self-aggregate in the solutions at aforementioned concentrations

[40, 41]. The  $\tau_2$  lifetime for CBZPC1 shows the ground state recovery of >1 ns with possible indications of long-lived triplet state formation. On the other hand, CBZPC2 showed relatively faster recovery which is in agreement with the typical fluorescence lifetimes (see section 3.2) and thus, is indicative to radiative decay for  $S_1 \rightarrow S_0$  transition. Our data were further compared with some of the recent studies in the field of phthalocyanines [42, 43, 44] and found our molecules to be quite promising for various ultrafast dynamics related applications, especially for the PDT. For the future, the present study can be extended to studying the optical nonlinearities of these molecules with varied pulse durations and varied wavelengths including the NIR wavelength range.

**Table 3.3**: Decay lifetimes of relaxation dynamics in CBZPC1 and CBZPC2 for different wavelengths.

λ (nm)	τ <sub>1</sub> (ps)	τ <sub>2</sub> (ps)					
CBZPC1							
514	473	1025					
625	725.3	1592					
750	2.2	26.33					
	CBZPC2	•					
514	25.46	185.2					
625	25.46	780					

 $\tau_R$ : Rise time;  $\tau_1/\tau_2$ : shorter decay component showing IC and/ or VC;  $\tau_3$ : longer decay component showing ISC. Error involved is  $\pm 10\%$ .

#### 3.3 Conclusions:

- The current study dives into the electrochemical, photophysical and NLO properties of two carbazole-induced phthalocyanines, CBZPC1 and CBZPC2.
- The carbazole group caused minimized molecular aggregation with a broadened absorption in Soret band. The computational DFT studies showed the molecular oxidation and reduction processes were ring-centered.

The femtosecond NLO studies of CBZPC1 and CBZPC2 have been investigated using
 Z-scan technique in kHz and MHz pulse regime at wavelengths from 600 to 900 nm.
 Large NLO coefficients were extracted from both the studies suggesting possible
 applications in optical limiting and optical switching. Also, the large 2PA cross section
 values can be effectively utilized in label-free biological imaging

• The excited state dynamics from fs-TAS studies were evaluated at each band maxima of the difference absorption spectra to reveal possibilities of long-lived triplet states in both the molecules. The fitted kinetics showed two distinct lifetimes – a shorter one (τ<sub>1</sub>) owing to intersystem crossing, ISC for CBZPC1 in THF while internal conversion, IC (S<sub>n</sub> → S<sub>1</sub>) for CBZPC2 in DCM and the longer lifetime (τ<sub>2</sub>) showed the molecular relaxation to the ground state from singlet or triplet state respectively, which was further verified from their structural and chemical studies.

#### 3.4 References:

- [1] B. Saleh and M. Teich, Fundamentals of photonics, New York: Wiley, 1991.
- [2] J. Dudley and J. R. J.R. Taylor, "Ten years of nonlinear optics in photonic crystal fibre," *Nat. Photonics*, vol. 3, p. 85–90, 2009.
- [3] P. Prasad, P.N. and D. Ulrich, *Nonlinear Optical and Electroactive P*, New York: Plenum Press, 1998.
- [4] W. Min, C. Freudiger, S. Lu and X. Xie, "Coherent nonlinear optical imaging: beyond fluorescence microscopy," *Annu. Rev. Phys. Chem.*, vol. 62, p. 507–530, 2011.
- [5] R. Boyd, *Nonlinear optics*, San Diego, CA: Academic Press, 1992.
- [6] J. Zyss, Molecular nonlinear optics: Materials, physics and devices, New York: Academic Press, 1994.
- [7] R. Philip, G. R. Kumar, P. Mathur and S. Ghosh, "Non-linear optical properties of the mixed-metal mixed-chalcogen clusters [[Fe<sub>2</sub>(CO)<sub>6</sub>{μ-SeC(Ph)=C(Se)}{(OEt)C = Cr(CO)<sub>5</sub>}] and [Fe<sub>2</sub>(CO)<sub>6</sub>Se<sub>2</sub>{μ-(CO)<sub>3</sub>Cr(η<sup>5</sup>-C<sub>5</sub>H(CH<sub>2</sub>Ph)(Ph)(OEt)}]," *Chem. Phys. Lett.*, vol. 313, p. 719–724, 1999.
- [8] K. Iliopoulos, I. Guezguez, A. Kerasidou, A. El-Ghayoury, D. Branzea, G. Nita, N. Avarvari, H. Belmabrouk, S. Couris and B. Sahraoui, "Effect of metal cation complexation on the nonlinear optical response of an electroactive bisiminopyridine ligand.," *Dyes Pigm.*, vol. 101, p. 229–233, 2014.
- [9] S. Zongo, K. Sanusi, J. Britton, P. Mthunzi, T. Nyokong, M. Maaza and B. Sahraoui., "Nonlinear optical properties of natural laccaic acid dye studied using Z-scan technique.," *Opt. Mater.*, vol. 46, p. 270–275, 2015.

- [10] B. Kulyk, S. Taboukhat, H. Akdas-Kilig, J.-L. Fillaut., Y. Boughaleb and B. Sahraoui., "Nonlinear refraction and absorption activity of dimethylaminostyryl substituted BODIPY dyes," *RSC Adv.*, vol. 6, p. 84854, 2016.
- [11] J. Riggs and Y. Sun, "Optical limiting properties of [60] fullerene derivatives.," *J. Phys. Chem. A*, vol. 103, p. 485–495, 1999.
- [12] X.-L. Zhang, X. Zhao, Z.-B. Liu, S. Shi, W.-Y. Zhou, J.-G. Tian, Y.-F. Xu and Y.-S., "Nonlinear optical and optical limiting properties of graphene oxide–Fe3O4 hybrid material," *J. Opt.*, vol. 13, pp. 7-11, 2013.
- [13] G. D. I. Torres, P. Vazquez, F. Agullo-Lopez and T. Torres, "Phthalocyanines and related compounds: organic targets for nonlinear optical applications," *J. Mater. Chem.*, vol. 8, p. 1671–1683, 1998.
- [14] D. Dini, M. Barthel and M. Hanack, "Phthalocyanines as active materials for optical limiting," *Eur. J. Org. Chem.*, vol. 2001, p. 3729-3769, 2001.
- [15] R. S. S. Kumar, S. V. Rao, L. Giribabu and D. N. Rao, "Femtosecond and nanosecond nonlinear optical properties of alkyl phthalocyanines studied using Z-scan technique.," *Chem. Phys. Lett.*, vol. 447, p. 274–278, 2007.
- [16] A. Zawadzka, P. Płóciennik, J. Strzelecki, M. Pranaitis, S. Dabos-Seignon and B. Sahraoui, "Structural and nonlinear optical properties of as-grown and annealed metallophthalocyanine thin films.," *Thin Solid Films*, vol. 545, p. 429–437, 2013.
- [17] A. Zawadzka, A. Karakas, P. Płociennik, J. Szatkowski, Z. Łukasiak, A. Kapceoglu, Y. Ceylan and B. Sahraoui, "Optical and structural characterization of thin films containing metallophthalocyanine chlorides.," *Dyes Pigm.*, vol. 112, p. 116–126, 2015.
- [18] S. Zongo, M. M.S. Dhlamini, P. Neethling, A. Yao, M. Maaza and B. Sahraoui, "Synthesis, characterization and femtosecond nonlinear saturable absorption behavior of copper phthalocyanine nanocrystals doped-PMMA polymer thin films.," *Opt. Mater.*, vol. 50, p. 138–143, 2015.
- [19] M. Larciprete, R. Ostuni, A. Belardini, M. Alonzo, G. Leahu, E. Fazio, C. Sibilia and M. Bertolotti, "Nonlinear optical absorption of zinc-phthalocyanines in polymeric matrix," *Photon. Nanostructures*, vol. 5, p. 73–78, 2007.

- [20] G. d. l. Torre, P. Vazquez, F. Agullo-Lopez and T. Torres, "Phthalocyanines and related compounds:organic targets for nonlinear optical applications," *J. Mater. Chem.*, vol. 8, pp. 1671-1683, 1998.
- [21] J. W. Perry, K. Mansour, I.-Y. Lee, X.-L. Wu, P. V. Bedworth, C.-T. Chen, D. Ng, S. R. Marder, P. Miles, T. Wada and et al., "Organic optical limiter with a strong nonlinear absorptive response," *Science*, vol. 273, p. 1533–1536, 1996.
- [22] M. E. Ragoussi, M. Ince and T. Torres, "Recent advances in phthalocyanine based sensitizers for dye-sensitized solar cells," *Eur. J. Inorg. Chem.*, vol. 13, p. 6475–6489, 2013.
- [23] K. Ishii, N. Kobayashi, K. M. Kadish, K. M. Smith and R. Guilard, *The Porphyrin Handbook*, Academic Press Elsevier: New York, 2003.
- [24] E. M. Maya, A. W. Snow, J. S. Shirk, R. G. S. Pong, G. L. Roberts and e. al., "Synthesis, aggregation behaviour and nonlinear absorption properties of lead phthalocyanine substituted with siloxane chains.," *J. Mater. Chem.*, vol. 13, p. 1603–1613, 2003.
- [25] F. Dumoulin, M. Durmus, V. Ahsen and T. Nyokong, "Synthetic pathways to water-soluble phthalocyanines and close analogs.," *Coord. Chem. Rev.*, vol. 254, p. 2792–2847, 2010.
- [26] L. Giribabu, C. V. Kumar, V. G. Reddy, P. Y. Reddy, C. S. Rao, S. Jang, J. Yum, M. K. Nazeeruddin and M. Gratzel, "Unsymmetrical alkoxy zinc phthalocyanine for sensitization of nanocrystalline TiO2 film," Sol. Energy Mater. Sol. Cells, vol. 91, p. 1611–1617, 2007.
- [27] L. Giribabu, V. K. Singh, C. V. Kumar, Y. Soujanya, P. Y. Reddy and M. L. Kantam, "Triphenylamine–phthalocyanine based sensitizer for sensitization of nanocrystalline TiO<sub>2</sub> films," *Sol. Energy*, vol. 85, p. 1204–1212, 2011.
- [28] S. Hamad, S. P. Tewari, L. Giribabu and S. Venugopal Rao, "Picosecond and femtosecond optical nonlinearities of novel corroles," *J. Porphy. Phth.*, vol. 16, p. 140–148, 2012.
- [29] D. Swain, V. K. Singh, N. V. Krishna, L. Giribabu and S. Venugopal Rao, "Optical, electrochemical, third-order nonlinear optical, excited state dynamics studies of Thio-Zinc Phthalocyanine.," *J. Porphy. Phth.*, vol. 18, p. 305–315, 2014.

- [30] D. Swain, R. Singh, V. K. Singh, N. V. Krishna, L. Giribabu and S. Venugopal Rao, "Sterically demanded zinc(II) phthalocyanines: synthesis, optical, electrochemical, nonlinear optical, excite state dynamics studies.," *J. Mater. Chem. C*, vol. 2, p. 1711–1722, 2014.
- [31] K. Srinivas, C. R. Kumar, M. A. Reddy, K. Bhanuprakash, V. J. Rao, and L. Giribabu, "D-π-A organic dyes with carbazole as donor for dye-sensitized solar cells," *Synth. Met.*, vol. 161, p. 96–105., 2011.
- [32] D. S. Lawrence, D. G. Whitten, "Photochemistry and photophysical properties of novel, unsymmetrically substituted metallophthalocyanines," *Photochem. Photobiol.*, vol. 64, p. 923–935, 1996.
- [33] S. Bhattacharya, C. Biswas, S. S. K. Raavi, J. V. S. Krishna, D. Koteshwar, L. Giribabu and S. V. Rao, "Optoelectronic, Nonlinear Optical Properties and Excited State Dynamics of a Triphenyl Imidazole Induced Phthalocyanine Derivative," *RSC Adv.*, vol. 9, pp. 36726-36741, 2019.
- [34] N. Krishna, P. T. Anusha, S. Venugopal Rao and L. Giribabu, "Optical, electrochemical and third-order nonlinear optical studies of triphenylamine substituted zinc phthalocyanine," *J. Porphy. Phth.*, vol. 20, p. 1173–1181, 2016.
- [35] D. Swain, R. Singh., V. Singh, N. Krishna, L. Giribabu. and S. Venugopal Rao, "Sterically demanded zinc(II) phthalocyanines:synthesis, optical, electrochemical, nonlinear optical, excite statedynamics studies," *J. Mater. Chem. C*, vol. 2, p. 1711–1722, 2014.
- [36] N. Venkatram, D. N. Rao, L. Giribabu and S. Venugopal Rao, "Nonlinear optical and optical limiting studies of alkoxy phthalocyanines in solutions studied at 532 nm with nanosecond pulses," *Chem. Phys. Lett.*, vol. 464, p. 211–215, 2008.
- [37] K. Balakrishna, R. Sampath, T. Vishwam, A. Samui, M. Joshi and S. Mohan, "Synthesis and Characterization of Carbazole Based Donor-Acceptor-Donor Type Polymer for NLO Applications," *J. Phys.: Conf. Ser.*, vol. 1495, p. 012026, 2020.
- [38] S. Majeed, N. Nwaji, J. Mack, T. Nyokong and S. Makhseed, "Nonlinear optical responses of carbazole-substituted phthalocyanines conjugated to graphene quantum dots and in thin films," *J. Lumin.*, vol. 213, p. 88-97, 2019.

- [39] D. Oulianov, A. Dvornikov and P. Rentzepis, "Femtosecond-to-nanosecond nonlinear spectroscopy of polymethine molecules," *Opt. Commun.*, vol. 205, p. 427–436, 2002.
- [40] W. Parson, "Electron-transfer dynamics in a Zn-porphyrin quinone cyclophane: effects of solvent, vibrational relaxations, and conical intersections," *J. Phys. Chem. B*, vol. 122, p. 3854–3863, 2018.
- [41] J. Savolainen., D. V. d. Linden, N. Dijkhuizen and J.L. Herek, "Characterizing the functional dynamics of zinc phthalocyanine from femtoseconds to nanoseconds," *J. Photochem. Photobiol. A*, vol. 196, pp. 99-105, 2008.
- [42] O. Adegoke, M. Ince., A. Mishra, A. Green, O. Varnavski, M. Martínez-Díaz, P. Bauerle, T. Torres and T. Goodson, "Synthesis and ultrafast time resolved spectroscopy of peripherally functionalized Zinc phthalocyanine bearing oligothienylene-ethynylene subunits," *J. Phys. Chem. C*, vol. 117, p. 20912–20918, 2013.
- [43] B. Brozek-Pluska, M. Orlikowski and H. Abramczyk, *Phthalocyanines*, Chapter IIA, pp 47–56., 2015.
- [44] V. Gulbinas, M. Chachisvilis, L. Valkunas and V. Sundstrom, "Excited state dynamics of phthalocyanine films," *J. Phys. Chem.*, vol. 100, p. 2213–2219, 1996.

# **Chapter 4**

# Excited State Dynamics and Nonlinear Optical Studies of a Triphenylamine Imidazole Substituted Novel Zinc Phthalocyanine.

The chapter encompasses the detailed photophysical studies of a ZnPc with triphenylamine group attached at its peripheral position by means of an ethylene bridge named as PBIPC [2(3), 9(10), 16(17), 23(24) tetrakis-4-((4-(1,4,5-triphenyl-1Himidazol-2-yl) phenyl) ethynyl) phthalocyanine zinc(II)]. A solution of PBIPC in THF or tetrahydrofuran was used for all the studies carried out. The molecule demonstrated a broad Soret (B) absorption band with emission around 700 nm. The time-resolved fluorescence data established the radiative lifetime to be ~3.7 ns with a quantum yield of 0.22. The computational studies [DFT, TD-DFT analysis by means of hybrid functional theory (B3LYP)] of energy optimized structures depicting HOMO-LUMO levels in PBIPC, revealed no distinctive donor-acceptor molecular system. The non-radiative lifetimes were measured using fs-TAS technique and global fit analysis. The results revealed 78% of the excited species underwent ISC with a decay rate,  $k_{isc} = 2.1 \times 10^8 \text{ s}^{-1}$ . This shows that PBIPC can be used as a potential photosensitizer in dye-sensitized solar cells (DSSCs) and phototherapy (PDT). The Pc molecule was also investigated for its third-order nonlinear optical behavior in the visible wavelengths and IR regime [600 nm  $-1.5 \mu m$ ] using the standard Z-scan technique. The data collected in the visible range from 600-800 nm exhibited two-photon absorption as the predominant NLO interaction while in the near-infrared wavelength range (1.0–1.5 μm) was dominated by three- and four-photon absorption processes. The nonlinear refractive index illustrated a self-focusing behaviour for the entire wavelength range.

#### Part of the presented work in this chapter has been published in the following.

- **1. S. Bhattacharya**, C. Biswas, S. S. K. Raavi, J. V. S. Krishna, D. Koteshwar, L. Giribabu and S. Venugopal Rao, "Optoelectronic, Nonlinear Optical Properties and Excited State Dynamics of a Triphenyl Imidazole Induced Phthalocyanine Derivative", *RSC Advances* **2019**, 9, 36726–36741.
- **2. S. Bhattacharya**, C. Biswas, S. S. K. Raavi, G. Lingamallu, S. Venugopal Rao, "Femtosecond transient absorption and nonlinear optical studies of a novel zinc phthalocyanine", **Topical meeting on nonlinear optics**, Waikoloa beach, Hawaii, U.S. **2019.** [**Proc. Photonics-2019- NTU4A.17**]

#### 4.1 Introduction

As discussed in the earlier chapters, phthalocyanines can be tailored through several synthetic procedures to possess superior thermal, chemical and optical stability including the ability to incorporate non-metallic and metallic ions in its cavity which can improve their nonlinear optical (NLO) properties [1, 2, 3]. Due to their favourable functionalization of various substituent groups at the peripheral positions, increased solubility in common organic solvents can be achieved with minimized aggregation [4, 5]. Triphenylamine imidazole molecule is currently being exploited for their applications in OLEDs (organic light emitting diodes) as fluorophores [6, 7, 8]. Its absorption window lies within the UV to near-UV region and generally emit in blue or green range. Additionally, the triphenylamine imidazole molecule was found to possess antimicrobial properties with an ability to photo-protect against PDT [9, 10]. Zinc phthalocyanine and its derivatives have proved to be excellent photosensitizers (PS) for PDT [11]. Recently, Ronguin et al. investigated Zn(II)Pcs in-vitro, 3D cells and in other complex structures in a combined therapeutic technique for clinical trials [12]. Kuzyniak et al. demonstrated the potential of ZnPc in treatment of oesophageal cancer by dose-dependent growth inhibition of adenocarcinoma and squamous cells by >90% [13]. When a PS is administered in a tissue and irradiated with a specific excitation wavelength, it releases cytotoxic species by undergoing certain photochemical interaction within the tissue, in presence of oxygen resulting in target tissue destruction. The efficacy of PDT relies on several factors like solubility, aggregation, intersystem crossing, etc [14, 15] for which the molecular structure of the PS and its excited state dynamics need to be studied thoroughly. To achieve larger penetration depth, a PS can be subjected to multi-photon excitation where a longer wavelength photon is nonlinearly absorbed by the PS to reach a higher energy excitation level, this mechanism has already been extensively used in 2PE-PDT or two photon excitation PDT [16]. The pre-requisite of this technique is a PS with large NLO absorption cross-section (σ) which is also discussed in this chapter. The NLO studies of Pcs have been studied since long enough to make us realize their application in Optical limiting and other multi-photon absorption applications [17, 18, 19]. However, most works have been focused on two-photon absorption and not beyond that. It was in 2000s that He et al. observed a highly directional and up-converted stimulated emission in an organic chromophore solution as an amplified spontaneous emission, produced by a strong simultaneous threephoton absorption at 1.3 µm [20]. Later on, a lot of groups started exploring 3PA

phenomenon for applications in OL, bio-imaging, short-pulse communications and frequency upconversion [21, 22, 23]. In 2017, Chen et al. [24] showed unusually large 5PA cross-section area of a family of halide perovskites colloidal nanocrystals at 1.3 µm. Other reported cases of organic chromophores with multi-photon absorption properties in the near-IR, have been exploited in the area of optical storage, communications, etc [25, 26, 27]. Unfortunately, very few studies have been conducted and reported in literature about the NLO properties of organic molecules, especially phthalocyanines, in the near-infrared spectral region. Hence, in this work, we have focused our efforts on understanding the ultrafast NLO studies of an imidazole substituted ZnPc through an ethynyl bridge (PBIPC) using femtosecond pulses from visible, 600–800 nm to the near infrared spectral region of 1.0–1.5 mm, using the Z-scan technique. The ultrafast studies of the excited molecule were achieved using the femtosecond transient absorption technique at B-band as well as Q-band excitation. The incorporation of triphenyl imidazole moiety in the phthalocyanine group has been observed to have significant effect on the electronic and sterical properties of the molecule using various optical spectroscopic techniques. The studies enabled us to identify the potential of PBIPC as a PS for photo-therapeutic and optoelectronic applications.

# **4.2** Experimental Details and Results:

PBIPC or 2(3), 9(10), 16(17), 23(24) tetrakis-4-((4-(1,4,5-triphenyl-1Himidazol-2-yl)phenyl)phthalocyanine zinc(II) with molecular weight of 2155.77 a.u. and structure as shown in figure 4.1(a), was studied for optical, NLO and photophysical properties. Shimadzu UV-3600, UV-visible-NIR spectrophotometer recorded the steady state absorption spectra of the given molecules. Fluorolog-3 spectrofluorometer (Spex model, JobinYvon) recorded the steady-state fluorescence spectra at 0.06 optical density. For fluorescence quantum yield calculations, zinc tertbutyl phthalocyanine (=0.37 in benzene) was used as the reference. [32]. A picosecond emitting diode laser (NanoLED,  $\lambda$ ex= 670 nm) by IBH Horiba Jobin Yvon - FluoroLog3- Triple Illuminator was used to record the corresponding fluorescence lifetimes of the molecules. The decay curves were recorded at  $\lambda$ em = 700 nm which is the phthalocyanine macrocycle fluorescence emission maxima. Detector used was the Photomultiplier tube (R928P, M/s Hamamatsu). A dilute solution of Ludox (in water) acted as a scatterer while recording the lamp profile. The instrument response function was calculated by the excitation source (~635 ps at 670 nm) full width half maximum (FWHM). Data fitting the decay curves were performed using

nonlinear least-squares iteration process with the help of IBH DAS6 (version 2.3) decay analysis software. The quality of the fits was adjudicated by the  $\chi^2$  values along with distribution of the residuals. The absorption of the PBIPC solution in THF were found to have a broadened Soret band with peak at 350 nm and an intense B-band at 695 nm which is typical to the Pc moiety, with a shoulder at 630 nm which is due to the presence of metal centre Zn as shown by blue solid line in figure 4.1(b). Emission studies demonstrated a shift in the Stokes peak at ~708 nm following the rule of mirror symmetry and indicated in figure 4.1(b) by the dashed line. The fluorescence lifetime, measured using the time correlated single photon counting (TCSPC) technique, was found to be ~3.68 ns with a yield of 22%.

The density functional theory (DFT) and time-dependent DFT studies were run in a functional basis set of the B3LYP/6-31G (d,p) level [Gaussian 09 package] to determine the theoretical information about structural, optical, and redox properties of the PBIPC. The PBIPC molecule constitutes the optimized energy structures as shown in Figures 4.2. Here, the HOMO, LUMO, and HOMO–LUMO gap energies with ground state dipole moment are given in Debye units. For PBIPC electron distribution, the optimized structure consists of HOMO and LUMO predominantly on the phthalocyanine ring at -4.830 and -2.871 levels respectively while the HOMO–1 was on phthalocyanine ring and at -5.124 and LUMO+1 at -2.785 on triphenyl imidazole moiety. Similarly, HOMO–2 electron cloud resided on triphenyl imidazole (-5.164) and LUMO+2 on phthalocyanine moiety at (-1.713). All these measurements were carried out at IICT, Hyderabad [28].

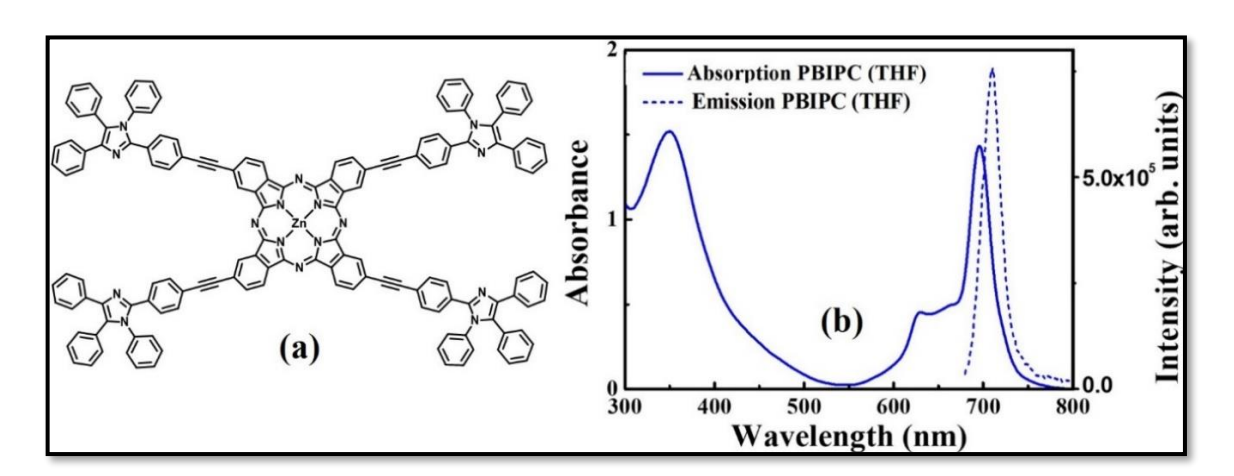


**Figure 4.1** (a) Molecular structure of PBIPC. (b) UV-visible absorption spectrum and emission spectrum of PBIPC in THF solvent depicted as solid blue line and dashed blue line respectively.

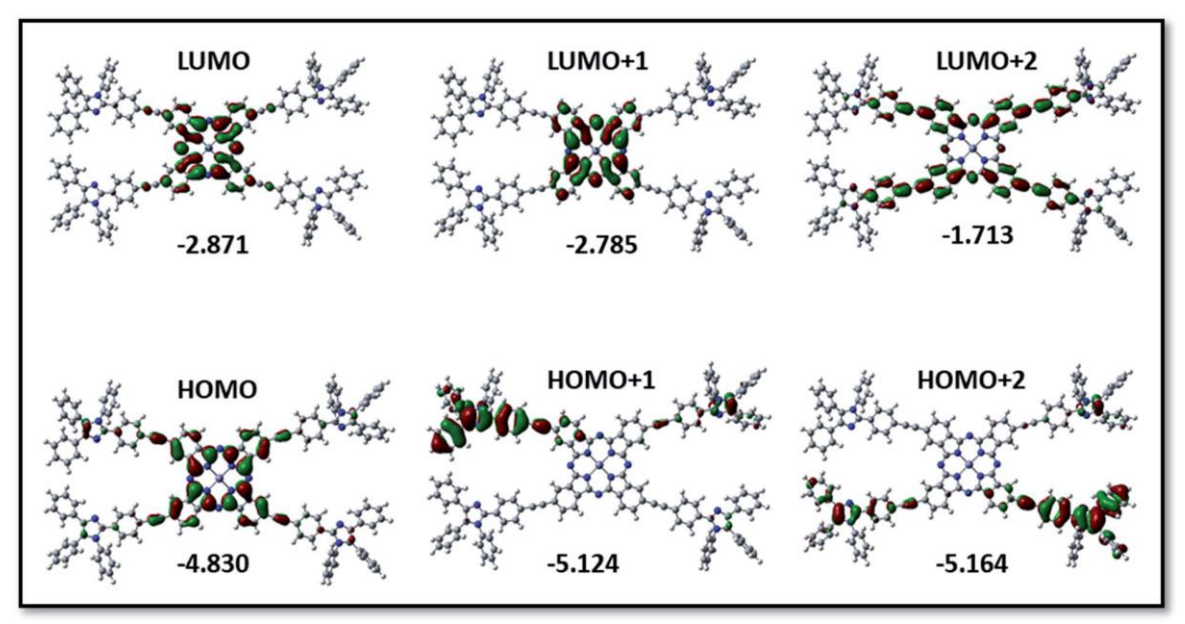


**Figure 4.2** Isodensity plots of FMOs and the energy values in eV by using the B3LYP method 6-31G (d,p) for PBIPC.

# 4.2.1. Z-scan with MHz pulses:

PBIPC was investigated in the 700–900 nm excitation range using 150 fs, 80 MHz pulses using the experimental setup described in the figure 2.11 of Chapter 2. Due to high molar extinction co-efficient of PBIPC in THF, a 70 µM concentration of the solution was used for the present study. Also, low concentration ensured the absence of any aggregation within the solution. The input peak intensity was in the 20-60 GW/cm<sup>2</sup> tange and the Rayleigh range were in the 1.9–2.8 mm range for given wavelength window. 1-mm glass cuvette was used for holding the sample solutions. The calculations and data fitting were performed using the formulae mentioned and discussed in Chapter 2. The open aperture studies showed RSA for the afore-mentioned input intensities with 2PA being the dominant phenomenon [see data in figures 4.3(a)–(c)]. The obtained 2PA coefficient was in the order of  $\sim (2.5-3.0)\times 10^{-8}$  W/cm<sup>2</sup> with an absorption cross-section,  $\sigma_2 \sim (1.6-2.9)\times 10^4$  GM. The closed aperture studies [figures 4.2 (d)–(f)] illustrate a positive nonlinearity with the coefficient,  $n_2 \sim (2.1-4.9)\times 10^{-16}$  cm<sup>2</sup>/W indicating a self-focusing behaviour. In the MHz regime, no solvent contribution was detected hence we can relate the obtained data to NLO behaviour of PBIPC only. Although, MHz pulses include contributions from both electronic and thermal phenomena (absorption of the laser light), from earlier studies on similar molecules demonstrated that the major contribution to the nonlinear absorption when excited with nJ, MHz, 800 nm pulses (from fs oscillator) was from the instantaneous TPA as shown in figure 4.7 (red arrow).

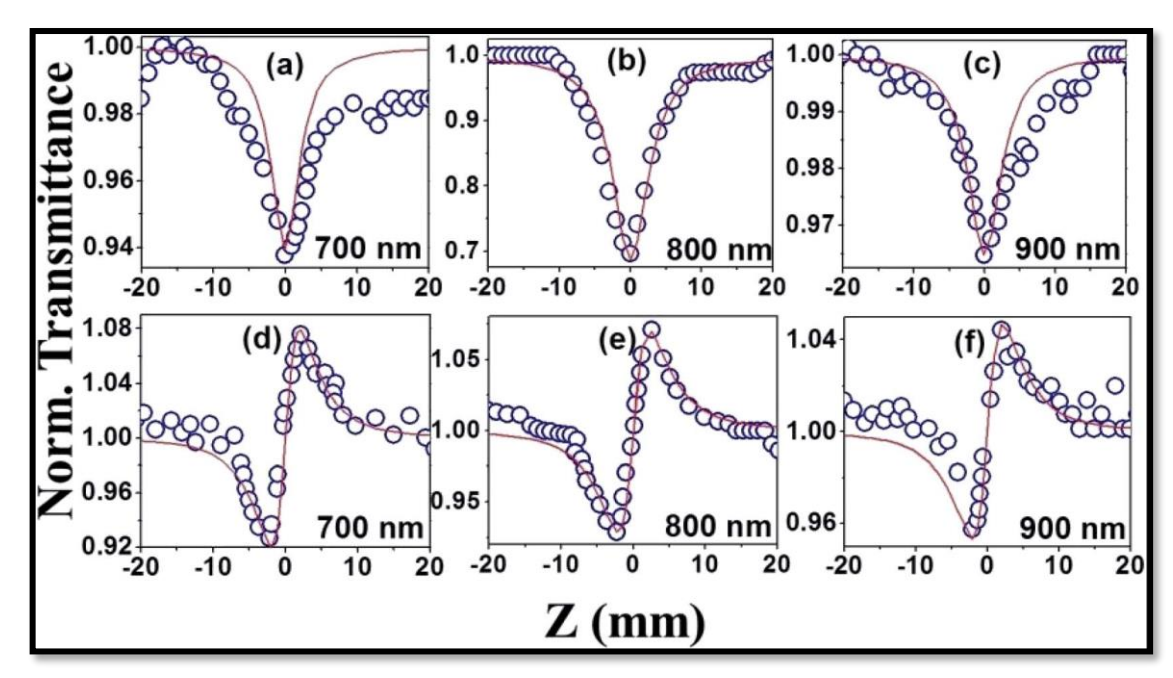


**Figure 4.3** (a), (b) and (c) Open aperture Z-scan data and (d), (e) and (f) closed aperture Z-scan data of PBIPC recorded at wavelengths of 700 nm, 800 nm and 900 nm, respectively, with 150 fs, 80 MHz pulses. The experimental data (blue, open circles) are best fitted (red, solid lines) for 2PA and positive nonlinear refraction.

# 4.2.2. Z-scan with kHz pulses:

The NLO results from MHz pulse regime might contain additional thermal contribution due to higher repetition rate with larger pulse width. Thus, in order to look at purely electronic contributions, PBIPC was studied for 600 nm – 1.5 µm excitation range using 70 fs, 1 kHz pulses using the setup as shown in figure 3 in Chapter 2. 70 µM concentration of the solution was used with the input intensity being in the range of 139– 370 GW/cm<sup>2</sup> and the Rayleigh range was in the 1.9–4.7 mm range for a given wavelength window. A 1-mm glass cuvette was used for all the Z-scan studies. For the visible range of 600 nm – 800 nm wavelength range, the RSA phenomena was predominantly 2PA [figures 4.4(a)–(c)] with absorption co-efficient of  $\alpha_2 \sim (2.0-12.0)\times 10^{-11}$  W/cm<sup>2</sup> and absorption cross-section in the range of 1570 – 7080 GM (see table 4.1). In the 2PA regime, PBIPC depicted positive nonlinearity with  $n_2 \sim (0.12-0.92)\times 10^{-16}$  cm<sup>2</sup>/W as shown in figures 4.4(d)–(f). For wavelengths 1.0 μm and 1.2 μm, the molecule exhibited RSA phenomenon that fitted best with 3PA calculation [figures 4.4 (a) and (b)] with 3PA coefficient,  $\alpha_3 \sim (2.7 - 1)$  $4.6)\times10^{-21}$  cm<sup>3</sup>/W<sup>2</sup> and 3P cross-section of  $\sigma_3 \sim (2.5-2.9)\times10^{-78}$  cm<sup>6</sup>s<sup>2</sup>. Positive nonlinearity was observed here as well with NLO refractive index,  $n_2 \sim (5.6-15.2)\times 10^{-16}$  cm<sup>2</sup>/W as shown in figure 4.5 (c) and (d). Beyond that, in the 1.3–1.5 µm spectral regime, 4PA was

the dominating phenomenon [figures 4.6(a)–(c)] with four-photon nonlinear absorption coefficient,  $\alpha_4 \sim (0.5-7.4)\times 10^{-32} \text{ cm}^5/\text{W}^3$  and cross-section,  $\sigma_3 \sim (3-62)\times 10^{-108} \text{ cm}^8\text{s}^3$ .

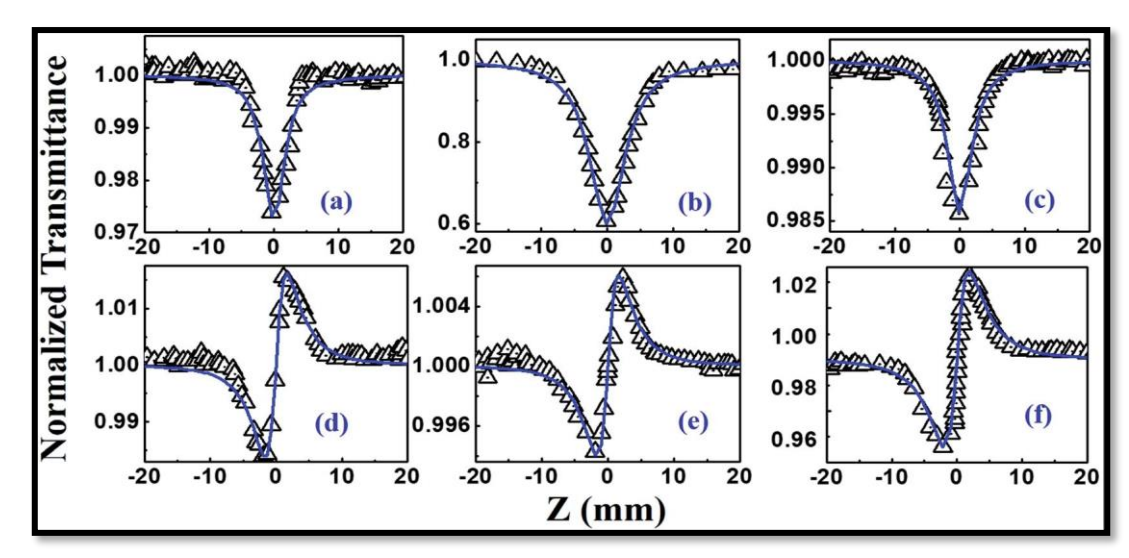


**Fig. 4.4** (a), (b) and (c) Open aperture Z-scan data (d), (e) and (f) closed aperture Z-scan data of PBIPC recorded at wavelengths of 600 nm, 700 nm and 800 nm, respectively, with 70 fs, 1 kHz pulses. The experimental data are represented by black, open triangles while the best fits are represented by blue, solid lines (for both 2PA and positive nonlinear refraction).

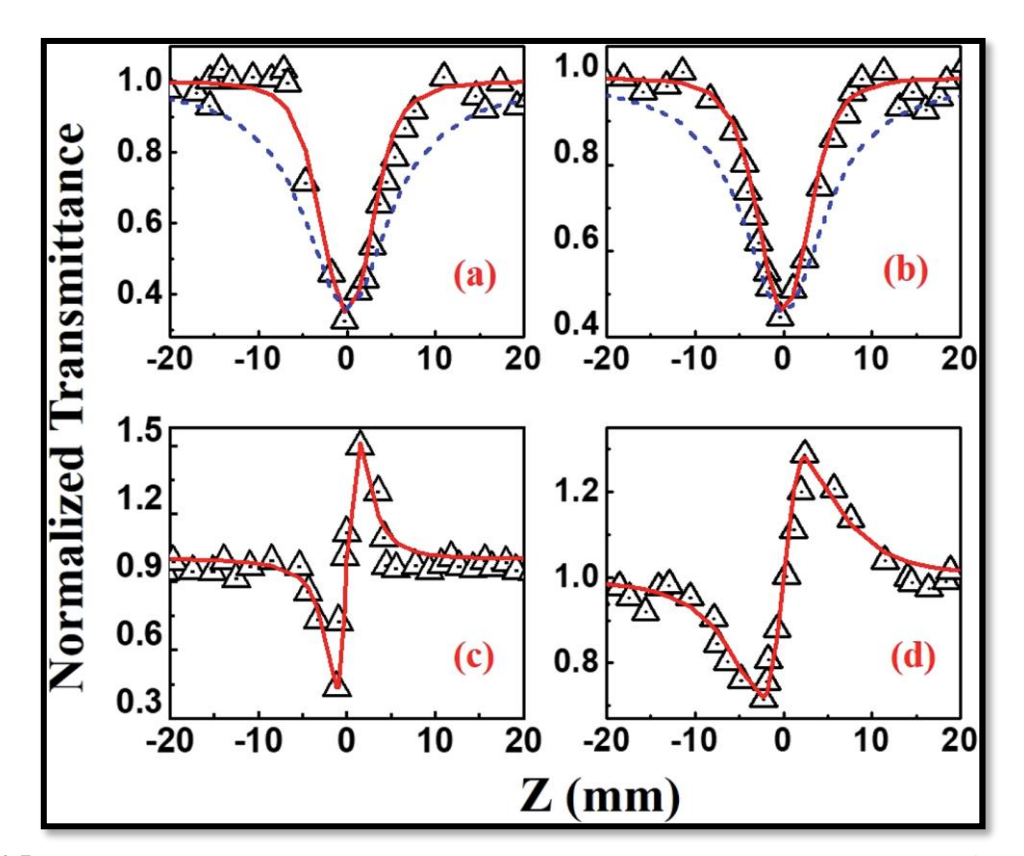


**Fig. 4.5** (a) and (b) Open aperture Z-scan data (c) and (d) closed aperture Z-scan data of PBIPC at wavelengths of 1000 nm and 1200 nm, respectively, and kHz excitation. Black triangles represent the experimental data while red, solid lines represent the 3PA fits. Blue, dashed lines represent 2PA fits in (a) and (b).

The nonlinear refractive index for the given wavelength range was found to be  $n_2 \sim (28-38)\times 10^{-16}~\text{cm}^2/\text{W}$  with data and the theoretical fits being presented in figures 4.6(d)–(f). Under the current experimental conditions ( $\sim 150~\text{fs}$ , MHz pulses), we can assume that the multi-photon absorption processes are not instantaneous (see figure 4.7) like in the kHz regime (where the pulse duration is < 50~fs and has lower probability of relaxing back in the upper excited states) but are sequential. In case there is no linear absorption of the single photon then the 2PA process (has to occur through virtual levels) is definitely instantaneous. Two-step 2PA occurs when the single photon is absorbed into the real states of the system being investigated. The detailed summary of all the NLO coefficients obtained from the present Z-scan study (MHz & kHz repetition rates) are summarized in Table 4.1.

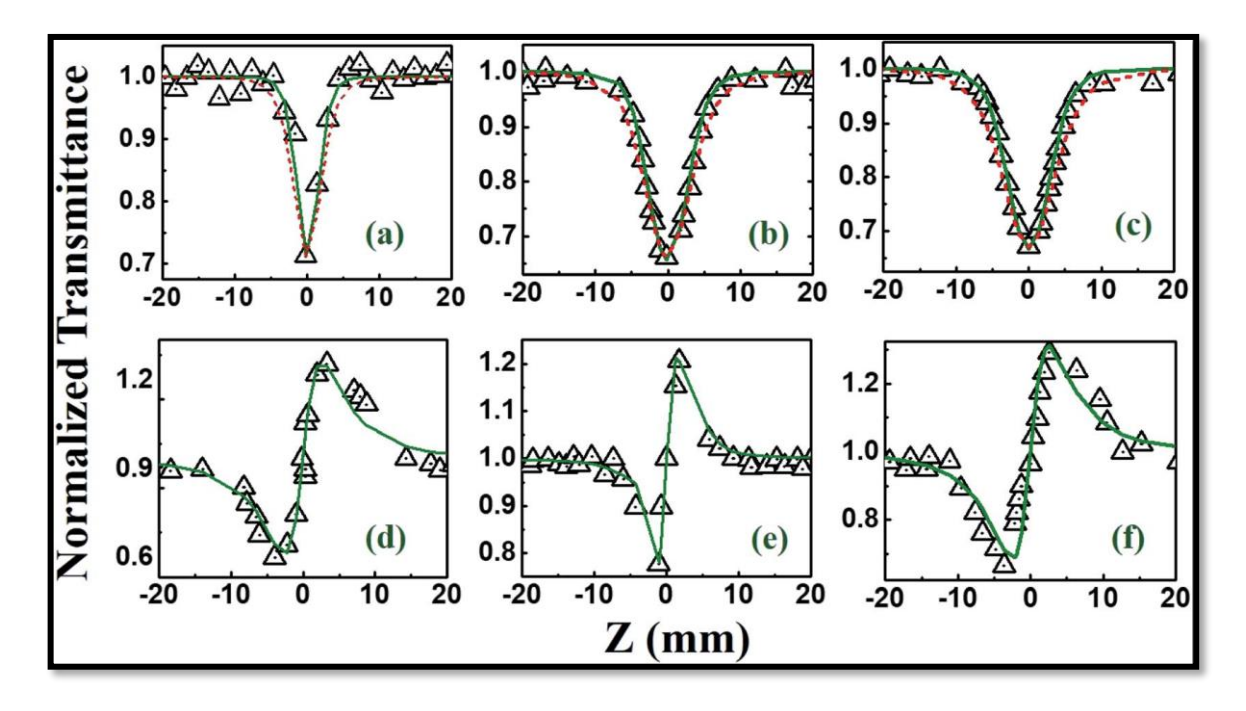


**Fig. 4.6** (a), (b) and (c) Open aperture Z-scan data (d), (e) and (f) Closed aperture Z-scan data of PBIPC recorded at wavelengths of 1300 nm, 1400 nm and 1500 nm, respectively, for kHz pulse regime. Black triangles represent the experimental data while green, solid lines represent the 4PA fits. Red, dashed lines represent 3PA fitted curves in (a), (b), and (c).

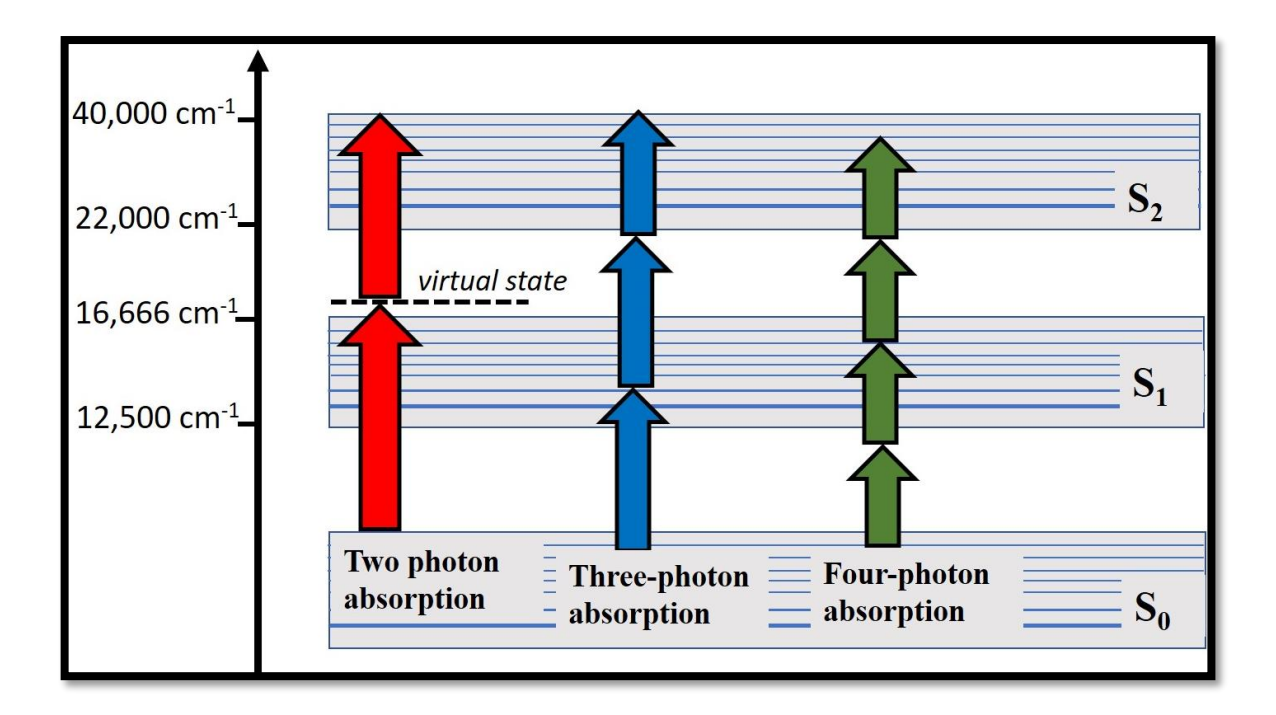


**Figure 4.7 RED:** Indicates instantaneous 2-photon absorption where the excited molecule absorbs 2 photons consecutively to reach a higher energy state using a virtual state as indicated in the diagram. **BLUE:** Indicates a sequential or non-instantaneous absorption process where the molecule reaches a certain excited state, losses energy before getting excited to the next level with photons of equal energies.

From the above studies and the data obtained, it is evident that molecule PBIPC possessed superior NLO properties with large 2PA cross-sections (retrieved with fs kHz pulses), which are on par with a few of the recently reported potential PS's used for two-photon excitation (TPE) PDT applications [16, 29, 30]. Additionally, the three- and four-photon absorption cross-sections were found to be equally large to many reported molecules making PBIPC ideal for applications such as three-photon pumped (3PP) and frequency upconverted lasing, 3PA based optical power limiting and stabilization, 3PA-based bio-imaging by means of IR to visible conversion, data storage, imaging and others [31, 32, 33].

**Table 4.1:** Summary of NLO coefficients of PBIPC for different wavelengths at both kHz and MHz pulse regime.

λ (nm)	n <sub>2</sub> (cm <sup>2</sup> /W) ×10 <sup>-16</sup>	n <sub>2</sub> (e.s.u.) ×10 <sup>-13</sup>	$\chi_{R}^{(3)}$ $m^2/V^2 \times 10^{-23}$	α <sub>2</sub> (cm/W) ×10 <sup>-11</sup>	(cm <sup>3</sup> /W <sup>2</sup> ) ×10 <sup>-21</sup>	α4 (cm <sup>5</sup> /W <sup>3</sup> ) ×10 <sup>-32</sup>	<b>6</b> 2Р ( <b>GM</b> )	$\sigma_{3P}$ $(cm^6s^2)$ $\times 10^{-78}$	σ4P (cm <sup>8</sup> s <sup>3</sup> ) ×10 <sup>-108</sup>	$\chi_{\rm I}^{(3)}$ ${\rm m}^2/{\rm V}^2$ $\times 10^{-23}$	χ <sup>(3)</sup> e.s.u. ×10 <sup>-15</sup>
					PBIPC kHz	pulses					
600	0.12	0.43	0.14	2.0	-	-	1570	-	-	1.14	1.31
700	0.81	2.90	0.97	3.0	-	-	2019	-	-	1.99	7.08
800	0.92	0.57	0.19	12.0	-	-	7080	-	-	9.13	6.68
1000	5.65	20.0	6.69	-	2.7	-	-	2.53	-	-	-
1200	15.2	54.0	18.4	-	4.6	-	-	2.99	-	-	-
1300	38.6	13.8	4.60	-	-	7.4	-	-	62.7	-	-
1400	31.9	11.4	3.81	-	-	0.49	-	-	3.32	-	-
1500	28.9	10.3	3.45	-	-	2.2	-	-	12.1	-	-
					PBIPC MHz	pulses					
λ (nm)	n <sub>2</sub> (cm <sup>2</sup> /W) ×10 <sup>-12</sup>	n <sub>2</sub> (e.s.u.) ×10 <sup>-8</sup>	$\chi_{R(^3)} $ $m^2/V^2 \times 10^{-18}$	α2 (cm/W) ×10 <sup>-8</sup>			$\sigma^2 \times 10^4$ (GM)			$\chi_{\rm I}^{(3)}$ ${\rm m}^2/{\rm V}^2$ $\times 10^{-20}$	χ <sup>(3)</sup> e.s.u. ×10 <sup>-10</sup>
700	2.14	0.76	2.55	2.48			1.67			16	1.83
800	2.14	0.76	2.55	5.00			2.94			38	1.85
900	4.89	1.75	5.84	3.20			1.67			27	4.19

# 4.2.3. fs-TAS with kHz pulses:

The molecule PBIPC in THF was excited at Soret band tail end, 400 nm and shoulder end of B-band at 650 nm. They were probed in the visible range of 440 – 800 nm up to a delay of 2 ns. The obtained data is shown in figures 4.8(a)–(d) indicating band maxima and minima. The data presented here, had been corrected for possible artifacts accompanying the transient absorption measurements (coherent artifact, chirp correction, background correction, etc.). The zero delay was around ~250 ps.

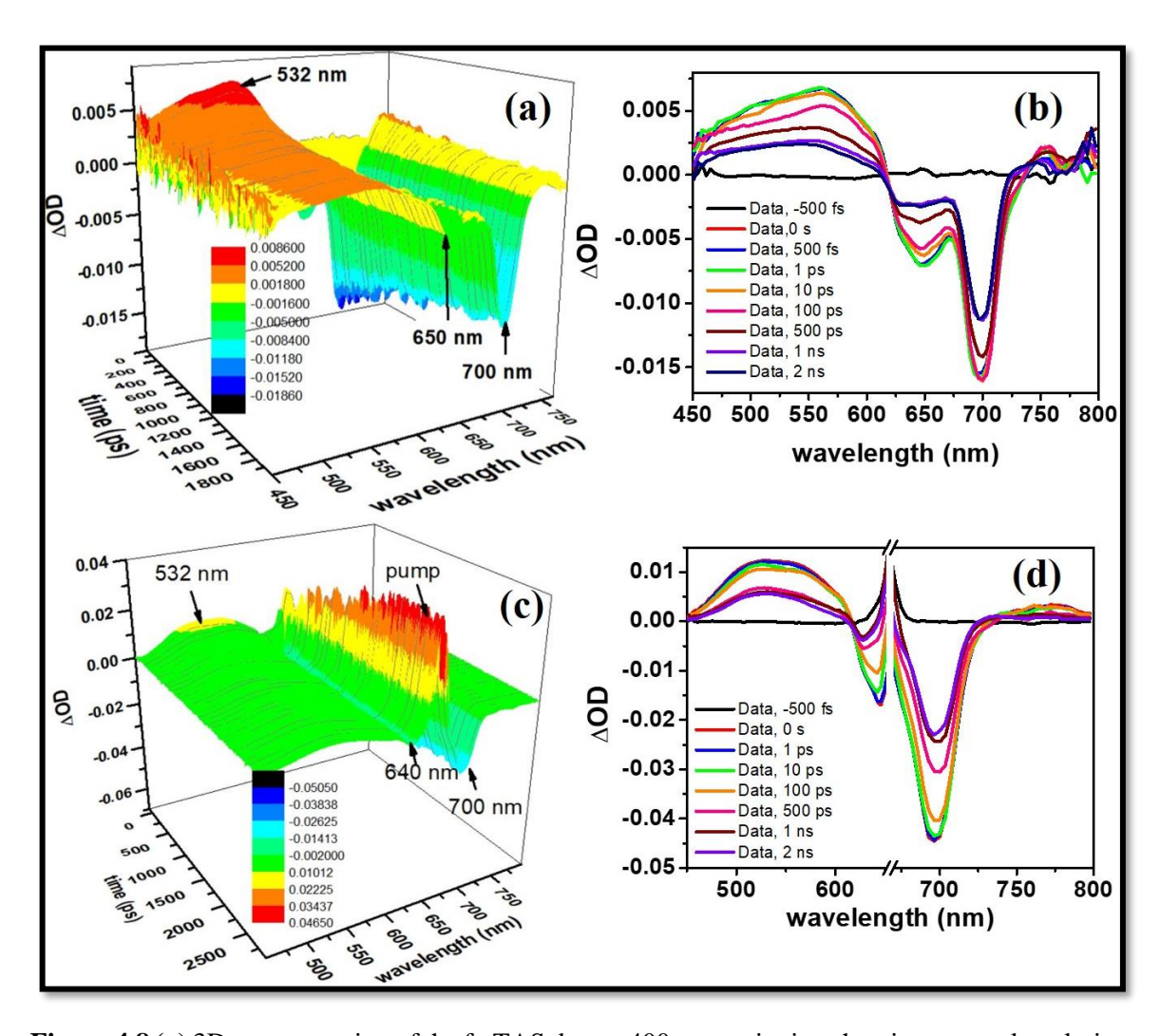


**Figure 4.8 (a)** 3D representation of the fs-TAS data at 400 nm excitation showing spectral evolution over 2 ns probe delay. **(b)** Spectral evolution of PBIPC at specific delays for 400 nm excitation. **(c)** 3D representation of the fs-TAS data at 650 nm excitation showing spectral evolution over 2 ns probe delay. The sharp spike around 650 nm is from the pump pulse and does not contribute to the transient data analysis **(d)** Spectral evolution of the sample PBIPC at specific delays for 650 nm excitation.

From the data presented in figures 4.8(a)–(d), it is evident that the transient data for PBIPC was independent of the excitation wavelength, depicting almost no change in each band maxima/minima. There was a presence of pump residue around 650 nm (figure 4.8 (c)) which is taken care of for later measurements. The molecule exhibited a broad ESA with peak at ~532 nm while the GSB minima seen at ~650 nm and 700 nm. From emission studies [figure 4.1(b)] we can assume additional SE contribution around 700 nm. The ESA spectra [figures 4.8(b), 4.8(d)] were seen to be broad, overlapping with the GSB spectra which indicated the possibility of triplet state transitions which is typical to phthalocyanines [29, 30]. The ESA band ( $\triangle$ OD>0) was observed to be long-lived and does not decay completely within the given delay time (~2 ns). This region shows the lifetime of singlet excited state S<sub>1</sub> which is filled from higher excited singlet states, S<sub>n</sub> via IC and/or vibrationally hot S<sub>1</sub> state via vibrational relaxation. From S<sub>1</sub> state, the excited species are likely to fill up the ground state  $S_0$  via radiative or non-radiative pathways or both. This is indicated by negative ΔOD band where the minima at ~650 nm and ~700 nm decreased concomitantly with S<sub>1</sub> state depopulation. The overlapping ESA and GSB spectra, observed as a slight spectral shift after 500 ps delay time, is indicative of a possible spin-forbidden transition ISC which can be confirmed in the kinetic studies. For kinetic studies, we chose each band extremes - ESA: 532 nm, GSB: 640 nm and 700 nm. The molecule was best fitted with a three-level kinetic model as shown in figures 4.9(a) and 4.9(b) with the obtained lifetimes being summarized in Table 4.2 below.

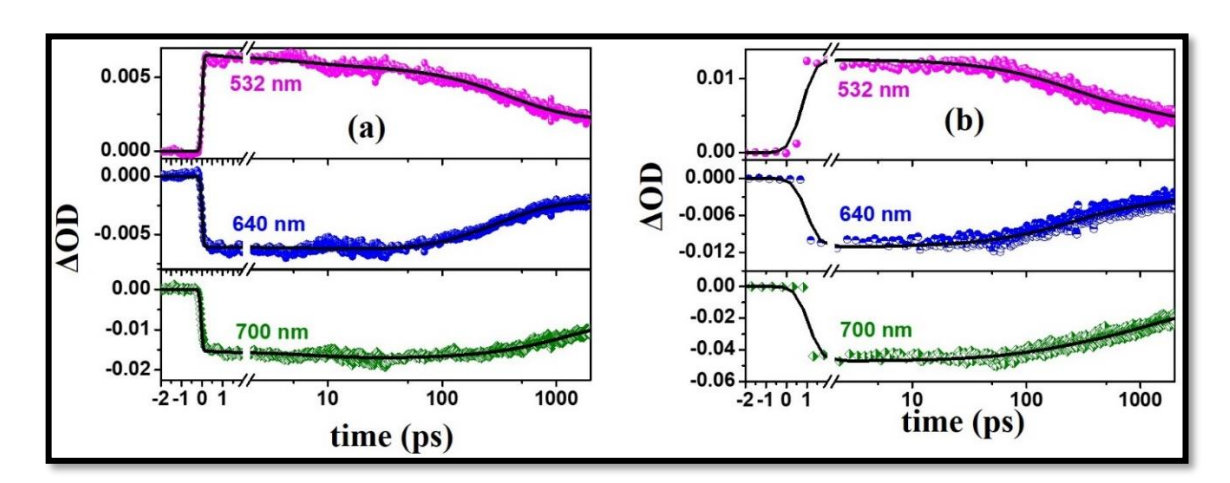


**Figure 4.9** (a) fs-TAS kinetics of PBIPC at an excitation wavelength of 400 nm for TA maximum 532 nm (magenta), GSB/SE maximum 640 nm (blue) and 700 nm (green) (b) fs-TAS kinetics of PBIPC at an excitation wavelength of 650 nm for TA maximum 532 nm (magenta), GSB/SE maximum 640 nm (blue) and 700 nm (green). The kinetics have been plotted in normal scale up to 2 ps and time scale beyond 2 ps is plotted in logarithmic scale. Symbols are the experimental data while the solid lines are theoretical fits.

**Table 4.2**. Decay lifetimes of relaxation dynamics in PBIPC for different wavelengths.

<b>Excitation wavelength</b>	Peak maxima	τ <sub>R</sub> (ps)	$\tau_1$ (ps), $\tau_2$ (ps)	τ <sub>3</sub> (ps)
400 nm	532 nm	0.131	5.59, 333.9	1300
	640 nm	0.123	21.02, 346	
	700 nm	0.241	8.60	1286
650 nm	532 nm	1.36	8, 216.3	1403
	640 nm	1.39	3.62, 408 ps	
	698 nm	1.32	142	1340

 $\tau_R$ : Rise time;  $\tau_1/\tau_2$ : shorter decay component showing IC and/ or VC;  $\tau_3$ : longer decay component showing ISC. Error involved is  $\pm 10\%$ .

The lifetimes majorly comprise of a short lifetime of few ps in ESA band which can account to  $S_1$  population of its vibrationally hot states ( $S_{1hot}$ ), the second lifetime in hundreds of picoseconds indicating energy reorientation of  $S_{1hot}$  state to  $S_1$ . The third lifetime of >1 ns is a slow process which can be indicative of the forbidden triplet state transition,  $T_1$ . In order to determine the lifetimes more accurately, here we apply Global fitting analysis with the same kinetic model. The sequential modelling gave us the following results:

**Global Fit:** To perform the global fitting, Glotaran 1.5.1 version was used. A sequential/unbranched three kinetic model was implemented for the analysis and 400 nm excitation data was used to achieve the global fit lifetime components. Figures 4.10(a)–(c) illustrate the EAS and DAS spectra obtained from the current model and how each excited species evolved with time in excited PBIPC. The accuracy of the global fit can be verified by looking at the spectral fit at extreme probe delays as shown in figure 4.10(d) and the corresponding kinetic trace shown as the inset.

The spectrum in red [figure 4.10(a)] corresponds to the first lifetime component which is very short-lived around 180 fs. In the DAS spectra, the spectrum corresponding to 180 fs (DAS 1, red line) is similar to the linear absorption spectrum of PBIPC shown by the black dashed line with the difference of an additional broad peak of DAS 1 in the range of 470–600 nm and a small dip around ~750 nm. The TAS spectra, being a difference spectra  $\Delta$ OD, can thus indicate to species population from higher excited states,  $S_n$  to

vibrationally higher  $S_1$  states or  $S_{1hot}$  state via internal conversion (IC) in the range 450–720 nm. Additionally, a small bleach (GSB) signal around 750 nm is observed corresponding to  $\pi \rightarrow \pi^*$  band of the Pc-moiety. The second lifetime in the DAS spectra (DAS 2, blue line) is ~317.8 ps and has a clear positive ESA band in the 450–600 nm region with a GSB in the 620–725 nm region which is nothing but the inverse of DAS 1 with a significant blue shift. This spectrum can be directly associated with  $S_1$  state population from  $S_{1hot}$  also termed as vibrational relaxation (VR).

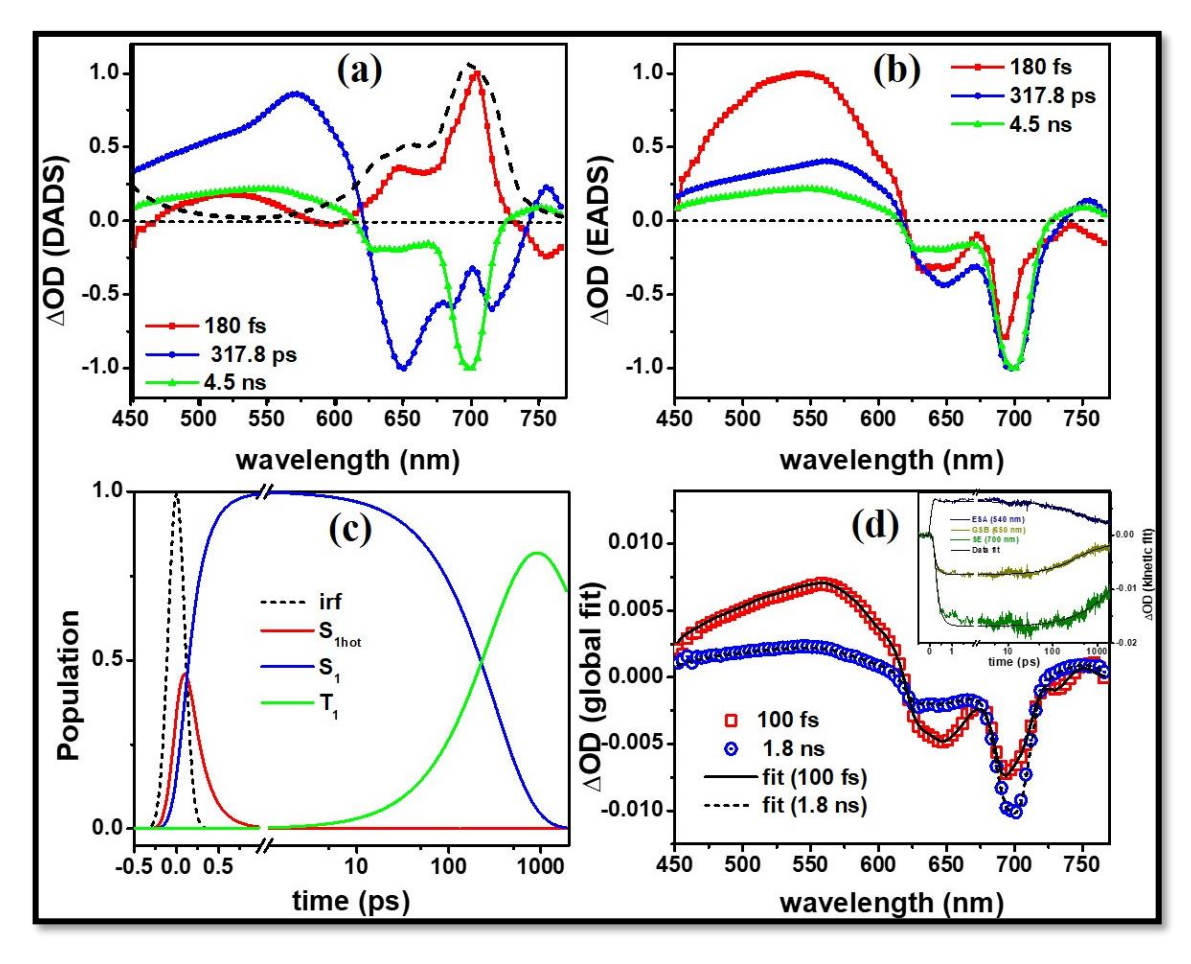


**Figure 4.10** (a) Difference associated spectra (DAS) of PBIPC (b) Evolution associated spectra of PBIPC. (c) Evolution of excited species over a probe delay of ~2 ns. Here red indicates internal conversion IC of  $S_n \rightarrow S_{1hot}$  in 180 fs, blue indicates vibrational relaxation of  $S_{1hot} \rightarrow S_1$  in 317.8 ps and green indicates intersystem crossing ISC of  $S_1 \rightarrow T_1$  in 4.5 ns (d) Global best fits of PBIPC spectra at 100 fs (red) and 1.8 ns (blue) with inset showing the corresponding band maxima kinetics – blue: 532 nm (ESA), yellow: 640 nm (GSB) and green: 700 nm (GSB/SE).

The excited species of the PBIPC solution, reorganizes themselves with the surrounding environment by exchanging their energy with neighboring atoms which in turn results in a blue shift in the spectrum. A photoinduced signal contribution also takes place in the 750 nm region corresponding to the  $S_1$  population due to excitation of the Pc-moiety in the Q-band by ESA. The third lifetime is a long-lived species lifetime of ~4.5 ns shown

as green line in figure 4.10(a), referred to as DAS 3. This lifetime is greater than the PBIPC fluorescence lifetime of ~3.7 ns with a spectral shift towards red. Here the ESA species have mostly undergone relaxation but the ground state haven't completely recovered which indicates the species migrating to a spin-forbidden triplet state via intersystem crossing or ISC with lifetime of ~4.5 ns. From DAS data, the corresponding evolution associated spectra, EAS was obtained as shown in figure 4.10(b) with the excited species evolution depicted by figure 4.10 c). Here we can see that the  $S_{1hot}$  state (red line) is extremely short-lived with low yield ~50% as compared to  $S_1$  (blue line) followed by the triplet state evolution given by the green line with a yield of ~70%. This shows that majority of the excited state species in PBIPC relaxed back to  $S_1$  state via IC than VR. Around ~70% of the  $S_1$  population underwent triplet state transition via ISC that evolved beyond the femtosecond delay range (i.e., >2 ns). From the above data, we can calculate the decay rate (k) of each transition by using the kinetic model as shown in figure 4.11. If the lifetime components are represented as  $\tau_{comp}$  then the decay constant can be determined as:  $k_{comp} = yield \ of \ comp$ . ( $\varphi_{comp}$ )

 $\tau_{comp}$ 

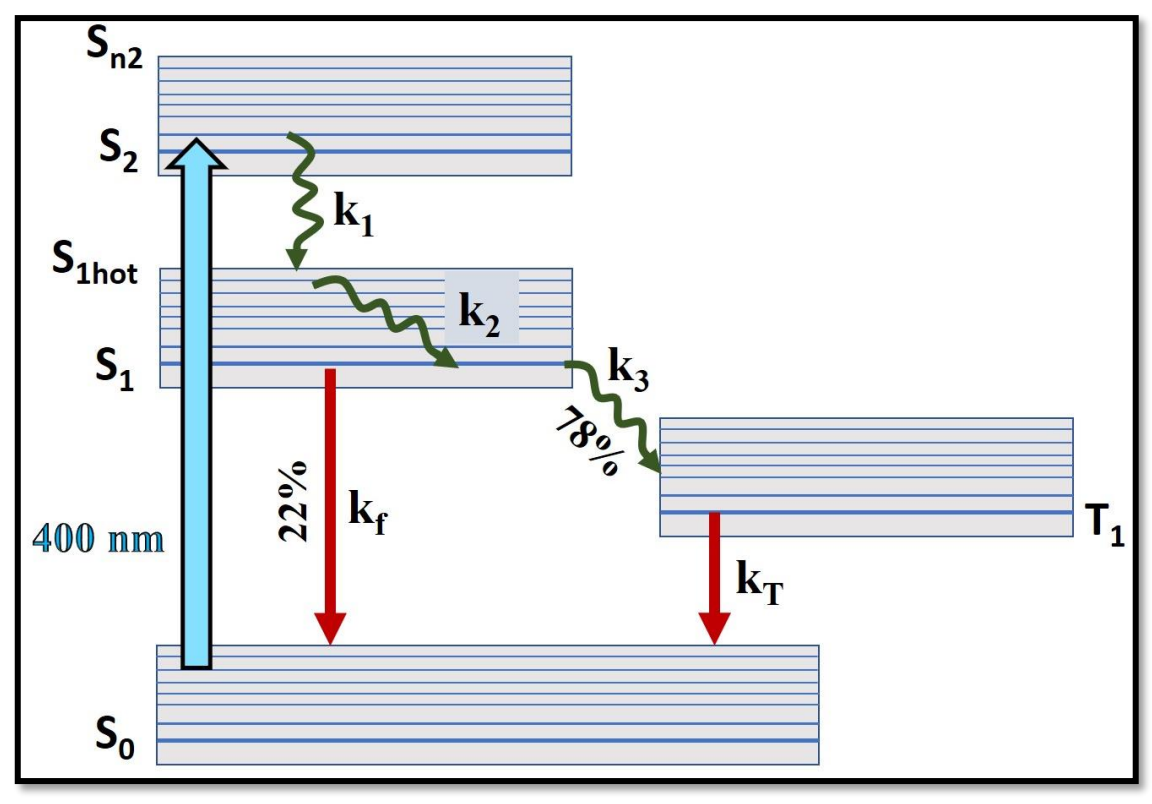


**Figure 4.11** Energy diagram of PBIPC where  $S_0$ ,  $S_1$ , ...,  $S_n$  are the singlet states whereas  $T_1$  is the triplet state. Blue arrow represents molecule excitation with 400 nm pump pulse. Green wriggly lines represent non-radiative transitions with decay constants of  $k_1$ ,  $k_2$  and  $k_3$  while red solid line represents radiative transition with  $k_f$  as fluorescence decay while  $k_T$  as decay via phosphorescence (typically in  $\mu$ s - ms).

The fluorescence lifetime ( $\tau_f$ ) studies revealed PBIPC decay to ground state S<sub>0</sub> within 3.68 ns with 0.22 or 22% quantum yield. Thus, the radiative decay rate was,  $k_r = \frac{0.22}{\tau_f} = 5.9 \times 10^7 \, \text{s}^{-1}$  [31]. For the remaining 78% to relax to triplet state via ISC, we calculated the decay constant to be  $k_3 = \frac{0.78}{\tau_f} = 2.1 \times 10^8 \, \text{s}^{-1}$  which is equal to the value obtained from our global analysis, thus confirming the kinetic model in figure 4.11. The detailed summary of all the decay rates obtained from global analysis is summarized in Table 4.3 below.

**Table 4.3**: Decay rates of PBIPC obtained using global fit at 400 nm excitation.

PBIPC (400 nm)								
Radiative lifetime		Non-radiative lifetime						
$k_r (\tau_f) s^{-1}$ $\Phi_f$		k <sub>1</sub> (τ <sub>1</sub> ) s <sup>-1</sup>	k <sub>2</sub> (τ <sub>2</sub> ) s <sup>-1</sup>	k <sub>3</sub> (τ <sub>3</sub> ) s <sup>-1</sup>	Фт			
5.9×10 <sup>7</sup>	0.22	5.5×10 <sup>12</sup>	3.1×10 <sup>11</sup>	2.2×10 <sup>8</sup>	0.78			
(3.68 ns)		(180.8 fs)	(317.8 ps)	(4.5 ns)				

Thus, fs-TAS studies of PBIPC indicated efficient intersystem crossing of the excited molecule with a high quantum yield of 78% which is quite high for a potential Pc monomer [37, 38]. Recent studies have been done to increase the triplet yield of Pc molecules for PDT applications by forming more complex structures like polymers and supramolecules which have resulted in high quantum yields [39, 40, 41]. The presence of triphenylamine imidazole group in the ZnPc molecule – PBIPC, with a triplet yield as high as 78%, proves its efficiency as a PS comparable to Pc complex derivatives. Zhang's group [42] extensively studied an imidazole and a methyl imidazole substituted zinc-phthalocyanine (ZnPc) whose triplet was compared to see the effect of peripheral substituent on ISC, triplet lifetimes and triplet yield. They found that the presence of a bulky imidazole group at the ZnPc periphery promoted faster singlet to triplet state charge transfer which in turn led to higher triplet yield and longer triplet lifetime. This result was found to be consistent in our molecule PBIPC. Thus, the triplet lifetime was not possible to be determined due to current experimental limitations. In order to experimentally determine the triplet lifetime with yield, ns-TAS studies need to be performed which was done for other imidazole substituted metal Pcs and presented in the coming chapters.

# 4.3 Conclusions:

- To summarize, the detailed study of NLO and photophysical studies of a novel triphenyl imidazole substituted zinc phthalocyanine PBIPC was performed using fs-TAS and the Z-scan techniques to realize its performance as a photosensitizer (PS). Presence of triphenyl imidazole moiety in the phthalocyanine molecule caused a broadening of absorption in the Soret band.
- The visible range from 600–800 nm showed two-photon absorption as the predominant NLO interaction while the NIR wavelength range (1.0–1.5  $\mu$ m) was was dominated by three- and four-photon absorption processes.
- The studied molecule displayed strong large multi-photon absorption cross-sections making it ideal for optical limiting, bioimaging applications [43, 44].
- PBIPC in THF exhibited a positive nonlinearity (self-focusing) for all wavelength ranges investigated which finds application as saturable absorbers [45, 46].
- Femtosecond transient absorption spectroscopy showed the excited state dynamics of PBIPC having possible triplet state transitions, evidenced by a broad transient absorption peak essentially overlapping the bleach signal for both excitation wavelengths 400 nm and 650 nm.
- A global fit analysis revealed three non-radiative lifetimes of 180 fs owing to internal conversion:  $S_n \rightarrow S_{1hot}$  followed by vibrational relaxation of  $S_{1hot} \rightarrow S_1$  state within 317.8 ps and then from  $S_1$  22% of the excited state species underwent radiative relaxation via fluorescence within 3.68 ns and 78% underwent intersystem crossing to the triplet state with a lifetime component of 4.5 ns.
- Combining high triplet yield and large two-photon absorption cross-section, we can conclude that PBIPC possess all crucial photophysical properties of a good photosensitizer and can be used in photovoltaics, PDT and 2PE-PDT applications [47, 48, 49, 50].

# 4.4 References:

- [1] X.-L. Zhang, X. Zhao, Z.-B. Liu, S. Shi, W.-Y. Zhou, J.-G. Tian, Y.-F. Xu and Y.-S., "Nonlinear optical and optical limiting properties of graphene oxide—Fe<sub>3</sub>O<sub>4</sub> hybrid material," *J. Opt.*, vol. 13, pp. 7-11, 2013.
- [2] G. de la Torre, P. Vazquez, F. Agullo-Lopez and T. Torres, "Phthalocyanines and related compounds:organic targets for nonlinear optical applications," *J. Mater. Chem.*, vol. 8, pp. 1671-1683, 1998.
- [3] D. Dini, M. Barthel and M. Hanack, "Phthalocyanines as active materials for optical limiting," *Eur. J. Org. Chem.*, vol. 20, pp. 3759-3769, 2001.
- [4] R. S. S. Kumar, S. V. Rao, L. Giribabu and D. N. Rao, "Femtosecond and nanosecond nonlinear optical properties of alkyl phthalocyanines studied using Z-scan technique," *Chem. Phys. Lett.*, vol. 447, pp. 274-278, 2007.
- [5] A. A. Chernonosov, E. A. Ermilov, B. Röder, L. I. Solovyova and O. S. Fedorova, "Effect of Some Substituents Increasing the Solubility of Zn(II) and Al(III) Phthalocyanines on Their Photophysical Properties," *Bioorg. Chem.*, 2014.
- [6] J. Tagare, D. K. Dubey, J.-H. Jou and S. Vaidyanathan, "Synthesis, photophysical, theoretical and electroluminescence study of triphenylamine-imidazole based blue fluorophores for solution-processed organic light emitting diodes," *Dyes Pigm.*, vol. 160, pp. 944-956, 2019.
- S. B. Yadav, S.S. Sonvane and N. Sekar, "Novel blue-green emitting NLOphoric triphenylamine-imidazole based donor-π-acceptor compound: Solvatochromism, DFT, TD-DFT and non-linear optical studies," *Spectrochim. Acta A.*, vol. 224, p. 117421, 2020.
- [8] J. Tagare, D. K. Dubey, R. A. K. Yadav and S. V. J-H Jou, "Triphenylamine-Imidazole based Luminophores for Deep-blue Organic Light Emitting Diodes: Experimental and Theoretical Investigations," *Mater. Adv.*, vol. Accepted Manuscript, 2020.
- [9] S. D. Burungale and M. J. Bhitre, "Synthesis of 2, 4, 5- triphenyl imidazole derivatives and biological evaluation for their antibacterial and anti-

- inflammatory activity," *Int. J. Pharm. Sci. Res.*, vol. 4, no. 10, pp. 4051-4057, 2013.
- [10] G. N. Bosio, F. S. G. E. J. Parisi and D. O. Mártire., "Imidazole and Beta-Carotene Photoprotection Against Photodynamic Therapy Evaluated by Synchrotron Infrared Microscopy," *Spectrochim Acta A Mol Biomol Spectrosc.*, vol. 195, pp. 53-61, 2018.
- [11] L. Howe and J. Z. Zhang., "Ultrafast Studies of Excited-State Dynamics of Phthalocyanine and Zinc Phthalocyanine Tetrasulfonate in Solution," *J. Phys. Chem. A*, vol. 101, p. 3207–3213, 1997.
- [12] L. P.Roguin, N. Chiarante, M. C. Vior and J. Marino, "Zinc(II) phthalocyanines as photosensitizers for antitumor photodynamic therapy," *Int. J. Biochem. Cell Biol.*, vol. 114, p. 105575, 2019.
- [13] W. Kuzyniak, J. Schmidt, W. Glac, J. Berkholz, G. Steinemann, B. Hoffmann, E. A. Ermilov, A. G. Gürek, V. Ahsen, B. Nitzsche and M. Höpfner, "Novel zinc phthalocyanine as a promising photosensitizer for photodynamic treatment of esophageal cancer," *Int J Oncol*, vol. 50, no. 3, pp. 953-963, 2017.
- [14] H. Abrahamse and M. R. Hamblin., "New photosensitizers for photodynamic therapy," *Biochem J.*, vol. 473, no. 4, pp. 347-364, 2016.
- [15] S. Kwiatkowski, B. Knap, D. Przystupski, J. Saczko, E. Kędziersk, K. K-Czope, J. Kotlińska, O. Michel, K. Kotowskia and J. Kulbacka., "Photodynamic therapy mechanisms, photosensitizers and combinations," *Biomed. Pharmacother*, vol. 106, pp. 1098-1107, 2018.
- [16] R. D. Nalda, R. D. Coso, J. Requejo-Isidro, J. Olivares, A. Suarez-Garcia, J. Solis and C. N. Afonso, "Limits to the determination of the nonlinear refractive index by the Z-scan method," *J. Opt. Soc. Am. B.*, vol. 19, pp. 289-296, 2002.
- [17] P. Zhao, Z. Wang, J. Chen, Y. Zhou and F. Zhang, "Nonlinear optical and optical limiting properties of polymeric carboxyl phthalocyanine coordinated with rare earth atom," *Opt. Mater.*, vol. 66, pp. 98-105, 2017.
- [18] J. W. Perry, K. Mansou, I. Y. S. L. X. L. Wu, P. V. Bedworth, C. T. Chen, D. Ng, S. R. Marder, P. Miles, T. Wada, M. Tian and H. Sasabe, "Organic optical limiter with a strong nonlinear absorptive response," *Science*, vol. 273, pp. 1533-1536, 1996.

- [19] K. V. A. Kumar, S. V. Rao, S. Hamad and S. M. Dharmaprakash, "Wavelength dependent nonlinear optical switching in electron beam irradiated CuTTBPc thin film," *RSc. Adv.*, vol. 6, pp. 22083-22089, 2016.
- [20] G. S. He, P. P. Markowicz, T.-C. Lin and P. N. Prasad, "Observation of stimulated emission by direct three-photon excitation," *Nature*, vol. 415, pp. 767-770, 2002.
- [21] C. J. Rowlands, D. Park, O. T. Bruns, K. D. Piatkevich, D. Fukumura, R. K. Jain, M. G. Bawendi, E. S. Boyden and P. T. So, "Wide-field three-photon excitation in biological samples," *Light Sci Appl*, vol. 16, p. e16255, 2017.
- [22] B. Anand, M. Molli, S. Aditha, T. M. Ratan, S. S. Sai and S. V. Kamisetti, "Excited state assisted three-photon absorption based optical limiting in nanocrystalline Cu<sub>2</sub>Se and FeSe<sub>2</sub>," *Opt. Commun.*, vol. 304, pp. 75-79, 2013.
- [23] B. Fang, M. Menotti, M. Liscidini, J. Sipe and V. Lorenz, "Three-Photon Discrete-Energy-Entangled," *Phys. Rev. Lett.*, vol. 123, no. 7, p. 070508, 2019.
- [24] W. Chen, S. Bhaumik, S. A. Veldhuis, G. Xing, Q. Xu, M. Grätzel, S. Mhaisalkar, N. Mathews and T. C. Sum, "Giant five-photon absorption from multidimensional core-shell halide perovskite colloidal nanocrystals," *Nat. Commun.*, vol. 8, p. 15198, 2017.
- [25] D. H. Friese, R. Bast and K. Ruud, "Five-Photon Absorption and Selective Enhancement of Multiphoton Absorption Processes," *ACS Photonics*, vol. 5, pp. 572-577, 2015.
- [26] F. E. Hernández, K. D. Belfield, I. Cohanoschi, M. Balu and K. J. Schafer, "Three- and four-photon absorption of a multiphoton absorbing fluorescent probe," *Appl. Opt.*, vol. 43, pp. 5394-5398, 2004.
- [27] K. N. Krishnakanth, S. Seth, A. Samanta and S. V. Rao, "Broadband ultrafast nonlinear optical studies revealing exciting multi-photon absorption coefficients in phase pure zero-dimensional Cs4PbBr6 perovskite films," *Nanoscale*, vol. 11, pp. 945-954, 2019.
- [28] S. Bhattacharya, C. Biswas, S. S. K. Raavi, J. V. S. Krishna, D. Koteshwar, L. Giribabu and S. V. Rao, "Optoelectronic, Nonlinear Optical Properties and Excited State Dynamics of a Triphenyl Imidazole Induced Phthalocyanine Derivative," *RSC Adv.*, vol. 9, pp. 36726-36741, 2019.

- [29] L. M. Mazur, T. Roland, S. Leroy-Lhez, V. Sol, M. Samoc, I. D. W. Samuel and K. Matczyszyn, "Efficient singlet oxygen photogeneration by zinc porphyrin dimers upon one- and two-photon excitation," *J. Phys. Chem. B*, vol. 23, pp. 4271-4277, 2019.
- [30] Y. Mir, J. E. v. Lier, J.-F. Allard, D. Morris and D. Houde, "Two-photon absorption cross section of excited phthalocyanines by a femtosecond Tisapphire laser," *Photochem. Photobiol. Sci.*, vol. 8, pp. 391-395, 2009.
- [31] B. Ren, N. Sheng, B. Gu, Y. Wan, G. Rui, C. Lv and Y. Cui, "Changing optical nonlinearities of homoleptic bis(phthalocyaninato) rare earth praseodymium double-decker complexes by the redox reaction," *Dyes Pigm.*, vol. 139, p. 788–794, 2017.
- [32] G. S. He and P. N. Prasad, "Three-photon absorbing materials: characterization and applications," in *Proc. SPIE 5211*, San Diego, California, 2003.
- [33] H. Lu and N. Kobayashi, "Optically Active Porphyrin and Phthalocyanine Systems," *Chem. Rev.*, vol. 610, p. 6184–6261, 2016.
- [34] F. Bolze, S. Jenni, A. Sour and V. Heitz, "Molecular photosensitisers for two-photon photodynamic therapy," *Chem. Commun.*, vol. 53, p. 12857–12877, 2017.
- [35] E. M. Maya, A. W. Snow, J. S. Shirk, R. G. S. Pong and G. L. Roberts, *J. Mater. Chem.*, vol. 13, pp. 1603-1613, 2003.
- [36] T. G. B. d. Souza, M. G. Vivasb, C. R. Mendonçaa, S. Plunkett, M. A. Filatov, M. O. Senge and L. D. Boni, "Studying the intersystem crossing rate and triplet quantum yield of meso-substituted porphyrins by means of pulse train fluorescence technique," *Journal of Porphyrins and Phthalocyanines*, vol. 20, pp. 282-291, 2016.
- [37] A. Ogunsipe, J.-Y. Chen and T. Nyokong, "Photophysical and photochemical studies of zinc(ii) phthalocyanine derivatives—effects of substituents and solvents," *New J. Chem.*, vol. 28, pp. 822-827, 2004.
- [38] D. Frackowiak, A. Planner, A. Waszkowiak, A. Boguta, R.-M. Ion and K. Wiktorowicz, "Yield of intersystem (singlet-triplet) crossing in phthalocyanines evaluated on the basis of a time in resolved photothermal method," *J. Photochem. Photobiol. A*, vol. 141, pp. 101-108, 2001.

- [39] Z. Iqbal, A. Ogunsipe, T. Nyokong, A. Lyubimtsev, M. Hanack and T. Ziegler, "Photophysics and photochemistry of octaglucosylated zinc phthalocyanine derivatives," *J. Porphyr. Phthalocyanines*, vol. 16, pp. 413-422, 2012.
- [40] A.I. Awaji, B. Köksoy, M. Durmuş, A. Aljuhani and S.Y. Alraqa, "Novel Hexadeca-Substituted Metal Free and Zinc(II) Phthalocyanines; Design, Synthesis and Photophysicochemical Properties," *Molecules*, vol. 24, p. 77, 2019.
- [41] N. Mehraban and H. S. Freeman, "Developments in PDT sensitizers for increased selectivity and singlet oxygen production," *Materials (Basel, Switzerland)*, vol. 8, no. 7, p. 4421–4456, 2015.
- [42] X.-F. Zhang, Y. Lin, W. Guo and J. Zhu, "Spectroscopic Insights on Imidazole Substituted Phthalocyanine Photosensitizers: Fluorescence Properties, Triplet State and Singlet Oxygen Generation," *Spectrochim Acta A: Mol. Biomol. Spectrosc.*, vol. 133, p. 752-758, 2014.
- [43] E. Öztürk, H. Eserci and E. Okutan., "Perylenebisimide-fullerene dyads as heavy atom free triplet photosensitizers with unique singlet oxygen generation efficiencies," *J. Photochem. Photobiol. A*, vol. 385, p. 112022., 2019.
- [44] S. S. K. Raavi, J. Yin, G. Grancini, C. Soci and V. R. Soma, G. Lanzani, L. Giribabu, "Femtosecond to microsecond dynamics of soret-band excited corroles," *J. Phys. Chem. C*, vol. 119, p. 28691–28700., 2015.
- [45] P. Bowe, W. Gibbs and J. Tregellas-Williams, "Lifetimes of Saturable Absorbers," *Nature*, vol. 209, pp. 65-66, 1996.
- [46] R.S.M. Soboh, A. Al-Masoodi, F.N.A.Erman, A. H.H.Al-Masoodi, H. Arof, M. Yasin and S.W.Harun, "Zinc phthalocyanine thin film as saturable absorber for Q-switched pulse generation," *Opt. Fiber Technol.*, vol. 57, p. 102235, 2020.
- [47] M. Urbani, M.-E. Ragoussi, M. K. Nazeeruddin and T. Torres, "Phthalocyanines for dye-sensitized solar cells," *Coord. Chem. Rev.*, vol. 381, pp. 1-64, 2019.
- [48] R. Milan, G. S. Selopal, M. Cavazzini, S. Orlandi, R. Boaretto, S. Caramori, I. Concina and G. Pozzi, "Zinc phthalocyanines as light harvesters for SnO2-based solar cells: a case study," *Sci. Rep.*, vol. 10, p. 1176, 2020.

- [49] Z. Zheng, H. Liu, S. Zhai, H. Zhang, G. Shan, R. T. K. Kwok, C. Ma, H. H. Y. Sung and I. D. Williams, J.W.Y. Lam, K.S. Wong, X. Hu, B.Z. Tang, "Highly efficient singlet oxygen generation, two-photon photodynamic therapy and melanoma ablation by rationally designed mitochondria-specific near-infrared AIEgens," *Chem. Sci.*, vol. 11, pp. 2494-2503, 2020.
- [50] S. Abid, S. B. Hassine, N. Richy, F. Camerel, B. Jamoussi, M. B.-Desce, O. Mongin, F. Paul and C. O. Paul-Roth, "Phthalocyanine-Cored Fluorophores with Fluorene-Containing Peripheral Two-Photon Antennae as Photosensitizers for Singlet Oxygen Generation," *Molecules*, vol. 25, no. 2, p. 239, 2020.

# **Chapter 5**

# Femtosecond to Microsecond Photophysical Studies and NLO Properties of Novel Imidazole Substituted Metal Phthalocyanines.

The chapter encompasses the detailed photophysical studies of two phthalocyanines (ZnPc and CuPc) with phenanthroimidazole group attached at its peripheral position via a phenyl bridge named as ImCuPc, [3,9,17,23-tetrakis(4-(1-hexyl-1H-phenanthro[9,10dlimidazole-2-yl)phenyl)-8H,9H-copper(II) phthalocyanine] and ImZnPc [3,9,17,23tetrakis(4-(1-hexyl-1H-phenanthro[9,10-d]imidazole-2-yl)phenyl)-8H,9H-Zinc(II) phthalocyanine]. A solution of ImMPc (M = Cu and Zn) in dichloromethane (DCM) was used for all the studies. They were investigated for their potential as photosensitizers through DFT, optical, and excited state dynamics, including their ultrafast nonlinear optical (NLO) studies. The steady state absorption and emission spectra of both the molecules, exhibited negligible Stokes shift in various solvents. They showed a broad Soret band due to the presence of phenanthro [9,10-d] imidazole moiety while the Q-bands were characteristic to their metal phthalocyanine group. Fluorescence lifetimes were measured to be in nanoseconds range for both the molecules. Their energy-optimized structures were generated using DFT, TD-DFT analysis showing the HOMO-LUMO (4.99-2.90 eV) levels of these molecules. The TAS spectra of both the molecules, in fs timescale, exhibited contribution from singlet-singlet excited state absorption, accompanying a transition to the triplet state via intersystem crossing, ISC. The calculated kinetic data at specific wavelengths along with global fitting demonstrated slow singlet to triplet state intersystem crossing in ImCuPc (decay rate of 1.6×10<sup>8</sup> s<sup>-1</sup>) and ImZnPc (decay rate of 1.4×10<sup>8</sup> s<sup>-1</sup>). The ns-TAS studies showed triplet state lifetimes of ~1.4 µs in ImCuPc and ~1.2 µs in ImZnPc. The triplet quantum yields  $(\phi_T)$  were calculated to be 0.51 for ImCuPc while it was 0.27 for ImZnPc rendering ImCuPc a better photosensitizer (PS) over ImZnPc. Third-order nonlinear optical studies at excitation of 800 nm (50 fs, 1 kHz pulses) demonstrated large two-photon absorption coefficients. ImCuPc had better self-defocusing ability than ImZnPc, whereas ImZnPc had a larger two-photon absorption cross-section (994 GM) when compared to ImCuPc (381 GM). All the above studies indicated that ImCuPc and ImZnPc have the potential for optoelectronic and biological applications.

Part of the presented work in this chapter has been published in the following.

- 1. **S. Bhattacharya,** G. Reddy, S. Paul, Sk. S. Hossain, S.S.K. Raavi, L. Giribabu, A. Samanta and S. Venugopal Rao, "Comparative Photophysical and Femtosecond Nonlinear Optical Properties of Novel Imidazole Substituted Metal Phthalocyanines", (*Under Revision, Dyes and Pigments April 2020*).
- 2. **S. Bhattacharya,** S. Paul, Sk. Saddam Hossain, S. S. K. Raavi, G. Lingamallu, S. Venugopal Rao "Femtosecond to Microsecond Photophysical Properties of a Novel Free Base Phthalocyanine", Ultrafast Optics XII, Bol, Croatia 2019. [*Proc. of SPIE* Vol. 11370, 1137001-483, UFO XII].

# 5.1 Introduction:

Photodynamic therapy (PDT) is a minimally invasive treatment where a photosensitizer (PS) is administered in a tissue that undergoes photochemical reaction when activated by visible light irradiation and generates cytotoxic species in the presence of oxygen. The general use is for the treatment of cancerous tumors as well as noncancerous diseases such as age-related psoriasis, macular degeneration, infectious diseases and atherosclerosis [1, 2, 3, 4, 5]. The efficacy of PDT relies on the photophysical properties and the chemical nature of the PS, which determine its dark toxicity, light absorption efficiency, singlet oxygen production quantum yield  $(\phi_D)$ , and photostability [6]. The light penetration depth varies a lot with the wavelength, the intensity of light used, and the tissues it has been exposed to and, longer wavelength light i.e. near-infrared (NIR) to IR has better penetration because of reduced scattering from tissue components. Since most of the PS absorbs in the maximum wavelength time window of 650 nm - 750 nm, we can use twophoton excitation (TPE) on appropriate PSs to achieve NIR penetration depth. Two-photon excitation (TPE) is defined as the simultaneous absorption of two photons instead of one to reach an excited state. It is a third-order nonlinear optical process whereby the rate of transition for the two-photon absorption is proportional to the square of the excitation light intensity.

$$R_{2P} \propto \sigma_2 I^2$$
 (5.1)

where  $\sigma_2$  is TPA cross-section representing the probability of reaching the excited state following light absorption, and I is the intensity of excitation light [6]. To determine  $\sigma_2$ , we employ the Z-scan technique in which the transmitted light is monitored while a sample is translated axially through the focus of a laser beam. The obtained data (open aperture and closed aperture) are fitted with a standard set of formulae reported by Sheik Bahae et al. in 1990 [7]. The parameters (nonlinear absorption coefficient and nonlinear refractive index) obtained from the fitted data were used to determine 2PA cross-sections using equation 5.2.

$$\sigma_{2PA} = \frac{h\omega\beta}{2\pi \times N_A \times o \times 0.001}$$
 (5.2)

where, 'h' is the Planck constant,'  $N_A$ ' is Avogadro's number, and ' $\rho$ ' is the concentration in mole per liter. ' $\sigma_{2PA}$ ' is commonly given in a new SI unit (GM) defined as 1 GM= $10^{-50}$ cm<sup>4</sup> s photon<sup>-1</sup> molecule<sup>-1</sup>. A PS is required to have high triplet quantum yield and long triplet state lifetime to successfully undergo photochemical reaction with singlet O2 via type I or II pathway [8]. Hence, a comprehensive photophysical study of a PS is crucial, which can be achieved with transient absorption spectroscopy (TAS). The widely studied molecule Phenanthroimidazole, is extensively studied due to its strong electrochemical properties with the most frequent application as blue emissive material in OLEDs and as a sensitizer in organic photovoltaics [9, 10, 11, 12]. The bulky phenanthroimidazole group, bridged with an aromatic group, such as phenyl, tends to form a very stable Pc derivative with minimized aggregation. The molecular structure of the Pc can be modified with a long alkyl chain attached to the nitrogen atom of the phenanthroimidazole group for improved solubility in common organic solvents. Charge transfer is promoted from phenanthroimidazole moiety to the Pc macrocycle in the presence of transition central metal (Cu and Zn) in the Pc moiety, making it an efficient donor-acceptor system. Thus, the minimized aggregation with enhanced solubility of the phenanthroimidazole substituted metallophthalocyanines along with their effective D- $\pi$ -A system make them very efficient as potential photosensitizers and optoelectronic applications in PDT and DSSC [13, 14, 15]. Based on the aforementioned factors, a phenanthroimidazole–phthalocyanine system have been designed for the current study, in which the phenanthroimidazole group is covalently attached to either zinc phthalocyanine (ImZnPc) or copper phthalocyanine (ImCuPc) at its peripheral position using phenyl spacers (see Figure 5.1) and investigated for their electrochemical, optical, excited state dynamics and ultrafast nonlinear optical (NLO) properties by employing various spectroscopic techniques.

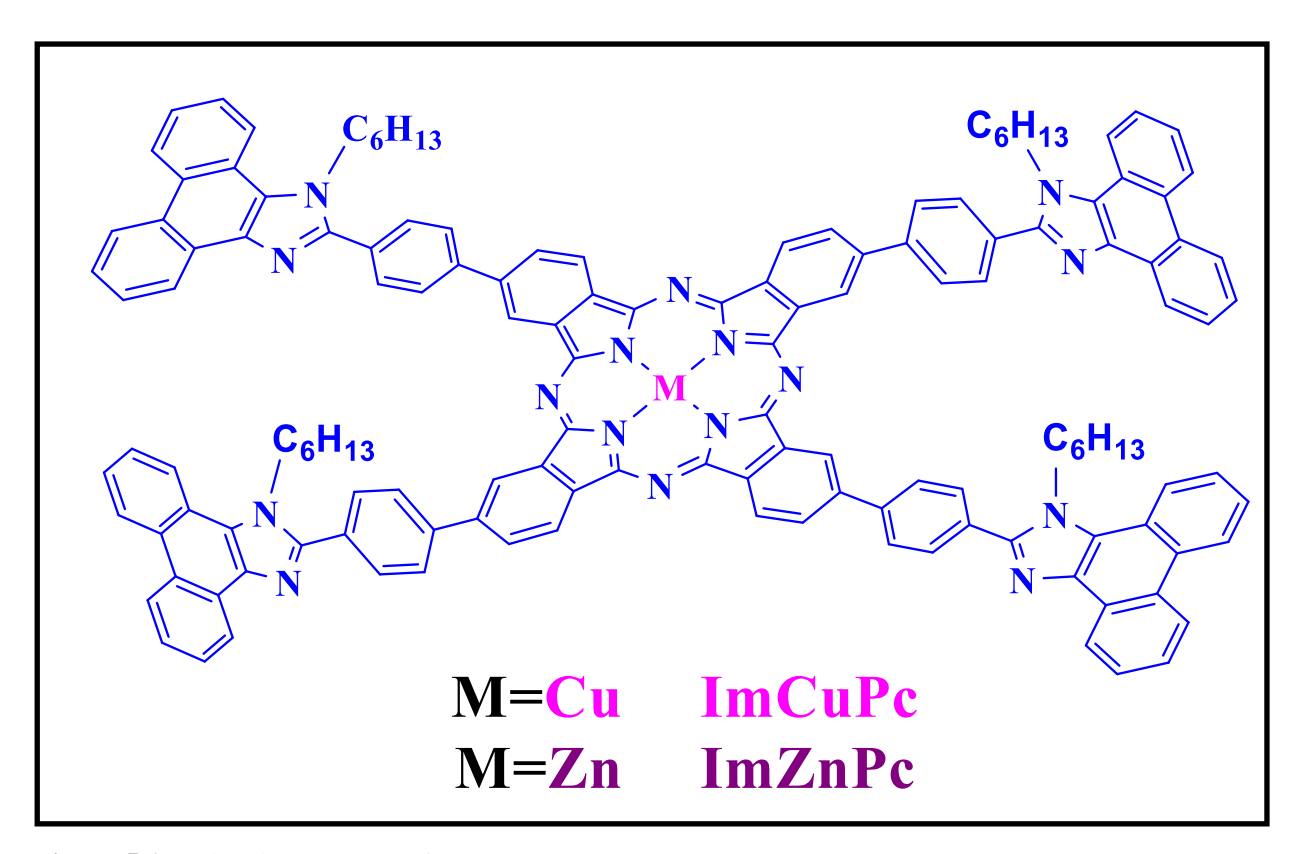


Figure 5.1 Molecular structure of ImMPc [M: Cu, Zn].

# **5.2** Experimental Details and Results:

The molecular synthesis and characterization of two novel phenanthro[9,10-d]imidazole substituted metal phthalocyanines, 3,9,17,23-tetrakis(4-(1-hexyl-1H-phenanthro[9,10-d]imidazole-2-yl)phenyl)-8H,9H-copper(II) phthalocyanine, ImCuPc and 3,9,17,23-tetrakis(4-(1-hexyl-1H-phenanthro[9,10-d]imidazole-2-yl)phenyl)-8H,9H Zinc (II) phthalocyanine, ImZnPc, were performed at IICT, Hyderabad, India.

# 5.2.1. Absorption and Emission studies:

Shimadzu UV-Visible-NIR (UV-3600) spectrophotometer was used to record the absorption spectra of studied complexes. Fluorolog-3 spectrofluorometer (Spex model from JobinYvon) was used to record steady-state fluorescence measurements at OD of ~0.06 at the wavelength of excitation ( $\lambda_{ex}$ ) 670 nm. Fluorescence lifetime was recorded using time-correlated single-photon counting (TCSPC) setup where the fluorescence

decays were recorded at the emission maxima of the molecules ( $\lambda_{em} = \sim 700$  nm). For detection, a photomultiplier tube (R928P, Hamamatsu) was used. To record the lamp profile, a scatterer (a dilute solution of Ludox in water) was used for calibration purpose. The instrument response function was limited by of the source of excitation at FWHM was ~635 ps at 670 nm. Decay curves were analyzed using IBH DAS6 (version 2.3) decay analysis software [nonlinear least-squares iteration]. The  $\chi^2$  values and distribution of the residuals indicate the best fit data analysis. The absorption properties of ImZnPc and ImCuPc (2.56 µM concentration) in various solvents (DMF, toluene, THF and DCM) are shown in Figures 5.2(a) and 5.2(c). On changing the solvent polarity, the Q-band shape of ImCuPc intensity at ~640 nm has increased as compared to other solvents due to lack of solubility whereas, ImZnPc at the absorption maximum was not significantly altered. Still, the range of absorption remained unchanged in all solvents (~570-750 nm). The emission spectra of ImZnPc and ImCuPc (1.28 µM) was recorded in different solvents at 650 nm excitation, as presented in figures 5.2(b) and 5.2(d). Only notable observation being the emission maxima of ImZnPc was blue-shifted in THF as compared to other solvents. To check the aggregation behavior of our molecules in DCM solution, the absorption spectra at different concentrations were carried out within the Beer-Lambert's law, as can be seen in figure 5.4 below. As Pc concentration increased, a linear increase in the Q-band was observed with no shift in wavelengths or new bands, indicating the absence of aggregated species. Similar studies were carried out in other common solvents (see figure 5.5) to observe that the Q-band shape at absorption maximum of ImZnPc remained nearly unchanged with changing polarity of the solvent, on the contrary, ImCuPc intensity of the high energy band at ~640 nm increased [due to lack of solubility in solvents such as DMF (a), (b) and toluene (c), (d)] but absorption range remained the same in all solvents (~570-750 nm).

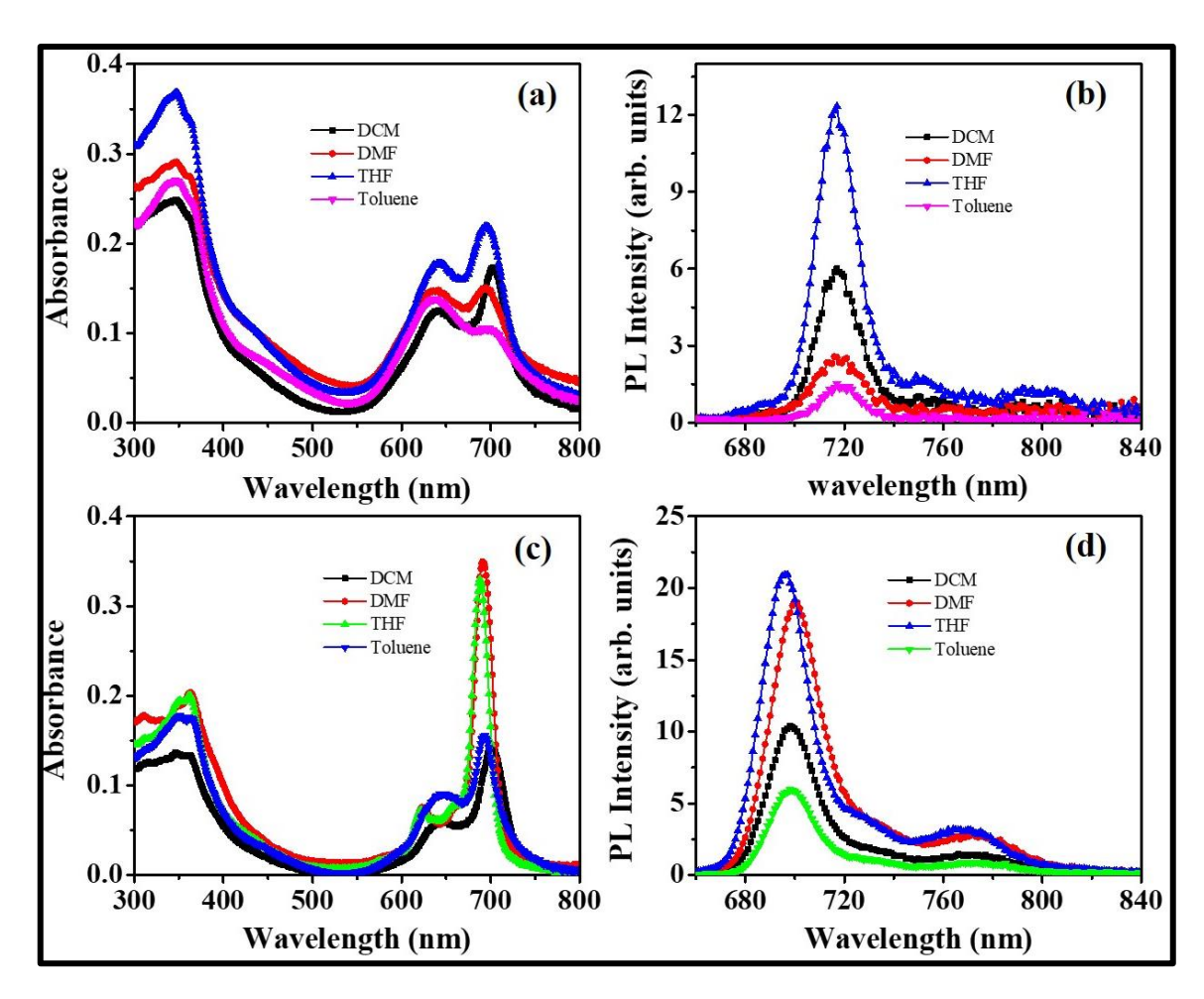


**Figure 5.2 (a)** Steady-state absorption and (b) emission spectra of ImCuPc (c) Steady-state absorption and (d) emission spectra of ImZnPc in different solvents at RT. The molecules were excited near 650 nm for the emission measurements.

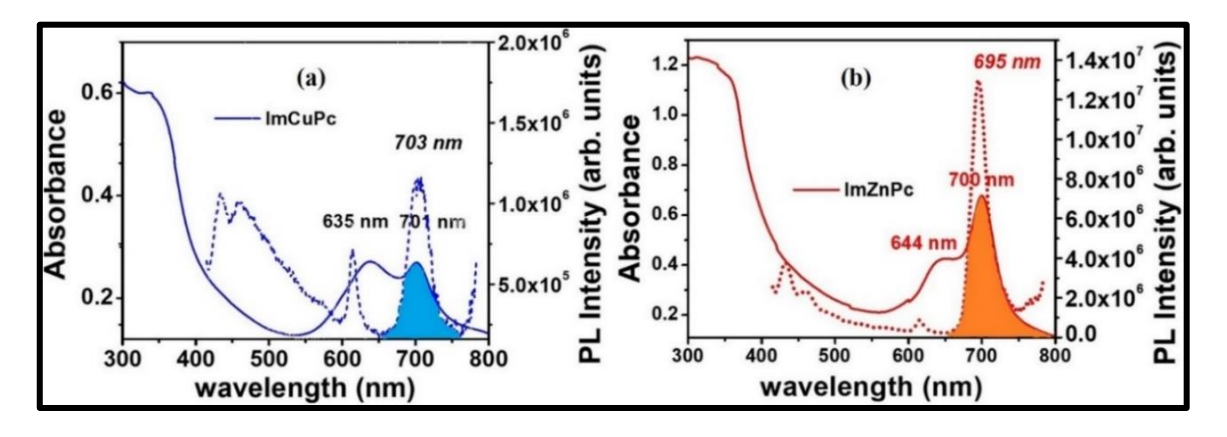


**Figure 5.3** Steady-state absorption (solid line) and emission (dashed line) spectra of (a) ImCuPc and (b) ImZnPc in DCM. The molecules were excited near 400 nm for emission measurements. The shaded area depicts the amount of overlap between the absorption and emission band.

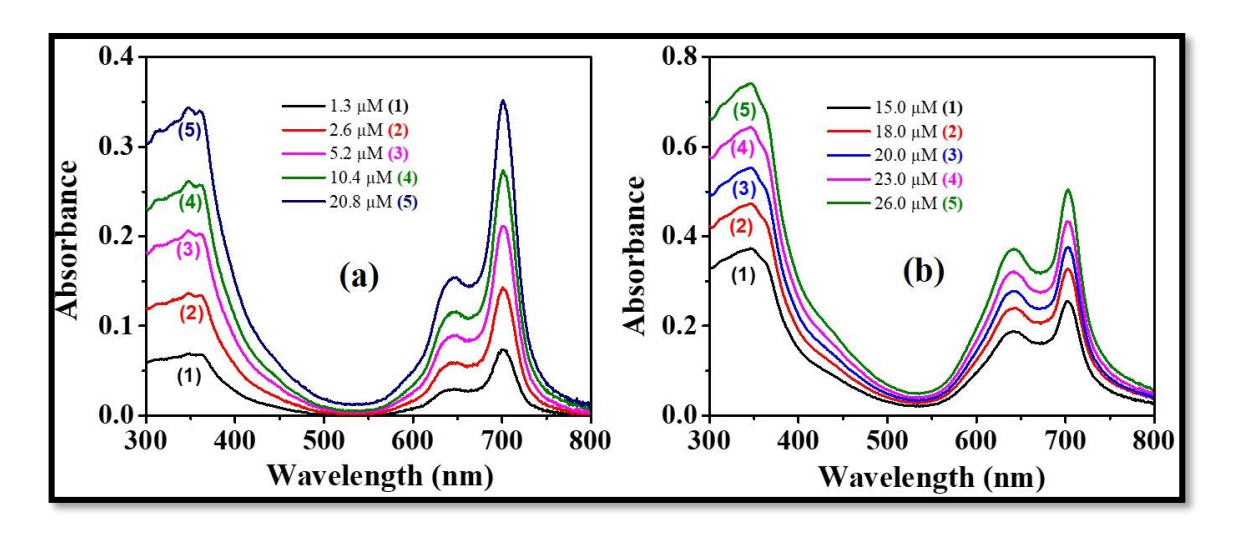


**Figure 5.4** Steady-state absorption spectra of (a) **ImZnPc** and (b) **ImCuPc** at different concentrations in DCM at room temperature (RT).

The steady-state absorption and emission spectra of ImCuPc and ImZnPc in DCM is shown in Figure 5.3. The overlap of absorption band for phenanthro[9,10-d]imidazole group with MPc moieties, results in a broad Soret band. The two Q-bands at 600-700 nm region are characteristics of CuPc and ZnPc, and appear due to  $\pi$ - $\pi$ \* transitions [13, 16, 17]. The lack of any significant Stokes shift in the emission band of both the molecules (~701 nm) with overlapping Pc absorption Q-band and the phenanthroimidazole emission band can promote intramolecular energy transfer via Förster's resonance energy transfer (FRET). In this process, the excited donor 'D\*' group within the molecule (i.e. phenanthroimidazole in ImMPc) relaxes back to the ground state, while simultaneously transferring the energy to the acceptor 'A' electron as shown by the relation:  $D^* + A \rightarrow D$ + A\* (see figure 5.6). FRET can affect the photoactivity of a photosensitizer and hence is important to PDT studies [18]. Being a competing factor in the molecular relaxation via fluorescence decay, FRET affects the fluorescence quantum yield of the molecule as it permits the nonradiative intramolecular transfer of energy within the molecule. A detailed summary of the optical studies (absorption/emission) has been summarized in table 5.1 below (section 5.2.2).

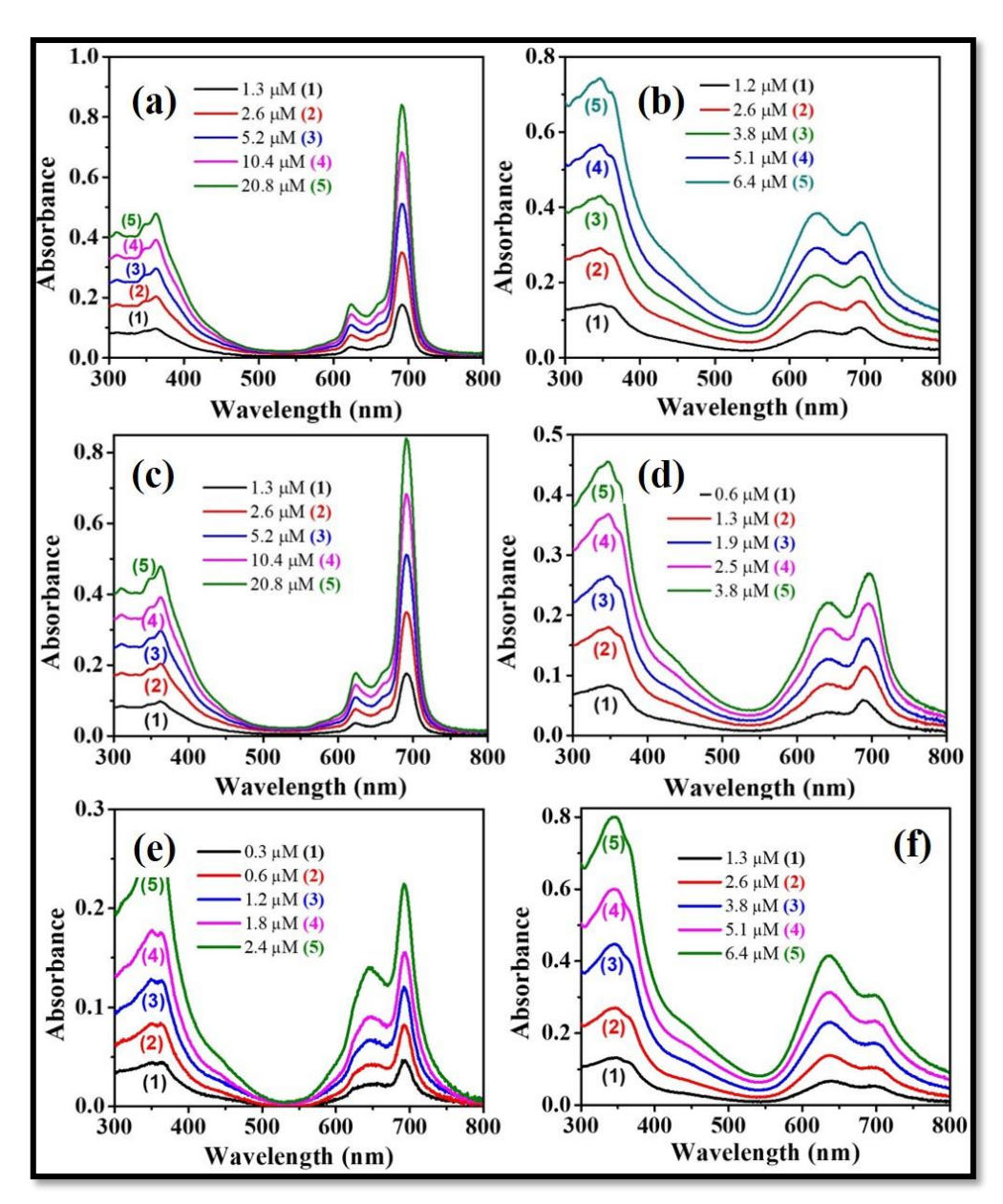


**Figure 5.5:** Absorption spectral changes of (a) ImZnPc and (b) ImCuPc in **DMF** at different concentrations, (c) ImZnPc and (d) ImCuPc in **toluene** and (e) ImZnPc and (f) ImCuPc in **THF**.

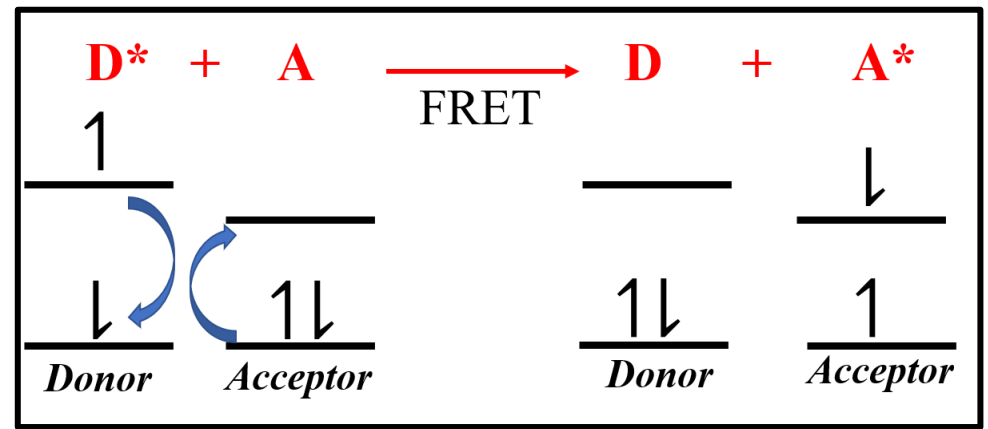


**Figure 5.6** Molecular orbital schematic illustration for resonance energy transfer (RET) via Förster's mechanism.

### 5.2.2. Theoretical Studies

For theoretical analysis of the structural and electronic properties of both ImCuPc and ImZnPc, computer simulations based on DFT was adopted. The density functional theory (DFT) and time-dependent DFT studies are run in a functional basis set of the B3LYP/6-31G (d,p) level [Gaussian 09 package] to determine the theoretical information about structural, optical, and redox properties of ImCuPc and ImZnPc. Both top and side views of the optimized structures of ImCuPc and ImZnPc are shown in Figure 5.7(a), which suggest that the phenyl bridge is perpendicular between phenanthro-imidazole and phthalocyanine macrocycle.

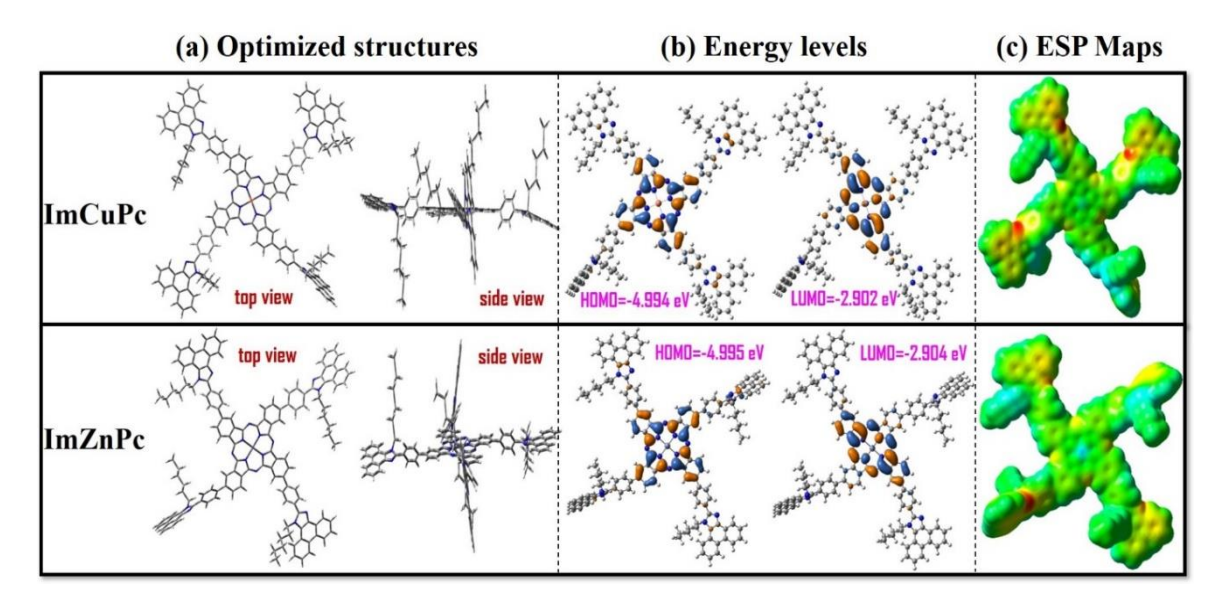


**Figure 5.7** B3LYP/6-31G(d,p)-calculated (a) optimized structure, (b) frontier HOMO and HOMO, and (c) molecular electrostatic potential map of ImCuPc and ImZnPc. The red and blue colors in (c) indicate the negative and positive potentials.

Both molecules constitute the optimized energy structures as shown in Figures 5.7. Here, the HOMO, LUMO, and HOMO–LUMO gap energies with ground state dipole moment are given in Debye units. The electron distribution of ImMPc (M=Cu,Zn), the optimized structure consists of HOMO and LUMO predominantly on the phenanthroimidazole donor present in both Pcs and acceptor Pc ring at -4.99 eV and -2.90 eV levels respectively while the HOMOs with higher electron density was on phenanthroimidazole group with the Pcs occupying the lower LUMOs (see table 5.1). Similarly, HOMO–2 electron cloud resided on triphenyl imidazole (–5.164) and LUMO+2 on phthalocyanine moiety at (–1.713). The electrostatic potential (ESP) maps distinctively indicate the electron cloud distribution in the molecules' energy optimized structures where more electron cloud indicates yellowish-red areas, whereas less electron cloud indicates

blue-green color on ESP [Figure 5.7(c)]. In is to be noted that no charge transfer process involves the alkyl chains whose major role is to improve the solubility in the molecular solutions. Thus, we can say that for our current molecules, phenanthroimidazole act as a good electron donor and phthalocyanine macrocycle act as an acceptor (weak).

**Table 5.1** Optical, electrochemical and theoretical data of ImCuPc and ImZnPc.

System	Solvent	λ <sub>max</sub> nm <sup>a</sup>	$\lambda_{em.max}$ $(\phi_f) nm^b$	τ <sub>f</sub> (Α%) (ns) <sup>c</sup>	Oxidation (V) <sup>d</sup>	$\mathbf{E_g}^\mathbf{e}$	HOMO <sup>a</sup> (eV)	LUMO <sup>a</sup> (eV)	$\mathbf{E_g}^{\mathbf{a}}$	μg <sup>a</sup> (debye)
IMZnPc	DCM DMF THF Toluene	702 691 688 693	698 (0.27) 700 (0.25) 696 (0.31) 698 (0.28)	0.6(47.3) 3.1(52.7)	0.58, 1.28	1.67	-4.995	-2.904	2.091	6.26
IMCuPc	DCM DMF THF Toluene	702 693 695 636	717 (0.14) 718 (0.12) 716 (0.13) 718 (0.15)	0.1(34.3) 4.7(65.7)	0.67, 1.12	1.65	-4.994	-2.902	2.092	6.74

 $\tau_f$ , A: fluorescence lifetime, amplitude.  $\Phi_f$ : fluorescence quantum yield. <sup>a</sup>Error limits:  $\lambda_{max}$ ,  $\pm 1$  nm. <sup>b</sup>Error limits:  $\lambda_{em}$ ,  $\pm 1$  nm. <sup>c</sup>Error limits in  $\tau$  are  $\pm 8\%$ . <sup>d</sup>The oxidation potentials of the dyes were measured in DCM with 0.1 M tetrabutylammonium perchlorate (TBAP) with a scan rate of 100 mVs<sup>-1</sup>. <sup>c</sup>Values are in eV.

# 5.2.3. Z-scan studies with kHz pulses:

The two-photon excitation PDT or 2PE PDT can be best understood by studying the NLO properties of the ImMPcs NIR window at 800 using the Z-scan technique. The open aperture Z-scan [Figures 5.8(a)] showed reverse saturable absorption (RSA) at 84 GW/cm² (an average input power of 0.15 mW) input intensity which is at non-resonant absorption band as shown in the steady-state absorption spectra of ImCuPc and ImZnPc [Figures 5.3(a), 5.3(b)]. The obtained data was fitted using a set of formulae, as mentioned in Chapter 2. The best fit for RSA signal in case of ImCuPc and ImZnPc was two-photon absorption (2PA) with the calculated coefficient,  $\alpha_2$ , to be  $2.3 \times 10^{-12}$  cm/W for ImCuPc and  $6.0 \times 10^{-12}$  cm/W for ImZnPc. The transitions are purely electronic contributions (and negligible thermal contribution) with instantaneous two-photon absorption as the dominant phenomenon [as ~50 fs pulse duration and 1 kHz repetition laser source]. Closed aperture z-scan showed negative nonlinearity [shown as the peak followed by a valley in figures 5.8(b)] in DCM solution whose solvent nonlinear refraction was negligible ( $n_2 \sim 1.6 \times 10^{-16}$  cm²/W) and NLO absorption  $\alpha_2 = 5 \times 10^{-13}$  cm/W as shown in see figure 5.9. The coefficient of nonlinear refractive index was found to be  $-n_2$ , to be  $3.7 \times 10^{-15}$  cm²/W for ImCuPc and

 $1.7\times10^{-15}~{\rm cm^2/W}$  for ImZnPc. The negative sign is reflective of the defocusing ability of the NLO molecules with ImCuPc having a slightly higher magnitude than ImZnPc. This self-defocusing property finds applications in imaging, cloaking, and sensing [19], which can be explored with our present macromolecules. The estimated error in measurements are roughly within the range of  $\pm 10\%$  which includes - errors in beam waist measurements, input beam intensity fluctuations, instrumental errors (detectors, etc.), among few. Thus, based on the measured NLO properties of ImCuPc and ImZnPc, the molecules can be useful in optoelectronics as well as in multi-photon biomedical imaging. The large 2PA cross-section values of ImCuPc and ImZnPc (see the summary of coefficients in table 3) at 800 nm proves superior photosensitizers in 2PE PDT procedure as compared to other equivalent phthalocyanine based photosensitizers [6, 20, 21].

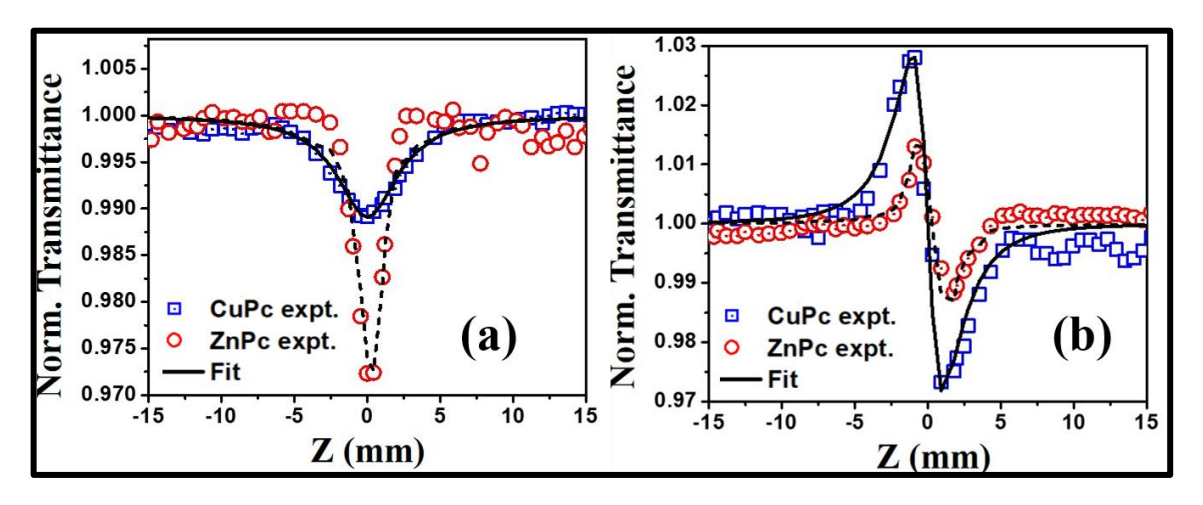


**Figure 5.8** 50 fs, 1 kHz Z-scan data at 800 nm excitation wavelength of ImCuPc (blue squares) and ImZnPc (red circles) where (a) shows open aperture experimental signatures and (b) shows closed aperture experimental results with black solid line being best fit for ImCuPc and dashed line for ImZnPc, respectively.

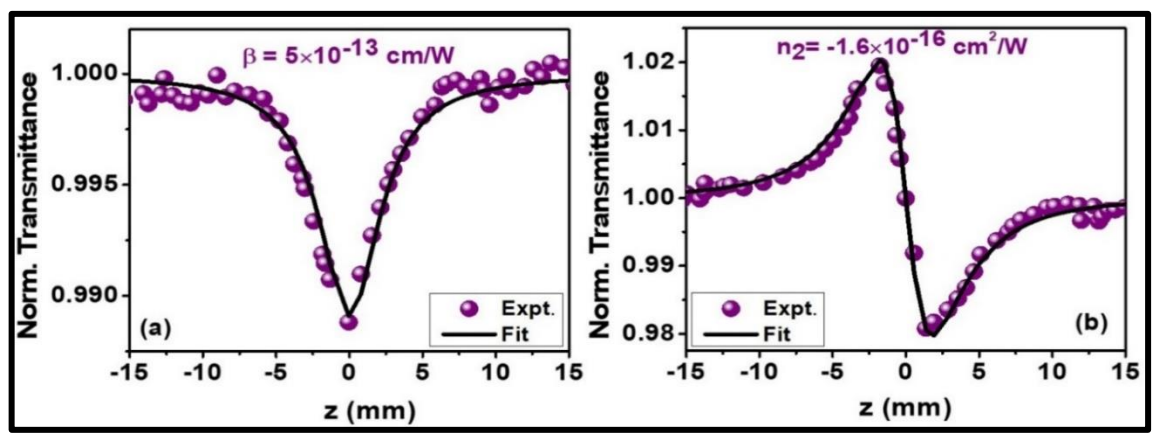


**Figure 5.9:** (a) Open aperture Z-scan data for **DCM** (dichloromethane) solvent and (b) closed aperture Z-scan data for DCM (dichloromethane) solvent obtained with ~70fs, 1kHz pulses at 800 nm wavelength. The purple spheres represent the experimental data while black solid line represents the fitted data.

#### 5.2.4. fs-TAS studies:

To understand the potential properties of ImCuPc and ImZnPc for PDT applications, the excited-state dynamics of ImCuPc and ImZnPc plays a crucial role. To do so, fs and ns-TAS studies were conducted on ImMPcs (M = Cu, Zn) solutions (in DCM). The fs-TAS studies gave information about the singlet excited state transition pathways in the molecules. The DFT studies demonstrated similar optimized HOMO-LUMO levels in ImCuPc and ImZnPc (see Table 5.1), with ImCuPc at slightly higher chemical potential. It also revealed the strong donor nature of phenanthroimidazole group to weak acceptor MPc moiety. The slight difference in the energy levels of ImZnPc and ImCuPc can be associated to filled 3d subshell of Zn [atomic # 30] compared to Cu [atomic # 29], which gives ImCuPc higher probability of donor-acceptor interaction than ImZnPc [38,39].

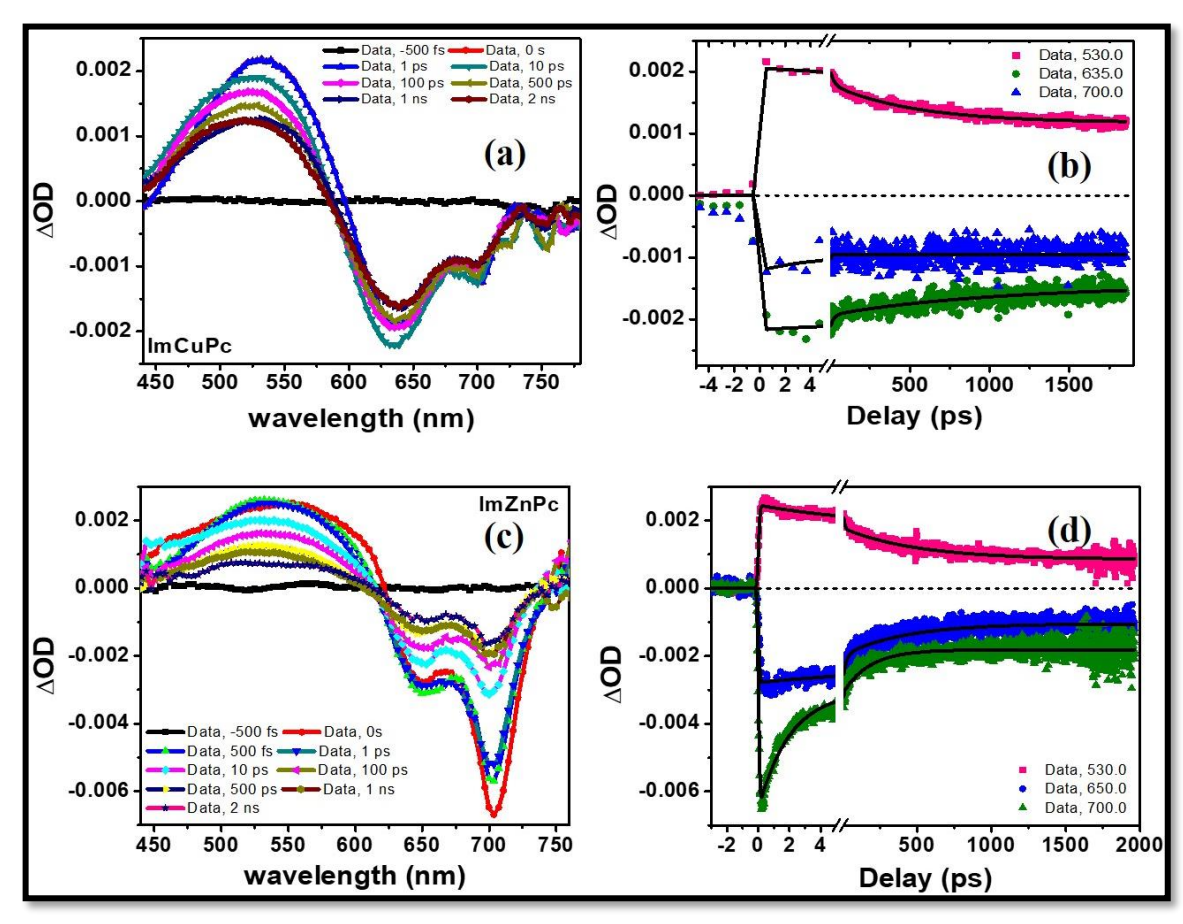


**Figure 5.10** fs-TAS spectra of (a) ImCuPc and (c) ImZnPc recorded up to 2 ns delay. Fitted kinetics of (b)ImCuPc at ESA maximum 530 nm (pink squares) and GSB minima 635 nm (green circles) and 700 nm (blue triangles) and (d) ImZnPc at ESA maximum 530 nm (pink squares) and GSB minima 650 nm (green triangles) and 700 nm (blue diamonds).

Figures 5.10(a) and 5.10(c) illustrate the difference absorption spectra of ImCuPc and ImZnPc at Soret band excitation (400 nm) respectively, for a delay range of 2 ns.

Throughout the difference absorption spectral evolution for both ImCuPc [Fig. 5.10(a)] and ImZnPc [ Fig. 5.10(c)], a redshift of ~4 nm was observed which was suggestive to the presence of excited state transitions from the singlet to the triplet state [22, 23]. These results were consistent at Q-band (610 nm) pump excitation as well, as shown in Figures 5.11(a) - 5.11(d). The ground state bleach (GSB) and stimulated emission (SE) appears as a superposed negative TA signal in both the molecules' spectra which was centered around 700 nm. A detailed kinetic analysis of each molecule at their ESA maxima and GSB/SE minima was performed using a multi-exponential decay model [22, 24] and the fitted data is illustrated in Figures 5.11(b) and 5.11(d). (0.1–0.15) ps was the measured TA signal rise time. The ESA maxima (530 nm) in both molecules showed a tri-exponential decay while GSB minima showed a bi-exponential decay with consistent relaxation lifetime of the molecules to the ground state – longer lifetimes (20–50 ps) and (0.5–1 ns) were comparable in ESA and GSB band in both molecules. The redshifted GSB minima could result due to possible overlap of some other low-lying transition state (like the triplet state). Thus, a global fit analysis was followed by the above data fitting using a specialized software, Glotaran, using standard modeling techniques [25].

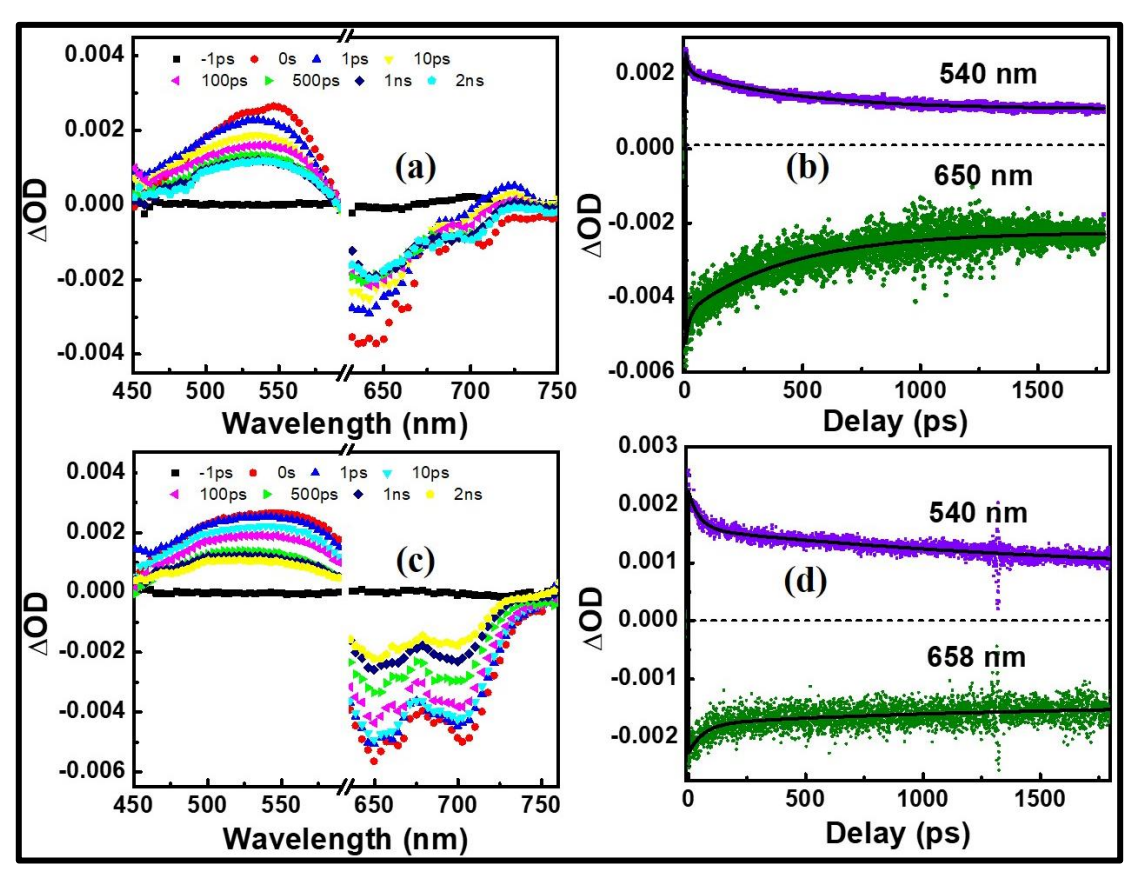


**Figure 5.11** (a) fs-TAS spectra of ImCuPc at 610 nm excitation (b) fs-TAS kinetics of ImCuPc at ESA maxima 540 nm and GSB minima 650 nm (c) fs-TAS spectra of ImZnPc at 610 nm excitation (d) fs-TAS kinetics of ImZnPc at ESA maxima 540 nm and GSB minima 658 nm.

Global fit analysis: The decay associated difference spectra (DADS) for globally fitted ImCuPc (figure 5.12 (a)) along with the corresponding excited state population (figure 5.12(b)) shows the following transitions - DADS 1 (red, squares) shows an ESA maximum at 554 nm and GSB minima at 634 nm and 701 nm, which can be found agreeable with the ImCuPc absorption spectrum (figure 5.3(a)). The SE contribution around 700 nm contains two bands at 703 nm and 727 nm which denotes  $S_1$  state recovery bands with a lifetime component of 1.7 ps. Shorter lifetime measurements weren't possible due to the instrumental limit (irf) of the measurement being 100 fs. Thus, the internal conversion from  $S_{nhot}$  to vibrationally hot  $S_1$  ( $S_{1hot}$ ) state can be assumed to be of magnitude lower than the irf (i.e. <100 fs). Hence, the DADS1 signal corresponds to the energy reorientation of  $S_{1hot}$  state to  $S_1$  state via vibrational relaxation within 1.7 ps.

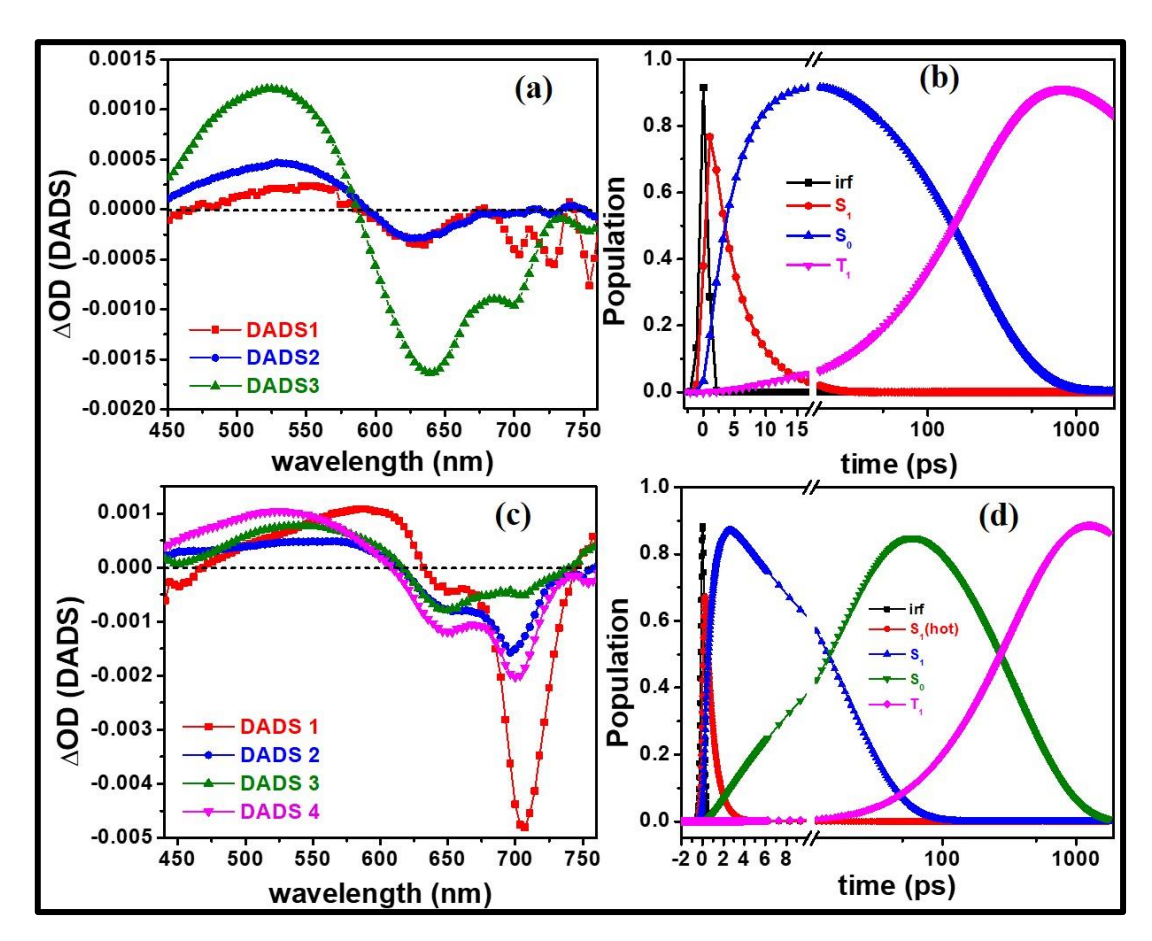


**Figure 5.12** (a) Decay associated difference spectra (DADS) for ImCuPc showing three lifetimes – DADS1 (1.7 ps): red squares, DADS2 (208.8ps): blue circles, DADS3 (7.1ns): green triangles. (b) excited species population showing singlet states: S<sub>1</sub> as red circles, S<sub>0</sub> as blue triangles and triplet state T<sub>1</sub> as magenta inverted triangle. The black square signal represents the instrument response limit (irf). (c) DADS for ImZnPc showing four lifetimes – DADS1 (772.5 fs): red squares, DADS2 (3.1 ps): blue circles, DADS3 (355.6 ps): green triangles and DADS4 (7.9 ns): magenta inverted triangles. (d) excited species population showing singlet states: S<sub>1</sub>(hot) as red circles, S<sub>1</sub> as blue

triangles,  $S_0$  as green inverted triangles and triplet state  $T_1$  as magenta diamonds. The black square signal represents the instrument response function (irf) of  $\sim 0.1$  ps.

A broader blue-shifted band similar to DADS 1 was observed in DADS 2 (blue, circles) consisting of an equally intense GSB band at 634 nm and no SE contribution at 700 nm. This can correspond to the nonradiative  $S_1$  state relaxation pathway (i.e. relaxation from  $S_1$  states to  $S_0$  state) with a lifetime component of 208.8 ps. The SE band disappearance also indicated that  $S_1$  state population does not entirely relaxes to the ground state but rather to an alternate pathway (preferably triplet  $T_1$  state). The  $S_1 \rightarrow S_0$  transition is nothing but the internal conversion (IC) of the excited molecular form to its ground state. The DADS 3 (green) corresponds to a long-lived spectrum (of ~7.1 ns), which is unlike DADS 1 and 2 (GSB is red-shifted with larger ESA band) and is likely to contribute to the intersystem crossing (ISC) between  $S_1$  state and triplet state  $T_1$ . The species population throughout the molecular transition of ImCuPc is given in figure 5.12(b) - instrumental limit of measurement is plotted as black squares,  $S_1$  state depopulation as red circles,  $S_0$  population by blue triangles and triplet state population  $T_1$  as magenta inverted triangles. While  $S_0$  populates faster via IC, the slow population evolution of  $T_1$  grows beyond the fs-TAS measurement limits.

Similarly, DADS for ImZnPc (Figure 5.12(c)) and the corresponding excited state molecular population (figure 5.12(d)) shows ESA maximum at 600 nm with negligible GSB around 650 nm and an intense SE minimum at 700 nm, as evidenced by the absorption spectrum of ImZnPc Q-band [figure 5.3(b)]. This shows that the excited species contribution from upper excited singlet states S<sub>n</sub> via SE with no GSB recovery in the Q-band. Thus, this band is not associated with S<sub>1</sub> state population but internal conversion (IC) from upper singlet states S<sub>nhot</sub> to vibrationally hot S<sub>1</sub> state (S<sub>1hot</sub>) with a short-lived component ~772.5 fs. This is followed by the blue-shifted ESA maximum and 650 nm GSB minimum in DADS 2 (blue) spectrum, with respect to DADS 1. This is the energy redistribution lifetime (~3.1 ps) of S<sub>1hot</sub> state to its surroundings to reach S<sub>1</sub> state. In the DADS 3 (green) spectrum ESA band was more prominent to DADS 2 and with similarly intense 650 nm GSB band where the 700 nm SE contribution disappears. This 355.6 ps lifetime component shows the ground state S<sub>0</sub> populating in a non-radiative pathway from S<sub>1</sub>. The DADS 4 (magenta) spectrum showed a shift in ESA maxima, which starts populating simultaneously with DADS 3 [shown as green inverted triangles in figure

5.12(b)] while the  $S_1$  state depopulates [shown as blue triangles in figure 5.12(b)]. This long-lived state of ~7.9 ns had lifetime longer than fluorescence decay time (see table 5.1) and has been assigned to the intersystem crossing (ISC) of the population to the triplet state.

### 5.2.5. ns-TAS Analysis

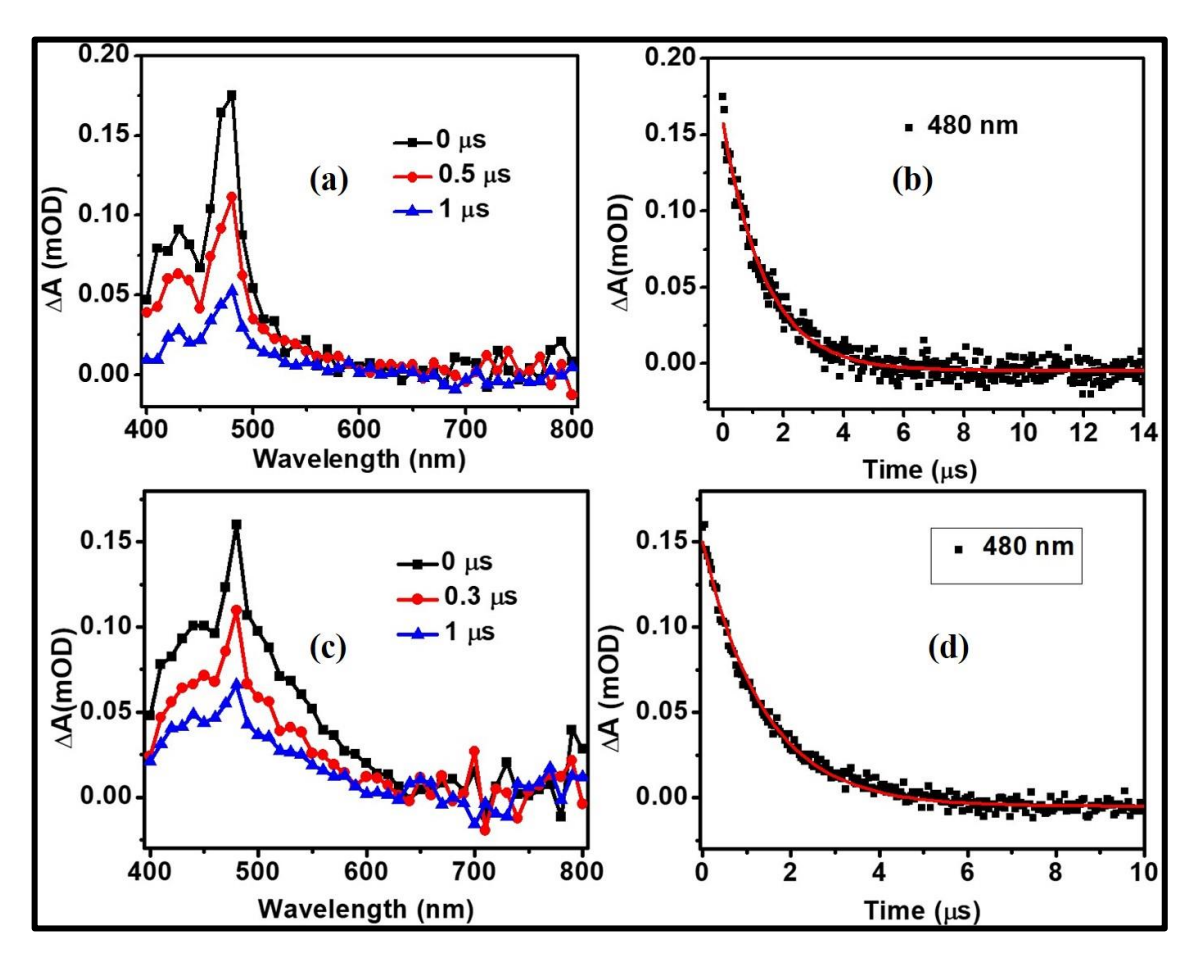


**Figure 5.13** (a) ns-TAS spectra of ImCuPc recorded up to 1  $\mu$ s delay. (b) Fitted kinetics of ImCuPc at ESA maximum 480 nm (black squares). Red solid line shows the best fit. (c) ns-TAS spectra of ImZnPc recorded up to 1  $\mu$ s delay. (d) Fitted kinetics of ImZnPc at ESA maximum 480 nm (black squares). Red, solid lines are the best fits.

The ns-TAS studies showed a defined triplet ESA at 480 nm maxima for ImCuPc and ImZnPc [Figures 5.13 (a), (b), and 5.13 (c), (d), respectively]. The kinetics were best fitted with mono-exponential lifetimes, ImCuPc showed triplet state lifetime ( $\tau_T$ ) of 1.4  $\mu$ s (ImCuPc) and 1.2  $\mu$ s (ImZnPc), respectively. Assuming the three-kinetic model of our photophysical system for both the molecules, the triplet quantum yields were calculated to be 0.51 for ImCuPc and 0.27 for ImZnPc [26]. The experimentally obtained decay rates were compared with theoretical calculation of the decay transfer rates using a suitable

kinetic model [24], as shown in figure 5.14, which showed excellent agreement, justifying our current kinetic model. The decay rate of transition, k, with corresponding lifetimes ( $\tau$ ) and triplet quantum yield  $\phi_T$  is summarized in Table 5.2.

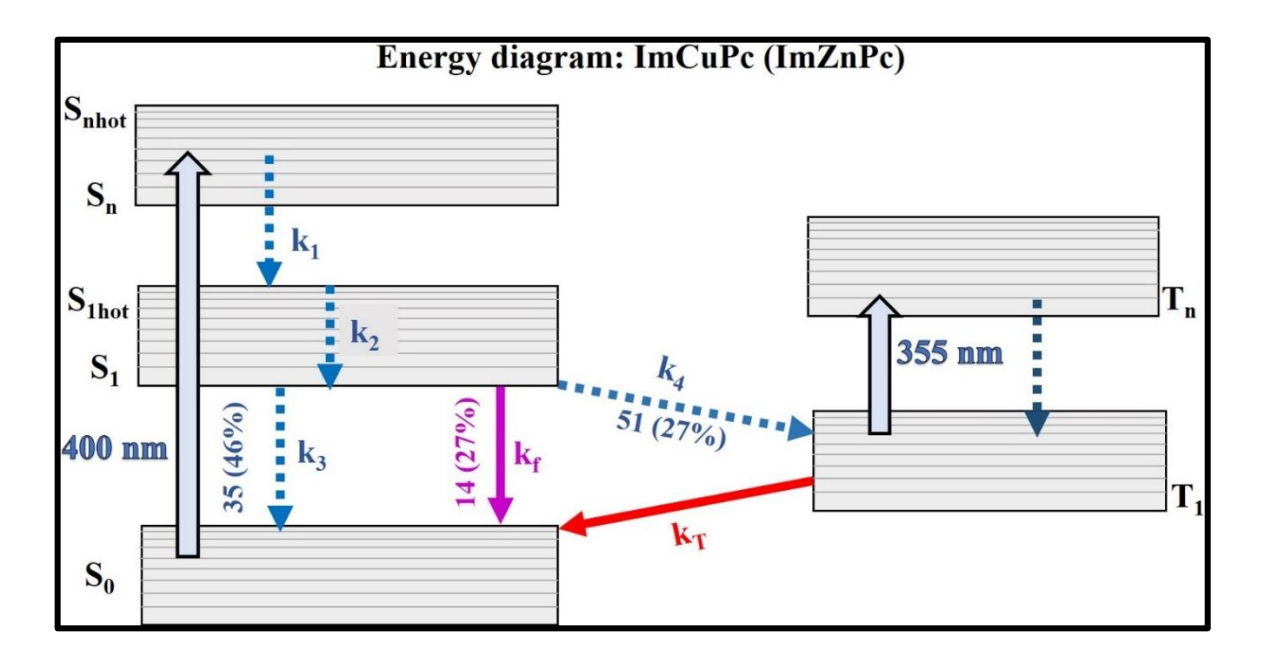


**Figure 5.14** Relaxation pathways of ImCuPc and ImZnPc obtained from TAS studies where  ${}^{\circ}k_{i}{}^{\circ}$  denotes the rate transition parameters. Here,  ${}^{\circ}S{}^{\circ}$  denotes to singlet states while  ${}^{\circ}T{}^{\circ}$  denotes to triplet states. The solid upward arrows indicate absorption. The downward dashed arrows indicate nonradiative relaxation while solid arrow indicates radiative relaxation. The branching percentages are mentioned for  $S_{1}$  state with ImZnPc values in brackets and ImCuPc outside the brackets.

Table 4.2 summarizes all the lifetimes for the molecules investigated in the present study and obtained from the TCSPC experiments, transient absorption studies using both fs and ns pulses. The results obtained were in excellent agreement from both theoretical experimental aspects, as discussed in the previous sections. Consistent with previously published literature [16, 27, 28, 29], our studies have confirmed that ImCuPc exhibited a faster intersystem crossing than ImZnPc. By principle, a longer-lived photosensitizer in its triplet state has higher chances of interacting with oxygen molecules as their non-excited state is the triplet state. This in turn can create larger number of cytotoxic singlet oxygen or free radicals that helps in targeted tissue destruction via apoptosis or autophagy, making it a potential photodrug for PDT applications. Considering the above factors, it is evident that phenanthroimidazole substituted metal phthalocyanines ImCuPc and ImZnPc can be potential photosensitizers with Cu incorporated ImMPc showing better performance over Zn incorporated moiety. Few recent studies relate intersystem crossing (ISC) to a higher

triplet yield [30, 31] which can clearly indicate our results of ImCuPc having higher triplet yield (0.51) than ImZnPc.

**Table 4.2.** Decay lifetimes of relaxation dynamics in PBIPC for different wavelengths.

Sample	k <sub>f</sub> s <sup>-1</sup> (τ <sub>f</sub> ) fluoresce nce	φf	$\begin{array}{c} k_1 \ s^{\text{-}1}(\tau_1) \\ S_n {\rightarrow} S_{1hot} \end{array}$	$k_2 s^{-1}(\tau_2)$ $S_{1hot} \rightarrow S_1$	$\begin{array}{c} k_3 \ s^{\text{-}1}(\tau_3) \\ S_1 {\rightarrow} S_0 \end{array}$	$\begin{matrix} k_4 \ s^{\text{-}1}(\tau_4) \\ S_1 \rightarrow T_1 \end{matrix}$	$\begin{array}{c} k_T  s^{\text{-}1}(\tau_T) \\ T_1 {\rightarrow} S_0 \end{array}$	φт
	TCSPC		fs-TAS				ns-TAS	
ImCuPc	4.5×10 <sup>7</sup> (~3.1 ns)	0.1 4	<10 <sup>13</sup> (<100 fs)	5.8×10 <sup>11</sup> (1.7 ps)	1.1×10 <sup>9</sup> (0.20 ns)	1.6×10 <sup>8</sup> (7.1 ns)	7.1×10 <sup>5</sup> (1.4 µs)	0.51
ImZnPc	1.4×10 <sup>8</sup> (~1.9 ns)	0.2 7	1.3×10 <sup>12</sup> (772.5 fs)	3.2×10 <sup>11</sup> (3.1 ps)	2.4×10 <sup>9</sup> (0.35 ns)	1.4×10 <sup>8</sup> (7.9 ns)	8.3×10 <sup>5</sup> (1.2 μs)	0.27

Here,  $k = \phi/\tau$ , denotes the rate of transition between excited states.  $\tau$ : decay lifetime component.  $\phi$  = quantum yield. IC: Internal Conversion. VR: Vibrational Relaxation. ISC: Intersystem Crossing. T: Triplet lifetime.

#### **5.3** Conclusions:

- In summary, we have discussed the optical, photophysical and nonlinear optical properties of two 1H phenanthro [9,10-d]-imidazole substituted metal phthalocyanines ImCuPc and ImZnPc to explore their potential as a photosensitizer in PDT and/or 2PE-PDT treatment procedures.
- Computational studies regarding the energy optimized structures in the concerned molecules indicated possibility of a donor (phenanthroimidazole group) acceptor (metallophthalocyanine moiety) interaction within the monomer(s) in solution. The phenanthro [9,10-d]-imidazole group broadens the MPc Soret absorption band.
- Ultrafast NLO properties of ImMPc with 50 fs, 1 kHz repetition rate pulses revealed
  a distinguished two-photon process being dominant at 800 nm. The molecules
  displayed reliable two-photon absorption cross-sections with ImZnPc showing a
  superior 2PA coefficient than ImCuPc. They exhibited negative nonlinearity (selfdefocusing).
- Femtosecond to microsecond timescale of photophysical studies were conducted with the ImMPc (M = Zn, Cu) using fs and ns-TAS studies which showed a consistent broad transient peak which essentially overlapped the bleach signal at Soret band (400 nm) and Q-band (610 nm) pump excitation indicating presence of possible triplet state transitions.

- A global fit analysis with triplet state measurements, revealed long-lived triplet states in both the molecules with ImCuPc triplet lifetime (1.4 μs) to be slightly longer than ImZnPc (1.2 μs) while the ISC lifetime was opposite with ImCuPc (~7.1 ns) having a faster intersystem crossing over ImZnPc (~7.3 ns).
- The triplet yield was also in aggregability with the TAS lifetimes showing higher yield for ImCuPc (0.51) than ImZnPc (0.27). Comparing the two molecules, it can be clearly concluded that phenanthro [9,10-d] imidazole substituted metal phthalocyanines—ImCuPc and ImZnPc are ideal photosensitizers for their use in PDT/2PE PDT applications owing to efficient charge-transfer mechanism, excellent nonlinear optical coefficients and large triplet lifetimes.
- Furthermore, the donor-acceptor interaction is faster in ImCuPc over ImZnPc, which can be assigned to the difference in 3d orbital configuration between CuPc and ZnPc.

#### **5.4** References:

- [1] S. B. Brown, E. A. Brown and I. Walker, "The present and future role of photodynamic therapy in cancer treatment," *Lancet Oncol.*, vol. 5, p. 497, 2004.
- [2] J. M. R. Detty, S. L. Gibson and S. J. Wagner, "Current clinical and preclinical photosensitizers for use in photodynamic therapy," *J. Med. Chem.*, vol. 47, p. 3897, 2004.
- [3] R. R. Allison, G. H. Downie, R. Cuenca, X.-H. Hu, C. J. Childs and C. H. Sibata, "Photosensitizers in clinical PDT," *Photodiagn. Photodyn. Ther.*, vol. 1, p. 27, 2004.
- [4] R. R. Allison and C. H. Sibata, "Oncologic photodynamic therapy photosensitizers: a clinical review," *Photodiagn. Photodyn. Ther.*, vol. 7, p. 61, 2010.
- [5] B. C. Wilson and M. S. Patterson, "The physics, biophysics and technology of photodynamic therapy," *Phys. Med. Biol.*, vol. 53, p. R61, 2008.
- [6] F. Bolze, S. Jenni, A. Sour and V. Heitz, "Molecular photosensitisers for two-photon photodynamic therapy," *Chem. Commun.*, vol. 53, p. 12857, 2017.
- [7] M. Sheik-Bahae, A. Said, T.-H. Wei, D. Hagan and E. V. Stryland, "Sensitive measurement of optical nonlinearities using a single beam," *IEEE journal of quantum electronics*, vol. 26, pp. 760-769, 1990.
- [8] M. Fournier, C. Pépin, D. Houde, R. Ouellet and J. v. Lier, "Ultrafast studies of the excited-state dynamics of copper and nickel phthalocyanine tetrasulfonates: potential sensitizers for the two-photon photodynamic therapy of tumors," *Photochem Photobiol Sci.*, vol. 3, pp. 120-126, 2004.
- [9] R. Francke and R. Little, "Optimizing electron transfer mediators based on arylimidazoles by ring fusion: Synthesis, electrochemistry, and computational analysis of 2-aryl-1-methylphenanthro[9,10-d] imidazoles.," *J. Am. Chem. Soc.*, vol. 136, p. 427–435, 2014.
- [10] W. Chen, Y. Yuan, Y. Xiong, A. Rogach, Q.-X. Tong and C. Lee, "Aromatically C6-and C9-substituted phenanthro[9,10-d]imidazole blue fluorophores: structure—property relationship and electroluminescent application.," *ACS Appl. Mater. Interfaces*, vol. 9, no. 31, p. 26, 2017.

- [11] N. Krishna, J. Krishna, S. Singh, L. Giribabu, A. Islam and I. Bedja, "Bulky nature phenanthroimidazole-based porphyrin sensitizers for dye-sensitized solar cell applications," *J. Phys. Chem. C*, vol. 121, p. 25691–25704, 2017.
- [12] X. Li, X. Peng, B. Zheng, J. Tang, Y. Zhao, B. Zheng, M. Ke and J. Huang, "New application of phthalocyanine molecules from photodynamic therapy to photothermal therapy by means of structural regulation rather than formation of aggregates," *Chem. Sci.*, vol. 9, pp. 2098-2104, 2018.
- [13] C. Allen, W. Sharman and J. v. Lier, "Current status of phthalocyanines in the photodynamic therapy of cancer," *J. Porphy. Phth.*, vol. 5, pp. 161-169, 2001.
- [14] F. Bellina, S. Cauteruccio, S. Montib and R. Rossi, "Novel imidazole-based combretastatin A-4 analogues: evaluation of their In vitro antitumor activity and molecular modelling study of their binding to the colchicines site of tubulin.," *Bioorg. Med. Chem. Lett.*, vol. 16, pp. 5757-5762, 2006.
- [15] P. Mroz, J. Bhaumik, D. Dogutan, Z. Aly, Z. Kamal, L. Khalid, H. Kee, D. Bocian, D. Holten, J. Lindsey and M. Hamblin, "Imidazole metalloporphyrins as photosensitizers for photodynamic therapy: role of molecular charge, central metal and hydroxyl radical production," *Cancer Lett.*, vol. 282, no. 1, pp. 63-76, 2009.
- [16] H. Abramczyk, B. Brozek-Płuska, K. Kurczewski, M. Kurczewska, I. Szymczyk, P. Krzyczmonik, T. Błaszczyk, H. Scholl and W. Czajkowski:, "Femtosecond transient absorption, raman, and electrochemistry studies of tetrasulfonated copper phthalocyanine in water solution," *J. Phys. Chem. A.*, vol. 110, pp. 8627-36, 2006.
- [17] M.-S. Liao and S. Scheiner, "Electronic structure and bonding in metal phthalocyanines, metal=Fe, Co, Ni, Cu, Zn, Mg," *J. Chem. Phys.*, vol. 114, p. 9780–9791, 2001.
- [18] S.-A. Omari:, "Resonance energy transfer and competing processes in donor–acceptor of sodium zinc (II)-2,9,16,23-phthalocyanine tetracarboxylate molecule," *J. Biol. Phys.*, vol. 42, no. 3, p. 373–382., 2016.
- [19] J. Cao, D. Shen, Y. Feng and W. Wan, "Nonlinear refraction by difference frequency generation," *Appl. Phys. Lett.*, vol. 108, p. 191101–5, 2016.
- [20] L. M. Mazur, T. Roland, S. Leroy-Lhez, V. Sol, M. Samoc, I. D. W. Samuel and K. Matczyszyn, "Efficient singlet oxygen photogeneration by zinc porphyrin dimers

- upon one- and two-photon excitation," *J. Phys. Chem. B*, vol. 23, pp. 4271-4277, 2019.
- [21] Y. Mir, J. E. v. Lier, J.-F. Allard, D. Morris and D. Houde, "Two-photon absorption cross section of excited phthalocyanines by a femtosecond Ti-sapphire laser," *Photochem. Photobiol. Sci.*, vol. 8, pp. 391-395, 2009.
- [22] S. Bhattacharya, C. Biswas, S. Raavi, J. Krishna, N. Krishna, L. Giribabu and S. V. Rao, "Synthesis, optical, electrochemical, DFT studies, NLO properties, and ultrafast excited state dynamics of carbazole-induced phthalocyanine derivatives," *J. Phys. Chem. C.*, vol. 123, pp. 11118-33, 2019.
- [23] S. Bhattacharya, C. Biswas, S. Raavi, J. Krishna, D. Koteshwar, L. Giribabu and S. V. Rao, "Optoelectronic, Nonlinear Optical Properties and Excited State Dynamics of a Triphenyl Imidazole Induced Phthalocyanine Derivative," *RSC Adv.*, vol. 9, pp. 36726-36741, 2019.
- [24] S. Raavi, J. Yin, G. Grancini, C. Soci and S. V. Rao, "Femtosecond to microsecond dynamics of soret-band excited corroles," *J. Phys. Chem. C*, vol. 119, p. 28691– 28700, 2015.
- [25] J. Snellenburg, S. Laptenok, R. Seger, K. Mullen and I. v. Stokkum, "Glotaran: A java-based graphical user interface for the R package TIMP," *Glotaran, J. Stat Softw.*, vol. 49, no. 3, p. 1–22., 2012.
- [26] M. Vivas, L. de Boni, L. Gaffo and C. Mendonca, "Investigation of Ground and Excited State Photophysical Properties of Gadolinium Phthalocyanine," *Dyes Pigm.*, vol. 101, p. 338–343, 2014.
- [27] L. Howe and J. Z. Zhang., "Ultrafast Studies of Excited-State Dynamics of Phthalocyanine and Zinc Phthalocyanine Tetrasulfonate in Solution," *J. Phys. Chem. A*, vol. 101, p. 3207–3213, 1997.
- [28] X. He, G. Zhu, J. Yang, H. Chang, Q. Meng, H. Zhao, X. Zhou, S. Yue, Z. Wang, J. Shi, L. Gu, D. Yan and Y. Weng, "Photogenerated Intrinsic Free Carriers in Small-molecule Organic Semiconductors Visualized by Ultrafast Spectroscopy," *Sci. Rep.*, vol. 5, p. 17076–87, 2015.
- [29] B. Caplins, T. Mullenbach, R. Holmes and D. Blank, "Femtosecond to nanosecond excited state dynamics of vapor deposited copper phthalocyanine thin films.," *Phys. Chem. Chem. Phys.*, vol. 18, p. 11454—11459, 2016.

- [30] F. Gotardo, L. Cocca, T. Acunha, A. Longoni, J. Toldo, P. Gonçalves, B. Iglesias and L. D. Boni, "Investigating the intersystem crossing rate and triplet quantum yield of protoporphyrin IX by means of pulse train fluorescence technique.," *Chem. Phys. Lett.*, vol. 674, pp. 48-57, 2017.
- [31] K. Sakamoto, T. Kato, E. Okumura, M. Watanabe and M. Cook, "Synthesis of novel cationic amphiphilic phthalocyanine derivatives for next generation photosensitizer using photodynamic therapy of cancer," *Dyes and Pigments*, vol. 64, no. 1, p. 63–71, 2005.

# Chapter 6

# Excited State Dynamics of Octa-alkoxy Substituted Porphyrins in the Presence of Nitroaromatic and Nitramine Energetic Materials.

In this chapter, we exploit the photophysical properties of three alkyl and alkoxy substituted porphyrins for their application as explosives sensors utilizing the fluorescence quenching mechanism. The molecules –H<sub>2</sub>EP (β-octaethylporphyrin) (S9), H<sub>2</sub>OMP (βoctamethoxyporphyrin) (S10) and H<sub>2</sub>OBuP (β-octabutoxyporphyrin) (S11) were investigated for their quenching abilities in the presence of three most commonly used high energy materials (HEMs)/explosives – TNT, HMX, and RDX. Based on the studies previously conducted [1], these porphyrins have been found to be excellent fluorophores exhibiting dynamic fluorescence quenching in the presence of nitroaromatic HEMs such as TNT using fluorescence spectroscopy and, therefore, can be used as an explosive detection tool. Fluorescence quenching is a radiative process and hence the ease in sensing using fluorescence spectroscopy. In this work we performed the measurement of radiative lifetimes as well as the non-radiative lifetimes using the fs-TAS technique to understand the quenching pathways in each fluorophore, quantitatively. The results revealed that TNT with the electron-rich porphyrin samples 9–11, demonstrated quenching in fluorescence via photoinduced electron transfer (PET). Whereas, for HMX and RDX, energy transfer was dominant with no significant quenching of fluorescence in the porphyrins. However, due to energy transfer between porphyrin donor molecules and the explosive acceptor molecules, a significant quenching in decay rates was evident. This data explains the reasons behind the selective detection of porphyrins towards nitroaromatics like TNT and not nitramines such as RDX, HMX.

Part of the presented work in this chapter has been published in the following:

**S. Bhattacharya,** C. Biswas, S.S. Sahoo, S.S.K. Raavi, P.K. Panda and S. Venugopal Rao, "Photophysical studies behind selective trace detection of nitroaromatics in  $\beta$  octaalkyl/alkoxy porphyrins". [Submitted, 2020].

#### **6.1** Introduction

Fluorescence-based detection mechanism takes place via photoinduced electron transfer between high-electron affinity analytes and excited fluorescent molecules that leads to a fluorescence quenching. Nitroaromatic explosives such as TNT (trinitrotoluene) are strong quenchers of the fluorescence due to their high electron affinities in a number of fluorophores [2, 3, 4]. Two major reasons that shape the nature of the excited state responsible for the luminescence challenging are:

- i. Chromophores that are excited and adjacent to each other can form inter-molecular electronic species with varied degrees of energetics and delocalisation [5], that can affect the nature and the sensitivity of the specific material to be used as a sensor.
- ii. Inter-molecular species could be excited directly or populated via energy transfer by either forming the ground state (aggregates) or electronic excited states (excimers).

Owing to the security issues and threat perception across the globe in the present times, detection of hazardous chemicals such as explosives is of great interest. In particular, there is a great demand for chemosensors (like fluorescence quenching mechanism) that can-do rapid detection of ultra-trace analytes from the explosives [6, 7]. Explosive sensing via fluorescence quenching can be performed using either analyte vapours or in solution form. Due to higher diffusivity, fluorescence quenching is more prominent in vapour detection than in solution [8]. However, traces of explosive remain often can be found in water or swamps for which a thorough study of their solution form is equally important. Sensors that are porphyrin-based can fit as both solution as well as vapor phase detection due their superior photo-stability and ease of synthesis. A major virtue of porphyrin-based sensors is their ability to selectively modulate their physico-chemical properties via suitable functionalization of the peripheral positions and/or incorporation of various metal ions into their core in order which can tailor the molecules' emission characteristics and coordination behavior. Contact between the fluorophore and the quencher at molecular level is crucial for the phenomenon of fluorescence quenching. The type of contact can be 'dynamic' that arises from a diffusive encounter, or 'static' which results from an intermediate complex formation. Recently, fluorescent conjugated polymers (CPs) have successfully detected nitrated explosive detection [9, 10, 11]. Molecular imprinted polymers [12], metal organic frameworks [13, 14], quantum dots [15, 16], nanoparticles [17, 18], coordination polymers [19, 20] and graphene [21] have also been exploited for explosives sensing applications. Fluorophores that are smaller molecules are equally efficient fluorescence sensors with other advantages over macromolecules such as easy synthesis, multiple quenching pathways for fluorescence and detection ability for a broad range of explosives. From recent studies on single molecule fluorophores [22, 23, 24] like porphyrin based sensors [25, 26, 27]. Pump-probe spectroscopy or TAS studies play an important role in understanding the charge transfer or energy transfer dynamics between the fluorophore and an analyte, quantitatively. This in turn, enables in improved sensor design. Recent studies with PETN [28] using ultrafast IR pump-probe spectroscopy, the molecule reveals a sub-ps vibrational energy transfer followed by a 150 ps energy transfer process that is incomplete. Recently, a combination of femtosecond TAS IR spectroscopy and 2D IR spectroscopy was used to study HHTT (RDX) [29]. The results demonstrated an accelerated energy relaxation as well as that energy-transfer processes in vibrational levels of the excited states in the microcrystal form of HHTT. Other studies have been carried out with dendrimers and polymeric fluorophores [30, 31] showing selective quenching via dynamic as well as instantaneous quenching that essentially helps in understanding the relaxation pathways of nitroaromatics. Here, we explore the sensing properties of alkyl and alkoxy groups of βsubstituted porphyrins in vapor phase sensing of Nitro-based energetic (NE) materials. Herein,  $\beta$ -octabutoxyporphyrin (**H<sub>2</sub>OBuP**; 11) and  $\beta$ -octamethoxyporphyrin (**H<sub>2</sub>OMP**; 10) as alkoxy counterparts and  $\beta$ -octaethylporphyrin (H<sub>2</sub>EP; 9) were used to systematically study how the porphyrin peripheral substituents behave towards NE vapor/solution sensing solution enabling to effectively design of superior sensors. Keeping it in mind, we exploited effect trinitrotoluene (TNT), 3,5-trinitro-1,3,5-triazine (RDX) the cyclotetramethylene-tetranitramine (HMX) on the above porphyrins and compare their photophysical characteristics using fs-TAS studies with global fitting.

# **6.2** Experimental Details and Results:

The molecular synthesis and characterization of three novel beta octa alkoxy porphyrins –  $H_2EP$  ( $\beta$ -octaethylporphyrin),  $H_2OMP$  ( $\beta$ -octamethoxyporphyrin) and  $H_2OBuP$  ( $\beta$ -octabutoxyporphyrin), labelled as samples S9, S10 and S11 respectively, were studied for explosives (HEM) sensing including TNT (trinitrotoluene), RDX (Research Department Explosive) and HMX (High Melting Explosive). The chemical synthesis and

characterization of the three fluorophores were carried out by Prof. P.K. Panda and his group at ACRHEM, University of Hyderabad as given in [1].

#### **6.2.1.** Absorption and Emission studies:

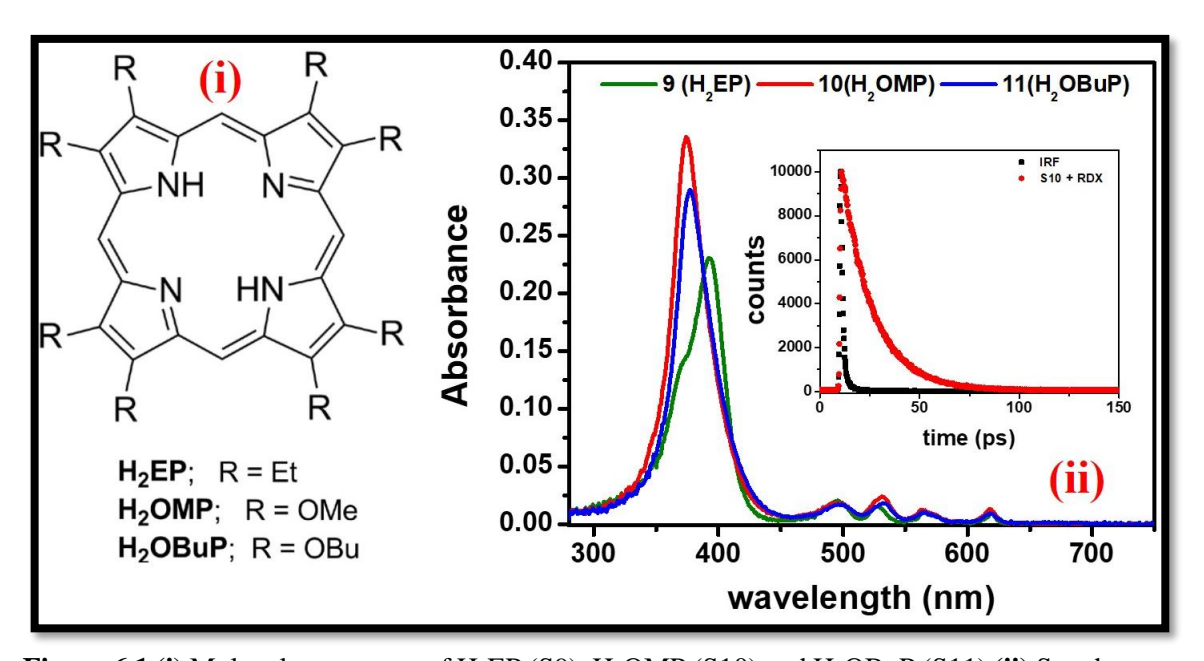


**Figure 6.1 (i)** Molecular structure of H<sub>2</sub>EP (S9), H<sub>2</sub>OMP (S10) and H<sub>2</sub>OBuP (S11) (**ii**) Steady-state absorption of S9 (green line), S10 (red line) and S11 (blue line) with fluorescence lifetime of S10 in presence of RDX as inset.

Shimadzu UV-3600, UV-visible-NIR spectrophotometer recorded the steady state absorption spectra of the given molecules. Fluorolog-3 spectrofluorometer (Spex model, JobinYvon) recorded the steady-state fluorescence spectra at 0.06 optical density. For fluorescence quantum yield calculations, zinc tertbutyl phthalocyanine (=0.37 in benzene) was used as the reference. [32]. A picosecond emitting diode laser (NanoLED,  $\lambda$ ex= 670 nm) by IBH Horiba Jobin Yvon - FluoroLog3- Triple Illuminator was used to record the corresponding fluorescence lifetimes of the molecules. The decay curves were recorded at  $\lambda$ em = 700 nm which is the phthalocyanine macrocycle fluorescence emission maxima. Detector used was the Photomultiplier tube (R928P, M/s Hamamatsu). The instrument response function was calculated by the excitation source (~635 ps at 670 nm) full width half maximum (FWHM). Data fitting the decay curves were performed using nonlinear least-squares iteration process with the help of IBH DAS6 (version 2.3) decay analysis software. For the best fit analysis, the  $\chi^2$  values and distribution of the residuals are compared. The absorption properties of both S9, S10, and S11 (50  $\mu$ M concentration) in different solvents (DCM, DMF, THF, toluene) are illustrated in Figures 6.1(ii). The solvent

used was Chloroform. The free base alkyl/alkoxy porphyrins had an intense absorption peak in the Soret band region (300 nm - 450 nm) and a multiple Q-bands in the visible region (500 nm - 650 nm) owing to degenerate  $D_{2h}$  splitting. Similarly, the emission spectra recorded in different chloroform at 650 nm excitation wavelength, followed by lifetime measurement is presented as inset of figure 6.1(ii).

The steady-state absorption and emission spectra of S9, S10 and S11 in chloroform, show a broad Soret band, which includes absorption band of the alkyl/alkoxy group attached at the periphery of the Por moieties. The degenerate Q-bands at 600-700 nm region are characteristics of  $D_{2h}$  band splitting, and appear due to  $\pi$ - $\pi$ \* transitions [32, 33, 34]. The emission band for all the molecules appeared at ~630 nm followed by 690 nm, illustrating an agreement with the rule of mirror symmetry. The clear overlap of absorption and emission spectra of porphyrin and energetic molecules – HMX and RDX denoted to possible intramolecular Förster's resonance energy transfer (FRET) within the monomeric structure. As we have discussed in the previous chapter, in FRET, the donor molecular group is in an excited state which transfers an electron to the ground acceptor state while relaxing to its ground state simultaneously:  $D^* + A \rightarrow D + A^*$  [35]. This phenomenon can be a competing process to the fluorescence during ground state recovery thus, reducing the fluorescence quantum yield permitting the nonradiative intramolecular transfer of energy in the porphyrins. This can negligibly affect the fluorescence quenching in these sensors.

#### 6.2.2. fs-TAS studies:

The excited-state dynamics of the fluorophores – S9, S10 and S11 is of crucial to study nitroaromatics (TNT) and nitramines (HMX, RDX) detection via fluorescence quenching. Here we used the TAS technique with 50 fs, 1 kHz pulses to understand the singlet excited state dynamics of the porphyrins. Initially, we want to look at the individual TAS spectra of each alkyl and alkoxy porphyrins – S9, S10, and S11. From the absorption spectra, we observe an intense Soret band in the 250–450 nm region for all three molecules. On exciting a 0.5 mM solution of each porphyrin in DMF (dimethyl formaldehyde) solvent, at 400 nm, we monitored the excited state kinetics up to a probe delay of 1 ns (see figure 6.2). Clearly, S9 is the longest-lived fluorophore while S10 is shortest lived followed by S11. In the above figure, the blue regions show a negative difference absorption (-ΔOD) given by the intensity profile at top right corner of the spectra. This shows the GSB region

for the porphyrins, arising due to  $S_0 \rightarrow S_1$  transition. The regions towards red indicates positive difference absorption ( $+\Delta$ OD) owing to excited state absorption or ESA. For S9 and S10, the ESA intensifies over the period of delay time denoting long-lived transient lifetime components. The fluorescence measurements of S9, S10, and S11 were found to result in radiative lifetimes of 9.1 ns, 7 ns, and 6.6 ns, respectively [see figure 6.1 (ii)]. For the fs-TAS lifetime measurements, we performed a global fitting [see figures 6.3 – 6.5 (a)-(h)] on all the three molecules with 0.5 mM solutions in chloroform and DMF. The obtained lifetime components along with the decay rate constants are tabulated in Table 6.1 below.

The globally fitted data revealed the following information. Figures 6.3(a)–6.3(h) illustrate the globally fitted TAS data of H<sub>2</sub>EP (S9) using standard state kinetic model. For both solvents – DMF and chloroform, four distinguished lifetime components were found with the first shorter lifetimes within 30 ps. Based on the corresponding DADS, it is clear that  $\tau_1$  indicates internal conversion to  $S_1$  hot states shown by red spectral lines in figures 6.3(c) and 6.3(g). The spectrum corresponding to  $\tau_1$  (red line) is similar to the linear absorption spectrum of S9 which the difference spectra can indicate to species population from higher excited states, Sn to vibrationally higher S1 states or S1hot state via internal conversion (IC) i.e.  $S_n \rightarrow S_1$ . The transient spectra around 630 nm is indicative to photoinduced excited state species that appears almost immediate to the molecular excitation owing to the contribution from the adjacent 620 nm absorption band [see figure 6.1(ii)]. This particle band evolves rapidly over each different excited state transition in S9, also evident in S10. This rapid evolution of the 630 nm band is not so distinguishable in S11. This can be assumed due to the fact that the butoxy group in S11 is rather bulky in comparison to ethyl and methoxy groups, restricting the rapid excited species transition from higher singlet states  $(S_n \rightarrow S_1)$ . The second lifetime  $\tau_2$  given by blue line in the figures 6.3(c) and 6.3(g). Here, we clearly see an inverted spectrum to  $\tau_1$  indicative of transient behavior with distinct photoinduced absorption (PIA) at 450 nm, 520 nm, 560 nm, 670 nm and 720 nm. This is owing to S<sub>1</sub> state repopulation via vibrational relaxation (VR) i.e.,  $S_{1hot} \rightarrow S_1$ . The next component  $\tau_3$ , is comparatively a long-lived component indicated by green line which is red-shifted to the  $\tau_2$  component indicating the lower state relaxation which is to  $S_0$  or ground state. This lifetime was found to be shorter in case of polar solvents like DMF than chloroform. However, the next component  $\tau_4$  had longer lifetime with a different absorption spectrum to the previous one, indicating a different relaxation pathway. We can assign  $\tau_4$  to triplet state transition via intersystem crossing (ISC) i.e.  $S_1 \rightarrow T_1$ . Similar observations were made for S10 (figure 6.4) with comparatively shorter lifetime components to S9 [figures 6.3(c) and 6.3(g)]. The corresponding species population are shown in figures 6.3(d) and 6.4(d), 6.4(h) which is in clear resonance with DADS analysis. For S11 in chloroform [figures 6.5(a)–(d)], three best fit components were studied. Here, while the first component can be  $S_1$  state vibrational relaxation, the other two was assigned to and  $S_1 \rightarrow S_0$  and  $T_1$  transitions respectively. The higher energy level transitions were most likely to be faster than the instrumental limit. With the above knowledge about our fluorophores, we added the analytes - TNT (nitroaromatic) with 2 mg and 4 mg concentration in chloroform solution whereas HMX and RDX (nitramines) in DMF and performed fs-TAS analysis under similar conditions.

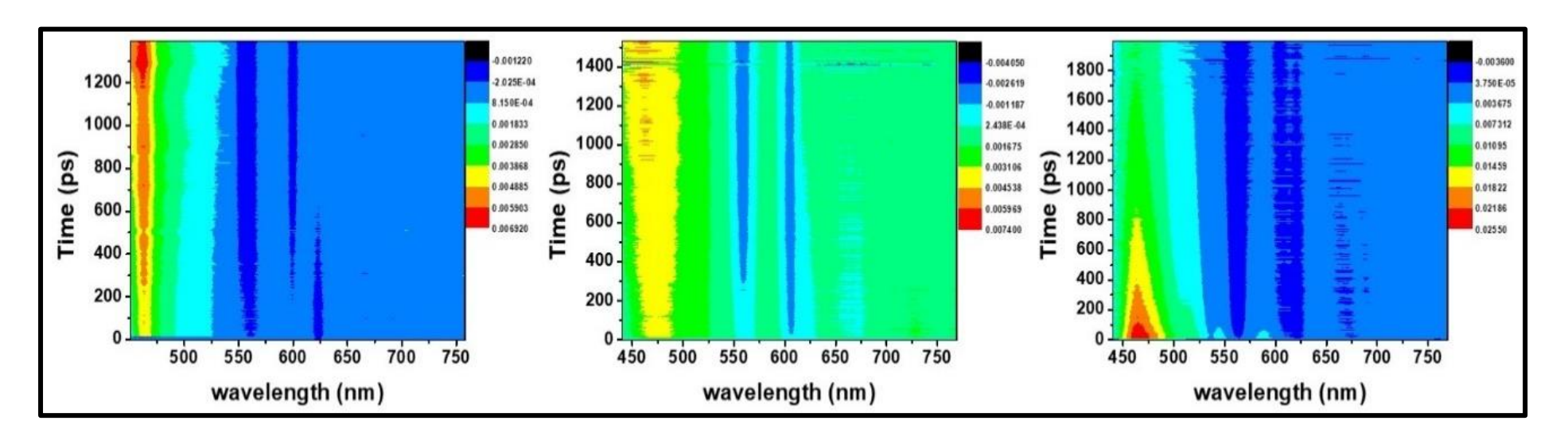
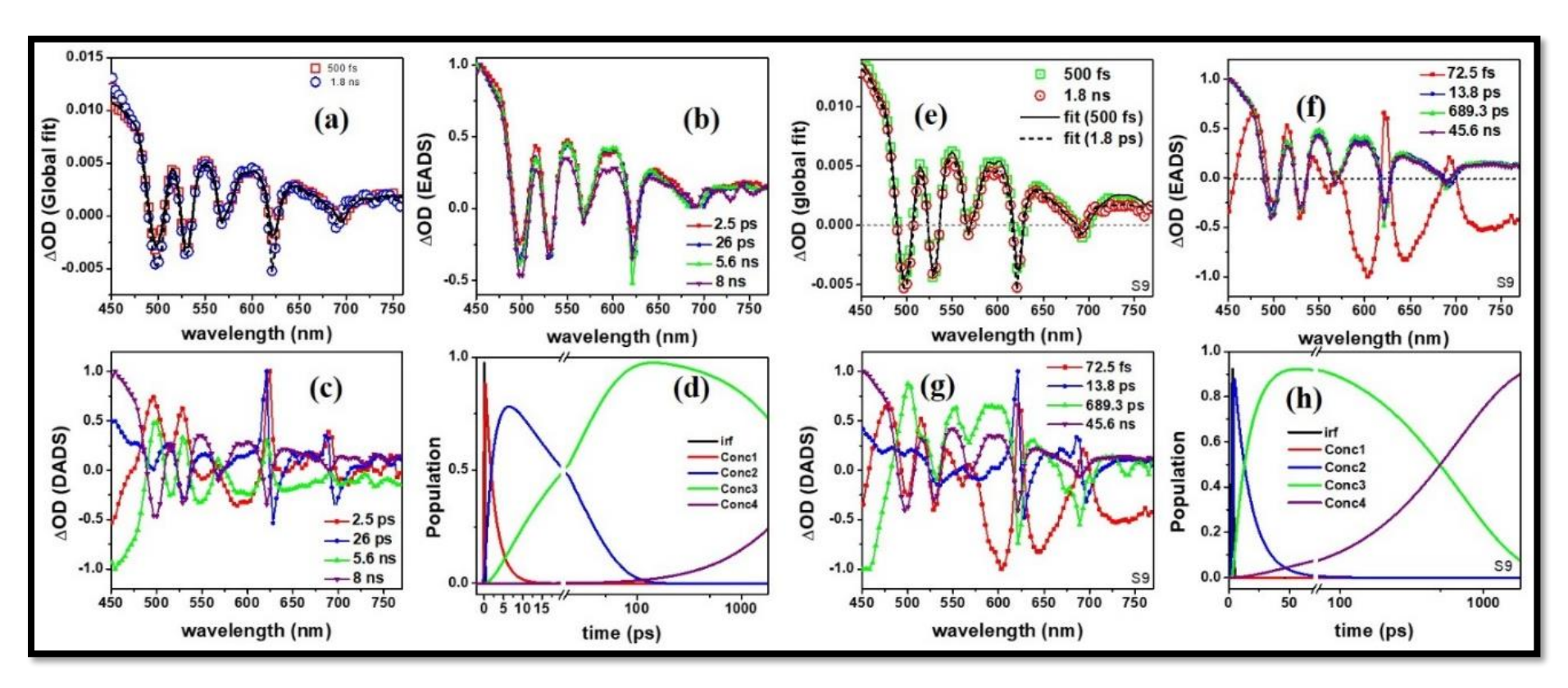
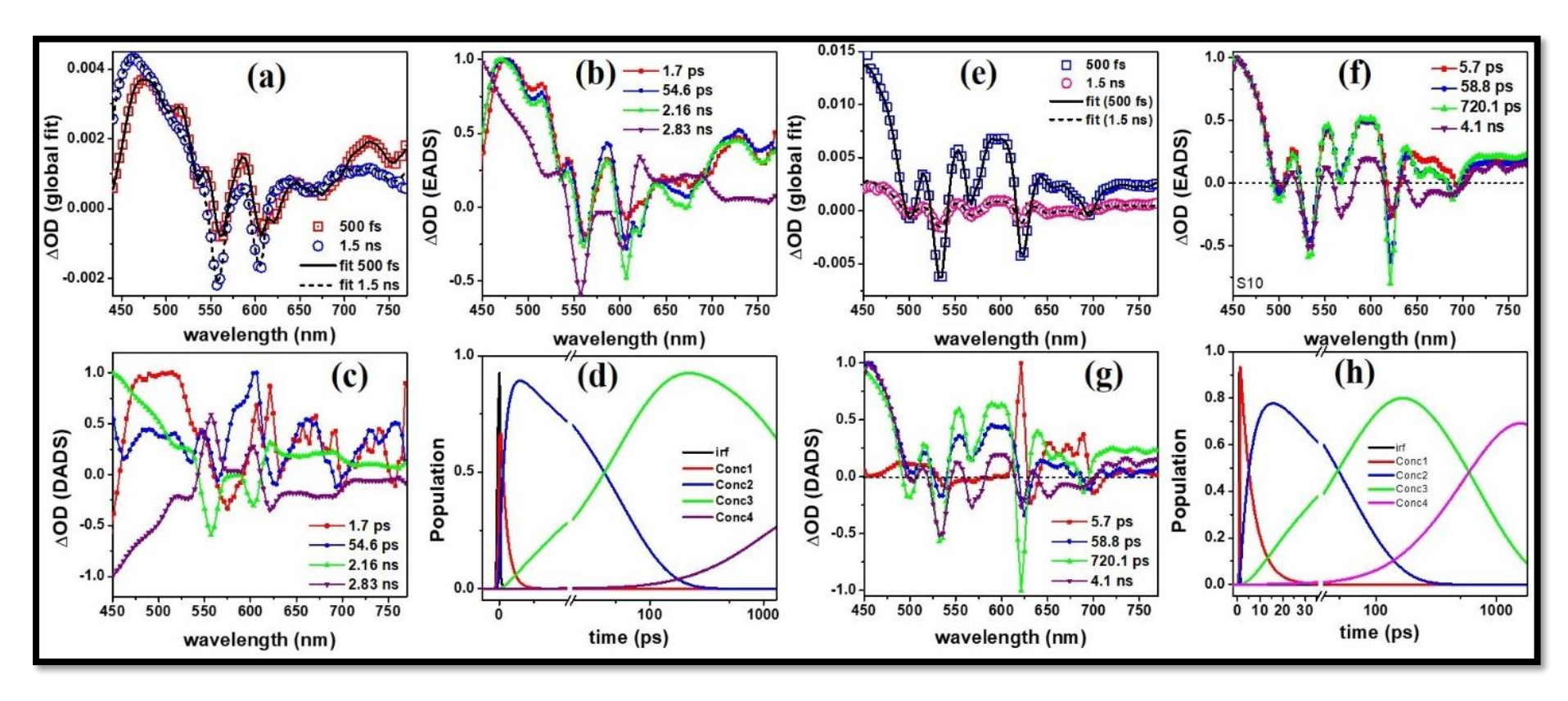


Figure 6.2 fs-TAS 3D spectra of (left) S9, (middle) S10 and (right) S11. The X-axis is wavelength, Y-axis shows spectra evolution over probe delay (in ps) and X-axis shows the difference absorption ( $\Delta$ OD) on a color scheme shown at the top right corner of each spectra.



**Figure 6.3** Global fit of fs-TAS spectra of S9 where (a), (e) spectra were recorded at 500 fs (red) and 1.8 ns (blue). Best fits show accuracy of the global fitting (b), (f) EADS of S9 in chloroform and DMF, respectively for various time delays (c), (g) DADS of S9 in chloroform and DMF, respectively for various time delays (d), (h) excited species population evolution of S9 in chloroform and DMF, respectively.



**Figure 6.4** Global fit of fs-TAS spectra of S10 where (a), (e) spectra were recorded at 500 fs (red) and 1.5 ns (blue). Best fits show accuracy of the global fitting (b), (f) EADS of S10 in chloroform and DMF, respectively for various time delays (c), (g) DADS of S10 in chloroform and DMF, respectively for various time delays (d), (h) excited species population evolution of S10 in chloroform and DMF, respectively.

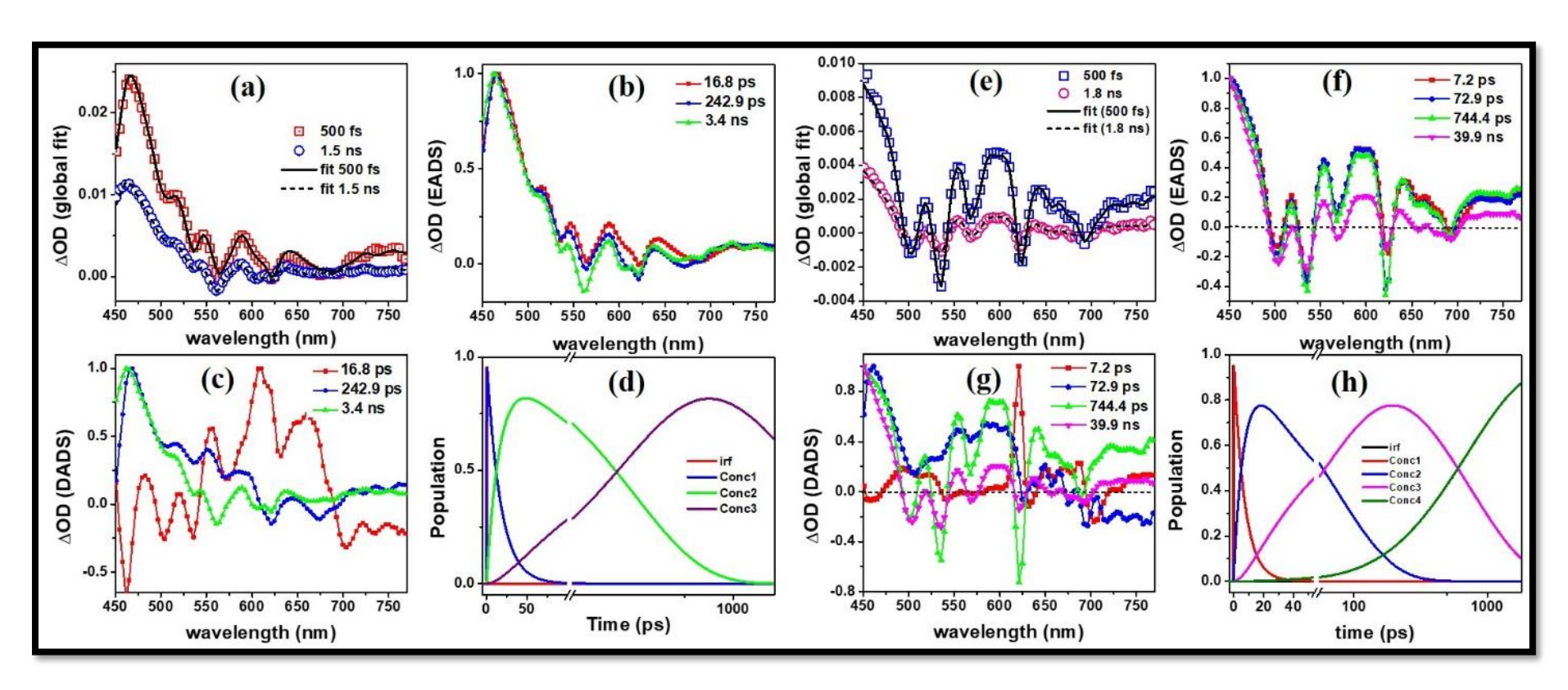


**Figure 6.5** Global fit of fs-TAS spectra of S11 where (a), (e) spectra were recorded at 500 fs (red) and 1.5 ns (blue). Best fits show accuracy of the global fitting (b), (f) EADS of S11 in chloroform and DMF, respectively for various time delays (c), (g) DADS of S11 in chloroform and DMF, respectively for various time delays (d), (h) excited species population evolution of S11 in chloroform and DMF, respectively.

**Table 6.1** fs-TAS global fit parameters of S9, S10, and S11 in various solvents at 400 nm excitation wavelength.

Sample	τ <sub>f</sub> (ns) fluorescence	$\begin{matrix}\tau_1(ps)\\S_n{\rightarrow}S_{1hot}\end{matrix}$	$\begin{matrix}\tau_2(ps)\\S_{1hot}{\longrightarrow}S_1\end{matrix}$	$\begin{matrix}\tau_3(ns)\\S_1{\rightarrow}S_0\end{matrix}$	$\begin{matrix}\tau_4(ns)\\S_1{\rightarrow}T_1\end{matrix}$
	TCSPC	fs-TAS			
		Chloroform, DMF			
S9 (H <sub>2</sub> EP)	9.1	2.5, 0.07	26, 13.8	5.6, 0.69	8, 4.5
S10 (H <sub>2</sub> OMP)	7.0	1.7, 5.7	54.6, 58.8	2.2, 0.72	2.8, 4.1
S11 (H <sub>2</sub> OBuP)	6.6	-, 7.2	16.8, 72.9	0.24, 0.74	3.4, 3.9

#### **6.2.3. Porphyrins with Nitroaromatics:**

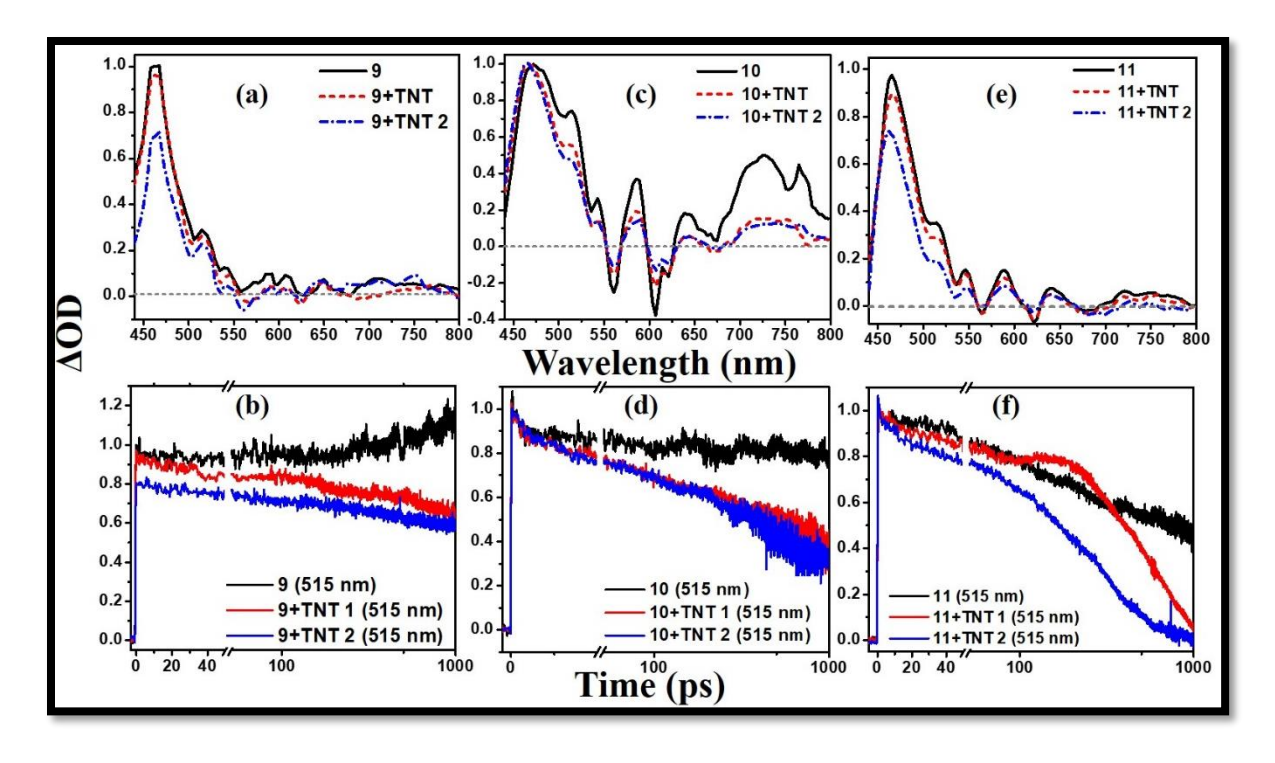


**Figure 6.6** (a) fs-TAS spectra of S9 recorded at 100 ps delay. (b) Corresponding kinetics of S9 at ESA maximum 515 nm. (c) fs-TAS spectra of S10 recorded at 100 ps delay. (d) Corresponding kinetics of S10 at ESA maximum 515 nm. (e) fs-TAS spectra of S11 recorded at 100 ps delay. (f) Corresponding kinetics of S11 at ESA maximum 515 nm. Here, TNT 1 corresponds to 2 mg of TNT in the porphyrin solution whereas TNT 2 is 4 mg TNT in porphyrin solution.

The influence of nitroaromatics (DNT, TNT, etc.) on the current molecules under study have been studied via steady state fluorescence spectroscopy and reported to have shown excellent fluorescence quenching in the presence of TNT in earlier works [1, 36]. The results revealed significant dynamic quenching in all three molecules in the presence of TNT with S10 showing maximum efficiency in the solution form. In order to understand the complete pathway, we performed fs-TAS studies to compare both spectral and kinetic features of the fluorophores in the presence and absence of TNT. The results are shown in figure 6.6 and an analysis was performed qualitatively.

From figures 6.6(a), 6.6(c), and 6.6(e), it is evident that all three molecules depicted significant quenching of the overall transient spectra. The corresponding kinetics recorded at the TA maximum 515 nm, matches the spectral signatures showing distinct quenching in the lifetimes. With increasing concentration, the quenching tendency consistently increased. However, on analyzing the quenching efficiency, S10 quenches the most in presence of TNT. Being electron deficient in nature, TNT acts as an acceptor (A) to an electron rich fluorophore (donor D) in its vicinity via photoinduced electron transfer (PET). In the PET, the excited-state of fluorophores act as donors (D) to the explosive compounds or analytes (A) in the ground-state as shown in figure 6.7 [37]. Here, the oxidative electron transfer process between the LUMO of the donor fluorophore and that of the acceptor explosive is driven. Frontier molecular orbital (FMO) studies confirmed that H<sub>2</sub>OMP and H<sub>2</sub>OBuP are more electron rich compared to H<sub>2</sub>EP [36]. Comparing with the HOMO-LUMO states of TNT [38], it is clear that the interaction is best with the alkoxy porphyrins (S10 and S11). Since negligible changes in FMO energy level is witnessed upon replacement of methoxy groups (S10) with butoxy groups (S11), the resultant alkoxy chain length elongation in S11 has very little effect on its electronic states. Thus, the interaction of TNT or nitroaromatics with our respective fluorophores can be indicated to PET where the fluorophore acts as the donor to TNT as the acceptor (D-A interaction) with the quenching efficiency ( $\frac{\Delta I}{I} \times 100$ ) in the order of S10 >S11 >S9. The corresponding lifetimes at TA maxima were fitted using bi-exponential decay fit and the results are summarized in Table 6.2.

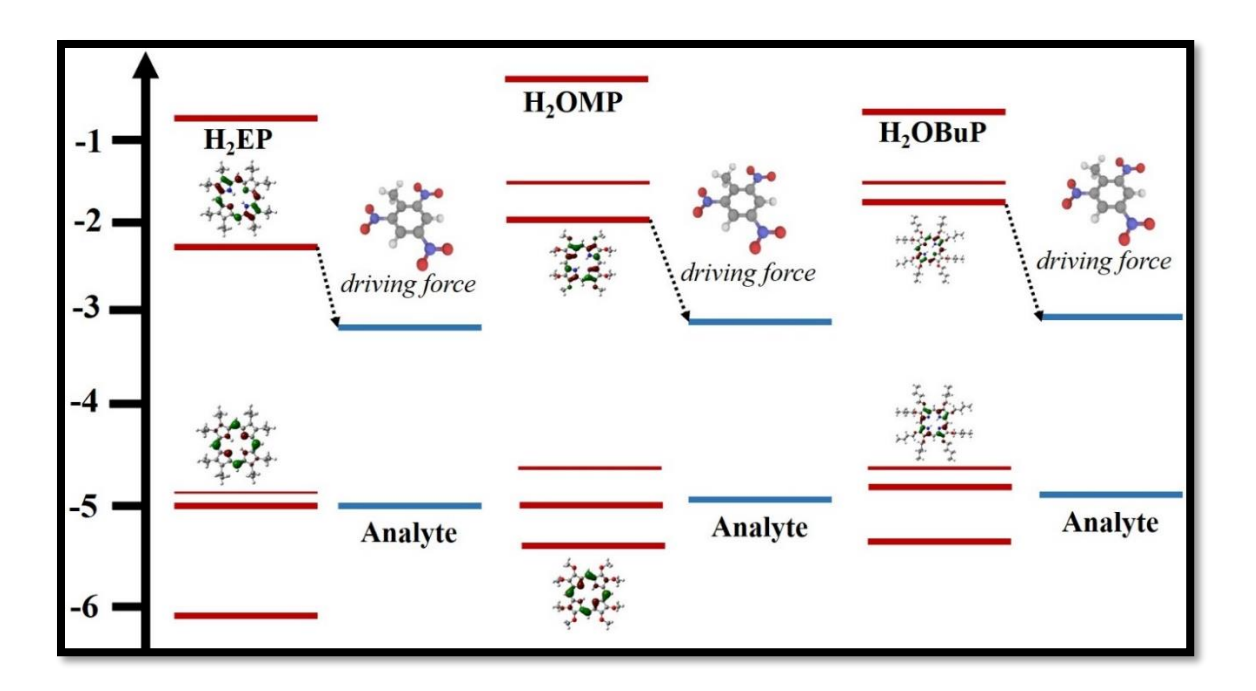


**Figure 6.7** Schematic drawings of the electronic structure of the fluorescence quenching process between S9, S10 and S11 with TNT.

**Table 6.2.** Decay lifetimes of relaxation dynamics in S9, S10 and S11 with TNT for different concentration at 515 nm.

Sample	τ <sub>1</sub> (ps)	$\tau_2$ (ps)
S9	252.3 ± 1.05	9860 ± 84.7
S9 + TNT (2 mg)	$10.9 \pm 0.061$	$3873.1 \pm 96$
S9 + TNT (4 mg)	$9.05 \pm 0.03$	$1316.3 \pm 15.4$
S10	$13.4 \pm 6.12$	$7450 \pm 10.5$
S10 + TNT (2 mg)	$16.3 \pm 9.95$	$1550 \pm 21.2$
S10 + TNT (4 mg)	$10.8 \pm 5.05$	292.7 ± 12.7
S11	$74.7 \pm 37.6$	$1820 \pm 27.8$
S11 + TNT (2 mg)	$66.07 \pm 23.5$	$1410 \pm 92$
S11 + TNT (4 mg)	$50.9 \pm 23.5$	$495.3 \pm 46.7$

## **6.2.4. Porphyrins with Nitro-amines:**

The influence of nitramines (HMX, RDX, etc.) on the current molecules under study have been studied via steady state fluorescence spectroscopy and reported to have shown no distinct fluorescence quenching in the presence of nitramines like HMX or RDX in their solution form.

This indicates that the molecules do not favor the electronic states to facilitate PET leading to radiative relaxation pathways. On the other hand, the steady state absorption of RDX and HMX is seen to overlap the fluorophore emission spectra. This can possibly facilitate energy transfer from fluorophores to the nitramines which can be observed as non-radiative lifetimes in their kinetic picture. Hence, in this chapter, we explore the non-radiative excited state pathways of the porphyrins in presence of HMX and RDX to explain the exact phenomenon qualitatively.

Figures 6.8(a)–6.8(f) and 6.9(a)–6.9(f) depict the influence of HMX and RDX on S9, S10 and S11 in DMF solvent, respectively. We can clearly observe a distinct quenching of the lifetimes in all three porphyrins in presence of nitramines. However, no apparent quenching in the spectral profile of the fluorophore was observed for any of the porphyrins. Table 6.2 summarizes the various relaxation lifetimes obtained from data fitting the kinetic profiles of each case scenarios. We can clearly notice that S10 shows the highest non-radiative lifetime quenching in the presence of HMX and RDX [see data from figures 6.8(c), 6.8(d) and 6.9(c), 6.9(d)], this being consistent with the case with TNT. The longer lifetime τ<sub>2</sub> shows a significant decrease in lifetime for all the cases in all three molecules. This indicates that whatever transfer of excited species happens between the sensor and the analyte, occurs in the first excited state or  $S_1$  state to lower. As there is a spectral overlap in absorption/emission spectra between the fluorophores and nitramines [1, 39], the non-radiative relaxation can be assigned to resonance energy transfer (RET) between electron rich porphyrins and electron deficit nitramines, as shown in figure 6.10. The lower quenching ability of S11 over S10 can be due to the bulkiness of the peripheral flexible butoxy groups in the porphyrin moiety which possibly resulted in slight hindrance of the excited state p-p donoracceptor interaction. Till date, several investigations have been performed showing the selective quenching mechanism of porphyrin sensors towards detection of nitroaromatics [40, 41, 42]. However, not many works include a detailed report analysing the reason behind the selective fluorescent quenching of porphyrins on nitroaromatics over nitramines. Here, through fs-TAS technique, we verify that due to favourable HOMO-LUMO level in TNT promote photoinduced charge transfer via donor-acceptor interaction in porphyrins over the less electron deficient RDX and HMX. The alkoxy porphyrins had higher LUMO levels over alkyl porphyrins hence greater PET driving force in TNT and RET in HMX and RDX.

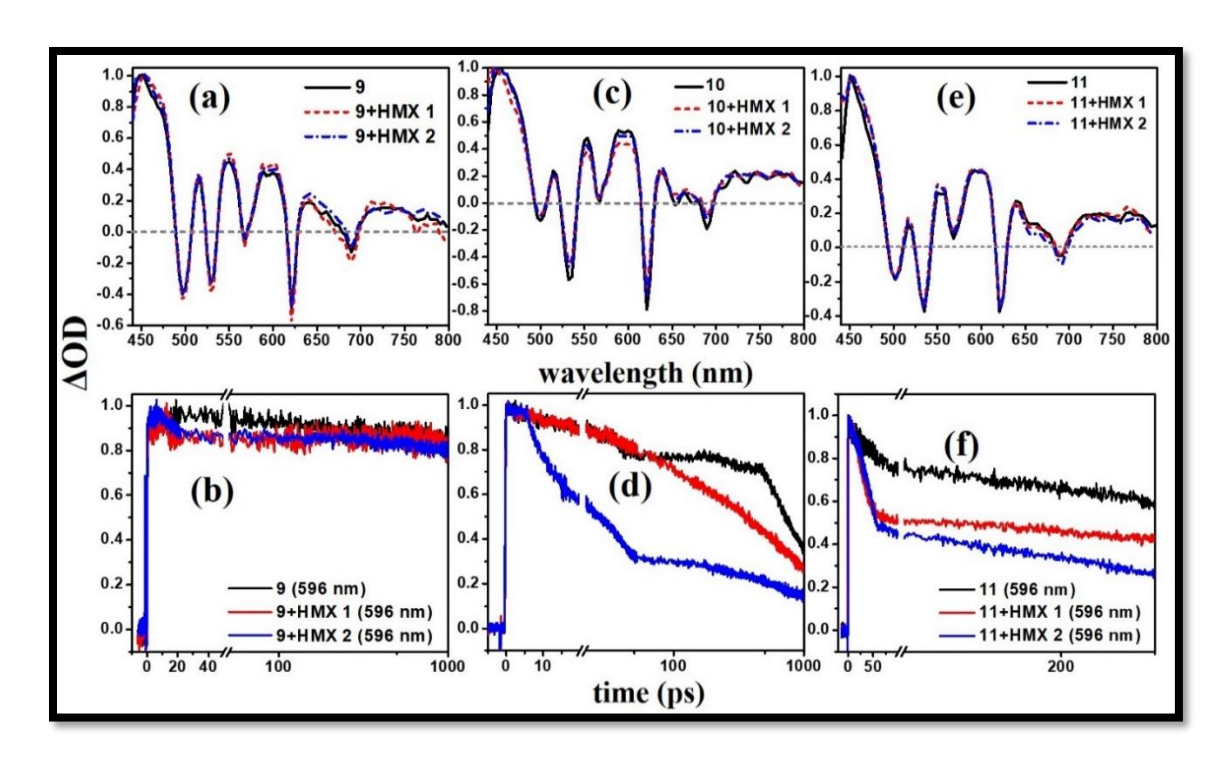


**Figure 6.8** (a) fs-TAS spectra of S9 recorded at 100 ps delay. (b) Corresponding kinetics of S9 at ESA maximum 515 nm. (c) fs-TAS spectra of S10 recorded at 100 ps delay. (d) Corresponding kinetics of S10 at ESA maximum 515 nm. (e) fs-TAS spectra of S11 recorded at 100 ps delay. (f) Corresponding kinetics of S11 at ESA maximum 515 nm. Here, HMX 1 corresponds to 2 mg of HMX in the porphyrin solution whereas HMX 2 is 4 mg HMX in porphyrin solution.

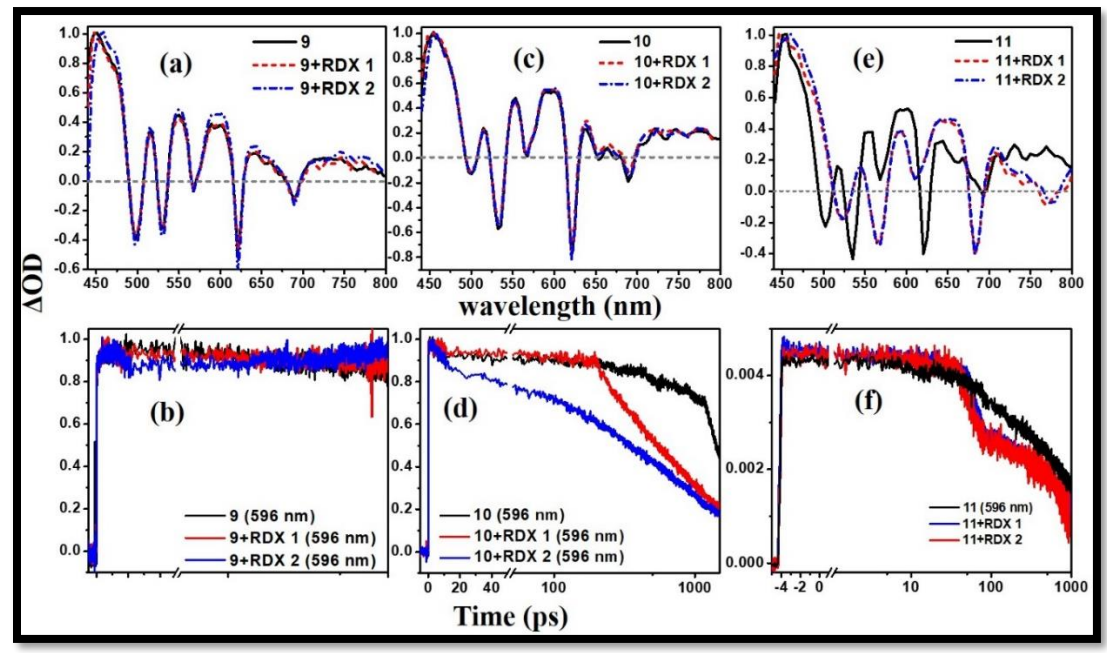


**Figure 6.9** (a) fs-TAS spectra of S9 recorded at 100 ps delay. (b) Corresponding kinetics of S9 at ESA maximum 515 nm. (c) fs-TAS spectra of S10 recorded at 100 ps delay. (d) Corresponding kinetics of S10 at ESA maximum 515 nm. (e) fs-TAS spectra of S11 recorded at 100 ps delay. (f) Corresponding kinetics of S11 at ESA maximum 515 nm. Here, RDX 1 corresponds to 2 mg of RDX in the porphyrin solution whereas RDX 2 is 4 mg RDX in porphyrin solution.

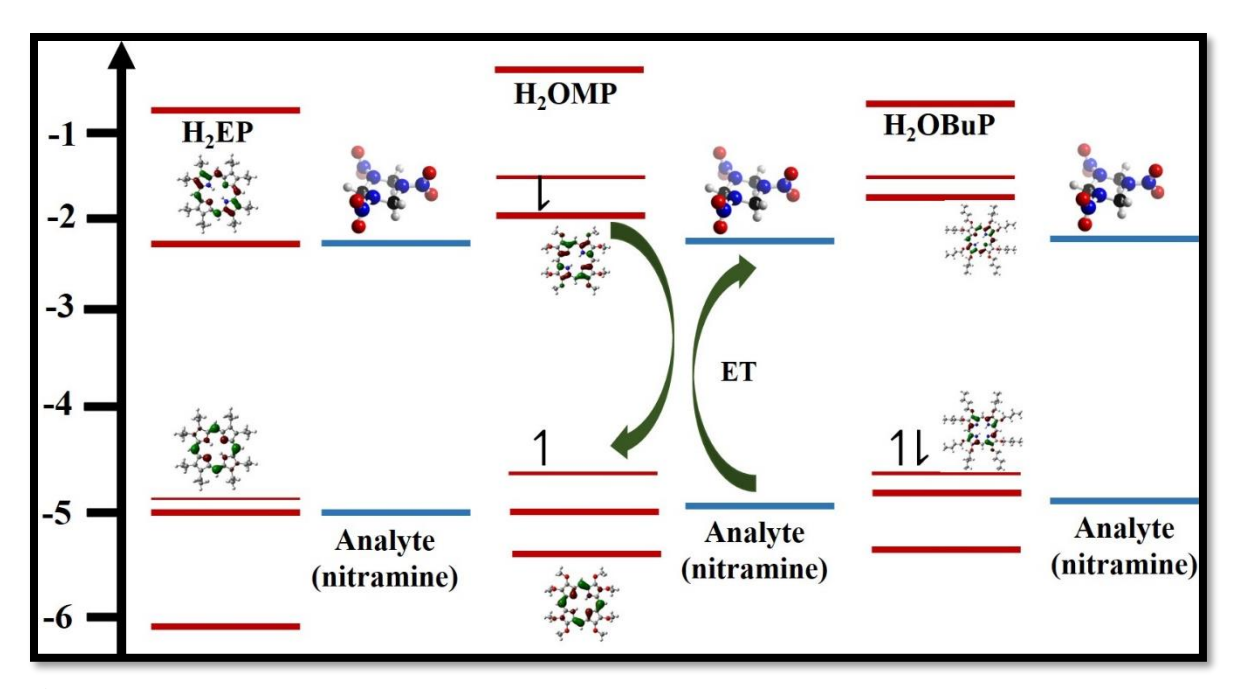


**Figure 6.10**: Schematic drawings of the electronic structure of the non-radiative pathways S9, S10 and S11 with nitramines (here RDX) via energy transfer (ET) between the porphyrin sensor and analyte (RDX).

**Table 6.3** Decay lifetimes of non-radiative relaxation dynamics in S9, S10 and S11 with HMX and RDX for different concentration at 515 nm.

Sample	τ <sub>1</sub> (ps)	τ <sub>2</sub> (ps)
S9	$3.06 \pm 0.73$	$3460 \pm 69.1$
S9 + HMX (2 mg)	$2.06 \pm 0.87$	$3544 \pm 57.5$
S9 + HMX (4 mg)	$2.16 \pm 0.05$	$2436.2 \pm 98.3$
S9 + RDX (2 mg)	$2.18 \pm 0.04$	$1326.3 \pm 53.1$
S9 + RDX (4 mg)	$3.08 \pm 0.04$	$1234.6 \pm 23.1$
S10	$77.69 \pm 6.86$	$2823.5 \pm 32.5$
S10 + HMX (2 mg)	$68.9 \pm 3.41$	$752.4 \pm 21.9$
S10 + HMX (4 mg)	$67 \pm 2.6$	$746.2 \pm 26.9$
S10 + RDX (2 mg)	$76.88 \pm 6.99$	$757.1 \pm 28.1$
S10 + RDX (4 mg)	$65.12 \pm 6.62$	$546.6 \pm 26.3$
S11	$76.7 \pm 8.88$	$2835.4 \pm 35.4$
S11 + HMX (2 mg)	$65.3 \pm 4.7$	$801.5 \pm 16.9$
S11 + HMX (4 mg)	$74.9 \pm 3.97$	$659.7 \pm 18.4$
S11 + RDX (2 mg)	$79.3 \pm 14.4$	$790 \pm 53.1$
S11 + RDX (4 mg)	$67.3 \pm 0.03$	$666.8 \pm 11.2$

## **6.3** Conclusions:

- In conclusion, this chapter discusses the mechanism of selective fluorescence quenching in three porphyrin derivatives S9, S10, and S11 in presence of TNT, RDX and HMX, in their solution form.
- The studies were performed using the fs-TAS technique with their possible application as sensors in trace explosive detection in water, swamps, etc. We observed distinguished fluorescence quenching in case of TNT which was assigned to PET, and non-radiative quenching for RDX and HMX.
- Spectral studies with lifetime studies revealed S10 to be most sensitive to detection in the solution form. The reason was that TNT being more electron deficient to the nitramines – RDX and HMX, leading to favorable donor-acceptor interaction with the porphyrins.
- Alkoxy porphyrins demonstrated superior sensor capabilities to their alkyl alternatives as
  they are more electron rich. However, the bulkiness in butoxy (S11) let to hinderance in the
  D-A interaction, rendering S10 to be better sensor for detection.
- This data can explain the reasons behind selective detection of porphyrins towards nitroaromatics like TNT and not nitramines such as RDX, HMX and help us to design a sensor that can distinctly sense not only nitroaromatics but nitramines as well.

#### **6.4** References:

- [1] A. Rana, S. Sahoo and P. Panda, "β-Octaalkoxyporphyrins: Versatile fluorometric sensors towards nitrated explosives," *J. Porphy. Phth.*, vol. 23, pp. 1-9, 2019.
- [2] G. B. Demirel, B. Daglarac and M. Bayindir, "Extremely fast and highly selective detection of nitroaromatic explosive vapours using fluorescent polymer thin films," *Chem. Commun.*, vol. 49, p. 6140–6142, 2013.
- [3] Y. Geng, M. A. Ali, A. J. Clulow, S. Fan, P. L. Burn, I. R. Gentle, P. Meredith and P. E. Shaw, "Unambiguous detection of nitrated explosive vapours by fluorescence quenching of dendrimer films," *Nat. Commun.*, vol. 6, p. 8240., 2015.
- [4] H. Nie, Y. Zhao, M. Zhang, Y. M. Baumgarten and K. Mullen, "Detection of TNT explosives with a new fluorescent conjugated polycarbazole polymer," *Chem. Commun.*, vol. 47, p. 1234–1236, 2011.
- [5] I. Hwang, U. Selig, S. C. Chen, P. E. Shaw, T. Brixner, P. L. Burn and G. D. Scholes, "Photophysics of detection of explosive vapours via luminescence quenching of thin films: impact of inter-molecular interactions," *J. Phys. Chem. A.*, vol. 117, p. 6270–6278, 2013.
- [6] A.W.Czarnik, "A sense for landmines.," *Nature*, vol. 394, p. 417, 1998.
- [7] C. A. F. C. J. Cumming, M. Fox, M. J. Grone, D. Reust, M. G. Rockley, T. M. Swager, E. Tower and V. William, "Using novel fluorescent polymers as sensory materials for above-ground sensing of chemical signature compounds emanating from buried landmines," *IEEE Trans. Geosci. Remote Sens.*, vol. 39, p. 1119, 2001.
- [8] S. Shoaee, S. Fan, P. Burn and P. Shaw, "Photophysics of detection of explosive vapours via luminescence quenching of thin films: impact of inter-molecular interactions," *Phys. Chem. Chem. Phys.*, vol. 18, p. 25861, 2016.
- [9] S. Rochat and T. M. Swager, "Conjugated amplifying polymers for optical sensing applications," *ACS Appl. Mater. Interfaces*, vol. 5, p. 4488–4502, 2013.
- [10] T. M. Swager, "The molecular wire approach to sensory signal amplification," *Acc. Chem. Res.*, vol. 31, p. 201–207, 1998.

- [11] J. S. Yang and T. M. Swager, "Fluorescent porous polymer films as TNT chemosensors: electronic and structural effects.," *J. Am. Chem. Soc.*, vol. 120, p. 5321–5322, 1998.
- [12] J. Li, C. Kenclig and E. Nesterov, "Chemosensory performance of molecularly imprinted fluorescent conjugated polymer materials," *J. Am. Chem. Soc.*, vol. 129, p. 15911–15918, 2007.
- [13] Z. Hu, B. Deibert and J. Li, "Luminescent metal-organic frameworks for chemical sensing and explosive detection," *Chem. Soc. Rev.*, vol. 43, p. 5815–5840, 2014.
- [14] S. Surya, S. Nagarkar, S. Ghosh, P. Sonar and V. Rao, "OFET based explosive sensors using diketopyrrolopyrrole and metal organic framework composite active channel material," *Sens. Actuators, B*, vol. 223, p. 114–122., 2016.
- [15] Y. Xia, L. Song and C. Zhu, "Turn-on and near-infrared fluorescent sensing for 2, 4, 6-trinitrotoluene based on hybrid (gold nanorod)—(quantum dots) assembly," *Anal. Chem.*, vol. 83, p. 1401–1407, 2011.
- [16] K. Zhang, H. Zhou, Q. Mei, S. Wang, G. Guan, R. Liu, J. Zhang and Z. Zhang, "Instant visual detection of trinitrotoluene particulates on various surfaces by ratiometric fluorescence of dual-emission quantum dots hybrid," *J. Am. Chem. Soc.*, vol. 133, p. 8424–8427, 2011.
- [17] Y. Long, H. Chen, Y. Yang, H. Wang, Y. Yang, N. Li, K. Li, J. Pei and F. Liu, "Electrospun nanofibrous film doped with a conjugated polymer for DNT fluorescence sensor," *Macromolecules*, vol. 42, p. 6501–6509, 2009.
- [18] Y. Salinas, E. Climent, R. –Máñez, F. Sancenón, M. Marcos, J. Soto, A. Costero, S. Gil, M. Parra and A. Diego, "Highly selective and sensitive chromo-fluorogenic detection of the tetryl explosive using functional silica nanoparticles," *Chem. Commun.*, vol. 47, p. 11885–11887, 2011.
- [19] C. Zhang, Y. Che, Z. Zhang, X. Yang and L. Zang, "Fluorescent nanoscale zinc (II)-carboxylate coordination polymers for explosive sensing," *Chem. Commun.*, vol. 47, p. 2336–2338, 2011.
- [20] S. Shanmugaraju, C. Dabadie, K. Byrne, A. Savyasachi, D. Umadevi, W. Schmitt, J. Kitchen and T. Gunnlaugsson, "A supramolecular Tröger's base derived coordination zinc

- polymer for fluorescent sensing of phenolic-nitroaromatic explosives in water," *Chem. Sci.*, vol. 8, p. 1535–1546, 2017.
- [21] L. Tang, H. Feng, J. Cheng and J. Li, "Uniform and rich-wrinkled electrophoretic deposited graphene film: a robust electrochemical platform for TNT sensing," *Chem. Commun.*, vol. 46, p. 5882–5884, 2010.
- [22] S. Shanmugaraju and P. Mukherjee, "π-Electron rich small molecule sensors for the recognition of nitroaromatics," *Chem. Commun.*, vol. 51, p. 16014–16032, 2015.
- [23] M. Meaney and V. McGuffin, "Investigation of common fluorophores for the detection of nitrated explosives by fluorescence quenching," *Anal. Chim. Acta*, vol. 610, p. 57–67, 2008.
- [24] M. Germain and M. Knapp, "Discrimination of nitroaromatics and explosives mimics by a fluorescent Zn (salicylaldimine) sensor array," *J. Am. Chem. Soc.*, vol. 130, p. 5422–5423, 2008.
- [25] M. Kielmann, C. Prior and M. Senge, "Porphyrins in troubled times: a spotlight on porphyrins and their metal complexes for explosives testing and CBRN defense," *New J. Chem.*, vol. 42, p. 7529–7550, 2018.
- [26] S. Tao, Z. Shi, G. Li and P. Li, "Hierarchically structured nanocomposite films as highly sensitive chemosensory materials for TNT detection," *Chem. Phys. Chem.*, vol. 7, p. 1902–1905, 2006.
- [27] S. Tao, G. Li and H. Zhu, "Metalloporphyrins as sensing elements for the rapid detection of trace TNT vapor," *J. Mater. Chem.*, vol. 16, p. 4521–4528., 2006.
- [28] N. Cole-Filipiak, R. Knepper, M. Wood and K. Ramasesha, "Sub-picosecond to Sub-nanosecond Vibrational Energy Transfer Dynamics in Pentaerythritol Tetranitrate," *J. Phys. Chem. Lett.*, vol. 11, p. 6664–6669, 2020.
- [29] L. Shi, P. Yu, J. Zhao and J. Wang, "Ultrafast Intermolecular Vibrational Energy Transfer in Hexahydro-1,3,5-trinitro-1,3,5-triazine in Molecular Crystal by 2D IR Spectroscopy," *J. Phys. Chem. C*, vol. 124, p. 2388–2398, 2020.
- [30] K. Hutchinson, D. Stoltzfus, P. Burn and P. Shaw, "Luminescent poly(dendrimer)s for the detection of explosives," *Mater. Adv.*, vol. 1, p. 837, 2020.

- [31] Y. Geng, M. Ali, A. Clulow, S. Fan, P. Burn and I. Gentle, "Unambiguous detection of nitrated explosive vapours by fluorescence quenching of dendrimer films," *Nat. Commun.*, vol. 6, p. 8240, 2015.
- [32] C. Allen, W. Sharman and J. v. Lier, "Current Status of Phthalocyanines in the Photodynamic Therapy of Cancer," *J. Porphy. Phth.*, vol. 5, pp. 161-169, 2001.
- [33] H. Abramczyk, B. Brozek-Płuska, K. Kurczewski, M. Kurczewska, I. Szymczyk, T. K. Błaszczyk, H. Scholl and W. Czajkowski, "Femtosecond Transient Absorption, Raman, and Electrochemistry Studies of Tetrasulfonated Copper Phthalocyanine in Water Solution," *J. Phys. Chem. A.*, vol. 110, pp. 8627-8636, 2006.
- [34] M.-S. Liao and S. Scheiner, "Electronic Structure and Bonding in Metal Phthalocyanines, Metal=Fe, Co, Ni, Cu, Zn, Mg.," *J. Chem. Phys.*, vol. 114, p. 9780–9791, 2001.
- [35] S.-A. Omari, "Resonance Energy Transfer and Competing Processes in Donor–Acceptor of Sodium Zinc (II)-2,9,16,23-Phthalocyanine Tetracarboxylate Molecule.," *J. Biol. Phys.*, vol. 42, no. 3, p. 373–382, 2016.
- [36] A. Rana and P. Panda, "Fluorescent turn-off based sensing of nitrated explosives using porphyrins and their Zn(II)-derivatives.," *RSC Adv.*, vol. 2, p. 12164–68, 2012.
- [37] B. Valeur, Molecular Fluorescence: Principles and Applications, NY: Wiley-VCH, 2002.
- [38] Y. Xiao, X. Su, L.S.-Vargas, E. Lacaze, B. Heinrich, B. Donnio, D. Kreher, F. Mathevet and A.-J. Attias, "Chemical engineering of donor–acceptor liquid crystalline dyads and triads for the controlled nanostructuration of organic semiconductors," *CrystEngComm.*, vol. 18, pp. 4787-4798, 2016.
- [39] C. Wang, H. Huang, B. Bunes, N. Wu, M. Xu, X. Yang, L. Yu and L. Zang, "Trace Detection of RDX, HMX and PETN Explosives Using a Fluorescence Spot Sensor," *Scientific Reports*, vol. 6, p. 25015, 2016.
- [40] S. Shanmugaraju, S. Joshia and P. Mukherjee, "Fluorescence and visual sensing of nitroaromatic explosives using electron rich discrete fluorophores," *J. Mater. Chem.*, vol. 21, pp. 9130-9138, 2011.
- [41] I. Kovalev, O. Taniya, D. Kopchuk, K. Giri, A. Mukherjee, S. Santra, A. Majee, M. Rahman, G. Zyryanov and V. Bakulev, "1-Hydroxypyrene-based micelle-forming sensors

- for the visual detection of RDX/TNG/PETN-based bomb plots in water," *New J. Chem.*, vol. 42, pp. 19864-19871, 2018.
- [42] K. Reddy, A. Kumar, A. Dhir and V. Krishnan, "New Ni-Anthracene Complex for Selective and Sensitive Detection of 2,4,6-Trinitrophenol," *Int. J. Spectroscopy*, vol. 1321427, no. https://doi.org/10.1155/2018/1321427, p. 5, 2018.

# **Chapter 7**

# **Conclusion and Future Scope**

This chapter summarizes some of the important results obtained and achievements during the course of this study as included in this thesis. There is a brief section explaining the current trends of ultrafast spectroscopic studies on newly developed organic molecules. Finally, the chapter ends with discussion on the future scope in the world of ultrafast spectroscopy and plausible ways to achieve it. The future applications of phthalocyanines and related molecules are also discussed in this chapter.

#### 7.1 Conclusions:

Non-degenerate transient absorption spectroscopy (TAS) is a well-established technique to understand the excited state dynamics in a particular physical system. This ultrafast third-order nonlinear spectroscopic technique has been improvised over the years in an attempt to encompass more and more information about the photophysical world. TAS studies on organic chromophores have been used to exploit their potential in opto-electronic and photo-medicinal applications extensively [1, 2, 3]. Tetrapyrrolic molecules such as porphyrins and phthalocyanines have caught particular attention from chemists, material scientists, physicists due to their delocalized electronic structure with the ability to be tailored on structural level leading to different photophysical as well as photochemical properties. They are known to be excellent photosensitizers as dyes in DSSCs (dye sensitized solar cell) applications and in photodynamic therapy (PDT). Additionally, they can be highly fluorescent molecules with their absorption spectrum within the biological window of 600 nm – 1350 nm. This makes them excellent biosensors and biomarkers as well as other potential bioimaging purposes [4, 5]. The porphyrins and phthalocyanines possess excellent nonlinear optical (NLO) properties due to the presence of delocalized electrons which can lead to interesting multiphoton absorption phenomena. This thesis had been an attempt to explore novel porphyrin and phthalocyanine derivatives for NLO and photophysical properties. Some of the important deductions have been listed below:

i. NLO coefficients: Porphyrins (Por) and Phthalocyanines (Pc) are recognized to possess excellent third-order NLO coefficients [6, 7, 8]. From our detailed NLO studies in the previous chapters, we have found large multiphoton absorption in metallo-porphyrins. *Chapter 2* compared the NLO coefficients of a Zinc porphyrin (ZnTPP) with a Zinc phthalocyanine (TPA-ZnPc). The results indicated large multi-photon absorption coefficients in both the molecules, making them excellent candidates for Optical limiting applications. However, the comparative study indicated slightly superior NLO properties in the phthalocyanine over porphyrin. This suggested that phthalocyanines are possibly better NLO materials over porphyrins sue to higher number of delocalized electrons being photochemically stabler with higher damage threshold. Hence, for later *chapters 3–5*, we dealt with Zinc phthalocyanines and their derivatives for superior NLO applications. It was observed that nature of peripheral substituents plays an equally important role in affecting

the NLO behaviour, i.e. the bulkier the substituent, the greater number of delocalized electrons with lesser tendency to aggregation and hence larger NLO coefficients. Hence, the triphenylamine imidazole substituted ZnPc, PBIPC in Chapter 4 was found to possess superior NLO properties than carbazole substituted ZnPcs in *Chapter 3*. The laser properties (i.e. input intensity, pulse duration, repetition rate and wavelength) are equally crucial in NLO measurements and needs to be evaluated carefully. Femtosecond pulses (~10<sup>-15</sup> s) are ideal for understanding the NLO phenomenon related to singlet excited state transitions. The NLO data obtained from higher repetition rate femtosecond pulses (80 MHz or above) contains not only electronic contributions but also thermal contributions that can increase the NLO coefficient values by at least 1-2 degrees of magnitude. This can be clearly visible from our studies with 80 MHz, 150 fs and 1 kHz, 50 fs laser pulses on the phthalocyanine derivatives in Chapters 3 and 4 to compare the coefficients. Since, 1 kHz data had purely electronic transitional contributions, we carried out the later NLO studies (using z-scan technique) with 50 fs, 1 kHz laser pulses over multiple excitation wavelengths. All data agreed that triphenylamine imidazole substituted ZnPc (Chapter 4) had best NLO coefficients over their carbazole (Chapter 3) and phenanthroimidazole (Chapter 5) counterparts due to bulkier nature and increased number of delocalized electrons. Also, Chapter 5 demonstrated that incorporation of central metal ion in Pc moiety can drastically affect the NLO properties of the molecule. When compared to the Pc free-base – ImHPc, incorporation of a central metal ion (like Cu/Zn) quenches the excited state of Pc molecule because of their d-orbitals which are highly reactive resulting in decrease of the NLO properties (measured as NLO coefficients). With Cu ([Ar]3d<sup>10</sup>4s<sup>1</sup>) having partially filled and Zn ([Ar]3d<sup>10</sup>4s<sup>2</sup>) having filled d-orbitals, ImZnPc showed superior NLO properties to ImCuPc [9].

**ii. Solvent effects:** Free-base porphyrins and phthalocyanine molecules tend to show limited solubility in various common polar and non-polar solvents [10, 11]. The incorporation of central metal has been found to increase the solubility of these molecules in common organic solvents such as DCM, THF, DMF, toluene, etc. due to solvation phenomenon [12]. This has led to increased search of suitable metallo-Por and metallo-Pc with various peripheral substituents that promote desired solubility in various solvents including aqueous [13]. Bulky groups prevent molecular aggregation that can negatively affect the photophysical properties

of the molecule. Especially, photosensitizers in DSSCs and PDT applications can often reduce their excited state quantum yield as a result of molecular aggregation in solution form. Again, it was observed from the chapters that an increase in solvent polarity can lead to increase in possibility of molecular aggregation which can reduction in quantum yield of emission ( $\varphi_f$ ). This, including solvation factor, results in different radiative lifetimes in a particular chromophore (Por/Pc) under different solvent conditions as is evident in *Chapters 3 -5*. Another interesting revelation to the effect of substituents on Por and Pc moieties is the addition of all the substituents used in the experiments to have broadened the Soret or B-band of the metallo-phthalocyanine moiety.

iii. **Donor-Acceptor interactions:** The Pc molecule has the ability to lose 1-2 electrons in its oxidative state while gain 1-4 electrons in its reductive state. This makes them excellent candidates for redox properties. Incorporation of appropriate metal ion at the center (transition to heavy metal) of the Pc moiety while attaching electron withdrawing or accepting groups at the periphery, can lead to interesting Donor-Acceptor (D-A) interactions within the molecule. Often the ease of electron movement between the metal and the ligand can be made possible by building a  $\pi$ -conjugated bridge (e.g. ethylene bridge in PBIPC in Chapter 4). This ensures efficient transfer of free electrons between the donor moiety to the acceptor (D- $\pi$ -A). Depending upon the redox properties within the molecule, one can observe photophysical properties such as Intramolecular Charge Transfer (ICT) or Intramolecular Energy Transfer (via FRET like in *Chapter 5*). In *chapter 6*, the porphyrins were electron rich molecules acting as donor molecules to electron deficit TNT (nitroaromatics), HMX and RDX (nitramines). While the fluorophores showed charge transfer (CT) mechanism with TNT, energy transfer (ET) was the dominant phenomenon with HMX and RDX. Throughout this thesis, we have tried to understand that D- $\pi$ -A systems are one of the most prominent forms of photophysical interactions in metalloporphyrins and metallophthalocyanines, the mechanism of which (CT or ET) depends on the electronic structure of both the donor and the acceptor redox properties.

#### iv. Effect of Central Metal Ion:

Although throughout the thesis, we have used Zinc as the central metal to a porphyrin (Chapter 2) as well as phthalocyanines (Chapters 3,4), studies have shown that the central ion

in a Por or Pc molecule has a significant effect on the photophysical and photochemical properties of the Por/Pc derivative. In *Chapter 5*, we studied the effect of metal ion on the NLO and photophysical properties of the phenanthroimidazole substituted Pc-moiety (ImCuPc and ImZnPc). Interestingly, the results revealed that the change in central metal ion from Zn to Cu improved the triplet yield in a photosensitizer. The possible explanation was the presence of open 3d shells in Cu over closed shell in Zn. This enabled ImCuPc to have stronger D- $\pi$ -A interaction over ImZnPc leading to better triplet state quantum yields. Similar observations have been reported in many works [14, 15] with recent advances on heavy metal ion as central metal for increased triplet state quantum yield. The reason being the increased spin orbit coupling in the molecule which in turn increases the intersystem crossing ISC efficiency within the molecule. Thus, this thesis also discusses that the central metal ion is imperative to potential optoelectronic and PDT applications in organic chromophores.

## **7.2** Future Scope in the experiments:

The transient absorption spectroscopy (TAS) or pump-probe spectroscopy was first proposed as the method of flash photolysis (femtochemistry) by Prof. Ahmed Zewail (Nobel laureate 1999) and have since been modified and improved on many levels till we reached attosecond pulse regime [16, 17]. While a lot of variations are possible to the TAS technique, the broader the spectral range of transient spectra, the better is the information we can deduct from the data regarding a photophysical phenomenon. Further, signal to noise ratio (SNR) is essential for a good clean interpretable data. Keeping in mind the above two reasons, the future scope of the non-degenerate fs-TAS used in this thesis, can be modified in the future as follows:

## 7.2.1. fs-TAS UV-mid IR wavelength range:

The current fs-TAS setup HELIOS (by M/s Ultrafast Systems) is a commercially built TAS setup with a delay of ~5 ns and probe spectrum in the visible range of ~420 nm to 820 nm. The white light continuum is achieved with the help of a Sapphire crystal. Organic chromophores (like porphyrins and phthalocyanines) whose absorption lies within the visible spectrum of an EM wave can be studied with easy and accuracy in the current experimental setup. However, molecules like energetic materials, water or biological molecules have their absorption in the UV and NIR regions

respectively. In order to achieve this broader spectrum, a CaF<sub>2</sub> crystal (UV-VIS-midinfrared) can be replaced with Sapphire crystal while another fiber-coupled multichannel InGaAs detector can be placed for IR detection. A rough schematic is shown in figure 7.1.

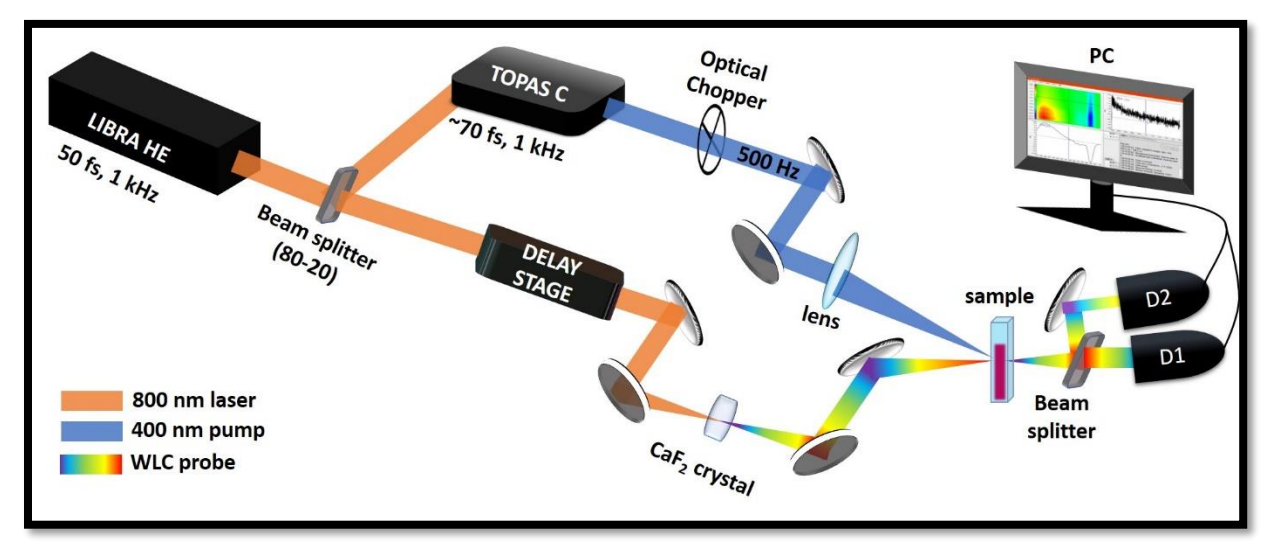


**Figure 7.1** Schematic suggesting a broadband non-degenerate fs-TAS setup in the wavelength range of UV to mid-IR.

#### **Fs-TAS Studies of Energetic Materials**

When it comes to study of energetic materials, the major purpose is to develop novel energetic materials with higher energy released at short time scales which is cost effective, enhanced stability, long shelf-life in addition to environmentally safe by-products the same time. The detonation mechanisms in these explosives need to be extensively studies with the dynamics of their decomposition which plays a crucial role in designing superior materials. Many commonly available energetic materials have their absorption in the Soret band (UV region) [18]. The excited state dynamics shapes the capability of explosive potential in the concerned molecule which is studied using TAS technique. Till date, reports have shown that excited state lifetime in energetic molecules range from few femtoseconds to picoseconds. Yi et al. [19] used femto-second transient absorption to study the relaxation dynamics behavior of 2, 2', 4, 4', 6, 6' hexanitrostilbene (HNS) after excitation at 266 nm and proposed a relaxation process of  $S_2 \rightarrow S^* \rightarrow S_1 \rightarrow T_1$ . They found a fast decay of  $S_1 \rightarrow S^*$  within 6.4 ps while the ISC decay time from the intermediate  $S^*$  state to the  $T_1$  one was estimated to be 19.6 ps. Wakeham et al. [20] demonstrate a fs-TAS technique on energetic solids to examine their irreversible decomposition which was found to be ~10 ps. Such examples clearly demonstrate the potential of fs-TAS studies with explosives using UV excitation

wavelength by exciting in the UV region. These studies are possible to be carried out using a CaF<sub>2</sub> crystal in our present HELIOS fs-TAS setup as shown in figure 7.1.

## 7.2.2. Hyperspectral fs-TAS study:

The Hyperspectral fs-TAS study is based on femtosecond laser sources as proposed by Gesuele [21]. An optical parametric amplifier is used to optically pump a sample at a tunable excitation wavelength while probes in transmission mode for a broad spectral range using a white light laser-generated supercontinuum. Transmission data collected by a pair of multichannel detectors, allowed retrieval of the absorbance change in a wide spectral range in one time. The probe artifacts created in the 2D system can be corrected by chirp calibration. In hyperspectral TAS configuration, the cross polarized pump-probe interaction between a s-polarized pump and p-polarized probe, extends the spectral measured range above and below the pump energy in the sample study. The hyperspectral fs-TAS studies were carried out with Single Layer Graphene to understand the excited state dynamics of the ultrafast charge carriers.

## 7.3 Future Scope with Phthalocyanines:

Phthalocyanines have evolved greatly over few decades and have been tailored with several complex structures thus enhancing their potential in several opto-electronic and biomedical applications [22, 23]. Due to their extensive  $\pi$ -conjugated aromatic structures, phthalocyanines can exist in polymeric, stacked, supramolecular, and other forms [24]. Here, we discuss some of the most recently discovered phthalocyanine conjugated structures that enhances their photophysical properties for efficient transition energy leading to superior photosensitizer properties.

## 7.3.1. Phthalocyanines as Supramolecular complexes.

A new area of chemistry deals with secondary interactions rather than covalent bonds in molecules focuses on the chemical systems made up of a discrete number of assembled molecular subunits or components and is known as Supramolecular chemistry. Probable intermolecular interactions present in supramolecular systems are – hydrogen bonding, hydrophobic forces, metal coordination, Van der Waals forces, electrostatic effects and  $\pi$ - $\pi$  interactions. It was inspired from basic biological systems crucial to cell structure and vision and developed over time by the

research works on molecular self-assembly, folding molecular recognition, mechanically-interlocked, molecular architectures and dynamic covalent chemistry [25].

Phthalocyanines have a structural advantage over many other organic and inorganic molecules, enabling them to form complex conjugates with both organic and inorganic moieties. Studies have proved yet and again that conjugating Pc moieties in supramolecular structures have increased several NLO and photophysical properties in materials [26, 27, 28]. Numerous covalent and supramolecular Pc-based donor - acceptor systems have been prepared and studied in recent years by incorporation of electroactive acceptor moieties such as fullerenes, carbon nanotubes (CNTs), graphene, anthraquinone, ferrocene, flavin or porphyrin. Of all these compounds, derivatives ranging from carbon nanostructures such as fullerenes, carbon nanotubes and graphene are clearly distinguished due to their remarkable physical-chemical properties [3, 29]. C<sub>60</sub> (fullerene) exhibits excellent electron acceptor properties that may lead, when part of a D - A system, to the formation of stable species. Similar to C<sub>60</sub> fullerene, CNTs show affinity for electrons that, once accepted, can be transported along their one-dimensional (1D) tubular structure. Therefore, both C<sub>60</sub> fullerene and carbon nanotubes are widely used as acceptor compounds in solar or hybrid cells [30, 31]. Thus, this opens up scope towards new and improved Phthalocyanine derivatives in the world of Optoelectronics and can be further pursued with the novel molecules developed and studied in this thesis.

## 7.3.2. Phthalocyanines in Organic LEDs (OLEDs).

Organic light-emitting diodes OLEDs are electroluminescent device that are light weight, transparent, flexible with color tunability that emit current when apllied an external voltage. The principle behind working of OLEDs involve excitation of the light emitting layer by recombination energy of cathode and hole electrons in anode followed by light emission from the light emitting layer when it reaches the ground state (see figure 7.2). Since their invention [32] in the late 1980s, remarkable improvements can be observed in OLEDs which can be broadly classified as energy conversion devices that transforms electric power into light (unitless). One of the major criteria is the power efficiency, along with durability and emission color. Recent studies with phthalocyanines have shown that reverse intersystem crossing (RISC) is possible in Pc derivatives with heavy-metal ion at the center and is responsible for optimizing OLED materials [33, 34].

Reverse intersystem crossing (RISC) is a forbidden energy transfer mechanism but recently it was observed that purely organic materials can be enabled for RISC by minimizing the energy gap between the lowest singlet excited state (S<sub>1</sub>) and lowest triplet state (T<sub>1</sub>) in thermally activated delayed fluorescence (TADF) systems [35, 36]. The large decay rate of RISC (k<sub>RISC</sub>) of the emitter can result in great device performance leading to TADF assisted fluorescence organic light-emitting diodes (OLEDs) as well as TADF-emitter OLEDs.

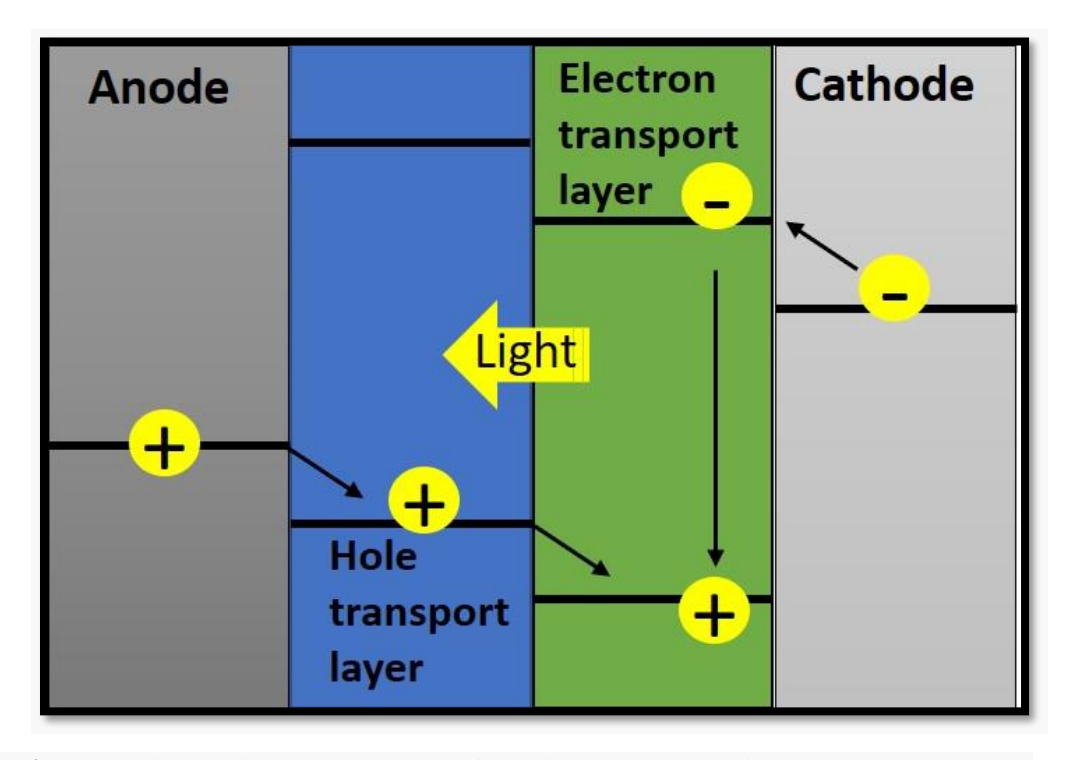


**Figure 7.2** Schematic showing the OLED working principle when subjected to electric energy.

## 7.3.3. Phthalocyanines in triplet-triplet annihilated upconversion.

A nonlinear optical process in which the energy of two photons are combined to a single high energy photon is termed as 'upconversion'. In triplet-triplet annihilation photon upconversion (TTA-UC), the upconversion occurs via triplet state energy transfer between the concerned molecules [37]. Unlike most luminescent materials that emit lower energy photons than the incident one showing a Stokes shift, an upconverted molecule undergoes an anti-Stokes process wherein the consolidated energy of multiple lower energy photons, produce a single higher energy photon. The TTA-UC differs from other upconversion approaches as it can upconvert from low-power light (unlike intense laser light only), which can include incoherent excitation sources, an

hence its appeal in practical applications [38]. In this process, a chromophore sensitizer is excited at long wavelength (low energy) light which excites the sensitizer from ground state to first singlet excited state  $(S_1)$ . The  $S_1$  state relaxes to the triplet state  $(T_1)$  of the sensitizer via intersystem crossing (ISC). This is followed by a triplet-triplet energy transfer (TTET) to an annihilator via Dexter's mechanism (see figure 7.3). The TTA-UC mechanism finds its potential application in the field of bioimaging, as well as photodynamic therapy because of its efficient use in noninvasive deep tissue penetration [39]. Phthalocyanines can be used as excellent photosensitizers for PDT or DSSCs (solar cells) using TTA UC process. Singh-Rachford et. al. [37] showed studies on upconverted yellow singlet fluorescence from rubene (5,6,11,12-tetraphenyl napthacene), generated from selective excitation at 725 nm that absorbed triplet sensitizer Pd(II) octabutoxyphthalocyanine PdPc(OBu)<sub>8</sub> in degassed toluene solutions. This study confirmed the anti-Stokes light producing sensitized TTA to be a general phenomenon as long as proper energy criteria were met. Similar studies had been carried out by Che et al. [40] with two tetrasulfonylsubstituted phthalocyanine (Pc) Pt(II) and Pd(II) complexes (Pd-Pc and Pt-Pc). They showed triplet-triplet-annihilation upconversion, with deep red excitation at 658 nm, upconversion with a quantum yield of 0.63% and an anti-Stokes shift of 3996 cm<sup>-1</sup>. Thus, TTA-UC holds immense potential in the world on Pc for applications in solar cells, bio imaging and PDT. These are only a few avenues to exploit the application of phthalocyanines or porphyrins. Pc and Por molecules can also be further be investigated for applications as QD-conjugates, micro-resonators and so on.

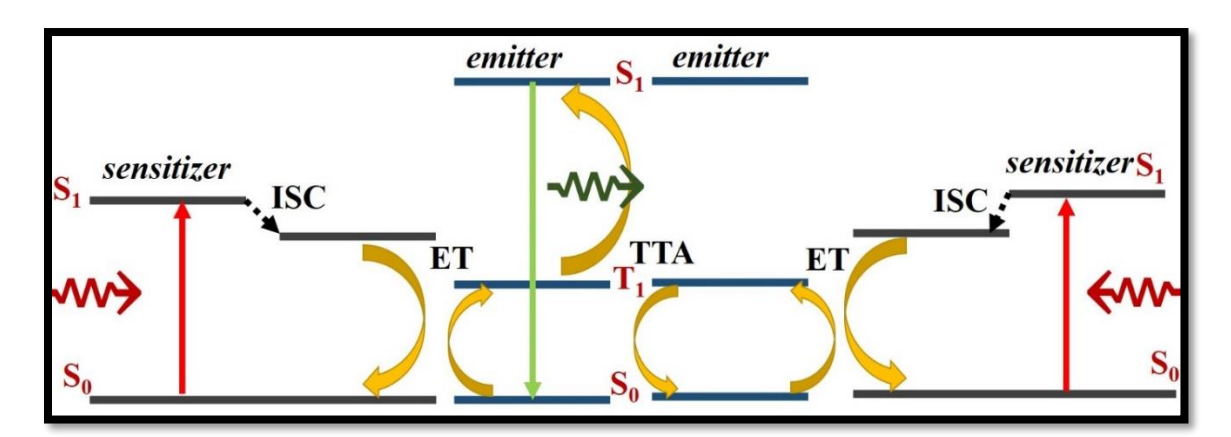


**Figure 7.3** Schematic of energy diagram showing the triplet-triplet annihilation upconversion TTA-UC process in a photosensitizer.

## 7.4 References:

- [1] R. R. Allison and C. H. Sibata, "Oncologic photodynamic therapy photosensitizers: a clinical review," *Photodiagn. Photodyn. Ther.*, vol. 7, p. 61, 2010.
- [2] B. Caplins, T. Mullenbach, R. Holmes and D. Blank, "Femtosecond to Nanosecond Excited State Dynamics of Vapor Deposited Copper Phthalocyanine Thin Films.," *Phys. Chem. Chem. Phys.*, vol. 18, p. 11454—11459., 2016.
- [3] D. Gonzalez-Rodriguez and G. Bottari, "Phthalocyanines, subphthalocyanines and porphyrins for energy and electron transfer applications," *J. Porphyrins Phth.*, vol. 13, p. 624–636, 2009.
- [4] J. Escobedo, O. Rusin, S. Lim and R. Strongin, "NIR Dyes for Bioimaging Applications," *Curr. Opin. Chem. Biol.*, vol. 14, no. 1, p. 64., 2010.
- [5] Y. Zhang and J. Lovell, "Recent applications of phthalocyanines and naphthalocyanines for imaging and therapy," Wiley Interdiscip. Rev. Nanomed. Nanobiotechnol., vol. 9, e1420, 2016. https://doi.org/10.1002/wnan.1420
- [6] J. Cao, D. Shen, Y. Feng and W. Wan, "Nonlinear Refraction by Difference Frequency Generation," *Appl. Phys. Lett.*, vol. 108, p. 191101–5, 2016.
- [7] P. Bowe, W. Gibbs and J. T-Williams, "Lifetimes of Saturable Absorbers," *Nature*, vol. 209, p. 65-66, 1996.
- [8] G. S. He and P. N. Prasad, "Three-photon absorbing materials: characterization and applications," in *Proc. SPIE*, *5211*, *1*–*12*, San Diego, California, 2003.
- [9] D. Mwanza, M. Louzada, J. Britton, E. Sekhosana, S. Khene, T. Nyokong and P. Mashazi, "The effect of the cobalt and manganese central metal ions on the nonlinear optical properties of tetra(4-propargyloxyphenoxy)phthalocyanines.," *New J. Chem.*, vol. 42, pp. 9857-9864, 2018.
- [10] K. Toyota, J.-Y. Hasegawa and H. Nakatsuji, "Excited States of Free Base Phthalocyanine Studied by the SAC-CI Method," *J. Phys. Chem. A*, vol. 101, no. 4, p. 446–45, 1997.

- [11] F. Yüksel, A. Gürek, C. Lebrunb and V. Ahsen, "Synthesis and solvent effects on the spectroscopic properties of octatosylamido phthalocyanines," *New J. Chem.*, vol. 29, pp. 726-732, 2005.
- [12] R.-M. Ion, "Porphyrins and Phthalocyanines: Photosensitizers and Photocatalysts," in *Phthalocyanines and Some Current Applications*, Online, IntechOpen, 2017, pp. 189-221.
- [13] H. Abramczyk, B. Brozek-Płuska, K. Kurczewski, M. Kurczewska, I. Szymczyk, T. K. Błaszczyk, H. Scholl and W. Czajkowski, "Femtosecond Transient Absorption, Raman, and Electrochemistry Studies of Tetrasulfonated Copper Phthalocyanine in Water Solution," *J. Phys. Chem. A.*, vol. 110, pp. 8627-36, 2006.
- [14] A. Tuhl, S. Makhseed, P. Zimcik, N. Al-Awadi, V. Novakova and J. Samuel, "Heavy metal effects on physicochemical properties of non-aggregated azaphthalocyanine derivatives," *Journal of Porphyrins and Phthalocyanines*, vol. 16, pp. 817-825, 2012.
- [15] C. Çoban and E. Demirbas, "Determination of Heavy Metal Ions in Aqueous Solutions by Phthalocyanine Coated Quartz Crystal Microbalance," *Sensor Letters*, vol. 4, no. 3, pp. 312-318, 2006.
- [16] M. Lara-Astiaso, M. Galli, A. Trabattoni, A. Palacios, D. Ayuso, F. Frassetto, L. Poletto, S. D. Camillis, J. Greenwood, P. Decleva, I. Tavernelli, F. Calegari, M. Nisoli and F. Martín, "Attosecond Pump–Probe Spectroscopy of Charge Dynamics in Tryptophan," *J. Phys. Chem. Lett.*, vol. 9, no. 16, p. 4570–4577, 2018.
- [17] P. A. Carpeggiani, P. Tzallas, A. Palacios, D. Gray, F. Martín and D. Charalambidis, "Tracing molecular dynamics at the femto-/atto-second boundary through extremeultraviolet pump-probe spectroscopy," Cornell University, New York, 2013. https://arxiv.org/abs/1304.6914
- [18] K. Smit, "Ultraviolet and visible absorption spectroscopy of some energetic molecules in the solid state," *J. Energ. Mater.*, vol. 9, pp. 81-103, 2006.
- [19] J. Yi, Y. Xiong, K. Cheng, M. Li, G. Chu, X. Pu and T. Xub, "A Combination of Chemometrics and Quantum Mechanics Methods Applied to Analysis of Femtosecond Transient Absorption Spectrum of Ortho-Nitroaniline," *Sci. Rep.*, vol. 6, p. 19364, 2016.

- [20] G. Wakeham, D. Chung and K. Nelson, "Femtosecond time-resolved spectroscopy of energetic materials," *Thermochimica Acta*, vol. 384, pp. 7-21, 2002.
- [21] F. Gesuele, "Ultrafast Hyperspectral Transient Absorption Spectroscopy: Application to Single Layer Graphene," *Photonics*, vol. 6, no. 3, p. 95, 2019. https://www.mdpi.com/2304-6732/6/3/95
- [22] M. Fournier, C. Pépin, D. Houde, R. Ouellet and J. v. Lier, "Ultrafast studies of the excited-state dynamics of copper and nickel phthalocyanine tetrasulfonates: potential sensitizers for the two-photon photodynamic therapy of tumors," *Photochem Photobiol Sci.*, vol. 3, pp. 120-126, 2004.
- [23] Z. Zheng, H. Liu, S. Zhai, H. Zhang, G. Shan, R. T. K. Kwok, C. Ma, H. H. Y. Sung, I. D. Williams and e. al., "Highly efficient singlet oxygen generation, two-photon photodynamic therapy and melanoma ablation by rationally designed mitochondria-specific near-infrared AIEgens," *Chem. Sci.*, vol. 11, pp. 2494-2503, 2020.
- [24] Y. Wang, K. Wu, J. Kröger and R. Berndt, "Review Article: Structures of phthalocyanine molecules on surfaces studied by STM," *AIP Advances*, Vols. 2,, p. 041402, 2012.
- [25] B. Daas, "Supramolecular Chemistry and its Applications," PIJMS, p. 68, 2014.
- [26] B. Anand, M. Molli, S. Aditha, T. M. Ratan, S. S. Sai and S. V. Kamisetti, "Excited state assisted three-photon absorption based optical limiting in nanocrystalline Cu<sub>2</sub>Se and FeSe<sub>2</sub>," *Opt. Commun.*, vol. 304, pp. 75-79, 2013.
- [27] S. Bhattacharya, C. Biswas, S. S. K. Raavi, J. V. S. Krishna, D. Koteshwar, L. Giribabu and S. V. Rao, "Optoelectronic, Nonlinear Optical Properties and Excited State Dynamics of a Triphenyl Imidazole Induced Phthalocyanine Derivative," *RSC Adv.*, vol. 9, pp. 36726-36741, 2019.
- [28] K. N. Krishnakanth, S. Seth, A. Samanta and S. V. Rao, "Broadband ultrafast nonlinear optical studies revealing exciting multi-photon absorption coefficients in phase pure zero-dimensional Cs<sub>4</sub>PbBr<sub>6</sub> perovskite films," *Nanoscale*, vol. 11, pp. 945-954, 2019.
- [29] F. D'Souza and O. Ito, "Supramolecular donor-acceptor hybrids of porphyrins/phthalocyanines with fullerenes/carbon nanotubes: Electron transfer, sensing, switching, and catalytic applications," *Chem. Commun.*, p. 4913–4928, 2009.

- [30] S. Fukuzumi and D. M. Guldi, *Electron Transfer in Chemistry*, New York: ed. Wiley-VCH, 2001.
- [31] H. Imahori, T. Umeyama, K. Kurotobi and Y. Takano, "Self-assembling porphyrins and phthalocyanines for photoinduced charge separation and charge transport," *Chem. Commun.*, vol. 48, p. 4032–4045, 2012.
- [32] C. Tang and S. VanSlyke, "Organic electroluminescent diodes.," *Appl. Phys. Lett.*, vol. 51, p. 913–915, 1987.
- [33] T. Mori, T. Mitsuoka, M. Ishii, H. Fujikawa and Y. Taga, "Improving the thermal stability of organic light-emitting diodes by using a modified phthalocyanine layer," *Appl. Phys. Lett.*, vol. 80, p. 3895, 2002.
- [34] A. Pearson, T. Plint, S. Jones, B. Lessard, D. Credgington, T. Bender and N. Greenham, "Silicon phthalocyanines as dopant red emitters for efficient solution processed OLEDs," *J. Mater. Chem. C*, vol. 5, p. 12688-12698, 2017.
- [35] O. Melville, B. Lessard and T. Bender, "Phthalocyanine-Based Organic Thin-Film Transistors: A Review of Recent Advances," *ACS Appl. Mater. Interfaces*, vol. 7, p. 13105–13118, 2015.
- [36] T. El-Agez, M.S.A.-Qrinawi, M.S.A.-Latif and S. Taya, "The Influence of Thin Layer Copper Phthalocyanine on the Performance of PVK/ Rhodamine B Device," *IUG Journal of Natural and Engineering Studies*, vol. 24, no. 1, pp. 54-59, 2016.
- [37] T. Singh-Rachford and F. Castellano, "Photon upconversion based on sensitized triplet—triplet annihilation," *Coord. Chem. Rev.*, vol. 254, p. 2560, 2010.
- [38] J. Zhou, Q. Liu, W. Feng, Y. Sun and F. Li, "Upconversion luminescent materials: advances and applications," *Chem. Rev.*, vol. 115, p. 395, 2015.
- [39] S. Bonnet, "Shifting the light activation of metallodrugs to the red and near-infrared region in anticancer phototherapy," *Comments Inorg. Chem.*, vol. 35, p. 179, 2015.

Excited State Dynamics and Femtosecond Nonlinear Optical Studies of Novel Porphyrins, Phthalocyanines using Transient Absorption Spectroscopy and Zscan Techniques

by Somdatta Bhattacharya

Submission date: 03-Nov-2020 10:37AM (UTC+0530)

**Submission ID: 1434707608** 

File name: Thesis\_Somdatta\_Final\_02Nov2020\_ver\_LIBRARY.pdf (911.28K)

Word count: 34557

Character count: 183017

Flerigopal Rao 04/11/2020

Dr. S. VENUGOPAL RAO
Professor
Advance Centre of Research in
High Energy Materials (ACRHEM)
UNIVERSITY OF HYDERABAD
Hyderabad-500 046. T.S. INDIA.



somdatta bhattacharya <somdatta@uohyd.ac.in>

## Request to provide Anti-plagiarism report for Final Thesis Submission.

Antiplagiarism IGML <antiplagiarism@uohyd.ac.in>

Tue, Nov 3, 2020 at 10:45 AM

To: Venugopal Rao Soma <somavenu@gmail.com>

Cc: somdatta bhattacharya <somdatta@uohyd.ac.in>, Venugopal Rao Soma <soma\_venu@uohyd.ac.in>

Report attached.

With best regards

Librarian, IT Services Indira Gandhi Memorial Library, University of Hyderabad

E-mail: antiplagiarism@uohyd.ac.in

Phone: 91-40-23132616

[Quoted text hidden]

Excited State Dynamics and Femtosecond Nonlinear Optical Studies of Novel Porphyrins, Phthalocyanines 🔁 using Transient Absorption Spectroscopy and Z-scan Techniques.pdf 18696K

Dr. S. VENUGOPAL RAO

Professor
Professor
Advance Centre of Research in
High Energy Materials (ACRHEM)
UNIVERSITY OF HYDERABAD
Hyderabad-500 046. T.S. INDIA.
Hyderabad-500 046.

Excited State Dynamics and Femtosecond Nonlinear Optical Studies of Novel Porphyrins, Phthalocyanines using Transient

ORIGINALITY REPORT	ctroscopy and Z-		
20% SIMILARITY INDEX	9% INTERNET SOURCES	17% PUBLICATIONS	3% STUDENT PAPERS
PRIMARY SOURCES			
photophysi nonlinear o	Bhattacharya, Caddam Hossain cal and femtosoptical propertiemetal phthalog	et al. "Compecond third-o s of novel im	parative rder idazole
2 pubs.rsc.or Internet Source	g		2%
acrhem.org			2%
Santosh Ku Suman Kris Electrochen and Ultrafas Carbazole-I The Journal	hattacharya, C mar Raavi, Jon hna et al. "Synt hical, DFT Stud at Excited State nduced Phthalo of Physical Char of Physical Char harm shuders own	nadula Venka hesis, Optica ies, NLO Pro Dynamics of ocyanine Deri emistry C, 20	ata % perties, vatives"

5	Somdatta Bhattacharya, Govind Reddy, Sneha Paul, Sk Saddam Hossain et al. "Comparative Photophysical and Femtosecond Third-Order Nonlinear Optical Properties of Novel Imidazole Substituted Metal Phthalocyanines", Dyes and Pigments, 2020  Publication	1%
6	Submitted to Savitribai Phule Pune University  Student Paper	<1%
7	Submitted to University of Hyderabad, Hyderabad Student Paper	<1%
8	Danilo Dini, Mário J. F. Calvete, Michael Hanack. "Nonlinear Optical Materials for the Smart Filtering of Optical Radiation", Chemical Reviews, 2016  Publication	<1%
9	Submitted to Manipal University  Student Paper	<1%
10	hdl.handle.net Internet Source	<1%
	Somdatta Bhattacharya, Chinmoy Biswas, Sai Santosh Kumar Raavi, Jonnadula Venkata Suman Krishna et al. "Optoelectronic, femtosecond nonlinear optical properties and excited state dynamics of a triphenyl imidazole blications I-S & LL are Miderly own papers.  as first author  The Similarity after encluding these papers is advance Centre of Religible Energy Materials UNIVERSITY OF HYDERSTAND OF	AL RAO

## induced phthalocyanine derivative", RSC Advances, 2019

Publication

***************************************		
12	Anup Rana, Sipra Sucharita Sahoo, Pradeepta K. Panda. "β-Octaalkoxyporphyrins: Versatile fluorometric sensors towards nitrated explosives", Journal of Porphyrins and Phthalocyanines, 2019	<1%
13	F. Bolze, S. Jenni, A. Sour, V. Heitz. "Molecular photosensitisers for two-photon photodynamic therapy", Chemical Communications, 2017  Publication	<1%
14	Submitted to IIT Delhi Student Paper	<1%
15	P. Jayaprakash, M. Lydia Caroline, S. Sudha, R. Ravisankar, G. Vinitha, P. Ramesh, E. Raju. "Synthesis, growth, optical and third order nonlinear optical properties of I-Phenylalanine d-Mandelic acid single crystal for photonic device applications", Journal of Materials Science: Materials in Electronics, 2020	<1%

opus.bibliothek.uni-wuerzburg.de 16 Internet Source

<1<sub>%</sub>

www.intechopen.com 17 Internet Source

Publication

Heruppal Ras

Heruppalas 04/4/200

Dr. S. VENUGOPAL RAO Professor
Advance Centre of Research in
High Energy Materials (ACRHEM)
UNIVERSITY OF HYDERABAD
Hyderabad-500 046. T.S. INDIA. ELSEVIER

Contents lists available at ScienceDirect

### Dyes and Pigments

journal homepage: http://www.elsevier.com/locate/dyepig





## Comparative photophysical and femtosecond third-order nonlinear optical properties of novel imidazole substituted metal phthalocyanines

Somdatta Bhattacharya <sup>a</sup>, Govind Reddy <sup>b</sup>, Sneha Paul <sup>c</sup>, Sk Saddam Hossain <sup>c</sup>, Sai Santosh Kumar Raavi <sup>d</sup>, Lingamallu Giribabu <sup>b,e,\*\*</sup>, Anunay Samanta <sup>c</sup>, Venugopal Rao Soma <sup>a,\*</sup>

- <sup>a</sup> Advanced Centre of Research in High Energy Materials (ACRHEM), University of Hyderabad, South Campus, Hyderabad, 500046, Telangana, India
- <sup>b</sup> Polymers & Functional Materials Division, CSIR-Indian Institute of Chemical Technology, Tarnaka, Hyderabad, 500007, Telangana, India
- <sup>c</sup> School of Chemistry, University of Hyderabad, Hyderabad, 500046, Telangana, India
- d Ultrafast Photophysics and Photonics Laboratory, Department of Physics, Indian Institute of Technology Hyderabad, Kandi, 502285, Hyderabad, Telangana, India
- e Academy of Scientific and Innovative Research (AcSIR), Ghaziabad, 201002, India

#### ARTICLE INFO

Keywords:
Phthalocyanine
Imidazole
Photosensitizer
Femtosecond
Two-photon absorption

#### ABSTRACT

Two novel phenanthro [9,10-d]imidazole substituted metal phthalocyanines, ImCuPc and ImZnPc, have been synthesized and their potential as photosensitizers has been investigated through optical, electrochemical, and ultrafast nonlinear optical (NLO) studies, including their excited state dynamics. The absorption as well as emission spectra of both the title compounds exhibited negligible Stokes shift in different solvents. The molecules depicted a broad Soret band due to the incorporation of phenanthro[9,10-d]imidazole moiety while the Q-bands were characteristic to their metal phthalocyanine group. DFT studies elucidated the HOMO-LUMO (4.99-2.90 eV) levels of these molecules with their energy optimized structures generated using DFT, TD-DFT analysis. The fs-TAS spectra of both the molecules exhibited contribution from singlet-singlet excited state absorption followed by transition to triplet states via intersystem crossing, ISC. The lifetimes calculated from obtained kinetics at specific wavelengths using global fitting demonstrated slow singlet to triplet state intersystem crossing in ImCuPc (decay rate of  $1.6 \times 10^8 \, \mathrm{s}^{-1}$ ) and ImZnPc (decay rate of  $1.4 \times 10^8 \, \mathrm{s}^{-1}$ ). The ns-TAS studies established long lived triplet states in both the molecules with ImCuPc depicting a slightly higher triplet lifetime of  $\sim 1.4~\mu s$  over ImZnPc with a triplet lifetime of  $\sim$ 1.2  $\mu$ s The triplet quantum yields ( $\phi_T$ ) were calculated to be 0.51 for ImCuPc while it was 0.27 for ImZnPc suggesting ImCuPc to be a better photosensitizer (PS) over ImZnPc. We believe the intramolecular D- $\pi$ -A interaction is stronger in ImCuPc resulting in higher triplet yield. Third-order NLO studies performed at a non-resonant excitation of 800 nm (~50 fs, 1 kHz pulses) demonstrated ImZnPc had a larger twophoton absorption cross-section (994 GM), possibly due to heavy atom effect, while ImCuPc was found to possess superior  $n_2$  (3.7 × 10<sup>-15</sup> cm<sup>2</sup>/W). The slightly superior nonlinear optical (NLO) performance of ImCuPc over ImZnPc could also possibly be due to lower energy gap and Copper's open 3d shells as opposed to full 3d shell in Zinc which overlaps with Pc 2p shells making it more active.

#### 1. Introduction

Phthalocyanines (Pc's) are  $18-\pi$  electron tetrapyrrolic planar cyclic organic molecules that have various biological and optoelectronic applications based on their optical, electrochemical, and thermal properties [1–5]. The field of nonlinear optics (NLO) has been emerging over the last two decades because of its relevance and applications in optical limiting, optoelectronics and photonics. Further, NLO materials possess the ability to be tailored for recently evolving applications such as

optical telecommunications and optical signal processing. Phthalocyanines, with their extended two-dimensional 18  $\pi$ -electron system, are among the versatile and strongest organic NLO materials extensively investigated in recent times. The optical and electrochemical properties of Pc macrocycle can be tuned either by substitution at its peripheral positions or changing the metal ion in its central cavity. It has been also observed that asymmetry in a phthalocyanine can induce a strong dipole moment leading to large nonlinearity [6,7]. The central metal ion in metallophthalocyanines affects the optical nonlinearity based on the

<sup>\*</sup> Corresponding author.

<sup>\*\*</sup> Corresponding author. Polymers & Functional Materials Division, CSIR-Indian Institute of Chemical Technology, Tarnaka, Hyderabad, 500007, Telangana, India. E-mail addresses: giribabu@iict.res.in (L. Giribabu), anunay@uohyd.ac.in (A. Samanta), soma\_venu@uohyd.ac.in (V.R. Soma).

## **RSC Advances**



#### **PAPER**



Cite this: RSC Adv., 2019, 9, 36726

# Optoelectronic, femtosecond nonlinear optical properties and excited state dynamics of a triphenyl imidazole induced phthalocyanine derivative†

Somdatta Bhattacharya, <sup>a</sup> Chinmoy Biswas, <sup>b</sup> Sai Santosh Kumar Raavi, <sup>b</sup> Jonnadula Venkata Suman Krishna, <sup>c</sup> Devulapally Koteshwar, <sup>c</sup> Lingamallu Giribabu <sup>b</sup>\*cd and Soma Venugopal Rao <sup>b</sup>\*a

A novel zinc phthalocyanine derivative [2(3), 9(10), 16(17), 23(24) tetrakis-4-((4-(1,4,5-triphenyl-1Himidazol-2-yl)phenyl)ethynyl)phthalocyanine zinc(II) (PBIPC)] was synthesized by incorporating a triphenyl imidazole moiety at its peripheral positions. The detailed mechanisms of absorption, emission, electrochemical, nonlinear optical (NLO) and photophysical (excited state dynamics) properties of PBIPC were explored. The absorption and emission properties of the compound were studied in different solvents. The incorporation of a triphenyl imidazole moiety at the peripheral position of the zinc phthalocyanine slightly broadened the Soret band. The emission studies revealed fluorescence quantum yields to be in the range of 0.11-0.22. The time-resolved fluorescence data established the radiative lifetimes to be in the nanosecond range. The oxidation and reduction processes were found to be ring centered, which were studied using the cyclic voltammetry (CV) technique. The energy optimized structures and HOMO-LUMO levels were calculated using DFT, TD-DFT analysis and were employed by means of hybrid functional theory (B3LYP) at 6-31G (d,p) basis set in the Gaussian 09 package. Twophoton absorption was observed in the NLO studies performed in the visible wavelength range of 600-800 nm while the nonlinear absorption was dominated by three- and four-photon absorption processes in the NIR wavelength range (1.0-1.5 µm). The molecule exhibited self-focusing behavior for all the wavelengths. Finally, the excited state dynamics of the title molecule PBIPC were investigated using femtosecond transient absorption spectroscopy and the results obtained were understood on the basis of a simple three kinetic model, for excitation wavelengths of 400 nm (Soret band) and 650 nm (Qband). Both the spectra demonstrated a broad positive transient absorption (TA) data which overlapped with the ground state bleach (GSB), which in turn displayed a red shift over a delay of  $\sim$ 2 ns. The lifetimes revealed a possibility of intersystem crossing ( $\tau > 1$  ns) owing to the triplet state transition.

Received 24th September 2019 Accepted 5th November 2019

DOI: 10.1039/c9ra07758h

rsc.li/rsc-advances

#### Introduction

The design and synthesis of organic materials (solutions, thin films) with strong nonlinear optical (NLO) coefficients has received considerable attention from various chemists and material scientists over the last couple of decades leading to the

evolution of photonics, optoelectronic technologies and biomedicine.<sup>1-6</sup> Many of the optical devices developed for such applications have been realized with  $\pi$ -conjugated organic materials such as phthalocyanines, metallophthalocyanines and porphyrins.<sup>7,8</sup> The NLO properties have been widely investigated in the case of phthalocyanines and metallophthalocyanines. The extended de-localized  $\pi$ -electron conjugation is a structural prerequisite for the observation of strong third-order NLO phenomena in organic molecules. Phthalocyanines have been found to possess fabulous thermal, chemical and optical stability and the ability to hold non-metallic and metallic ions in its cavity through several synthetic procedures leading to a tremendous interest in the NLO properties of new molecules designed and/or synthesized.9-13 To realize NLO devices for optical signal processing and telecommunications a number of new materials have been developed and investigated. 14,15 Additionally, phthalocyanines demonstrate an optical limiting (OL) mechanism realized through reverse saturable absorption (RSA) and/or two-photon

<sup>&</sup>lt;sup>a</sup>Advanced Center for Research in High Energy Materials (ACRHEM), University of Hyderabad, South Campus, Hyderabad 500046, Telangana, India. E-mail: soma\_venu@uohyd.ac.in

<sup>&</sup>lt;sup>b</sup>Department of Physics, Ultrafast Photophysics and Photonics Laboratory, Indian Institute of Technology Hyderabad, Kandi 502285, Hyderabad, Telangana, India

Polymers & Functional Materials Division, CSIR-Indian Institute of Chemical Technology, Tarnaka, Hyderabad 500007, Telangana, India. E-mail: giribabu\_l@ vahoo.com

<sup>&</sup>lt;sup>d</sup>Academy of Scientific and Innovative Research (AcSIR), Anusandhan Bhawan, 2 Rafi Marg, New Delhi, 110001, India

<sup>†</sup> Electronic supplementary information (ESI) available. See DOI: 10.1039/c9ra07758h

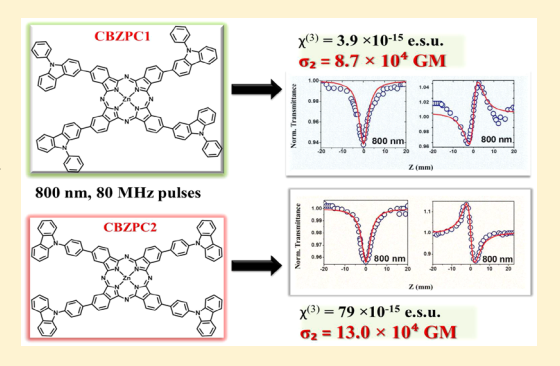


## Synthesis, Optical, Electrochemical, DFT Studies, NLO Properties, and Ultrafast Excited State Dynamics of Carbazole-Induced **Phthalocyanine Derivatives**

Somdatta Bhattacharya, † Chinmoy Biswas, ‡ Sai Santosh Kumar Raavi, ‡ Jonnadula Venkata Suman Krishna, Silo Narra Vamsi Krishna, Lingamallu Giribabu, Silo Narra Vamsi Krishna, Lingamallu Giribabu, and Venugopal Rao Soma\*,†

Supporting Information

ABSTRACT: In this paper, we present results from the detailed investigations on the synthesis, optical, emission, electrochemical, and ultrafast nonlinear optical (NLO) properties along with the excited state dynamics of zinc(II) 2,10,16,24-tetrakis(9-phenyl-9H-carbazol-2-yl)phthalocyanine (CBZPC1) and zinc(II) 2,10,16,24-tetrakis(4-(9Hcarbazol-9-yl)phenyl)phthalocyanine (CBZPC2). Due to the presence of carbazole moieties, the Soret band was found to be broadened. The emission studies performed using different solvents revealed the fluorescence yields in the range of 0.10-0.27 and the time-resolved fluorescence data revealed radiative lifetimes of, typically, a few nanoseconds. Femtosecond transient absorption measurements indicated the formation of triplet states within the first nanosecond of photo-



excitation. From the cyclic voltametric studies, the oxidation and reduction processes were found to be ring centered. Spectral changes in the UV-visible absorption were recorded by means of spectro-electrochemical analysis at an applied potential. The DFT and TD-DFT analysis was employed using B3LYP hybrid functional theory and 6-31G(d,p) basis set in the Gaussian 09 package. The NLO properties of CBZPC1 and CBZPC2 were investigated using the Z-scan technique and femtosecond (fs) pulses with kHz and MHz repetition rates. Closed and open aperture Z-scan data were recorded at three different wavelengths of 600, 700, and 800 nm, and the NLO coefficients were extracted from both types of data. Two-photon absorption (TPA) was the dominant mechanism observed in the open aperture Z-scan data. The real and imaginary parts of the  $\chi^{(3)}$  along with the two-photon absorption cross sections were evaluated. Our NLO data and large 2PA coefficients and cross sections obtained indicate the potential of these compounds for applications in optical limiting and optical switching applications.

#### 1. INTRODUCTION

Nonlinear optics (NLO) is considered to be the most promising technology toward the evolution of several fields such as photonics, optoelectronics, and biomedicine. 1-5 To date, several NLO moieties were developed to study their potential in applications of optical signal processing and telecommunications.<sup>6,7</sup> Organic compounds such as dyes have been found to be particularly good potential NLO candidates.<sup>8-10</sup> The strong NLO properties originate from the  $\pi$ -delocalized networks, resulting in a major intensification in the triplet excited state lifetimes. The research in this direction has led to progress in the study of novel  $\pi$ -conjugated materials. 11 Incidentally, the tetrapyrrolic pigments like phthalocyanines and its metallic derivatives have shown a

huge influence on the NLO properties, due to their ability of holding more than 70 (70) nonmetallic and metallic ions in the cavity, which yields incredible thermal, chemical, and optical stability. In addition, phthalocyanines possess ultrafast and large third-order nonlinearity, which can further be developed from their derivatives through rational synthetic procedures. 12-15 The metallic phthalocyanines (MPcs) can also exhibit interesting chemical and optical properties. The optical constants of MPc thin films provide information concerning microscopic characteristics of the material. It has also been

Received: February 18, 2019 Revised: April 9, 2019 Published: April 9, 2019

<sup>&</sup>lt;sup>†</sup>Advanced Centre of Research in High Energy Materials (ACRHEM), University of Hyderabad, Hyderabad 500046, Telangana, India

<sup>\*</sup>Ultrafast Photophysics and Photonics Laboratory, Department of Physics, Indian Institute of Technology Hyderabad, Kandi 502285, Telangana, India

<sup>§</sup>Polymers & Functional Materials Division, CSIR-Indian Institute of Chemical Technology, Tarnaka, Hyderabad-500007, India Academy of Scientific and Innovative Research (AcSIR), Anusandhan Bhawan, 2 Rafi Marg, New Delhi, 110001, India

Contents lists available at ScienceDirect

## Optics and Laser Technology

journal homepage: www.elsevier.com/locate/optlastec



Full length article

## Femtosecond, broadband nonlinear optical studies of a zinc porphyrin and zinc phthalocyanine



M.S.S. Bharati <sup>a</sup>, S. Bhattacharya <sup>a</sup>, J.V. Suman Krishna <sup>b</sup>, L. Giribabu <sup>b</sup>, S. Venugopal Rao <sup>a,\*</sup>

<sup>a</sup> Advanced Centre of Research in High Energy Materials (ACRHEM), University of Hyderabad, Hyderabad 500046, Telangana, India

#### ARTICLE INFO

Article history: Received 11 April 2018 Received in revised form 14 June 2018 Accepted 10 July 2018

Keywords: Two-photon absorption Three-photon absorption Optical limiting Z-scan Porphyrin Phthalocvanine

#### ABSTRACT

Broadband (700-950 nm) third order nonlinear optical (NLO) properties of porphyrin (ZnTPP) and phthalocyanine (TPA-ZnPc) molecules in solution form have been studied using the Z-scan technique with femtosecond, MHz pulses. Two-photon, three-photon absorption coefficients along with the third-order NLO susceptibility ( $\chi^3$ ) and their optical limiting thresholds are estimated from the theoretical fits to experimental data. Closed aperture Z-scan data provided the information on the sign and magnitude of nonlinear refractive indices  $(n_2)$  at different wavelengths. Our results clearly suggest that these molecules possess the potential for applications such as optical limiting and biological imaging at high repetition rates.

© 2018 Elsevier Ltd. All rights reserved.

#### 1. Introduction

Novel organic molecules with exceptional third-order nonlinear optical (NLO) coefficients are required for various device applications in the fields of optical communications, biomedical imaging. and photonics [1–3]. Both porphyrins and phthalocyanines are aromatic organic macromolecules with a huge number of delocalized  $\pi$  electrons [4–8]. Porphyrins, rigid square planar molecules made of four pyrroles, connect to form a larger ring. Porphyrin is stabilized by an aromatic character which extends over its entire structure. Phthalocyanines are a group of synthetic pigments that contain four isoindole units linked together in a large ring. A phthalocyanine is typically intensely blue-green-coloured and is widely used in dyes. Both porphyrins and phthalocyanines can carry a central metal ion in their rings which opens up lots of possibilities in tuning the NLO properties [9–13]. In fact, they can be used for tailoring the NLO coefficients to suit a specific application. For example, certain moieties depict saturable absorption (SA) and such molecules can be used in mode-locking of ultrafast lasers. A few others demonstrate strong nonlinear absorption, and these can be utilized in either bio-imaging applications [strong twophoton absorption (TPA) coefficient/cross-section] or as optical limiters. Some class of these molecules depict strong nonlinear

refractive index (n<sub>2</sub>) and such molecules have potential applications in all-optical switching provided they have ultrafast electronic response. The nonlinear absorption can be tuned in such molecules to achieve SA or reverse saturable absorption (RSA). Similarly, the  $n_2$  of a molecule can be modified by simply changing the central metal ion or the peripheral substituents. It is observed that the NLO properties strongly depend on the excitation wavelength and the input pulse duration used. Therefore, it is imperative to scrutinize the NLO properties of any novel molecules over a wide wavelength range. In the present work we present NLO properties of a porphyrin and a phthalocyanine molecule in the 700–950 nm spectral range achieved with femtosecond pulses.

The Z-scan technique is a single-beam technique that provides both the sign and magnitude of real and imaginary parts of third order nonlinear susceptibility  $\chi^{(3)}$ . This method is simple to perform and gives rapid, accurate results. This technique was originally introduced by Sheik Bahae et al. [14]. According to Beer-Lamberts law the amount of light transmitted is a linear function of incident light intensity.  $\alpha(I) = \alpha + \beta I$  and  $dI/dZ = -\alpha(I)I$ , where  $\alpha$  is linear absorption coefficient; I is the intensity of the light and  $\beta$  is a nonlinear absorption coefficient. The light induced refractive index change is described by the relationship  $n = n_0 +$ n<sub>2</sub>I, where n<sub>o</sub> is the linear refractive index; I is the intensity of the light and  $n_2$  is a nonlinear refractive index coefficient. In open aperture Z-scan the nonlinear absorption of the sample is measured. One can use the following equations  $dI/dz = -\alpha I - \alpha_2 I^2$ 

<sup>&</sup>lt;sup>b</sup> Polymers & Functional Materials Division, CSIR-Indian Institute of Chemical Technology, Tarnaka, Hyderabad 500007, Telangana, India

<sup>\*</sup> Corresponding author. E-mail address: soma\_venu@uohyd.ac.in (S. Venugopal Rao).

FISEVIER

#### Contents lists available at ScienceDirect

### Solar Energy

journal homepage: www.elsevier.com/locate/solener



## Low cost 'green' dye sensitized solar cells based on New Fuchsin dye with aqueous electrolyte and platinum-free counter electrodes



Ramesh K. Kokal<sup>a</sup>, Somdatta Bhattacharya<sup>b</sup>, Lilian S. Cardoso<sup>c</sup>, Paulo B. Miranda<sup>c</sup>, Venugopal Rao Soma<sup>b</sup>, Prabhakar Chetti<sup>d</sup>, Deepa Melepurath<sup>a</sup>, Sai Santosh Kumar Raavi<sup>e,\*</sup>

- <sup>a</sup> Department of Chemistry, Indian Institute of Technology Hyderabad, Kandi, Sangareddy, Telangana 502285, India
- <sup>b</sup> Advanced Centre of Research in High Energy Materials (ACRHEM), University of Hyderabad, Hyderabad, Telangana 500040, India
- <sup>c</sup> Instituto de Física de São Carlos, Universidade de São Paulo, C.P. 369, 13560-970 São Carlos, SP, Brazil
- <sup>d</sup> Department of Chemistry, National Institute of Technology, Kurukshetra 136119, Haryana, India
- e Department of Physics, Indian Institute of Technology Hyderabad, Kandi, Sangareddy, Telangana 502285, India

#### ARTICLE INFO

# Keywords: Aqueous DSSC Pt free counter electrodes Ultrafast spectroscopy, New Fuchsin, electrochemical impedance spectroscopy

#### ABSTRACT

In this work, we present the application of a inexpensive water-soluble New Fuchsin (NF) dye as a photosensitizer for dye sensitized solar cells (DSSC). A comprehensive study including computational, spectroscopy and cyclic voltammetry measurements established the efficacy of NF as a photosensitizer. Density functional theory (DFT) modelling of NF is performed to estimate the energy levels and experimentally verified using the cyclic voltammetry measurements. For the spectroscopy characterization time-resolved absorption and fluorescence studies are employed on NF in ethanol solution and as thin film deposited on glass and mesoporous  $TiO_2$ . Femtosecond transient absorption measurements revealed ultrafast electron injection within < 1 ps at the interface of NF and  $TiO_2$ . NF sensitized solar cells were fabricated and optimised using various liquid electrolytes and carbon-based counter electrodes. The fabricated devices were further characterized using electro-impedance spectroscopy and Mott-Schottky measurements. The best-performing device with photo-conversion efficiency of 2.9% was obtained using aqueous  $Fe^{3+}/Fe^{2+}$  electrolyte and CoS treated carbon fabric. These components are non-toxic and economical resulting in the fabrication of low cost and eco-friendly "green" solar cells.

#### 1. Introduction

Tremendous success of the dye-sensitized solar cell technology, notwithstanding, during the last three decades, (Gong et al., 2017; Grätzel, 2003; Hardin et al., 2012; Mathew et al., 2014) with a record efficiency of ≈13% (Mathew et al., 2014), few challenges that still plague the community are the long-term stability for commercialization & overall cell performance (Fakharuddin et al., 2014; Shahimin et al., 2015), use of expensive platinum-based counter electrodes (CE) (Iqbal and Khan, 2018; Mozaffari et al., 2017; Ye et al., 2015) and use of various organic solvent-based liquid electrolytes (Yu et al., 2011). Particularly, the use of liquid electrolytes come with various drawbacks such as high vapor pressure, toxic and sometimes explosive resulting in sever environmental impact. To further this issue, iodide based liquid electrolyte to be corrosive and damage the platinum electrodes in a long run (Shahimin et al., 2015). Moreover, a long-standing and critical issue still unresolved in the DSSC community is the contamination of standard aprotic DSSC systems by means of moisture/water. To counter the issues of corroding liquid electrolyte and instability in moisture environment, lot of efforts are directed towards the development of aqueous dye-sensitized solar cells (Bella et al., 2015; Law et al., 2010; Risbridger, 2013). Novel sensitizers were developed towards aqueous DSSC fabrication (Li et al., 2017). Considering naturally occurring dyes and pigments, most of which are soluble in water, offer cost-effective alternatives, the use of natural dyes and pigments as effective sensitizers are yet to fructify its potential (Hao et al., 2006; Iqbal et al., 2019; Richhariya et al., 2017; Sanjay et al., 2018; Shalini et al., 2015; Zhou et al., 2011). In view of being cost-effective and stable in the aqueous environment, an ideal DSSC should consist of inexpensive sensitizer, water-based non-toxic electrolytes, and platinum-free counter electrode, giving it the true definition of eco-friendly 'green' photovoltaic device.

In this report, we present our results on a 'green' DSSC making use of an inexpensive magenta dye, New Fuchsin, for the first time as a photosensitizer, employing a water based  $Fe^{3+}/Fe^{2+}$  electrolyte with CoS deposited on C-fabric as the counter electrode. New Fuchsin  $[C_{22}H_{24}N_3Cl,4-$ 

E-mail address: sskraavi@iith.ac.in (S.S.K. Raavi).

<sup>\*</sup> Corresponding author.

ELSEVIER

Contents lists available at ScienceDirect

## Dyes and Pigments

journal homepage: www.elsevier.com/locate/dyepig



# Synthesis and femtosecond third order nonlinear optical properties of push-pull *trans*-A<sub>2</sub>B-corroles



Pinky Yadav <sup>a</sup>, Thangaraj Anand <sup>a</sup>, Sree Satya Bharathi Moram <sup>b</sup>, Somdatta Bhattacharya <sup>b</sup>, Muniappan Sankar <sup>a, \*</sup>, Soma Venugopal Rao <sup>b, \*\*</sup>

- <sup>a</sup> Department of Chemistry, Indian Institute of Technology Roorkee, Roorkee 247667, India
- b Advanced Center for Research in High Energy Materials (ACRHEM), University of Hyderabad, Hyderabad 500046, Telangana, India

#### ARTICLE INFO

Article history:
Received 30 March 2017
Received in revised form
13 April 2017
Accepted 14 April 2017
Available online 25 April 2017

Keywords: Trans-A<sub>2</sub>B-corroles Femtosecond Charge-transfer Third order nonlinear optical properties DFT studies

#### ABSTRACT

Six novel push-pull trans-A<sub>2</sub>B free base corroles (1-6) were synthesized and characterized by various spectroscopic techniques. The charge-transfer ability of these trans-A<sub>2</sub>B-corroles was reflected from the broadness of the UV-visible absorption spectral bands. Corroles 1 and 2 exhibited absorption at lower wavelengths, higher quantum yield and longer singlet state lifetime as compared to 3-6. The ultrafast nonlinear optical (NLO) properties of these corroles were evaluated in visible range (at 800 nm) using the femtosecond Z-scan technique. The investigated corroles possess negative type of nonlinearity and selfdefocusing behavior with the magnitude of nonlinear refractive index  $(n_2)$  in the range of 0.36  $-2.84 \times 10^{-11}$  cm<sup>2</sup>/W, while the two-photon absorption ( $\beta$ ) coefficients were in the range of 6.5–68 cm/ GW with  $|\chi^{(3)}|$  in the range of  $10^{-9}$  e.s.u. The resultant dipole moments of these corroles were calculated theoretically and found to be 1.47–7.26 D depending on the nature of push-pull groups on the mesophenyl substituents. 1-6 demonstrated excellent NLO activity due to their 'push-pull' design. Among the investigated corroles, 1 and 2 possess strong two-photon absorption coefficient and large values of  $\chi^{(3)}$ suggesting that the nonlinearity of corrole molecules highly depends on the electronic nature and number of meso-substituents. Corroles 1 and 2 possessing two acceptor and one donor moieties depicted superior NLO behavior as compared to corroles (3-6) with one acceptor and two donors due to strong electron withdrawing nature of pentafluorophenyl groups as well as higher singlet excited state lifetime and quantum yield.

© 2017 Elsevier Ltd. All rights reserved.

#### 1. Introduction

Nonlinear optical (NLO) materials have attracted materials/ chemistry/physics researchers' interest since past two decades due to their tremendous potential in various applications such as optical communication, optical limiting, multi-photon imaging, fluorescence, data storage devices and surface-enhanced Raman scattering [1–3]. Mainly organic molecules which contain large conjugated  $\pi$ -systems with donor and acceptor sites at the opposite end of the periphery were used as NLO materials [4–7]. These molecules offer the advantages of strong optical nonlinearity and faster optical response. Recently, electron rich corroles based on D-

E-mail addresses: sankafcy@iitr.ac.in (M. Sankar), soma\_venu@uohyd.ac.in (S.V. Rao).

 $\pi$ -A systems were synthesized to study their third-order NLO properties [8-12]. Corroles, a class of contracted porphyrinoids processes  $18-\pi$  electron aromaticity. Chemistry of corroles was started 40 years before but the research in this area was slow due to lack of synthetic methodologies [13]. Corrole studies grew up tremendously with the revolution of one pot synthetic route of corroles [14,15]. This provided a new impetus to the synthesis of novel corroles particularly  $\beta$ - and meso-functionalization of the macrocycle [16-20]. Tribasic corroles exhibiting interesting properties such as lower oxidation potentials, higher fluorescence quantum yields, larger Stokes shift, and relatively more intense absorption phenomena as compared to their corresponding porphyrins. These macrocycles showed an intense Soret band and three less intense O-bands in the visible region. These versatile spectral, electrochemical and photophysical properties of corroles attracted the researchers' interest leading to their widespread applications [21–24]. In addition, the electron-rich  $\pi$ -system of these

<sup>\*</sup> Corresponding author.

<sup>\*\*</sup> Corresponding author.

